# Applications and Industry®



January 1958

## Transactions Papers



(This issue completes publication of all technical program papers presented during 1957.)



NUMBER 34

*Published Bimonthly by*

AMERICAN INSTITUTE OF ELECTRICAL ENGINEERS

## Communication and Electronics—January 1958



*(See inside back cover)*

---

*Applications and Industry.* Published bimonthly by the American Institute of Electrical Engineers, from 20th and Northampton Streets, Easton, Pa. AIEE Headquarters: 33 West 39th Street, New York 18, N. Y. Address changes must be received at AIEE Headquarters by the first of the month to be effective with the succeeding issue. Copies undelivered because of incorrect address cannot be replaced without charge. Editorial and Advertising offices: 33 West 39th Street, New York 18, N. Y. Nonmembers subscription $5.00 per year (plus 50 cents extra for foreign postage payable in advance in New York exchange). Member subscriptions: one annual subscription in consideration of payment of dues without additional charge to any one of three divisional publications: Communication and Electronics, Applications and Industry, or Power Apparatus and Systems; additional annual subscriptions $2.50 each. Single copies when available $1.00 each. Second-class mail privileges authorized at Easton, Pa.



Printed in United States of America

Number of copies in this issue 13,000

# Application of D-C Machines to Oil-Well Drilling

B. H. HEFNER
NONMEMBER AIEE

BECAUSE OF their flexibility, portability, and ease of operation, diesel-electric units are particularly well suited as power plants for drillings rigs. The diesel engine has long been recognized for its efficiency, reliability, and economy of operation. In many cases, the diesel engine has all but replaced other types of prime movers.

An electric-transmission system is an infinitely variable speed changer that matches engine output to load requirements. It eliminates the need for mechanical-torque multipliers and multiple-chain drives. Instead, it utilizes flexible cables that can be connected and disconnected quickly and easily without requiring bolting and taping. The need for alignment of basic power units with draw works, rotary tables, or mud pumps is thus eliminated and set-up time is greatly reduced. Multiple loads can be handled by one engine without gear-reduction complexity. The flexible connections permit the engines to be located on a tender while the rig and its equipment are on a platform. One engine can also be mounted on the platform to provide it with independent power should it be necessary to move the tender because of weather conditions.

Diesel-electric rigs are light and inherently compact. The latter is particularly important to offshore operations where space is at a premium. On land, the need for heavy foundations is avoided and set-up time is cut to a minimum. Driller's controls for the electric-transmission system are as simple as, if not simpler than, controls for conventional transmissions.

Some versions of of diesel-electric units utilized conventional switchgear and off-the-shelf industrial motors. The equipment was large and controls were complex and costly. Rig operators had to turn to specialists to take care of even minor difficulties.

Paper 57-978, recommended by the AIEE Petroleum Industry Committee and approved by the AIEE Technical Operations Department for presentation at the AIEE Conference of the Petroleum Industry, Philadelphia, Pa., September 9–11, 1957. Manuscript submitted January 14, 1957; made available for printing August 7, 1957.

B. H. HEFNER is with General Motors Corporation, La Grange, Ill.

With the use of the General Motors *567*-series 2-cycle *V*-type 8-cylinder 875-hp (horsepower) diesel engine as the prime mover, the design and building of an electric-transmission system that would satisfy as closely as possible the following criteria was initiated:

1. Over-all system as simple as possible.
2. Maximum interchangeability of components.
3. Maximum operational flexibility.
4. Built-in protection for all components.
5. Ease of operation and maintenance.

## Drill-Rig Load Requirements

Since any transmission, mechanical, electric, or otherwise, essentially functions to match engine output to load requirement, it is obvious that the load requirements of the drilling rig must be analyzed and compared with engine characteristics.

The *567* diesel engine at full load operates at constant speed and constant torque. Drilling-rig loads are varied and arise from the following:

1. Draw works.
2. Rotary table.
3. Mud pumps.
4. Miscellaneous loads including air compressors, motor-generator sets for a-c supply, small slush pumps, coring reels, etc.

The draw works is basically used as a hoist mechanism, although it is also used to power the breaking-out and making-up catheads and sometimes to drive the rotary table. Hoisting the drilling stem is essentially a tractive effort. It is necessary to start and to accelerate a heavy load when the stem is long and deep. It is necessary to operate at higher speeds and low torque when the load is light, i.e., when a single stand is being handled.

This traction loading can be seen clearly in Fig. 1 which compares the curve for draw-works hook pull versus hook speed, with the curve for locomotive tractive effort with locomotive speed. The two curves have almost identical shapes.

As currently built, draw works are equipped with either a friction clutch or a jaw clutch. To engage a jaw clutch, the transmission comes to a full stop, while a friction clutch engages "on the fly." In designing a transmission for a friction-clutch-equipped draw works, it is particularly important to provide good deceleration control so that pick-up speed is not excessive. A case in point would be breaking out or making up with the catheads—a low-speed light-load operation.

As long as the drilling conditions for which the driller sets the rotary table stay the same, the rotary table represents a steady load with little variation in torque or speed. But if drilling conditions change, for instance, if gumbo or heavy strata is encountered and the bit begins to ball, torque will increase and speed decrease. If an "easy" strata is encountered, speed will increase and torque will drop.

The characteristics of the load represented by mud pumps are similar to the rotary-table characteristics. As long as the conditions for which the mud pumps have been set do not change, pumping speed does not vary. But should a cavity, plugged hole, or other situation arise, a change in pumping speed is necessary.

The remainder of the load from auxiliary equipment and services represents a small percentage of the total power requirements of the rig and is essentially a steady-state load.

Based on a consideration of these load patterns, it would seem logical to proceed on the assumption that, among other things, the electric transmission for a drilling rig should provide extremely high torque at low speeds and, conversely low torque at high speeds. In general, the transmission of power should be responsive to changing-load conditions. These objectives were strived for in the design of the electric transmission for drilling units.

## Generator Selection

To supply power adequately to the load motors on a drilling rig, generator voltage should decrease as the current increases. In other words, a differential effect is required. The classical means of accomplishing this is to provide a differential field in the generator. In the original design studies the use of a generator of this type was considered. Its construction and characteristics are quite familiar from work in the locomotive field. However, upon further analysis, it was decided not to use it for the following reasons:

1. Multiplicity of load functions cannot be met without serious control complications.
2. Differential-field windings occupy space in the generator and require bigger forward-excitation windings. This results in the

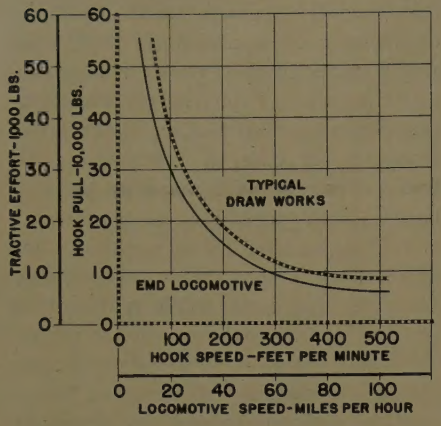


**Fig. 1. Comparison curves of locomotive tractive effort versus draw-works hook pull**

following: a heavier machine, and a larger machine.

It was decided, instead, to use a smaller generator with a separately excited field. The same machine, except for a change in the field winding, is used as a motor to power the draw works, mud pumps, and rotary table.

Designated as model *D39G*, the generator designed and built for drilling-rig application is a 4-pole machine rated at 500 kw. The armature has a progressive simplex lap winding and employs hot-pressed coils with a class *H* system insulation of glass and mica tape, glass and mica channels, and silicone varnish. Insulation on coil diamonds include varnished and melamine asbestos, fiber glass, and Teflon. Radial brush arrangement allows rotation of the armature in either direction. Main fields and interpoles have class *H* silicone-rubber insulation bonded to the copper which provides a positive moisture seal. Sealed-grease-lubricated cylindrical roller bearings at drive end and commutator end of the armature shaft provide extended maintenance-free service life.

The *D39G* generator is a force-ventilated machine, receiving its air from an engine-driven blower.

## Excitation-Control System

In the design of the control circuit and apparatus, simplicity, rugged construction, and compactness were the objectives in the choice of components. An a-c power source was chosen for the control of generator excitation because it permits the use of minimum sized equipment requiring very low voltage and current. The excitation-control circuit is shown in Fig. 2 and is described in the following.

The first requirement for the control system is a device for the driller's hand that will send a command to the power plant to supply power for a given load. A number of devices can be used including a rheostat or a potentiometer. A Variac (a variable-voltage transformer) was used, which is a rugged dependable low-watt-loss unit that keeps at a minimum the heat-dissipation level at the driller's station.

The 110-volt a-c power supply, which is common to almost every rig in the field, is taken through the Variac. Controlled excitation flows from this point through a multiple-conductor cable to a motor-control cabinet, and from there to the generator-control cabinet on the engine skids by means of appropriate interlocks. The 110-volt a-c power goes through an isolating transformer which steps the voltage down by a 4-to-1 ratio. The current is then rectified by a bridge rectifier, a full-wave rectifier of the dry-plate type which is conservatively rated so that its life will be almost indefinite. The rectified current is then supplied to the field of the engine-driven exciter generator, which amplifies the excitation current to the main-generator field. The main-generator field requires up to 100 amperes.

Up to this point this is, in effect, a

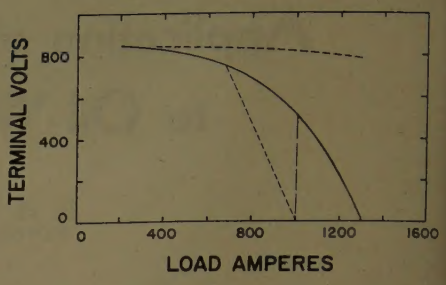


**Fig. 3. Net results of the control system**

shunt generator with the voltage dropping slightly with increased current demand. But to serve properly the constant-horsepower demand of the load motors, the control circuit must supply a differential effect so that voltage will drop as current demand increases. This is accomplished by means of a feedback circuit.

## Feedback Circuit in the Control System

A feedback current proportional to the armature current of the main generator is supplied by a transductor which is inserted in the power circuit between the generator and motor. The device is essentially a type of d-c transformer. The d-c load cable from the generator to the motor passes through steel cores with coil windings around them. These windings are supplied by a small alternating current from the 110-volt supply, and a rectifier is added so that the feedback current is rectified.

Little current flows through the transductor until the d-c load cable begins to carry current. Then, as the load current increases, the transductor core saturates, changing its impedance and allowing an increase in the transductor output current. This current is in a fixed ratio to the armature current—approximately 1 to 400 amperes, and is unaffected by any other regulating action.

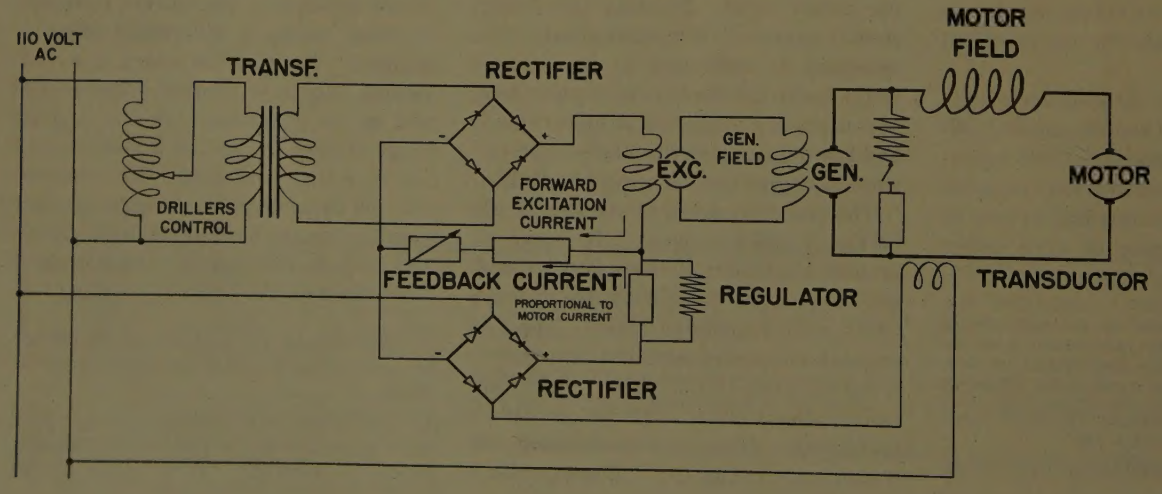


**Fig. 2. Excitation-control circuit**

The direct current from the transductor flows to a preset regulating resistor and a voltage drop is produced which subtracts from the voltage on the exciter generator field. The result is a reduction in exciter-field current and thus less voltage generated by the main generators.

Given a constant maximum voltage on the excitation circuit, the excitation current is determined by that voltage and by the resistance in the circuit. The feedback current is essentially independent of the resistance within its circuit and, as mentioned earlier, is proportional to the high-voltage d-c flow.

Thus, by using three simple low-cost static-control components, namely transductor, rectifier, and resistor, together with a relatively small generator, it is possible to obtain the characteristics of a much larger generator with a differential-field winding.

## Regulation for Thermal and Torque Limits

With the addition of a simple field regulator two other important objectives are attained with the excitation-control system. These objectives include provision for torque and thermal limit. The torque limit is utilized for intermittent generator output to prevent damage to the equipment being driven. The thermal limit is utilized for continuous generator output to prevent overheating of the motors.

The field regulator has two control coils, a current coil and a voltage coil. The torque limit is provided by the current coil. The thermal limit is provided by the combined action of the current and voltage coils. Both act so that when energized, the operator on the resistance element moves to cut in resistance. When de-energized, the spring-loaded operator returns to its minimum resistance. The current coil is in series with the transductor output and becomes operative when the transductor output tells it that the armature (load) current is approaching 1,000 amperes. The coil then cuts resistance into the circuit and the transductor current passing through it creates a voltage which opposes the voltage of the excitation current.

The voltage coil, in series with a calibrating resistor, is wired across the generator output so that as the generator voltage rises the voltage coil becomes stronger, causing resistance to be cut into the exciter-field circuit. A recalibration relay is arranged so that when an individual generator is used to power an intermittent load such as the draw works, the relay cuts out the action of the voltage coil. This causes a change in the generator characteristic to match the operating requirements of the draw works.

The net results of the control system can be seen in Fig. 3 in which terminal volts have been plotted against load amperes to show the generator characteristic curves. The horizontal dashed line (at the top) is the generator characteristic resulting from a given excitation without control. The solid line shows the differential effect of the feedback current. It is a close approximation of the constant-power curve desired for drill-rig generator operation. The vertical dashed line (long dashes) represents the control effect of the field-regulator current coil on intermittent generator output to limit torque.

The diagonal dashed line represents the continuous generator output obtained as a result of the control effect of the current and voltage coils of the field regulator. As can be seen, the volt-ampere relationship is a straight line whose slope can be varied by varying the relationship between the current and voltage coils of the field regulator.

It can be seen that the generator-and-control system offers unusual flexibility in performance. Generator characteristics can be adjusted by relatively simple circuit changes to meet the sometimes widely varying needs of mechanical equipment used on drilling rigs.

## Motor Selection and Control Design

The design approach used up to this point has not necessarily presupposed the use of a particular class of load motor. Rather, the choice of motor is dictated by the operational requirements of the drilling rig.

There are only two basic types of d-c motors, the shunt motor and the series motor. A variation of the shunt motor is the separately excited motor. A shunt motor with armature and fields connected in parallel with a common supply is immediately ruled out in view of the many high-starting-torque loads, such as in the case of the draw works. A shunt motor has a constant speed and a varying torque. It has very poor starting-torque characteristics. This type of motor requires added control such as accelerating resistors and contactors in the armature circuit or a separate excitation supply to provide the desirable starting characteristics.

The net result is a choice between a series motor and a separately excited motor. The series motor is widely accepted as the standard class of motor for traction type of loading; and traction loading is encountered in the draw works and to a certain extent in mud-pump operation. On the other hand, since a separately excited generator is used, a separately excited motor would be a wholly identical machine—certainly a desirable feature. With an added control system, the torque characteristics of a separately excited motor would be improved. The choice between the series motor and the separately excited motor is not clear until all of the factors involved are considered. In the judgment of some, the choice is clearly the series motor.

For a major portion of the load demand, the series motor is a self-regulating machine. Its speed-torque characteristics follow the load pattern; high starting torque at low speed, high speed at low torque. Its self-regulating characteristic requires modification near the no-load end of the operational sequence. At light load, its decelerating characteristics need improvement; and at mechanical failure of the load, the motor overspeeds.

The separately excited motor is inherently unable to regulate itself; it has very poor torque response and therefore a control system is required to provide the needed characteristics. In other words, the motor itself will not respond to load change, it must be adjusted to meet the new load requirements. Its decelerating characteristics and performance at light load are good. While it is not affected by a mechanical loss of load, it must be protected against an electric (field) failure, which would cause it to "run away."

It thus becomes a question of which motor requires less effort, equipment, and cost to compensate for its disadvantages. It has been found that the advantages of the series motor outweigh the advantages of the separately excited motor, and its disadvantages are easier to deal with than the disadvantages of the separately excited motor. To sum up, the following are the advantages and disadvantages of each type:

Series-motor advantages

1. Speed-torque characteristics suited to the needs of the draw works, mud pump, rotary table, and auxiliary and miscellaneous drives.
2. Standardization of all motor drives.
3. Simplified wiring for application.
4. Controls centralized in motor-control and generator-control cabinets.
5. Higher inherent torque characteristics.
6. Wider speed range.

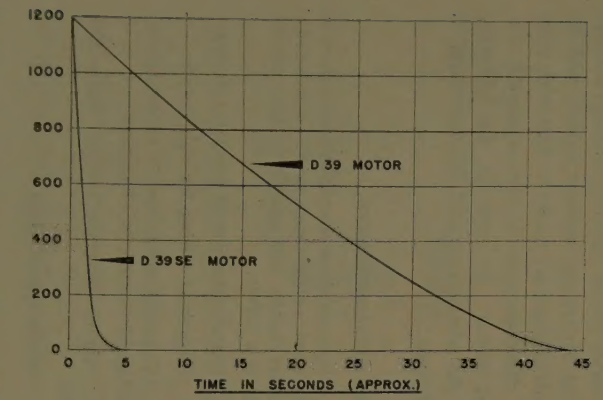


Fig. 4 (left). Typical draw-works deceleration curve for D39 and D39SE motors

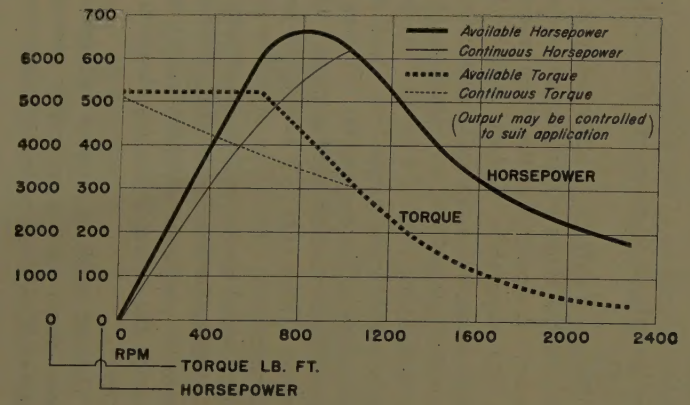


Fig. 5. D39 industrial motor, torque and horsepower curve for applications from 150 to 625 hp

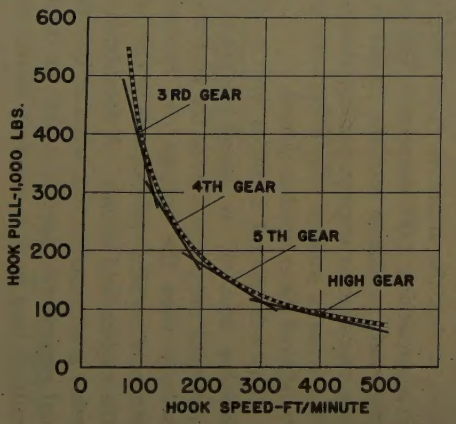


Fig. 6. Typical 1,200-hp draw-works curve compared with theoretical "ideal" curve

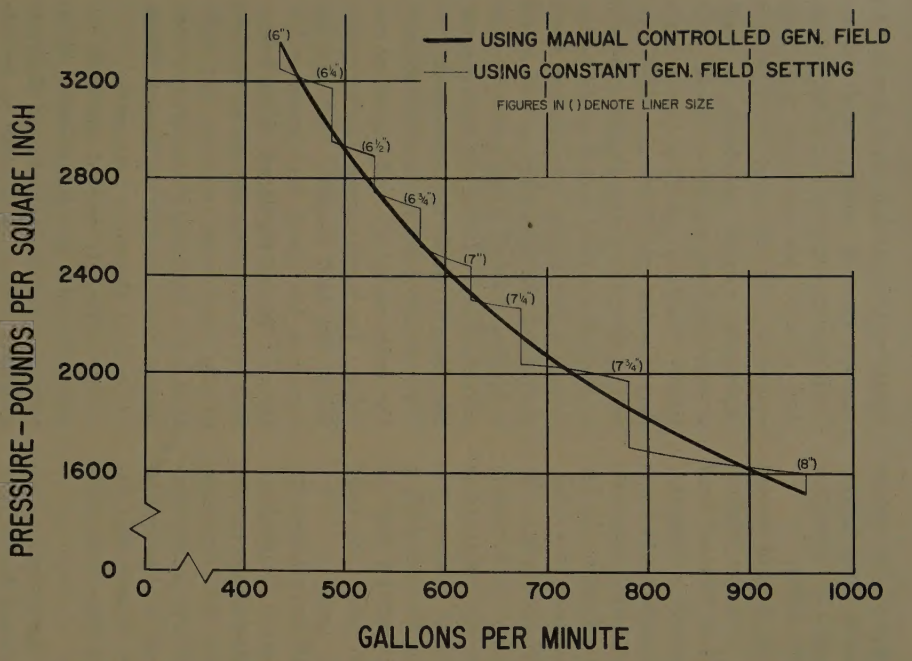


Fig. 7. Typical 1,000-hp mud-pump application curve using two D39M motors

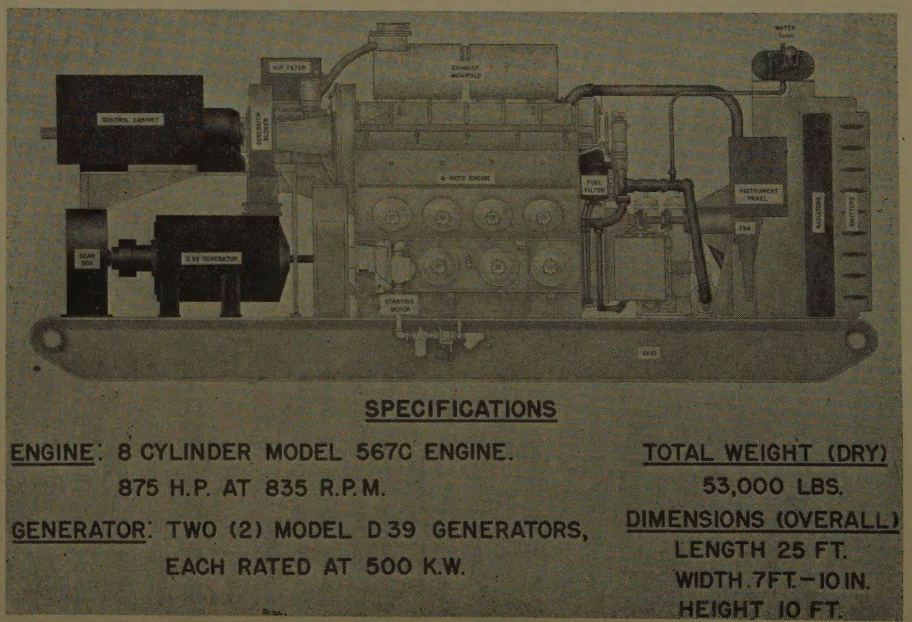


Fig. 8. Unit of 875 hp

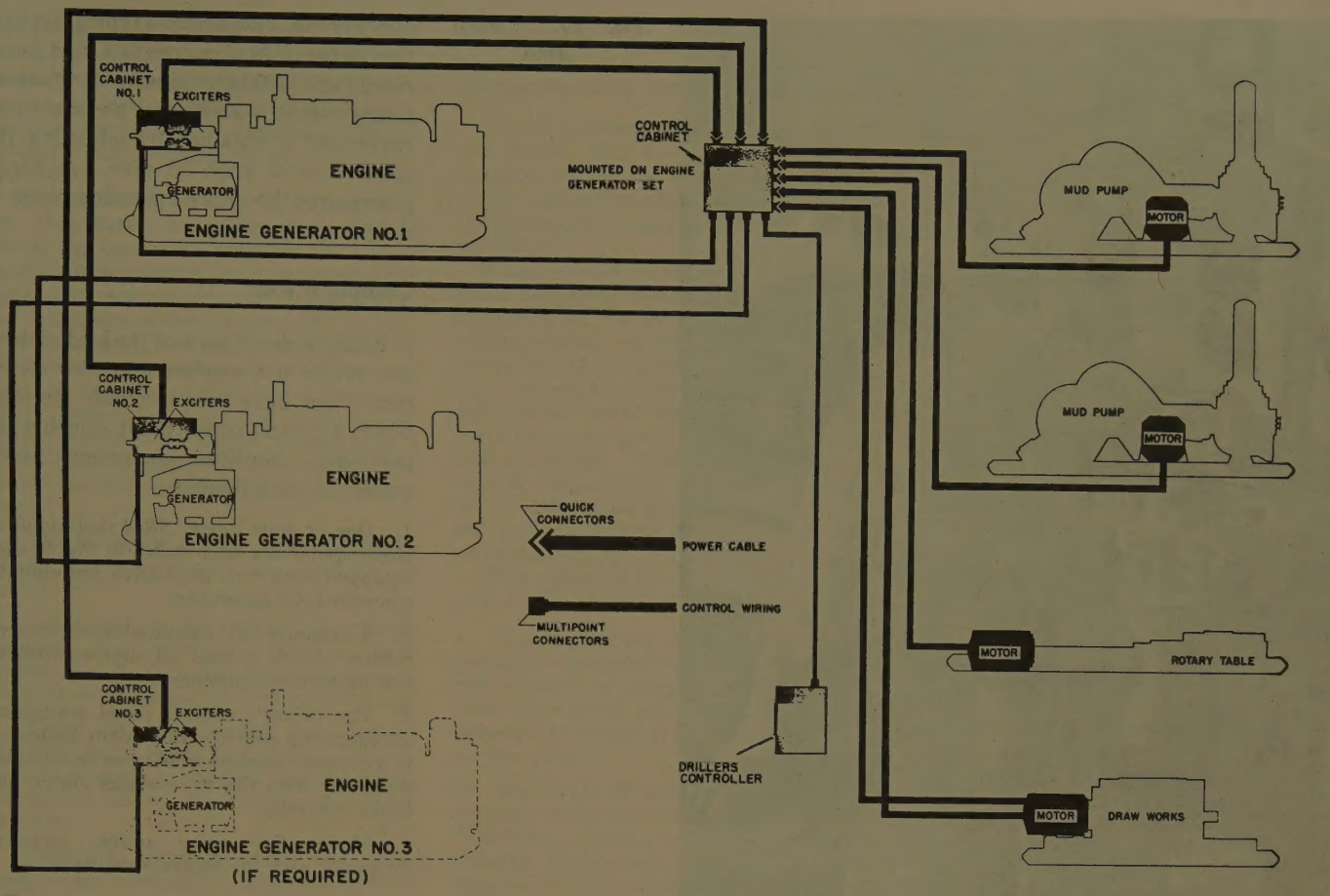


**Fig. 9. Diesel-electric drill-rig schematic**

Series-motor disadvantages

1. Safety control for speed limit in case of load loss due to mechanical failure.
2. Deceleration control for performance improvement.

Separately excited motor advantages

1. Does not overspeed with loss of load.
2. Better inherent decelerating characteristics.

Separately excited motor disadvantages

1. Speed-torque characteristics do not match load requirements; the motor runs at constant speed and does not respond to change in drilling conditions.
2. Requires voltage-failure protection for each motor field.
3. Machine transients need to be controlled.
4. Three kw per motor is required for control power.

## Motor-Overspeed Protection

Model *D39M* motor used in the electromotive diesel-electric unit is a d-c 4-pole series-wound machine, in which all parts, except the main-field windings, are interchangeable with the *D39* generators. It is conservatively rated at 625 hp for continuous operation. The machine has a continuous-current rating of 670 amperes with a short-time rating of 1,000 amperes for intermittent hoisting operations.

To protect the motor against overspeed, an *E*-type through-cable relay is used. It consists of four parts; a 2- by 3- by 1/4-inch magnet yoke, voltage coil, armature assembly, and contact assembly. The relay is biased by a generator current-carrying cable passing through the yoke of the relay, and operates on generator voltage by energizing a voltage-sensitive coil. In operation, the flux set up in the yoke by the two turns of the generator lead tends to keep the relay from picking up.

The relay operates to remove generator excitation when the generator voltage has reached the value which, for a given load, tends to result in motor overspeed. At this point the voltage-coil flux is of sufficient magnitude to overcome the biasing effect of the cable and to pick up the relay. Power to the motor is cut off until the driller shuts off his power control to re-establish the circuit.

## The New S-E Motor Control

As can be seen from the previous description, one of the two shortcomings of the series motor, overspeeding in case of mechanical failure, is easily handled. The motor literally shuts itself off by the use of a simple, rugged unit.

Providing the desired degree of deceleration control for operating equipment such as the draw works takes some ingenuity. A device is needed that gives the series motor the better decelerating response of the separately excited motor to light load without losing any of the series-motor advantages or taking on any of the separately excited motor disadvantages.

The device proved to be the new "super-excitation" (S-E) control. In effect, it consists of a selenium rectifier and a step-down transformer supplied from the 220/440-volt a-c utility system of the drilling rig. It maintains a small amount, approximately 20%, of excitation in the motor field.

At light or no load without the S-E control, the armature does not decelerate fast enough when power is removed. The S-E control slows the armature quickly and smoothly. It accomplishes this by converting the inertia of the motor and its load into electric energy which is in turn dissipated in the generator and engine. (The motor becomes a generator whose

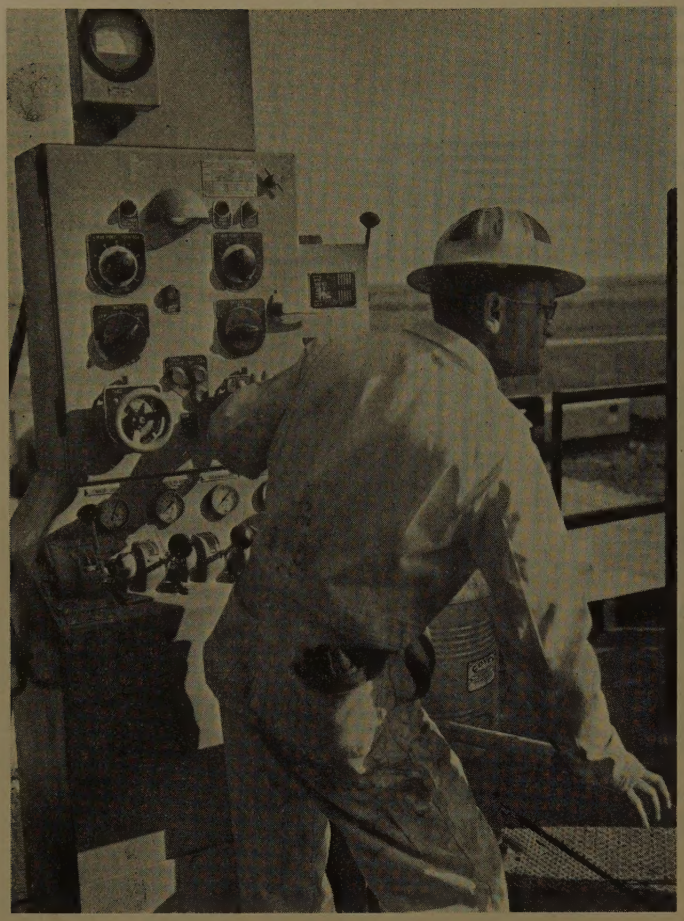

Fig. 10. Control stand

field is supplied by the superexcitation and drives the main generator and engine.)

So long as the normal excitation is at an appreciable value, the device has little if any effect on the motor characteristics. It becomes important only when the normal excitation falls off to the point where it is in the magnitude of the superexcitation current. The S-E control can be adjusted so that the decelerating current can be controlled to a desired value.

This device is a compact unit with no moving parts and with components that have long life. It can be added to a motor already in operation or built integrally into the control system.

Fig. 4 shows the effect of the S-E control on the operation of the electric transmission. Fig. 5 shows the torque and horsepower curves for the *D39M* motor. Fig. 6 shows the optimum draw-works curve and *D39M* operating curve for a typical draw-works application. The curve in Fig. 7 illustrates a typical application of two *D39M* motors to a mud pump rated at 1,000-hp input. Maximum pump output is shown by the saw-tooth curve and is obtained by adjusting the speed control knob to give full horsepower over the entire operating range of the pump.

### Complete Unit

With the description of the load motors, the major d-c machines in the diesel-electric set have been covered. In summary, a typical power plant utilizing the previously described equipment would consist of the following:

1. One or more model *SR-8* skid-mounted engine-generator sets, shown in Fig. 8, each equipped with two dual-drive individually controlled d-c generators.
2. A separate skid-mounted motor-control cabinet which houses all motor-switching and protective equipment.
3. The driller's control panel containing all operating controls and alarm indicators in a compact cabinet which can be mounted integrally with the draw-works clutch and brake controls.
4. Model *D39* drive motors mounted integrally with the driven equipment.

A typical field arrangement of the power plant is shown in Fig. 9. In this case, dual-drive motors are used on two mud pumps and the draw works while a single motor drives the rotary table. The 8-position selector switch located on the driller's control stand (Fig. 10) selects the desired arrangement for coupling available generator output to the various motor-drive units. For full-torque low-horsepower operation, a single generator is connected to the individual motor drive. For full-torque full-horsepower operation, two generators are connected in series to the motor-drive unit.

## Discussion

**G. W. Webb** (General Electric Company, Dallas, Tex.): I wish to congratulate the author on a comprehensive coverage of this very timely subject. Early versions of diesel-electric rigs were complex and costly. It is perhaps fortunate for the drilling industry that locomotive market conditions permitted manufacturers of traction equipment to turn their attention to other applications at a time when offshore drilling became active.

We are in complete accord with the author's design criteria of:

1. Simplicity.
2. Interchangeability.
3. Flexibility.
4. Built-in protection.
5. Ease of operation and maintenance.

Means of accomplishing these objectives electrically is a vital concern of the industry, and I feel constitute a profitable area for study and discussion. The following comments are offered in the interest of furthering our mutual objectives.

With reference to generator selection, the author states that a differential-generator characteristic is required, but proposes a shunt-wound generator with an external current-regulating system to attain this characteristic. This was used in earlier versions of electric rigs.

True, a differential field in the generator requires space and could mean a larger machine; however, if the motors and generators are to be interchangeable in frame size and armatures, the choice seems to be between a reduction in generator peak rating and the extra controls required for current- and voltage-regulating systems.

Our experience leads us to question the use of such regulating controls on drilling rigs when the job can be done by a few turns of heavy copper in the generator field, which is simple to understand, the ultimate in reliability, requires no critical adjustments or maintenance, and is fast in transient response.

I would appreciate clarification of the objection to a differential generator for the reason that "multiplicity of load functions cannot be met without serious control complications." It appears that either type generator can be assigned to various loads

on the rig with about the same number of switching contactors. Actually, it is quite simple to parallel two differential generators to obtain even higher intermittent output from the hoisting motors than could be obtained with a single higher rated shunt generator.

With reference to motor selection, it is felt that motor and generator selection should be considered together since it is their combined output which determines the significant performance characeristics from the standpoint of driving the load.

In considering the relative advantages of the series motor, universally used on locomotives, and the separately excited shunt motor, which for years has been the accepted standard for electric drilling rigs, I would like to compare briefly some features of the locomotive- and drilling-rig applications.

1. The locomotive motor is geared to the wheel. Drilling motors are chained or belted.

2. Light loads or loss of load are difficult to obtain on a locomotive. Even so, series motors are occasionally destroyed despite years of development or overspeed devices.

3. There are no mechanical gear changes provided in a locomotive drive. Steam-type draw works, commonly used, have four mechanical ratios. Mud pumps have liner changes.

4. Line-pull, pump-pressure, and drill-stem torque limitations I believe have more serious consequences than wheel slip in a locomotive.

5. In a locomotive the main controls are located much closer to the motors than on a drilling rig. This permits the switching of power circuits to put the traction motors in series or parallel and to change their fields to obtain the long smooth tractive effort curves.

Now in considering the series-motor advantages for drilling applications, the following applies:

1. It is readily conceded that the inherent speed-torque characteristic of the series motor is closer to ideal performance. However, the differential generator in itself provides high speed at low torque, and low speed at high torque with the shunt motor. This combination inherently limits no-load speed without reliance on external control devices and also limits stalled torque without external current regulation.

2. With either motor all motors can be standardized.

3. Simplified wiring is assumed to refer to elimination of shunt field connections. It is questioned whether the necessity for reversing the series field on draw works and rotary, the superexcitation supply and leads, and the torque-limiting and overspeed protection would not defeat the purpose of simplified wiring.

4. It would appear that controls would necessarily be centralized for either motor.

5. Is it not true that the higher inherent torque of the series motor must be limited by external controls to the same permissible maximums.

6. The wider constant-horsepower speed range of the series motor is not questioned, but the difference without field switching on a 4-speed draw works would not seem to warrant the extra control complications.

The series-motor disadvantages are not questioned. We do, however, seriously question its use on any chained or belt-driven application where external overspeed shutdown is depended on to protect life and property.

With reference to the shunt-motor advantages, the shunt motor not only will not overspeed on loss of load, but since it is always excited at full field, its speed is always closely proportional to applied voltage, permitting acurate speed control at light loads, speed indication with standard voltmeters, and good regenerative braking characteristics. Shunt-motor torque is directly proportional to current as limited by the differential generator characteristic, and can be measured directly with a standard ammeter.

With reference to the shunt-motor disadvantages, the following applies:

1. Considering the combined motor and generator characteristic, the shunt motor will respond to changes in drilling conditions, since as the generator trades volts for amperes, the motor trades speed for torque or vice versa.

2. Thousands of shunt-motor applications in many industries would indicate that the field-failure hazard (which can happen only through field-circuit discontinuity simultaneous with loss of load) is not a serious problem. A simple voltage relay can be used to protect against this if required.

3. Transient-current surges which might cause difficulty are felt to be minimized on the limited engine-generator power supply and with the voltage-control systems normally used.

4. Field-excitation power of approximately the same magnitude is required for either motor, the series motor taking this power from the main engines and from the superexcitation source, while the shunt motor takes it from an exciter.

With regard to controls, many references have been made to controls in the preceding discussion. The 3-field differential-generator and shunt-motor combination requires only commonly familiar power and field contactors, simple relays, rheostats, and resistors. All rectifiers, saturable reactors, variable-voltage transformers, and current- or voltage-regulating systems can be eliminated. With the use of commonly accepted air throttles, pressure switches, and actuators, the generator-field rheostats can be remotely controlled, eliminating individual exciters for each generator. A single exciter with a stand-by is adequate for all rig requirements. It is felt that this approach is consistent with the objectives of simplicity, built-in protection, and ease of operation and maintenance without sacrificing interchangeability or flexibility.

**L. L. Johnson** (General Motors Corporation, La Grange, Ill.): Mr. Webb interprets the recommendation of the separately excited generator as an objection to a differential generator, and this is not intended. The result of carefully studying oil-rig load requirements revealed a very wide range of parameters. For example, consider the rotary table. Certainly it is desirable to limit table torque, and this limit will vary as some function of the drill pipe size. To provide such flexibility will require control and it certainly is more easily and more accurately accomplished by operating on a feedback control system than on the field of a differential machine. In the feedback system, power, speed, or torque can be varied independently or together to obtain almost any desired characteristic. In other words, a differential generator adjusted to give desirable draw-works performance does not fit either a rotary-table or mud-pump requirement. Compromising so that a single generator characteristic be usable for all loads sacrifices much performance; and to apply control to modify the differential machine requires about the same apparatus used basically in the feedback system.

Mr. Webb suggests paralleling generators for intermittent-high-intermittent output on a hoist—if motors and generators are identical, no one machine establishes the limit, they all do.

In considering the pros and cons of a motor to oil-well drill rigs, similarities to electric traction were logical, but not necessarily the details. There are particular problems peculiar to each. No attempt will be made here to compare locomotive wheel slip with draw-works line pull, or locomotive motor connection with mud-pump liner-size changes.

Proceeding to series-motor advantages, Mr. Webb cites the inherent no-load speed limit of separately excited motors; if this is true, why are field-failure relays provided? Either series or separately excited motors require a protective relay.

It is true that all motors can be standardized.

Simplified wiring does mean wiring to separately excited fields, and also the power supply for them. Only one or two loads on the rig require reversing, and to accomplish this only one additional cable between the load and control is required when the series motor is used. The superexcitation capacity amounts to only a small fraction of the normal motor excitation of the separately excited motors. It puts out nothing except when the pump back braking is being utilized, and there is no additional rig wiring to accomodate it.

The controls are centralized regardless of motor type, and the torque limit is provided by either basic generator characteristics control, or by control requested by the user. The accuracy of these limits is not subject to several variables, such as field temperatures and field supply voltages.

Mr. Webb's comment on shunt-motor advantages tends toward the negative by repeating previously stated problems in applying the series motors, and overemphasizing the assumed desirability of shunt-motor characteristics. The need for braking is not required and perhaps not desired for all loads. There are also many conditions where, to get the desired speed on a given load, either motor-field control or engine speeds much higher than power requirements justify (or both) are necessary and result in control complexity or excessive fuel consumption, or both. The fact is that the requirements can be, and are, satisfied by both types of motors.

With reference to the comment on disadvantage of separately excited motors, we find that appropriate machine response to conditions can, as stated, be achieved, but the degree of meeting all desired conditions is too involved to consider here.

Reference is made to thousands of industrial applications of shunt-excited machines; these thousands of shunt-wound motor applications can be reduced to a fraction of that number if only separately excited motors are considered. Excluding the special one-of-a-kind elaborate reversing drives and very accurate speed-regulated motors reduces the number still more. In addition to that, either separate or shunt excited are almost universally protected with field-failure relays; relays which are the equivalent of speed-limit relays employed where series motors are used. It should also be pointed out that in the case of separately excited machines total excitation failure is not the only hazard; the motor behaves as predicted only when the field current is as assumed for the calculation. There are severel prominent influences such as field temperature which affect the value of field current. Troubles in the field circuit of one motor can affect all others on the system unless the complication of protection control is applied, or a separate excitation supply provided for each motor. As a final comment on details of this nature it should be emphasized that there are probably many times as many points as brought up here that have been considered by those who have satisfactory performance in their assigned responsibility.

Finally, Mr. Webb mentions controls; control is equally essential regardless of motor choice, and detail for detail, there is not a great deal of difference in the number of items. Reference is made to a single exciter with stand-by being all that is required for a rig; surely there must be some wiring to apply the power from it to motor and generator fields, some control to permit transferring from one exciter to the other, some kind of protection to prevent a failure in one circuit from affecting all the others. Some "complications" are admitted such as remotely controlled rheostats. As a suggestion, there are severe limitations as to how remote the rheostats can be for a practical mechanical connection. There certainly are reasons why the world's largest and most successful supplier of rheostat-controlled 3-field generators did not choose that system for this application, and there is no time to treat them in detail here.

**E. E. Hogwood** (Westinghouse Electric Corporation, East Pittsburgh, Pa.): Mr. Hefner is to be congratulated on his timely paper describing General Motors' equipment for drilling rigs. Integrally designed diesel-electric drilling equipment have been available in past years from one of the major supply companies. These equipments utilized standard-oil-field diesel engines and industrial-type electric equipment. In most cases, the control was designed to meet the specific requirement of the drilling customer.

The advantages of the d-c variable-voltage oil-well-drilling transmission have long been recognized; however, their general usage has been limited due to the initial investment required when industrial apparatus tailored to the customer's requirements is used. The introduction of mass-produced transportation-type equipment with its lighter weight and reduced space requirements has made it possible to lower the first cost of a diesel-electric rig to be more competitive with mechanical drilling rigs.

With reference to load requirements, the author's analysis of the load requirements of a drilling rig are quite correct, although it should be recognized that the torque-versus-speed requirements of a locomotive are not exactly parallel to those of a drilling rig. First, the locomotive is basically used for accelerating a load and maintaining a particular speed for reasonably long periods of time. On the drilling rig, the load must also be accelerated and brought up to a speed, but the speed is not maintained for any appreciable length of time. Also, the draw works effectively contain a set of gears whereby the required constant-horsepower curve is better accomplished; therefore, it is not necessary for the motor to cover the entire speed-torque range. The greatest difference between the locomotive and the drilling rig is at light loads, such as "fishing" and "making up."

It is important to have relatively good speed control and the ability to accurately position a light load when performing these operations. For this reason we do not agree with the author that the series-wound motor adequately fits the draw-works and rotary-table applications.

With reference to motor characteristics, the separately excited shunt motor has been successfully applied on quite a number of diesel-electric drilling rigs, mine hoists, and cranes where an adjustable variable-voltage system is employed. The separately excited motor operating from a variable-voltage generator will regulate itself to the load in a manner similar to the series motor, although over not as wide a speed-torque range. The author has indicated that the shunt motor is inherently unable to regulate itself to the load but this is true only if the motor is operating from a constant potential bus. When a separately excited motor operates from a variable-voltage generator, i.e., one whose voltage output droops markedly with increased load, the motor will regulate itself quite well to the load. Its speed-torque curve approximates the desired constant-horsepower curve in the full-load region, and has the additional advantages of no-load speed limit and stalled torque limit without any external control devices. The sacrifice in speed-torque range is considered desirable to gain the advantages of limited no-load speed, limited torque, and inherent braking characteristics.

With regard to generator characteristics, a more direct way of obtaining the desired volt-ampere generator characteristic is to use a differential-series field in either the main generator or its exciter. The differential-field strength is proportional to the main-armature current. This method ensures an inherent drooping characteristic and consequent current and torque limit without the use of external regulators and other control devices. We have chosen the foregoing method of obtaining our drooping characteristics because we consider the inherent means more reliable and less complicated.

With reference to overspeed protection, a considerable number of separately excited d-c motors are presently operating on diesel-electric drilling rigs without loss of field protection. To our knowledge, there has not been one report of a motor running away. The heavy loads on the main drives prevent the motor from running away; therefore, loss of field protection is not generally required because simultaneous loss of field and load are quite remote.

In general, the case for the separately excited motor has been presented in this discussion; however, the characteristics of the series-connected motor are considered adequate for the mud-pump drives and other auxiliaries where speed control is not of too much importance. The foregoing comments pertain to the application of series- or separately excited shunt motors on the draw-works and rotary-table drives where reversing and good speed control are usually required. Mud pumps do not require this type of control.

**B. H. Hefner:** The author appreciates sincerely the interest evidenced in this paper and wishes to thank the discussers for their excellent comments. The discussions by Mr. Webb, Mr. Johnson, and Mr. Hogwood provide an opportunity to examine the various systems objectively and in detail.

We recognize the fact that in the design of electric machines there are several routes that can be followed to achieve an end result. Each system of rotating electric machines and associated control equipment can be justified on the premise that it accomplishes its design goal.

Admittedly, there are definite advantages and disadvantages to every power system. I shall not take issue with designs that differ from ours. Our choice of design was dictated by studies of a number of power systems used in a wide range of applications, under all conditions of field drilling.

In the interest of providing a constantly better product, engineers are striving continuously to develop and to improve the design of both machines and controls to obtain ever higher levels of performance and reliability.

# Germanium Rectifier Equipment for Electrolytic Processes

L. G. MILLER
NONMEMBER AIEE

W. R. HODGSON
ASSOCIATE MEMBER AIEE

DIRECT-CURRENT power is being utilized along with alternating current in many industrial systems. Equipment employing sources of d-c power for electroplating, anodizing, electrochemical, adjustable speed drives, and other industrial applications are being used in increasing quantities. It is not convenient generally to power a combined a-c and d-c power system from two separate sources. Available power must either be rectified or inverted so that all electrical needs for a plant can be handled from the same source. The normal direction of change is from a-c to d-c, and it therefore seems reasonable that rectifiers will have considerable importance in the field of design and application for industrial systems.

There is always a demand to improve or develop electric equipment. Usually many years of tests, development, and field trials follow before a new development matures. Such is the case of germanium semiconductor rectifiers which are now coming into their own. The need for a low and medium voltage rectifying device spurred industry into a rapid development program to fill this gap. This energetic development of the germanium power rectifier has reached a point where its application is no longer restricted to the electronics and communications industry. Now the germanium power rectifier takes its place beside the other rectifying devices and promises to replace them in many applications.

Direct-current loads at almost any voltage and current can be supplied with germanium rectifier series-parallel combinations. The ultimate voltage and current size is generally a matter of economics. This paper will discuss germanium diodes, their construction, operation, and protection along with typical applications for germanium semiconductor rectifiers.

Paper 57-1178, recommended by the AIEE Industrial Power Rectifiers and Semiconductor Metallic Rectifiers Committees and approved by the AIEE Technical Operations Department for presentation at the AIEE Conference on Rectifiers in Industry, Chicago, Ill., June 4–5, 1957. Manuscript made available for printing September 20, 1957.

L. G. Miller and W. R. Hodgson are with Westinghouse Electric Corporation, East Pittsburgh, Pa.

## Description of the Semiconductor Diode Element

In order to compare this rectifier with other types, we should first become familiar with its physical construction. Fig. 1 shows a typical finished germanium diode. The heart of the semiconductor rectifier is a sandwich of five layers of material fused together. The central layer, the germanium itself, is a slice of single crystal *n*-type germanium. This single crystal is grown from a melt of ultrapure germanium to which small amounts of *n*-type impurities have been added. The top and bottom layers are the collectors which have approximately the same coefficient of thermal expansion as germanium, and have good heat and electrical conductivity. During the assembly process, germanium is soldered to the bottom collector layer with pure tin and to the top collector layer with pure indium. The bottom collector-tin layer is ohmic, but the indium on the top surface of the germanium forms a *p-n* junction by alloying into the germanium and changing its conductivity from *n* to *p* type in the upper region.

To form a workable rectifier device, the diode sandwich must have additional work performed on it. The diode assembly is soldered to the water-cooled copper base and a flexible lead is soldered to the top molybdenum layer. A glass-Kovar seal is then assembled around the diode and welded vacuum tight. The semiconductor rectifier is then tested for vacuum tightness with a helium leak detector. After degassing the internal parts, a dry gas is sealed in the semiconductor rectifier at atmospheric pressure. This hermetically sealed assembly assures that the diode surface will not be subjected to moisture and other impurities which may cause cell failures. The assembly must also be designed so that the crystal is not subjected to damaging mechanical forces, either from thermal expansion or outside forces such as shipping and handling.

A *p-n* junction has rectifying properties; these properties are illustrated in a simplified form in Fig. 2. If the *p* region is made positive with respect to the *n* region, holes from the *p* region and electrons from the *n* region are driven toward each other. The holes and electrons recombine, each electron filling one hole. This is the easy direction of current flow. If the polarity is reversed, the holes in the *p* region are attracted toward the negative polarity and the electrons in the *n* region are attracted toward the positive polarity, leaving what is essentially an insulator in the junction region and blocking the flow of current. Thus, this *p-n* junction allows current to pass unimpeded in one direction and offers a very high impedance to current flow in the opposite direction. Therefore the germanium rectifier described previously functions as a rectifier. Fig. 3 is a cutaway view showing the method of assembling a typical diode into a unit to provide cooling, hermetic sealing, and mechanical protection. Fig. 4 shows the completed assembly.

## Method of Rectifier Protection

The germanium diode having such a small mass must have proper protection. With proper protection the unit can be relied upon for continuous unattended reliable operation. This protection may conveniently be divided into several features as follows:

1. Overload
2. Surge voltage
3. Junction failure
4. Cooling water failure

The semiconductor rectifier diode has a very short thermal time constant compared to that of transformers, reactors, buswork, and other pieces of equipment with relatively large masses. For this reason, it cannot be protected against overloads by ordinary thermal inverse time devices. In general then, overload protection will be provided for by means of overcurrent relays on each parallel rectifier together with standard devices to protect the transformer and other associated equipment.

A diode failure occurs whenever the cell loses its ability to block inverse voltage. This places a short circuit on the transformer windings. In single-way circuits it also places a short circuit across the d-c bus. This short circuit will cause fault current to flow in the good diodes. A fast acting current-limiting fuse in series with the faulted diode will interrupt this fault current before it has built up to destructive values in the good units. A fuse-monitoring system provides an indication when a fuse has blown. Each fuse has an indicator on the outside to determine

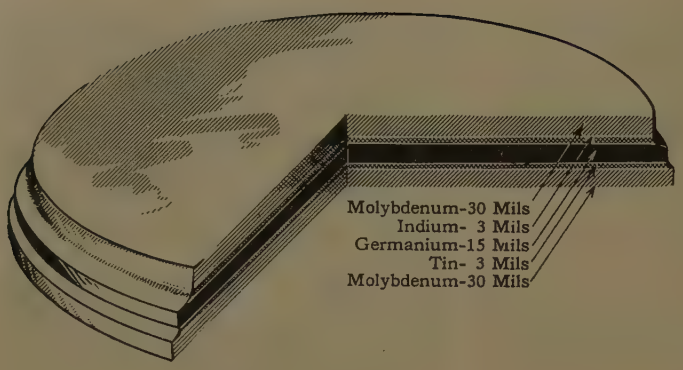


**Fig. 1 (left). Cutaway diagram of a germanium rectifier cell**

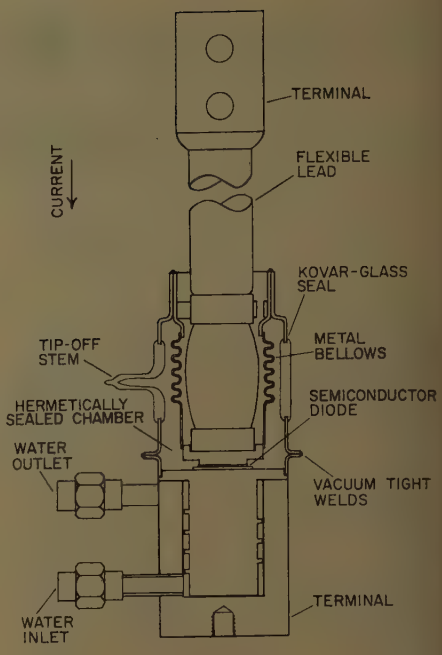


**Fig. 3 (right). Water-cooled semitron rectifier cutaway view**

which fuse has blown. Other means of removing the faults can be used depending on the number of units in parallel and the type of service.

The most common method of cooling is by liquid cooling which quickly removes heat. Thus the diodes are assured of the best thermal conditions for maximum life, and are independent of daily fluctuations of ambient air. Since the diodes are water cooled, means must be provided to protect against water supply failure. Consequently, if the water supply should fail, the rectifiers are shut down and an alarm is given.

## Methods of Output Control

The semiconductor diode is a free conducting device. That is, it will start conducting whenever the *p*-type material is made positive with respect to the *n*-type material. For this reason, control of the output voltage must be obtained through varying the input voltage or by changing the regulation of the rectifier by means of a variable reactance. The most common method of varying the input voltage is with induction regulators or step regulators with no-load or load taps or both. The most common means of varying the reactance is by means of saturable core reactors. The choice of the foregoing types of voltage control depends upon the application requirements and the economics of the types available.

The induction regulator provides a continuous variation of the input voltage and maintains the inherent high power factor and low output voltage ripple of the rectifier even at reduced output. The size of the regulator is dependent on the range of control desired. It would be most suitable for applications requiring a steady output with small a-c line variations.

The step regulator can vary the input voltage either by load or no load taps or a combination of both. Although the output is not continuously variable over the range, it can be made so with steps of sufficient fineness for some applications. It can also take the form of manual tap switching of taps on the rectifier transformer. The step regulator also maintains a high power factor and low ripple at reduced output.

The saturable reactor is the other chief means of varying the rectifier output. This type of control functions by varying the reactance and, hence, the regulation of the rectifier. Full range, stepless control is obtained by varying the d-c bias current in the saturable reactors. This control is obtained with very little power and it is fast, lending itself readily to applications requiring automatic voltage or current regulators.

The saturable reactor provides a different output characteristic than the induction or step regulator. From about 0 to 90% output voltage, the output current is approximately constant for a given bias and is proportional to the bias. Above 90% voltage the regulation curves are similar to those with no saturable reactor. The no-load voltage varies very little with bias. Variations of supply voltage affect the no-load voltage but do not change the characteristics below about 90% of normal voltage. This means that below 90% of normal d-c voltage, the output current will not vary appreciably with load resistance changes or with input voltage variations for a fixed bias current. This constant-current output characteristic provides a cur-

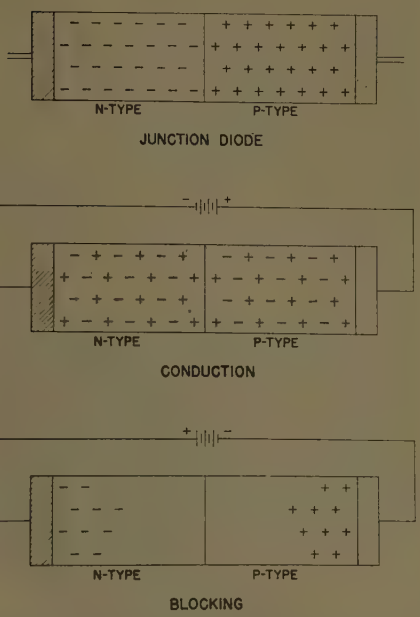


**Fig. 2. Semiconductor diode rectifier p-n regions**

**Fig. 4. Water-cooled semitron rectifier element**

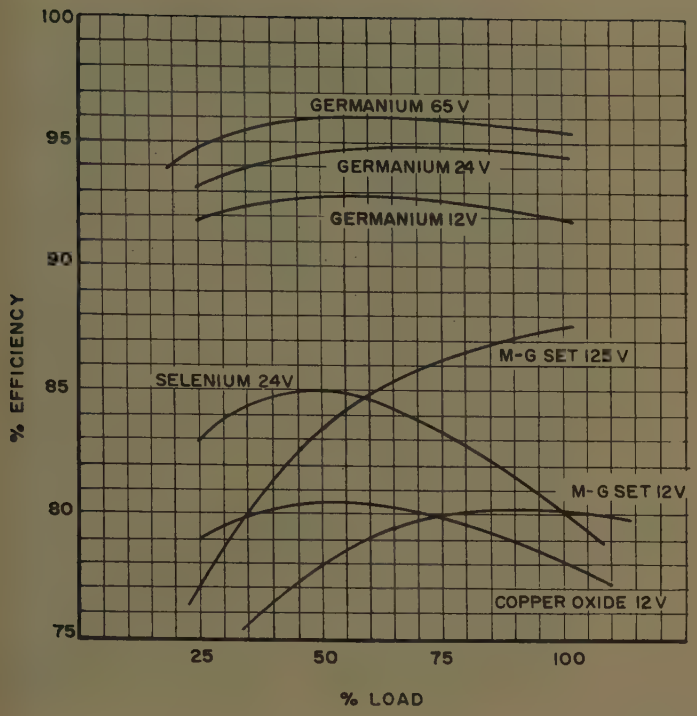


Fig. 5. Comparative efficiencies for several types of 4,000-ampere low-voltage conversion equipment

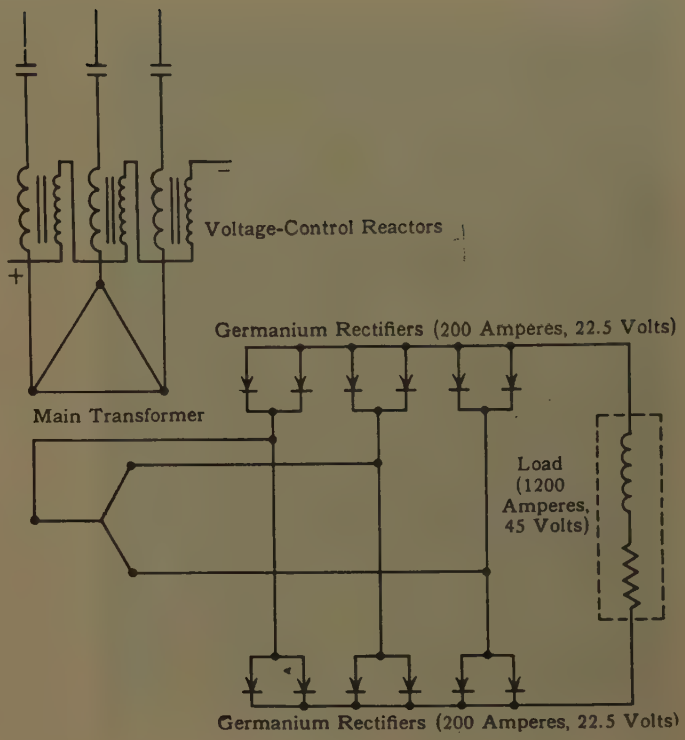


Fig. 7. A typical circuit for 6-phase double-way germanium rectifier

rent-limiting feature as well as a current-regulating characteristic. Since for a given output voltage the output current is very nearly proportional to the bias, a very simple voltage-compensation feature can be obtained by making the bias current proportional to the load current. This steep rise in voltage for very slight reductions of current provides arc stabilization for arc-casting furnaces.

A typical application of germanium semiconductor power supplies, with saturable core-reactor-type control is for continuous strip plating. The strip is continuously fed through several plating tanks with a rectifier for each plating tank. The total thickness of plating is directly proportional to the sum of all the rectifier plating currents and inversely proportional to the speed of the strip through the plating baths. Each rectifier has its own saturable core reactor. The d-c bias windings of all the rectifiers are connected in parallel to a regulated d-c bus. This regulated bus controls the total output of all the rectifiers in direct proportion to the line speed to maintain a uniform plating thickness with strip speed variations. The thickness of the plate can be varied by changing the regulating setting. The saturable core-reactor-type of control lends itself very well to this type of regulator application.

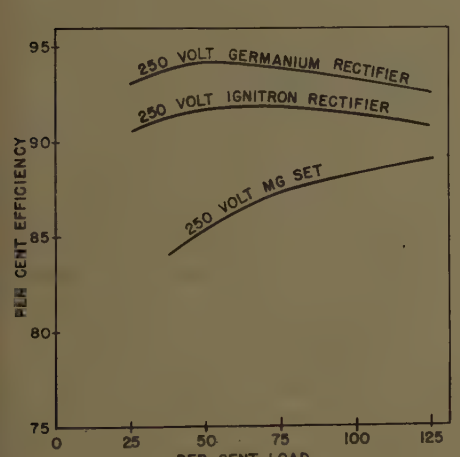


Fig. 6. Comparative efficiencies for germanium rectifier, Ignitron rectifier, and mg sets at 250 volts

## Comparison of Germanium Rectifiers with Other Types of Existing Rectifiers

The germanium semiconductor rectifiers when compared to other metallic rectifiers or to Ignitron rectifiers have certain inherent advantages. One of the most prominent advantages of germanium is its efficiency advantages. Reference is made to Fig. 5 showing the relative efficiencies of germanium along with copper oxide, selenium, and motor-generator (mg) sets. The curve depicts very clearly the large efficiency advantage over the other conversion methods in this low-voltage class.

Fig. 6 is an efficiency comparison of a 250-volt semiconductor rectifier with a comparably rated Ignitron rectifier and mg set. A large efficiency advantage in favor of the germanium is evident. The high arc drop of the Ignitron rectifier compared to the low forward drop of the germanium rectifier, even with the required number of diodes in series, provides the efficiency difference.

These large efficiency advantages provide a real savings in dollars to the ultimate user particularly where large blocks of power are to be utilized. The cells can be operated at very high current densities due to the low losses within the cell. It is these low losses that are responsible for the germanium rectifiers high efficiency. This saves dollars in copper, cooling equipment, and power costs; this also provides additional savings in size and weight of a germanium rectifier. These rectifiers do not have a forward aging characteristic as do selenium or copper oxide. It is therefore not necessary to adjust transformer taps over a period of time to compensate for changing characteristics. Thus there will be no reduction in initial efficiency as elapsed operating time increases.

A considerable savings in space, installation cost, and original building cost can be experienced with germanium semiconductor rectifiers. The high current density that germanium can be worked at in normal operation when compared to other metallic rectifiers provides real space saving. This is due to the fact that germanium can be worked at

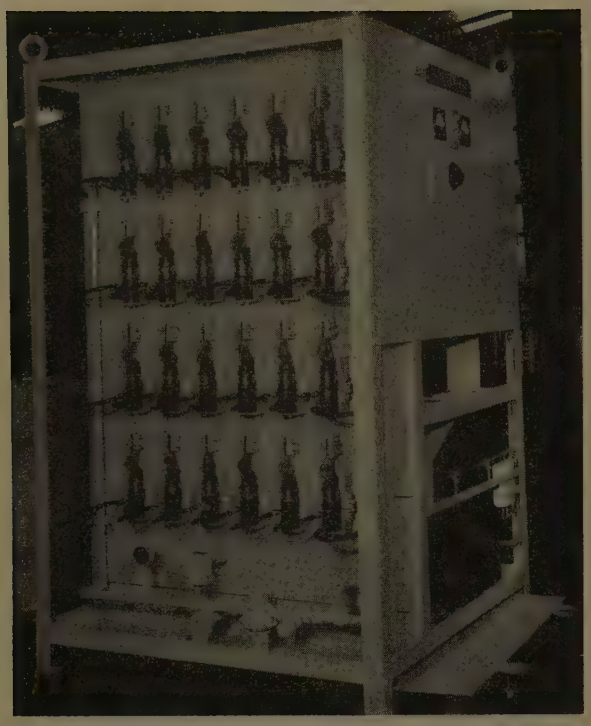

Fig. 8 (left). A complete 4,000-ampere 12-volt assembled unit shows accessibility of individual diodes

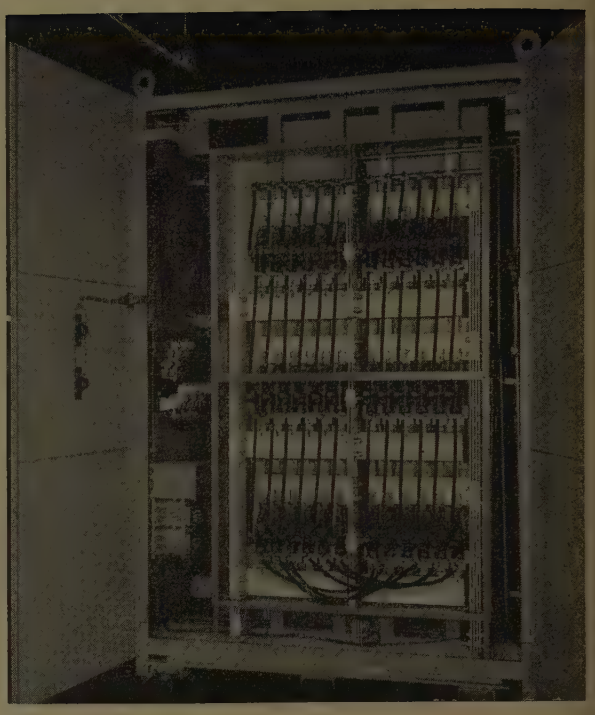

Fig. 10 (right). A complete 3,000 - ampere 40 - working - volt 80-volt open-circuit germanium semi-tron vacuum arc-melting furnace power supply

approximately 1,000 times the current density of selenium for the same forward drop, and approximately 300 times the current density of copper oxide for the same forward drop.

The germanium rectifier being a static device with no rotating parts means a savings in maintenance. All the component parts are designed and manufactured for many years of operation. No auxiliary circuits are required with semiconductor rectifiers as on mercury arc rectifiers with the resulting space and maintenance savings. Corrosion problems are minimized on the equipment and eliminated on the diodes due to their hermetically sealed construction.

Low installation costs are inherent with these devices since no special foundations are required. They can be quickly installed as it is generally a matter of making a-c and d-c connections along with the necessary water connections. Individual units can be arranged for close coupling when series or parallel connections are required.

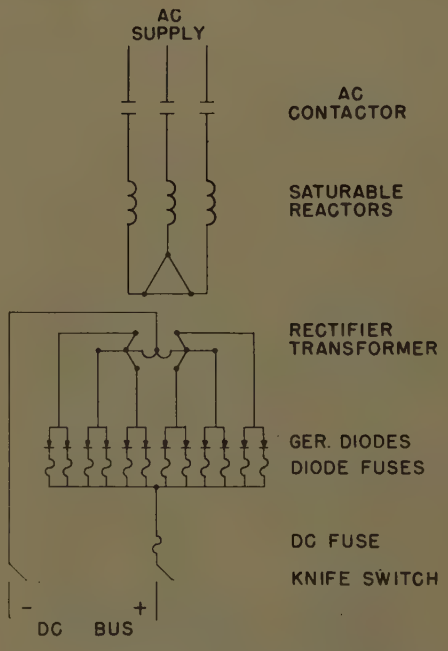


Fig. 9. A typical circuit for 6-phase single-way germanium rectifier

## Industrial Application

The field of germanium rectifier applications is broad, and it encompasses low-voltage plating and anodizing supplies up to higher voltage electrochemical and industrial applications. A few typical installations will be discussed in this paper.

Recently a large copper company installed additional refining capacity and the decision was made to purchase germanium rectifiers after thorough investigation of all types that are available in this voltage class. The equipment is utilized in electrolytic refining of copper. The load is constant at 16,000 amperes with a potentiality of 135 volts direct current. At present the equipment is capable of 16,000-ampere output at 90 volts direct current.

A group of four 4,000-ampere packages were installed along with their switching and transforming equipment. Each 4,000-ampere unit is composed of a 6-phase full-wave double-way bridge circuit with two such circuits connected in series for 90 volts direct current. This circuit connection is shown in Fig. 7. A throat-connected Inerteen-insulated self-cooled rectifier transformer provides the proper element voltage. In the same tank as the rectifier transformer is a saturable core reactor to provide current and voltage control of the units. The primary switching of the rectifier units is by means of 2,400-volt oil-immersed contactors.

The units are controlled from a central control panel which includes all metering and control switches conveniently located in one position. The station operates unattended except for periodic meter reading trips by the cell room personnel. The germanium cells themselves are arranged in a delta 6-phase double-way full-wave rectifier circuit as shown in Fig. 7. The required number of paralleled elements are utilized on each leg of the bridge circuit. The cells are direct water cooled. The cooling system and bus bar are so arranged that all paralleled diodes are operating at relatively the same junction temperature. This assures that parallel division of load is not upset due to varying junction temperatures.

Each diode has a high speed "Amp-Trap" fuse, which in case of failure of an element protects the remaining elements by opening the circuit of the faulted element. The primary switching of the rectifier transformers is by means of motor starter-type high-voltage oil-immersed contactors. These contactors are

bussed together to form a co-ordinated line-up with the a-c switchgear and d-c control compartment. Overload protection of the individual rectifier units is by means of high-speed relaying from the d-c side of the unit. Transformer fault protection is provided in the primary contactors by means of disconnecting-type fuses similar to those on motor-feeder circuits. An incoming line auxiliary compartment together with the station auxiliary transformer and the a-c incoming line breaker make up the remaining complement of a-c metal-clad equipment. Close coupled to the a-c switching equipment is located a d-c control and metering cubicle. All individual unit contactor switches, d-c ammeters, and individual and master manual current-control switches are conveniently located for the operator.

The rectifier transformer and saturable core reactor are in the same tank and are Inerteen-insulated, self-cooled, and throat-connected to the germanium rectifier. The transformer is connected delta on the primary and triple delta on the secondary. Each secondary delta is capable of furnishing 4,000 amperes at 45 volts direct current. The windings are so arranged that the rectifiers may be connected in series for 45, 90, or 135 volts direct current.

Included in the same tank is a saturable core reactor to provide manual current control for each transformer–rectifier combination. An additional feature of this saturable core reactor is the current limiting action of the reactor under short-circuit conditions. This reactor also to a certain degree limits inrush currents on the unit.

The foregoing application depicts a large installation where transformers, metering equipment, and switching equipment are not an integral part of the rectifier cubicles. For some applications such as tin-plating, arc-furnace supplies, anodizing, cathodic treatment, and cleaning applications the power level is such that a completely self-contained unit can be supplied.

Fig. 8 shows such a unit rated 4,000 amperes, 12 volts, direct current which would fit any of the above applications. This unit contains the germanium diodes connected in a single-way circuit as shown in Fig. 9. The unit contains a combination linestarter–AB breaker for primary protection and switching. A saturable core reactor is utilized for manual voltage control and a dry-type rectifier transformer, and germanium water-cooled diodes complete the assembly along with the necessary metering. This unit can easily be adapted to automatic current control as required on large tin plate lines and operated in parallel with many other like units.

A rather unique application is that of the unit shown in Fig. 10. This is a self-contained unit that is used for a vacuum arc-melting furnace. It is unique in that it has a high open-circuit voltage to strike the arc and a low operating voltage to maintain the arc. Operation of this unit at short-circuit conditions is not uncommon. The unit is rated 3,000 amperes at 40 working volts and 80 volts open circuit. Manual control is provided to preset the operating point and the furnace control then takes over to maintain the correct arc voltage and current. Recently four of these units have gone into service.

A conservative working level in peak inverse voltage of germanium is approximately 90 volts, therefore, a limitation on d-c voltages exists from a single element. As applications of higher d-c voltages are required, elements are placed in series. A typical example is a 300-kw 250-volt d-c industrial unit for crane power supply. A double way circuit similar to that shown in Fig. 7 is utilized except series elements are utilized to obtain the maximum d-c voltage required for this application. This unit station layout is similar to an Ignitron unit substation, that is, a metal-clad line-up consisting of an a-c breaker cubicle, a transformer cubicle, a germanium rectifier cubicle, and a control and d-c breaker cubicle.

A Magamp voltage regulator on this unit provides essentially flat voltage from no load to full load and allows compensating circuits to be used for proper division of load during parallel operation. This unit can be applied in existing substations where Ignitrons and mg sets already exist. The large efficiency advantage of the germanium rectifier at this voltage is shown in Fig. 6. Along with this efficiency advantage, low installation costs and relatively little maintenance make the semiconductor rectifier attractive in this field.

The afore-mentioned applications represent low-voltage units with a single diode in a single-way circuit or a series of diodes for higher voltages. For voltages in the 150-volt range, a different scheme is utilized. Here it would be necessary to put two diodes in series which means that if one diode fails, the peak inverse voltage applied to the second diode in series is doubled. The possibility of this diode failing is high. Therefore, in this voltage range, multiple-winding transformers are utilized and the rectifier units connected in series for the higher voltage. Two of the circuits shown in Fig. 7 are connected in series. The transformer therefore determines the peak inverse voltage that a diode will be subject to and failure of a single diode does not stress other diodes in the circuit.

A typical application in this category is the refining of cobalt which requires 150 volts direct current and amperes in the range of 8,000. At this power level, and due to the number of diodes in a unit, the transformer and regulating equipment would generally be separately mounted. A typical application consists of two 4,000-ampere packages consisting of an outdoor transformer, a rectifier cubicle, necessary a-c and d-c switching, and a control cubicle.

In addition to applications described in the foregoing, future applications in the 300-volt electrochemical field appear good; applications for hydrogen gas production, anodizing, and low voltage electroplating are also prominent.

## Conclusions

Although a relatively new device, the germanium rectifier has already become well established. The device itself is designed to obtain long life, low maintenance, high efficiency, and good service reliability. It is demonstrating its performance in electroplating, anodizing, electrolytic processes, and other related applications. Operating experience to date with germanium rectifiers has been good. The future appears bright for the germanium rectifier, evidenced by the activity along this line now taking place in industry.

## Reference

1. Power Rectification via Germanium and Silicon, J. L. Boyer. *Westinghouse Engineer*, Pittsburgh, Pa., Sept. 1954, pp. 183–86.

# A High-Current-Density Selenium Rectifier

C. C. GEIB
NONMEMBER AIEE

W. E. BROWN
NONMEMBER AIEE

THE semiconductor properties of selenium were discovered by Fritts in 1883. However, it was not until the period between 1939 and 1950 that the selenium rectifier came into its own in the United States as a means for converting relatively large amounts of power from alternating to direct current.

Up to the present, the development of the selenium rectifier has been characterized by a steady increase in the reverse voltage rating. The earliest voltage rating per cell was in the neighborhood of 12 volts, as compared to the most recent rating of about 45 volts. While the voltage rating was being increased, the current rating remained at approximately 160 milliamperes per square inch of rectifying area. Failure to increase the current rating may be explained by the fact that the current density of the selenium rectifier had a direct bearing upon the aging of the rectifier. Aging is defined here as an increase in the forward resistance of the rectifier and the resultant decrease in the output voltage.

The conventional selenium rectifier, when operated at the accepted current density of 160 milliamperes per square inch of rectifying area will, in general, reach a somewhat decreased but fairly stable output level within 20,000 hours of continuous service. After this initial decrease, there is an extended period of operation during which there is relatively little change in output. Rectifiers operating at less than normal current loads or on intermittent duty applications show a longer aging time. In view of this it has been assumed that an ampere-hour law governs the initial rate of rectifier aging. Conventional rectifiers, operating at current loads in excess of the accepted standard normal, follow this law to a great extent. However, a current density point is reached above which rather rapid and continuous aging takes place, even though the rectifier is maintained at a reasonable temperature through forced cooling.

The authors have been instrumental in recent developments in selenium rectifiers which have resulted in the production of a cell having a current-carrying capacity of 265 milliamperes per square inch of rectifying area with ordinary convection cooling. This cell is unlike the conventional selenium cell in many respects; actually, it behaves more like the high-temperature selenium rectifier. It was partially evolved from development work which was aimed at the improvement of the high-current-density cell is 105 C (degrees centigrade). This similarity to the high-temperature cell accounts for the fact that in this new type of cell current density has far less effect upon aging. Consequently, with adequate forced cooling, it can accommodate continuous current loads of 1.18 amperes per square inch The voltage rating of these rectifiers is 15 volts rms per cell.

The data shown in the figures were compiled from tests conducted with rectifiers of the type shown in Fig. 1, the cells in this type of rectifier are $4^1/_8$ inches square, and they have an effective rectifying area of 14.2 square inches.

Fig. 2 shows typical aging characteristics of the high-current-density rectifier operating at a current density of 850 milliamperes per square inch. In addition to showing the aging characteristics, this curve also substantiates the ampere-hour law governing the initial rate of rectifier aging, for in this case the rate of aging decreases markedly after about 3,500 hours.

Figs. 3 and 4 illustrate the static characteristics of the high-current-density rectifier at ambient temperatures of 25 and 105 C. The nonlinear characteristics of the forward voltage drop curve give an indication of the regulation of the rectifier when it is operated at different loads.

Fig. 5 shows a curve of nominal output voltage versus current for a 3-phase bridge rectifier made with six cells operating into a resistance load. The alternating voltage was held constant at 15 volts during the test. As was to be expected, the maximum change in output voltage fell within the region of the lighter loads. The absence of a greater flexure of the curve, especially at lighter loads, can be accounted for by the following: As the current load is decreased, a reduction in rectifier cell temperature occurs. The forward voltage of the rectifier cells increases slightly as the cells become cooler. The higher forward voltage causes a decrease in output voltage. The lower output voltage tends to neutralize the sharper rise in output which normally accompanies lighter current loads.

With ordinary convection cooling, the high-current-density cell has a current-carrying capacity of 265 milliamperes per square inch of rectifying area. This rating is fixed for rectifier stacks constructed with the cells normally spaced. For rectifier stacks constructed with one to four cells, or those having wide spaced cells, the convection-cooled rating is 345 milliamperes per square inch of rectifying area. Normal spacing, as applied here, varies with the size of the cell. In the case of cells of $1^3/_4$ inches in diameter, normal spacing is approximately 0.156 inch, center to center. Normal spacing for the 5- by 6-inch cells is about 0.312 inch. Wide spacing is approximately 1.6 times normal spacing. Table I lists some of the rectifier cell sizes available and their ratings with convection cooling.

To obtain the maximum output of 1.18 amperes per square inch from the high-current-density rectifier, adequate cooling must be maintained. Adequate cooling in this case refers to any method which will maintain a cell temperature below 105 C. The most common and effective method used to obtain the desired results is to employ a forced air draft. It has been found, during tests, that in order to obtain the maximum cooling effect with a minimum forced draft, a number of good practices should be observed. First, to avoid confusion, all measurements of air flow are made on the leeward side of the rectifier. Several measurements are made between the cells so that an average air flow through the rectifier can be determined. Air flow should be parallel to the plane of the rectifier cells. Conditions causing air turbulence such as obstructions which might impede the flow of air are to be avoided. Finally, wherever practical, the rectifier should be mounted, with relation to the air flow so that the air passes through the smallest dimension of the rectifier. For example, optimum cooling would be obtained in a rectifier constructed of cells which are 5 inches wide and 6 inches long if the air is made to enter and leave a path just 5 inches long instead of 6 inches long.

Paper 57-1174, recommended by the AIEE Industrial Power Rectifiers and Semiconductor Metallic Rectifiers Committees and approved by the AIEE Technical Operations Department for presentation at the AIEE Conference on Rectifiers in Industry, Chicago, Ill., June 4–5, 1957. Made available for printing September 20, 1957.

C. C. GEIB and W. E. BROWN are with the Fansteel Metallurgical Company, North Chicago, Ill.

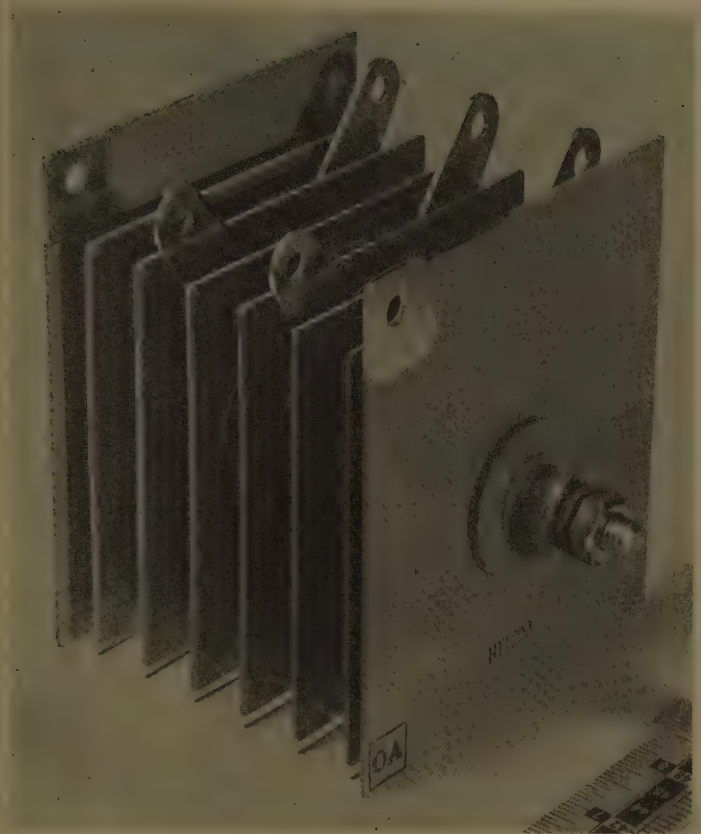

Fig. 1. Three-phase bridge rectifier made of $4^1/_8$-inch square cells: current rating 50 amperes

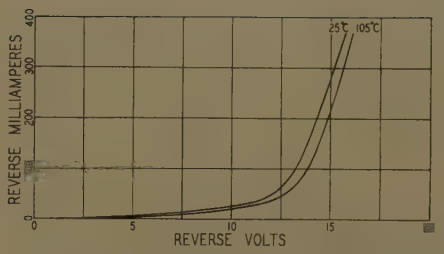


Fig. 4. Static characteristics, reverse direction

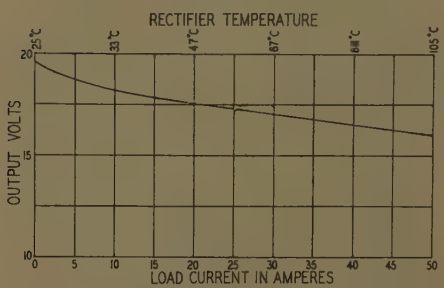


Fig. 5. Regulation curve: 3-phase bridge rectifier

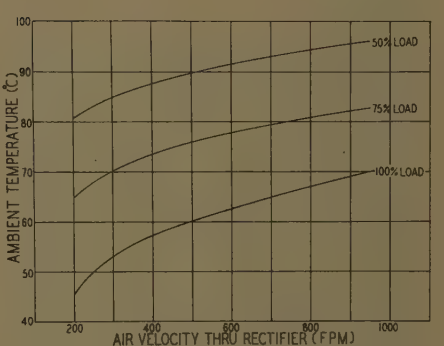


Fig. 6. Forced cooling curves: current loads based on density of 1.18 amperes per square inch

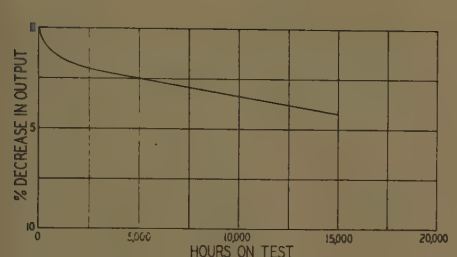


Fig. 2. Typical aging characteristics with current density of 850 milliamperes per square inch

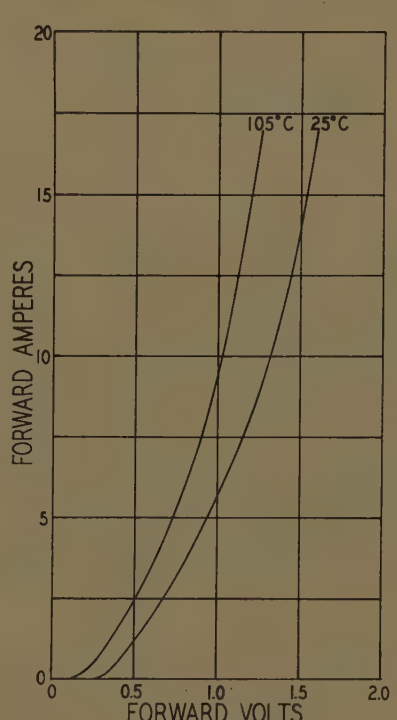


Fig. 3 (below). Static characteristics, forward direction

In the design of a rectifier stack for applications requiring forced cooling, a maximum cell spacing of about 0.6 inch is employed, provided that such spacing is consistent with other aspects of the design such as physical dimensions, circuit connections, and type of load. The rectifier terminals, which have a considerable effect on cooling since they are a cause for air turbulence, are made of a material as thin as is practical for a particular design.

Fig. 6 shows the air velocity required, at various ambient temperatures, to maintain the temperatures of the rectifier cells under 105 C. The per-cent load on this graph is based on a current density of 1.18 amperes per square inch.

Fig. 1 illustrates a typical high-current-density rectifier. This particular stack is referrred to as an automotive rectifier and, as its name implies, is one of several stacks designed especially for a-c to d-c conversion in automotive electric systems. This is a 3-phase bridge rectifier which has a current rating of 50 amperes d-c with forced cooling. The maximum a-c input rating is 15 volts rms.

The automotive application presents a particularly rigorous test of both the physical and the electrical capabilities of a rectifier. The environmental conditions which the rectifier must be able to withstand include rather severe vibration, in addition to corrosive atmospheres. Some of the materials with which an automotive rectifier might be expected to come in contact, either directly or in vapor form, are gasoline, oil, alcohol, ethylene glycol, road salts, dust- and grit-laden air, and moisture. Obviously, in order to function properly for a satisfactory length of time, the rectifier must be protected from these environmental conditions.

Rectifiers designed to withstand extreme environmental conditions are protected by three coats of an epoxy resin base paint. Improved methods of application and curing of this finish make possible a 50-hour guarantee against a salt fog corrosion test of the type described in the military standard *202.*[1] Rectifiers having the protective finish just described have been able to withstand salt fog testing for periods in excess of 100 hours with no indication of corrosive attack. On occasion, finished rectifiers have been able

**Table I. High-Current-Density Selenium Rectifier Cells, Standard Sizes and Ratings**

Maximum D-C Ampere Continuous Output of Element with One Cell Per Arm at Ambient Temperature 113 Degrees Fahrenheit (45 C) or Less
Maximum A-C Volts Per Cell, 15

| Basic Cell | | Single-Phase | | Three-Phase | | | Maximum Continuous D-C Rating as Valve, 113 | | Maximum No. of Cells Per Stack | Approximate Cell Spacing On Center |
|---|---|---|---|---|---|---|---|---|---|---|
| Size, Inches | Type | Half-Wave | Bridge or Center Tap | Half-Wave | Bridge | Center Tap | Amperes | Blocking Voltage | | |
| 2⅝ D* | *HE* | 1.270 | 2.54 | 3.4 | 3.810 | 4.6 | 1.95 | 12.5 | 1 to 4 | |
| | | 0.980 | 1.95 | 2.6 | 2.940 | 3.6 | 1.45 | 12.5 | 5 to 40 | 0.250 |
| 2⅝ D | *HE* | 1.270 | 2.54 | 3.4 | 3.810 | 4.6 | 1.95 | 12.5 | 1 to 28 | 0.390 |
| 3⅛ D | *HF* | 2.6 | 5.2 | 6.6 | 7.8 | 9.4 | 3.9 | 12.5 | 1 to 4 | |
| | | 1.950 | 3.9 | 5.2 | 5.850 | 7.3 | 2.9 | 12.5 | 5 to 40 | 0.250 |
| 3⅛ D | *HF* | 2.6 | 5.2 | 6.6 | 7.8 | 9.4 | 3.9 | 12.5 | 1 to 28 | 0.390 |
| 4⅛ D | *HG* | 4.2 | 8.4 | 11.5 | 12.6 | 15.8 | 6.5 | 12.5 | 1 to 4 | |
| | | 3.25 | 6.5 | 8.6 | 9.75 | 12.2 | 5.0 | 12.5 | 5 to 40 | 0.250 |
| 4⅛ D | *HG* | 4.2 | 8.4 | 11.5 | 12.6 | 15.8 | 6.5 | 12.5 | 1 to 28 | 0.406 |
| 4⅛ Sq† | *HT* | 4.9 | 9.8 | 13.1 | 14.7 | 18.2 | 6.5 | 12.5 | 1 to 4 | |
| | | 3.75 | 7.5 | 9.9 | 11.2 | 14.0 | 5.0 | 12.5 | 5 to 40 | 0.250 |
| 4⅛ Sq | *HT* | 4.9 | 9.8 | 13.1 | 14.7 | 18.2 | 6.5 | 12.5 | 1 to 28 | 0.406 |
| 4⅛ by 6 | *HP* | 7.3 | 14.6 | 19.5 | 21.9 | 27.7 | 11.8 | 12.5 | 1 to 4 | |
| | | 5.7 | 11.4 | 15.3 | 17.1 | 21.2 | 8.4 | 12.5 | 5 to 40 | 0.312 |
| 4⅛ by 6 | *HP* | 7.3 | 14.6 | 19.5 | 21.9 | 27.7 | 11.8 | 12.5 | 1 to 28 | 0.500 |
| 5 by 5 | *HH* | 7.3 | 14.6 | 19.5 | 21.9 | 27.7 | 11.8 | 12.5 | 1 to 4 | |
| | | 5.7 | 11.4 | 15.3 | 17.1 | 21.2 | 8.4 | 12.5 | 5 to 40 | 0.312 |
| 5 by 5 | *HH* | 7.3 | 14.6 | 19.5 | 21.9 | 27.7 | 11.8 | 12.5 | 1 to 28 | 0.500 |
| 5 by 6 | *HR* | 9.1 | 18.2 | 24.4 | 27.3 | 34.0 | 13.5 | 12.5 | 1 to 4 | |
| | | 7.0 | 14.0 | 18.7 | 21.0 | 26.1 | 10.4 | 12.5 | 5 to 40 | 0.312 |
| 5 by 6 | *HR* | 9.1 | 18.2 | 24.4 | 27.3 | 34.0 | 13.5 | 12.5 | 1 to 28 | 0.500 |

* In diameter.
† Square.

to withstand salt fog testing successfully for periods exceeding 500 hours.

The efficiency of a rectifier stack is usually determined as being the ratio of the product of the average values of the direct current and voltage to the effective value of the input power. The value obtained in this manner is the conversion efficiency, which can vary with the type of circuit and for the type of load. The wattmeter efficiency of the rectifier is the ratio of the d-c power output to the a-c power input, both values being measured by means of wattmeters. This is the true efficiency of the rectifier, since it is dependent upon the effective values of input and output power. In general, the difference between conversion efficiency and wattmeter efficiency will be small in the case of 3-phase circuits and single-phase circuits with capacitance loads. However, in order to change from conversion efficiency to wattmeter efficiency in the case of a single-phase bridge rectifier operating into a resistance load, the product of the average values of the direct current and voltage must be multiplied by the square of the form factor or approximately 1.23.

The high-current-density rectifier, as illustrated in Fig. 1, operating at 50 amperes or 1.18 amperes per square inch, exhibits a wattmeter efficiency in excess of 70%. It is very interesting to note that one of the rectifiers from which data were taken to give the aging curve of Fig. 2 exhibited a wattmeter efficiency of 70% even after 13,000 hours on test and a 3.95% decrease in output voltage. This can be accounted for by the fact that in practically all cases where failure does not actually occur, rectifier aging which increases the forward resistance of the rectifier normally increases the reverse resistance. Thus, the changes in the power losses in the forward and reverse direction tend to offset each other and the efficiency of the rectifier remains substantially the same.

Some applications which are particularly suited to the capabilities of the high-current-density selenium rectifier are a-c to d-c conversion in automotive electrical systems, high-current battery chargers, or "fast chargers," low-voltage–high-curent power supplies, and electrochemical applications such as plating, anodizing and polishing. These are but a few of the many fields of applications open to this type of selenium rectifier which has the ability to carry unusually large amounts of current without the rapid deterioration of the rectifying characteristics.

## Reference

1. Test Methods for Electronic and Electrical Component Parts. Military standard *MIL-202A*, Washington, D.C., Oct. 24, 1956.

# A 10-Kw Germanium Rectifier for Automatic Power Plants

E. A. HAKE
ASSOCIATE MEMBER AIEE

THE AVAILABILITY of high-current semiconductor rectifying devices, high-grain magnetic amplifiers, transistors, and semiconductor diodes prompted this development. The practical objective of this design was to develop a rectifier of 10-kw rating that could compete with a motor-generator set and its controls for use by the Bell System. Higher efficiency and a reduction in over-all size over rectifiers of earlier design were the major inducements.

The design of the saturable reactors was the chief problem, where cost and reproducibility were hurdles to be cleared. Also, protection, maintenance, and versatility of the unit had to be explored, as related to its use in past, present, and proposed automatic power plants. A preliminary investigation was made to determine the feasibility of using square-loop saturable reactors controlled directly by a transistor amplifier with two 2-watt transistors in the output stage. This fundamental approach is described in a previous paper.[1]

## Circuit Description

### General

Fig. 1 is a block diagram of the rectifier which is rated at 50-volts 200-amperes continuous duty and 63-volt 200-amperes intermittent duty operating into a battery and resistance load. The power section of the rectifier consists of a self-saturated magnetic amplifier, with six germanium fan-cooled power rectifiers in a 3-phase full-wave bridge configuration. The control is by means of a transistorized push-pull amplifier using germanium transistors and rectifying diodes; and silicon diodes for blocking and as a voltage reference. Under normal conditions the rectifier operates as a constant voltage device up to rated load current. Slightly beyond rated load, the rectifier is automatically current-limited to prevent overloading.

Paper 57-1175, recommended by the AIEE Industrial Power Rectifiers and Semiconductor Metallic Rectifiers Committees and approved by the AIEE Technical Operations Department for presentation at the AIEE Conference on Rectifiers in Industry, Chicago, Ill., June 4–5, 1957. Manuscript made available for printing September 20, 1957.

E. A. Hake is with Bell Telephone Laboratories Inc., New York, N. Y.

The rectifier was designed to float a storage battery and to maintain its voltage to better than ±1%, and to operate at a constant current of 101–103% of rated output current for any condition of battery discharge down to 1.75 volts per cell. Taps are provided on the main transformer to furnish voltage for charging two or four additional cells which are a part of the reserve power facilities in a central office. Built-in test features are provided to simplify maintenance and adjustment.

### Power Section

The power section, shown in Fig. 2, consists of a 3-phase step-down transformer $T1$ furnishing alternating voltage to a self-saturated magnetic amplifier $L1$, $L2$, and $L3$ equipped with fan-cooled germanium power diodes $CR1$-$CR6$. An inductor, $L4$, $L5$, capacitor, $C1$-$C10$, inductor, $L6$, filter reduces the ripple in the output to the desired level; $L4$ is a swinging inductor. The rectifier output current lead passes through the cores of the d-c transformer, $CT1$, in the current sensing circuit, which provides a signal proportional to the d-c load current. A fuse is in the negative output lead. The switch $S1$ disconnects the rectifier from the battery in position 1, and in positions 2, 3, and 4 selects the correct taps on transformer $T1$ for the number of battery cells in the circuit. Fig. 2 also includes $T2$ the bias current supply for the main reactors, as well as the a-c supply for the current sensing circuit.

### Magnetic Amplifier

The basic circuit shown on Fig. 2 is a 3-phase self-saturated magnetic-amplifier power stage in a full-wave bridge configuration. The saturable-reactor control windings are driven by an amplifier having two 2-watt transistors in the output stage in a push-pull arrangement. The high power gain required indicated the need for cores using square-loop material. However, the selection of saturable-reactors for this application was governed by cost as much as the technical considerations. The saturable-reactor design selected was a compromise of these factors. Three-legged saturable reactors composed of two cores made of square-loop $DU$ laminations having common d-c control windings satisfied the requirements of high gain, reasonable cost, use of form-wound coils, good reproducibility, and simple test procedures.

Although these saturable reactors were better balanced than other reactors investigated, the need for low output ripple and the limited margin of current overload of the germanium power rectifying elements, required additional means of balancing. The most effective method was found to be the introduction of adjustable amounts of negative feedback into each core by means of a rheostat across a separate winding (Fig. 2 winding 5-6, 7-8 on $L1$, $L2$, and $L3$) on each core, on the same leg as the gate winding. Fig. 3 illustrates the variations of rms and average current in each gate winding and power rectifying element with and without the balancing adjustment at full rated load current.

Unbalance causes high 60-cycle and 120-cycle components of ripple which the filter attenuates to a lesser degree than the 360 cycles for which it was designed. The output ripple measured at the battery was found to vary from 80 to 500 millivolts depending on the degree of unbalance of the various sets of reactors tested. Use of the balancing winding and its associated rheostat reduced the total ripple by a factor of 10 to 1. This adjustment will be made at the factory on the assembled rectifier. The process is simple, requiring only an oscilloscope connected to the input to the main filter and an a-c vacuum-tube voltmeter.

### Control Section

The control circuit is shown in Fig. 4. It consists essentially of a gate circuit to discriminate between voltage and current signals, and an amplifier operating in push-pull to drive the saturable-reactor control windings.

$CR18$ and $CR19$ are the gating diodes. Depending on the magnitude of the rectifier output current, a voltage signal received from the *ADJ VOLTS* potentiometer or a current signal from the current sensing circuit is connected to the base of transistor $Q1$ and is matched against the potential of the voltage reference diodes[2] $CR13$, 14, 15, 16 connected to the base of $Q2$. The amplified difference is applied to identical 2-stage current amplifiers consisting of $Q3$, $Q5$ and $Q4$, $Q6$ transistors, and associated apparatus. The push-pull output is connected to the control windings 11-12, and 13-14 of the saturable-reactors $L1$, $L2$, $L3$ shown in Fig. 2 through leads $A$ and $B$.

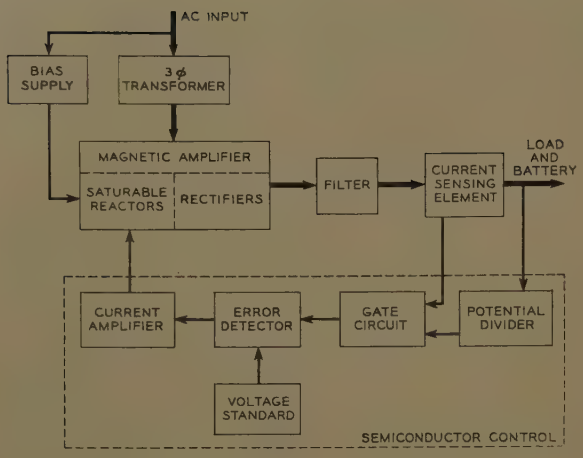


**Fig. 1 (left). Block diagram**

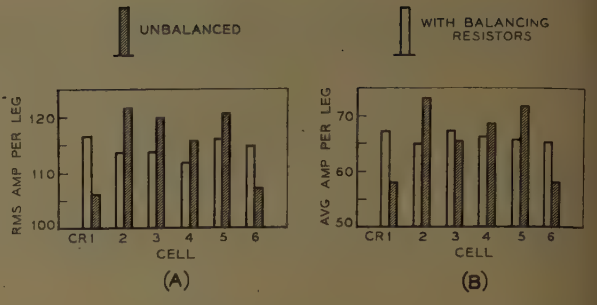


**Fig. 3 (right). Rms and average current through rectifying elements with and without balancing circuits**

Dual gain-control rheostats *P*7 and *P*8 permit adjustment of the stiffness of regulation of the rectifier. An adjustable stability-control rheostat, *P*13, is provided to compensate for variations in the control loop. Thermistor (*TH*1) minimizes the effects of ambient temperature variations. A feature peculiar to the application in a central office equipped with a pulsed switching load is the combination of capacitor *C*16 and resistor *R*44. This circuit prevents the output voltage from decreasing excessively when the load swings exceed the constant-current settings, for a limited time. If the overload persists, normal constant current protection is realized.

## Rectifying Elements

The six germanum power rectifying elements[3] used in this application are rated at 83 amperes per cell in a 3-phase bridge configuration when forced air cooled at the rate of 2,000 linear feet per minute. The quantity of cooling air provided was determined by test to give adequate cooling, while minimizing the noise produced by the high-velocity air passing between the fins of the rectifying cells. Fig. 5 illustrates the blower assembly.

The increased efficiency and small size of the semiconductor power rectifying elements must be accompanied by more complicated protection from short circuits or overloads. Selenium rectifiers have a relatively large surface for the conduction of current and have a time-overload characteristic such that normal fusing provides satisfactory protection. The small area semiconductor cells have a very low thermal capacity, so that the protective device must be extremely fast to prevent damage to the diodes.

The indefiniteness of the term "short circuit" makes the discussion of the subject an involved one. Depending on the impedance of the source, point of short-circuit occurrence, and impedance of the shorting element itself, a short circuit may range from a very slight overload of the

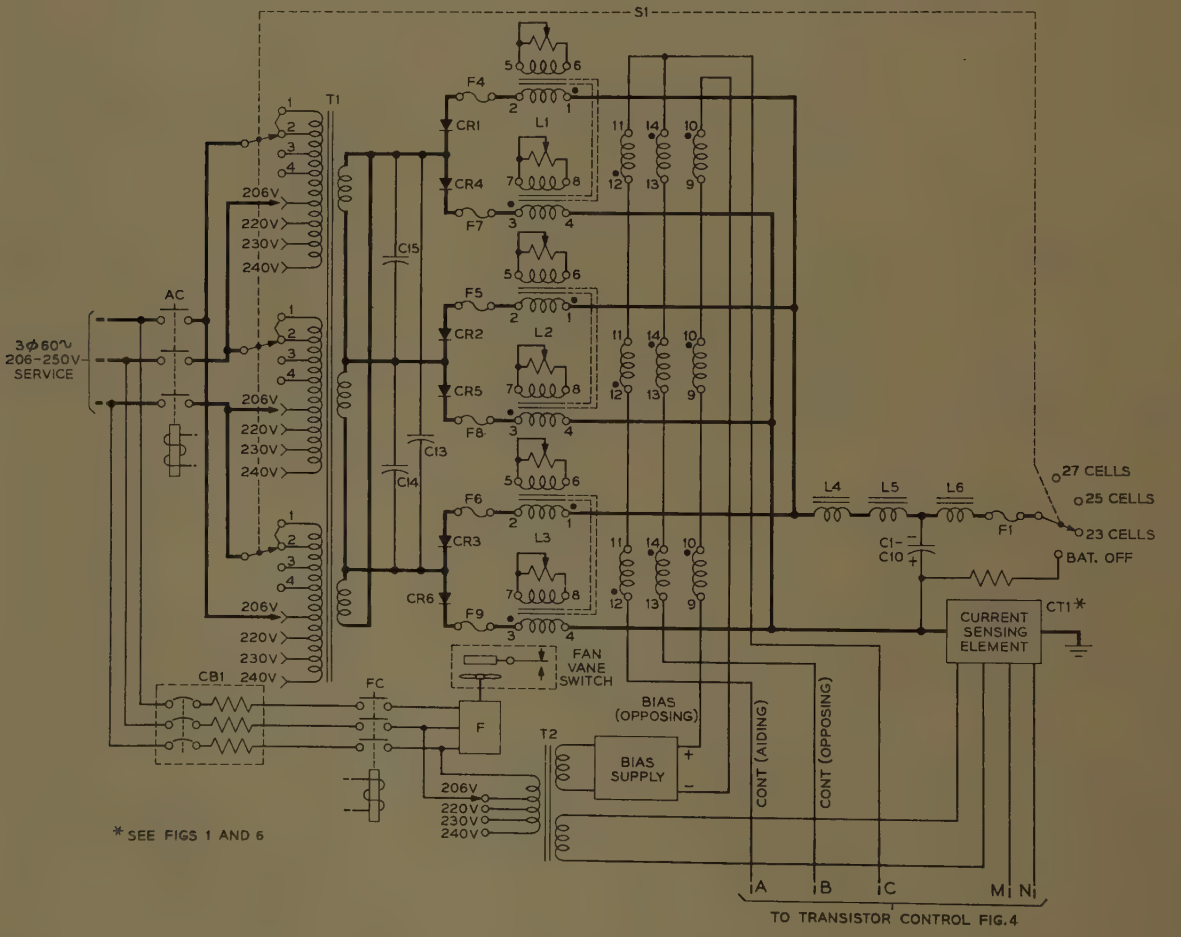


**Fig. 2. Schematic of power section**

rectifying cell to a current that may be many times the rating of the cell.

In cases where a number of rectifying cells are paralleled and the current capability of the source may be 10,000 amperes or more, the present recommended protection places a surge-type fuse[4] in series with each cell. The currrent-time characteristic of these fuses falls within the safe overload range of the germanium cells. In cases where the short-circuit current is limited by one or more of the factors enumerated above, protection is marginal at best. Protection may then be afforded by a surge-type fuse, a circuit breaker, a current-limiting circuit, or shut-down circuit feature.

In this rectifier three of these methods are utilized to cover specific loading conditions. To protect against short circuits at the rectifying cells, surge-type fuses (*F4-F9* Fig. 2) are used. To protect the cells from overloads external to the rectifier, the electronic control circuit (Figs. 4 and 6) automatically limits the output to a safe value. Failure of the electronic circuit permits an overload relay, *OL* (Fig. 6), to function to shut down the rectifier. However, a short circuit between the rectifying elements and the rectifier output may result in a rectifying cell failure. Since most cells "fail short" a total of three cells can be lost in this circuit. Additional study of this problem is under way since the problem is characteristic of most power supplies whose short-circuit capabilities are low.

Protection against fan failure is provided by a vane-type switch in the air stream. Electrical failure or an obstruction of the intake vent will cause a rectifier shutdown. Voltage surges across the cells are minimized by the use of capacitors across the secondary windings of the main transformer.

## Current-Sensing Circuit

The basic current-sensing circuit is the d-c measuring magnetic amplifier circuit[5] illustrated in Fig. 6(A). It has been been called a "d-c transformer" by usage. It is not a new device but its value has been increased by the availability of square-loop core materials.

The device was selected for this application because it provides a signal of considerable magnitude limited only by design. This eliminates the need for a d-c amplifier with its attendant circuit complication and problems of drift, replaceable parts, etc. In this application a 60-volt signal is provided at full load on the rectifier. Fig. 6(B) illustrates the actual circuit arrangement. The lead labeled *L* is the d-c output lead of the

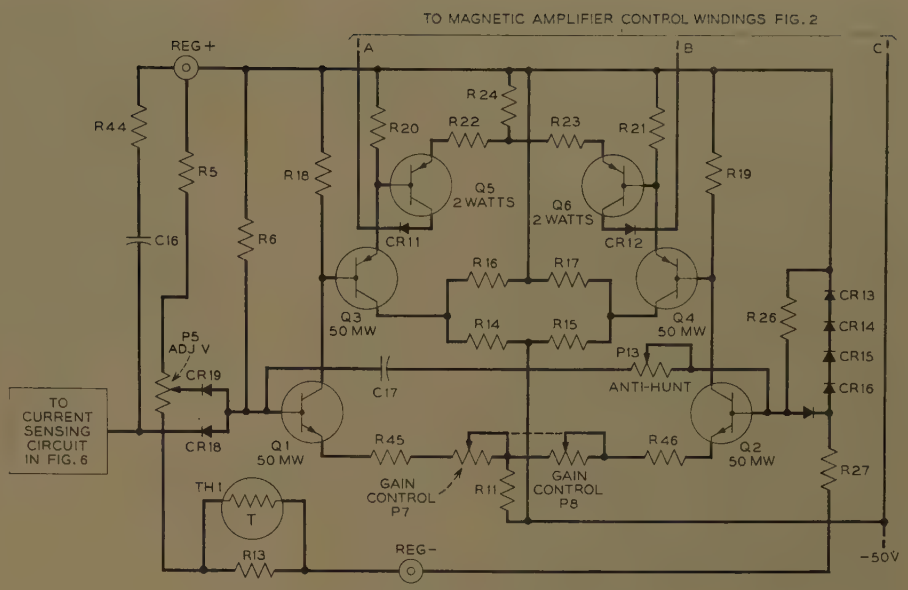


Fig. 4. Schematic of control section

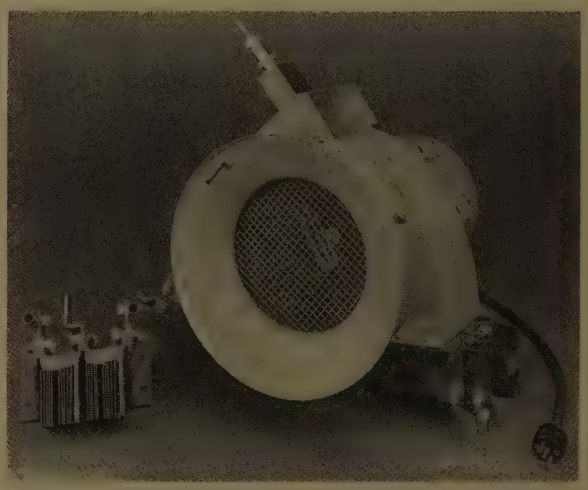

Fig. 5. Blower assembly with demountable rectifier assemblies

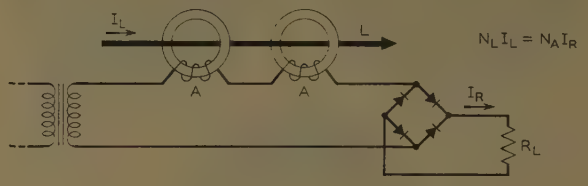


Fig. 6(A). D-c transformer, basic circuit

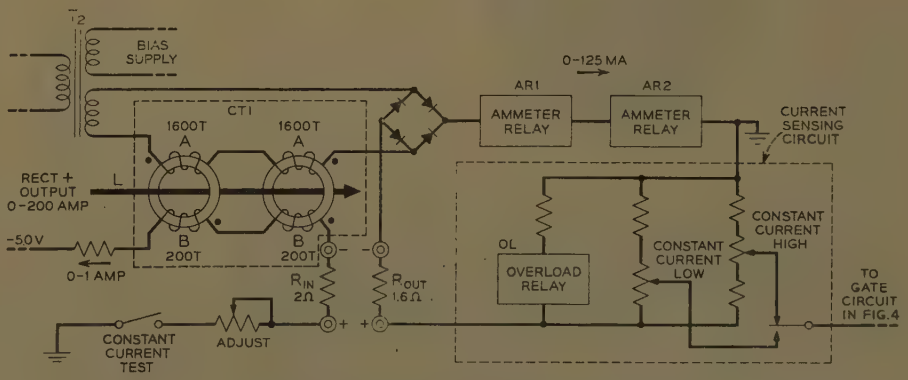


Fig. 6(B). D-c transformer, application schematic

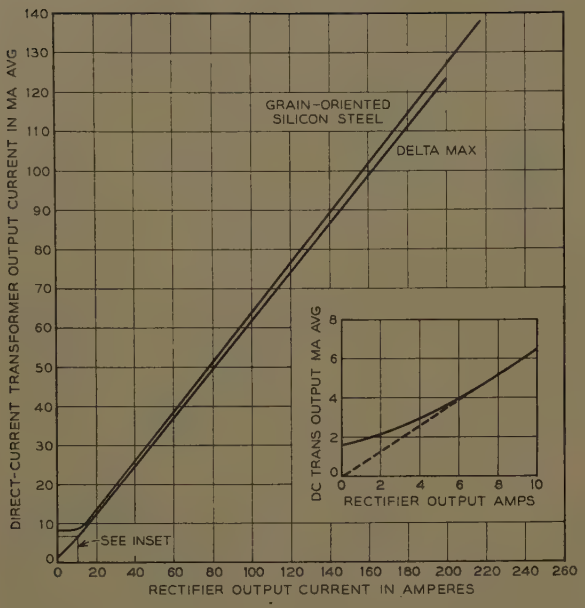


**Fig. 7 (left). Characteristic of d-c transformer**

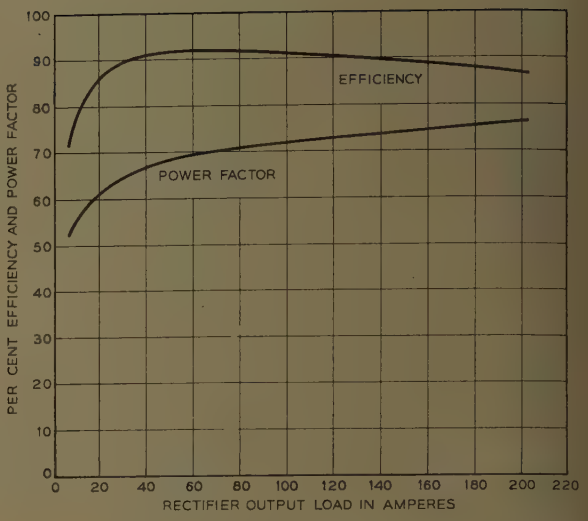


**Fig. 11 (right). Efficiency and power factor**

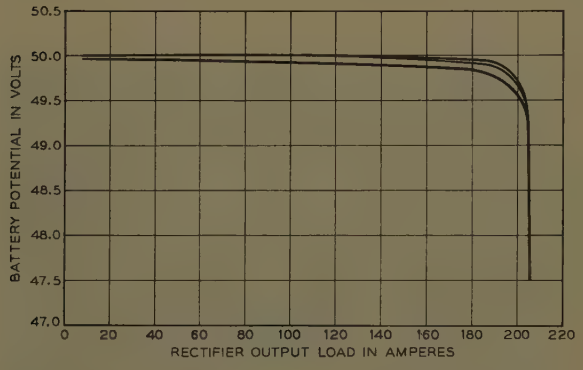


**Fig. 8 (left). Static line and load-voltage regulation**

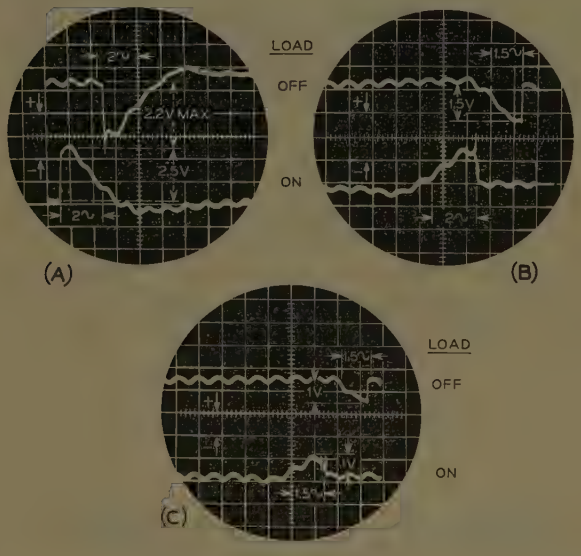


**Fig. 9 (left). Dynamic response to a single step-load change**

A—95%
B—55%
C—30%




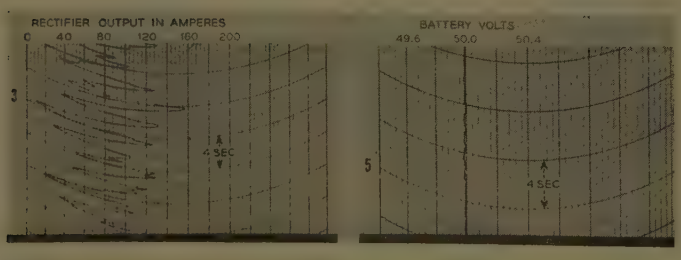


**Fig. 10. Dynamic response to random load pulses—six 20-ampere load steps of 0.3–0.5-second duration**

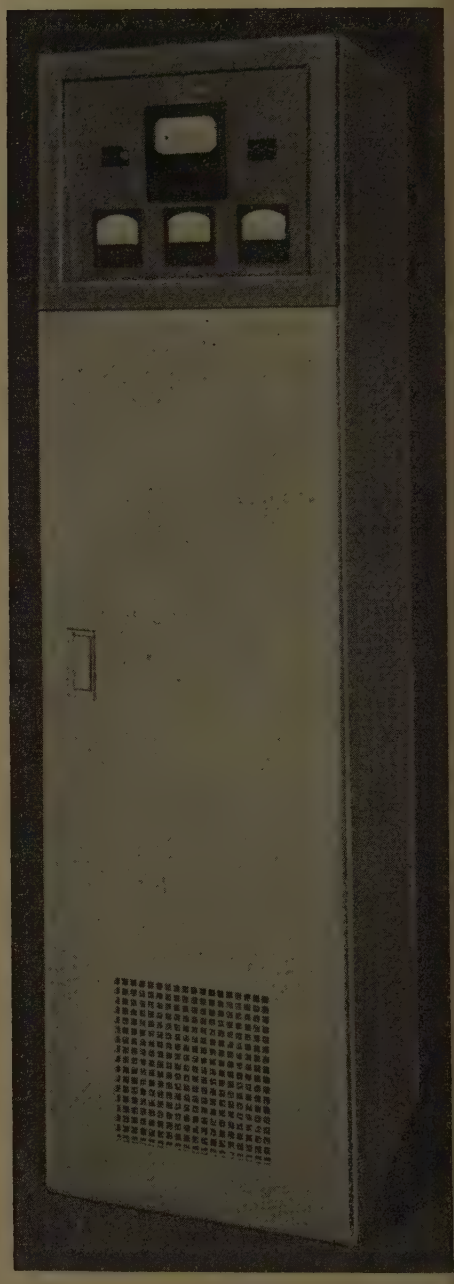

**Fig. 12. Model of rectifier**

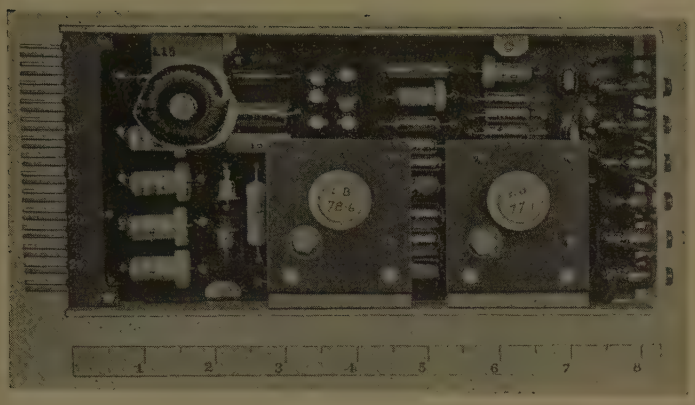

Fig. 13. Plug-in printed wiring control panel

rectifier. It serves as a single-turn primary winding for the toroids making up the current-sensing element *CT*1. The *A* windings are the a-c secondary windings. They are connected series opposing. The ratio of secondary to primary turns is 1,600/1. The rectified output current is proportional to the current in the load lead *L*.

The voltage drop across the group of resistors making up the current-sensing section in the output circuit of the d-c transformer (Fig. 6(B)) is connected to the current gate in the transistor control circuit (Fig. 4). As the load current in the *L* lead increases the voltage across these resistors will increase. If the load current exceeds the preset value permitted by the *CONCUR H* (constant-current high) adjustment, the rectifier output voltage will be decreased to maintain the current at this value. Winding *B* (Fig. 6(B)) is a 200-turn test winding provided to permit adjustment of the constant current level with the rectifier disconnected from the battery and load. A simulated change of 50-150% rated current is possible.

The two saturable cores are Magnetics Incorporated *50042-2A* toroids made of 0.002-inch Deltamax tape. The curve of the rectifier output current, *L*, and the d-c transformer output is plotted on Fig. 7 for a 480-ohm load and ±10% line voltage change. The characteristic for a similar set of coils using grain-oriented silicon steel is also plotted. The principal differences is the low minimum current (magnetizing current) for the high-gain cores.

The saturable-reactors are potted in an epoxy resin for ease of mounting and as physical protection for the windings to avoid abrasion due to contact with the load cable or bus bar. In a similar manner to standard a-c transformer practice, a single design can be used for a series of rectifiers of various current ratings by threading more than one turn through the cores.

## Maintenance and Reliability

Most present-day central-office power plants in the Bell System are wholly automatic, and in many cases the offices are unattended. Continuity of service is the paramount objective in the design of telephone systems. To achieve this, a high order of reliability and minimum maintenance of the power plant are essential. The present regulating equipments use electron tubes which are considered renewable items. This rectifier has only components which are considered non-renewable assuming the components are fabricated reliably. However, to assure prompt restoration of facilities in the event of a failure, a number of indicating devices and trouble shooting aids are incorporated in this design. Three lamps indicate the general area of failure. Circuit breakers or fuses have tell-tale indicators or are self-evident.

The transistor amplifier (Fig. 4) can be tested while the main power section is disconnected from the a-c supply. The transistor amplifier section is on a plug-in printed card making its replacement a simple operation if it becomes defective. The power section can be tested separately by disabling or removing the transistor control section, which also permits manual operation of the rectifier if a replacement transistor-card is not available.

Failure of the bias supply (Fig. 2) will prevent the application of a-c power to the power section and will give an alarm. Faulty behavior of the d-c transformer circuit or apparent inaccuracies in a meter or measuring circuit can be localized with the rectifier disconnected from the battery, using the test winding (*B*) in Fig. 6(B) in conjunction with resistors *R* (IN) and *R* (OUT).

## Performance Data

Static and dynamic characteristics of the rectifier model were measured when connected to a 1,000-ampere-hour battery and resistance load. The regulating leads and output voltmeter leads were connected to the battery terminals. All data shown on the attached figures were taken at room ambient (25-30 degrees centigrade). However, measurements indicated only a 0.2% change in output voltage for a 30-degree-centigrade variation in ambient.

### Output Voltage Regulation

Fig. 8 illustrates the static voltage regulation for a ±7% line-voltage change. The constant current adjustment was made at 205 amperes and 49.0 volts output. The transition from constant voltage to constant current requires a 10% change in load. Fig. 9 illustrates oscilloscope traces of the dynamic response to step changes in load. Response time noted is on a 60-cycle basis. Fig. 10 illustrates the response to a fast changing load simulating operation of the rectifier in a central office with a pulsating relay switching load. The load consisted of six 20-ampere steps appearing at random for approximately 0.3–0.5 second.

### Power Factor and Efficiency

Fig. 11 illustrates the efficiency and apparent power factor of the development model rectifier. Earlier selenium rectifiers used in the same application had a maximum efficiency of 76%.

## Equipment Features

Fig. 12 illustrates the appearance of the model rectifier. Note the sloping meter panel to improve readability. The control panels are mounted on a swinging gate behind the large front door. The control amplifier is mounted on a removable printed wiring card which is a part of the control panel, see Fig. 13. Control relays are of the wire spring type, and are mounted on the control panel. The saturable reactors, 3-phase transformer, and filter inductors are mounted in the bottom portion of the rectifier. Ventilated openings are provided in front and rear doors. The top is closed except for openings for incoming and outgoing leads. The air intake for the fan is in the rear door. Air must pass through a dust filter panel. The rectifiers are arranged for side-by-side mounting.

## Conclusions

The objective of designing a 10-kw rectifier utilizing solid-state devices, that competes with existing regulated motor-generator sets in telephone power plants,

has been realized. Semiconductor devices include high- and low-power germanium rectifiers, low-power silicon diodes, and germanium transistors. The use of laminated core saturable reactors with form-wound coils and an in-circuit balancing arrangement fulfills the requirements of reasonable cost and elimination of core selection while using square-loop core material in a high-gain self-saturated magnetic amplifier. High efficiency and good static and dynamic response resulted from the direct control of the large saturable reactors by a transistor control circuit equipped with two 2-watt transistors in a push-pull output stage. The base area of the unit was decreased approximately 10% over the earlier selenium rectifiers of lower output rating.

## References


1. Some Applications of Semiconductor Devices in the Feedback Loop of Regulated Metallic Rectifiers, **B. H. Hamilton.** *AIEE Transactions*, vol. 73, pt. I, 1954 (Jan. 1955 section), pp. 640–45.

2. The Suitability of the Silicon Alloy Junction Diode as a Reference Standard in Regulated Metallic Rectifier Circuits, **D. H. Smith.** *Ibid.*, pp. 645–51.

3. Germanium Rectifiers for Industrial Applications, **L. W. Burton.** *Ibid.*, vol. 75, pt. I, Mar. 1956, pp. 41–44.

4. Shawmut Amp-Trap. *Bulletin 514–7*, The Chase Shawmut Company, Newburyport, Mass.

5. Magnetic Amplifiers (book), **H. F. Storm.** John Wiley & Sons, Inc., New York, N. Y., 1955.


# Silicon Power Rectifier Equipments


**J. A. MARSHALL**
MEMBER AIEE

**V. N. STEWART**
MEMBER AIEE


A NOTABLE newcomer in the power rectifier field is the silicon power rectifier cell capable of handling, in some applications, power outputs up to 10,000 watts each. This paper illustrates one method of using silicon power rectifier cells in an equipment with an industrial rating of 300 kw at 250 volts and with overload duty of 125% for 2 hours and 200% for 1 minute. A review of the components, equipment design, and operating performance is presented along with general rules and their application to equipment protection.

## Circuit

The double-way or 3-phase full-wave bridge rectifier, Fig. 1, proved to be the most economical for this application because it allowed the use of simplified copper configurations and a standard transformer.

## Components

The silicon power rectifier cell was chosen for its peak inverse- and surge-voltage characteristics and higher operating temperature. The type *4JA60B* cell[1] most closely met the requirements of the normal peak inverse voltage of 276 volts and the surge duty of 600 volts as established in the section on application basis for components. The magnitude of the surge voltage demanded two cells in series, and current requirements dictated the total number of cells per phase. There are a total of 192 cells used with 16 parallel rectifying paths for each way, and two cells in series for each parallel path. The average current per cell with this arrangement is 25 amperes for the full-load rating of the equipment.

A-c power is supplied to the rectifier unit by a standard 500-kva delta-Y 480-volt to 208/120-volt transformer with four 2% taps. Voltage regulation is accomplished by an induction-type regulator rated 36 kva, 480 volts, capable of controlling the output voltage ±10%.

For best design, the cells should be mounted with consideration given to simple circuit connections, adequate cooling, and ease of maintenance. A removable tray was designed to accomplish the foregoing goals. Eight silicon power rectifier cells, their dividing resistors, a protective fuse, air baffles, disconnects, fin conductors, an indicating lamp, lift-off handle and latch are arranged on a tray as shown in Fig. 2.

The eight cells of each tray are connected electrically as shown in Fig. 1 and physically as shown in Fig. 2. The incoming and outgoing connections are terminated in finger-type disconnects.

The five copper fin conductors to which the cells are connected act as heat sinks and the area between them allows for the passage of cooling air, either natural or forced convection. Four of the fins provide the common point between series cells and the fifth fin is the common conductor for the four parallel paths.

The indicating lamp, connected in parallel with the fuse, lights whenever the fuse blows and the circuit is energized. It is possible to include an audible alarm or remote indication of fuse operation for unattended installations.

Three vertical rows of four trays each are mounted on the front and rear of the metal-enclosed unit which houses the bus. The bus consists of the three a-c power connections from the transformer and the two d-c outputs to the load air circuit breaker.

The unit shown in Fig. 3 has a fan mounted on the roof to provide forced air cooling for the trays.

Normal maintenance of the trays consists of a visual inspection and a check of the internal connections. This is quickly accomplished by disconnecting the tray as shown in Fig. 4. In the event of a cell failure, quick replacement of the tray having a faulty cell is possible under load. A spare tray can be inserted while necessary replacements are made to the original tray.

## Protection

A completely protected rectifier equipment is accomplished through a design combining the characteristics of the rectifier cells, transformers, fuses, and breakers. These components form an equipment to give a continuous-current rating and short-time ability as well as providing for the following abnormal conditions of an industrial system:

1. D-c overload.
2. External d-c faults.
3. Internal d-c faults.
4. Cell-blocking-characteristic failure.
5. A-c faults.

Applying protection under these conditions has established several general rules which give high continuity of service, rapid restoration of service after an overload outage, short-circuit protection, and removal of a defective cell. This applies particularly to power units having


Paper **57-1176**, recommended by the AIEE Industrial Power Rectifiers and Semiconductor Metallic Rectifiers Committees and approved by the AIEE Technical Operations Department for presentation at the AIEE Conference on Rectifiers in Industry, Chicago, Ill., June 4–5, 1957. Manuscript made available for printing September 20, 1957.



J. A. Marshall and V. N. Stewart are with General Electric Company, Philadelphia, Pa.

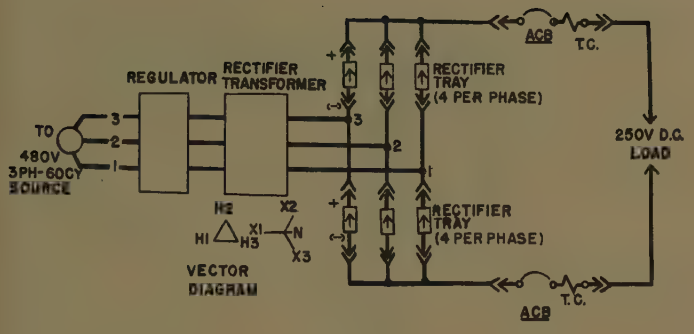


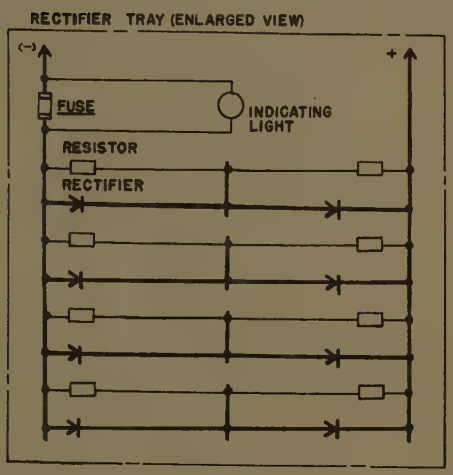


Fig. 1. Double-way silicon power rectifier circuit

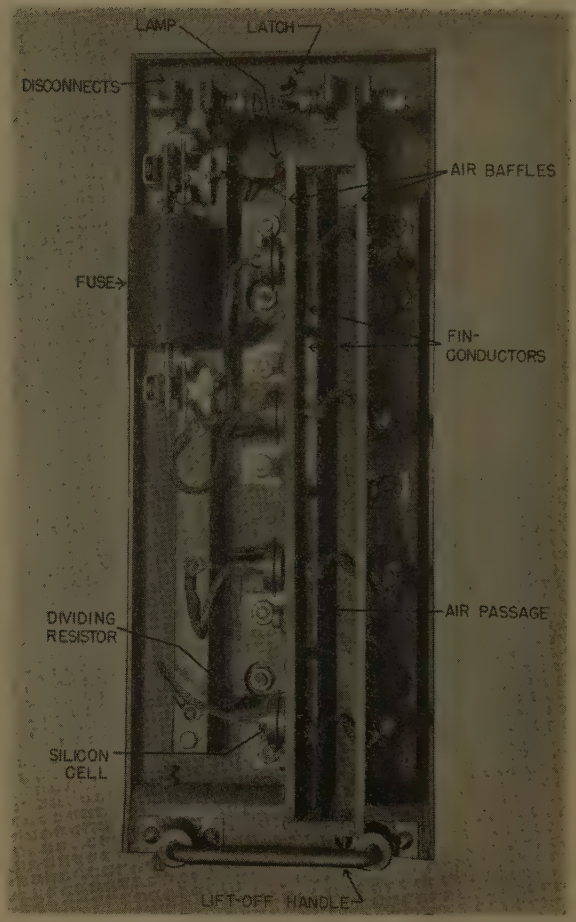


Fig. 2. Removable tray showing type SRF rectifier fuse and type 4JA60 silicon power rectifier

multiple rectifier cells per phase and capacities such as the 300-kw unit presented in this paper.

The following general rules can be partially demonstrated in the co-ordination curves of Fig. 5 and in the basis for selection of the components which follow this section.

1. Low thermal capacity of the rectifier cell makes the overload duty an influencing factor in the determination of unit size.

2. Momentary capacity of the equipment (rectifier cells) must be sufficient to withstand fault durations equal to the clearing time of the d-c line breaker.

3. Maximum fault conditions cannot exceed the surge-current limits of the cells without a probable loss of cells.

4. Fuse melting characteristics must allow sufficient time for circuit clearing by the d-c breaker over the entire range.

5. A fuse in series with a rectifier cell or parallel cells as used in this equipment can only provide cell isolation with a failure of the blocking characteristic. In general, fuses with a sufficient current capacity to meet the normal forward duty will not provide individual cell protection on overload or short-circuit currents. Further, with several fuses operating in parallel under balanced conditions and appearing to divide the available fault current, they will not clear simultaneously and thereby leave the total duty to the last fuse to clear. This means that the maximum duty of the cells must be based on the entire fault through the last fuse to clear. The extreme duty on the cells protected by the last fuse to clear would result in thermal damage and loss of the cells.

6. Fuse selectivity under failure of the blocking characteristic is dependent on the fuse-clearing, arcing, and melting $i^2t$ characteristics established for maximum system conditions. Performance for this function cannot be evaluated from the normal time-current melting characteristic of the fuse but must include the energy conditions with full voltage applied.

7. Surge voltages occurring during the operation of protective equipment as well as the normal voltage conditions will determine the selection of the operating peak inverse voltage rating of the rectifier cells.

## Application Basis for Components

The rectifier equipment presented in this paper readily illustrates the selection of components based on their characteristics and the requirements established for adequate protection. Using the system shown in Fig. 1, an equipment supplying a 300-kw load at 250 volts will require 16 parallel conduction cells in each phase to meet both the industrial overload and short-circuit momentary ability.

Fig. 3. Front view of the silicon rectifier equipment with type AK-1-50 air circuit breaker

Fig. 4. Method of tray removal

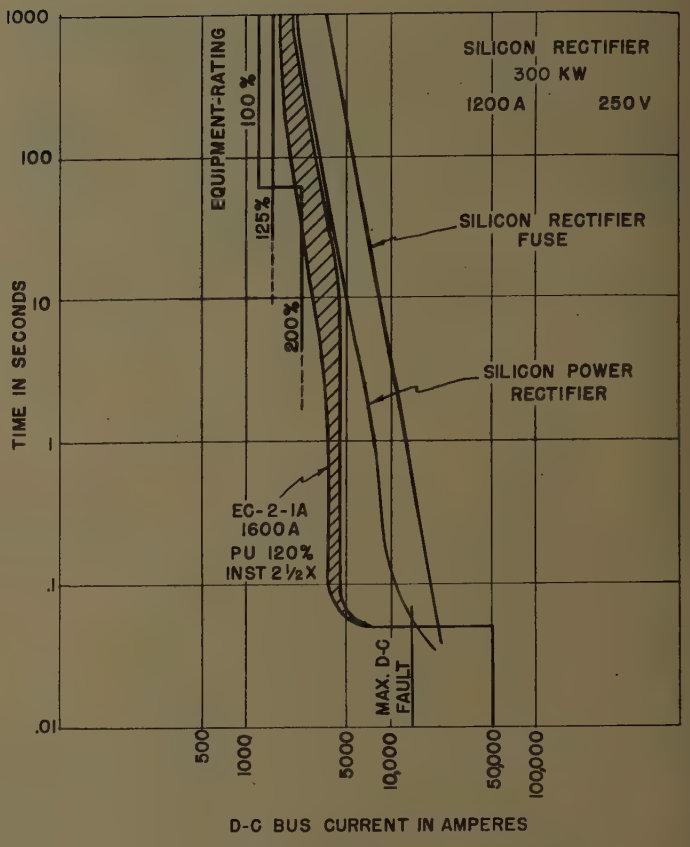


Fig. 5. Protective co-ordination characteristics

Each cell is applied to limits determined by cell heating due to losses, heat-dissipation rate, ambient conditions, thermal storage capacity of conducting parts, and thermal capacity of the cells.

In the selection of the number of cells a conservative continuous-current level is established when the numbers of cells are adequate for the overload protection associated with the 125% and 200% ratings of the industrial equipment. The 16 parallel cells of this unit have the characteristics of the silicon power rectifier in Fig. 5 and the long-time overload duty to the cells which is determined by the protective breaker characteristic can reach a maximum of 1,980 amperes (165%). For these overloads with very long times, the output of the cells is dependent on the power loss and the ability of the cells and equipment to dissipate this loss. Although the initial design data will be based on a desired copper conductor temperature for calculating the selected arrangement, such as illustrated in Figs. 1 and 2, it is necessary to evaluate the results through a test of a prototype and the completed equipment. Each degree rise in the bus limits the average current capacity of the cell which has a total operating temperature of 200 C (degrees centigrade). The cell temperature of this equipment is based on 48 cells averaging the normal d-c output and is related to the power losses of the 3-phase curves as given in a previous paper.[1]

As the values of overcurrent increase, the time to reach the temperature of the cells will reduce. Here, the rectifier characteristic has a resemblance to that of a fuse characteristic with an inverse time function in the range of 10 to 600 seconds. This damage characteristic for the rectifier cell must include the initial temperature conditions at 100% load, the maximum ambient of 40 C, the heat sink provided by both cooling fins and the rectifier parts, and the temperature generated by the junction losses.

As the peak currents increase to short-circuit conditions, the damage characteristic shifts from a temperature limitation to one of cell fracture under high currents. This alters the characteristic as can be noted for values less than 1/2 second. This has been verified through surge testing of individual and multiple cells as well as power tests of the entire equipment.

For this application the available faults levels are from 9,000 to 11,000 amperes d-c which is well below the momentary ability of the cells with a breaker clearing time of 0.05 second. The equipment with the 16 parallel cells per phase has momentary ability approaching 15,000 amperes.

The melting time-current characteristics of the fuse must be co-ordinated with the d-c breaker over the entire range of currents. This co-ordination is evident in the protective co-ordination curves for this application for values over the range and beyond the maximum d-c fault conditions.

The fuse conduction period in each cycle is related to the commutation characteristics of the cell which change from 120 electrical degrees conduction for the lower overload current to 180 electrical degrees for the fault conditions. Therefore, the normal fuse characteristic must be properly adjusted to show its current melting response in relation to the rectifier applications, and this has been made in Fig. 5.

Blocking characteristic failures cause direct line-to-line faults on the transformer through the normal conducting cells of another phase and must be isolated by limiting action to prevent damage of the good cells. This is the function of the fuses applied with the equipment and the minimum number of fuses, such as the four per phase used in this 300-kw unit, are determined by the contingency operation with one fuse open, the relation of total clearing energy to melting energy, and the peak let-through currents. The last two conditions are vitally affected by the system's voltage and available currents. For the contingency operation

with one fuse open, a phase with a defective cell will have to carry an increase of 33% over the 100% load during replacement of cell and fuse. This duty will be considerably less than the overload ability of the cells as indicated by the earlier analysis covering the overload damage characteristic.

Selective operation by the fuse to eliminate the failed cell is determined by the ratio of total clearing $\int i^2dt$ to melting $\int i^2dt$. The silicon rectifier fuse was measured to be less than three to one with controlled power testing using conditions of maximum severity. This ratio would also allow selectivity during contingency operation with three fuses in service and provide a margin with the normal four fuses per phase in service.

The fuse which is isolating an equipment tray having a rectifier blocking-characteristic failure must give current-limiting action under the worst condition to protect the 16 parallel cells in series with the faulted circuit. In this equipment the fuse design limited the current per cell to an approximate peak of 650 amperes while giving adequate co-ordination with the breaker. This is considerably less than the value which can be taken by the cells for several cycles. In this application the $\int i^2dt$ let-through energy is one fifth of the ability of the silicon cells and does not represent a factor in the design; however, this should be checked to assure sufficient margin with the particular rectifier characteristic and arrangement being used for the equipment.

The surge-voltage rating of the cells has been given as nominal continuous peak value with an additional amount for surge condition. The 200 volts of peak inverse voltage plus 100 volts for surge makes 300 volts for each unit and a total of 600 volts for the two cells in series. This is adequate for the maximum peaks which approach 600 volts for the fuse or breaker operation. This eliminates the consideration of the higher peak inverse voltage ratings such as the 300-volt cell with a total of 400 volts for surge conditions.

Internal faults in the equipment and transformers receive their protection through the breakers or fuses associated with the a-c system. These are applied according to practices now used extensively for load-center units and distribution systems supplying a-c power.

## Performance

An induction-voltage regulator with a range of ±10% is connected ahead of the main transformer and provides voltage regulation. The inherent regulation of the unit without the induction regulator is approximately 5%.

Using a forward-cell drop of approximately 1 volt, the efficiency of the rectifier element is approximately 98% and the efficiency of the equipment per American Standards Association mercury-arc rectifier standards is approximately 95.5%. The over-all efficiency including the induction-voltage regulator required for voltage control is approximately 94.3%. The vector power factor is approximately 97%.

## Conclusions

The performance of this equipment compares most favorably with other types of conversion equipment in the 250- to 500-volt range. It is felt that the voltage range will be extended higher in the near future. This type of equipment is best suited for use in industrial and electrochemical applications which do not require large voltage ranges.

## Reference

1. The Rating and Application of a Silicon Power Rectifier, D. K. Bisson. *AIEE Special Publication T-93*, "Rectifiers in Industry," June 1957, pp. 135–42.

# Selenium Rectifier Applications in Automotive Vehicles

EMERY J. SZABO
ASSOCIATE MEMBER AIEE

SELENIUM rectifiers were first tested in 1937 for possible application in automotive vehicles. The term "automotive vehicle" includes passenger cars, trucks, buses, off-highway construction equipment, and other self-propelled vehicles.

It was in 1937 that the Chrysler Corporation was doing experimental work with an alternator rectifier system, replacing the conventional d-c generator on passenger cars. The first selenium rectifiers for that application were imported from Europe since they were not manufactured in the United States until 1938. There was considerable development work done by the Chrysler Corporation on passenger car systems but the beginning of World War II stopped the commercial work and Chrysler continued development of an alternator rectifier system for military aircraft.[1] There was limited production of an aircraft alternator rectifier system rated at 30 volts, 400 amperes d-c output. The selenium rectifiers were air-blast-cooled for minimum size and weight.

In 1945, the Leece Neville Company took up development work on an alternator rectifier system for heavy duty applications on police cars, trucks, and buses.[2]

The first standard equipment application of selenium rectifiers was in 1946, when the Twin Coach Company introduced their postwar design motor coach, which was equipped with an alternator rectifier system rated at 14 volts, 100 amperes d-c output. Since that date, the use of selenium rectifiers in vehicle generating systems has expanded rapidly. Up until today there have been about 100,000 selenium rectifiers installed as a part of heavy-duty generating systems for automotive vehicles.

Before discussing the particular applications of various types of selenium rectifiers in generating systems, a comparison will be made of the conventional d-c generating system with the alternator rectifier system. The system consists of two units; a variable speed-belt-driven d-c generator, and the generator control unit, commonly referred to as the voltage regulator. The d-c generator is a shunt-type machine and is required to operate over a speed range established by the pulley diameters and speed range of the engine in the vehicle.

The alternator rectifier system consists of three units. The first of these is the

Paper 57-1177, recommended by the AIEE Industrial Power Rectifiers and Semiconductor Metallic Rectifiers Committees and approved by the AIEE Technical Operations Department for presentation at the AIEE Conference on Rectifiers in Industry, Chicago, Ill., June 4–5, 1957. Manuscript made available for printing September 20, 1957.

Emery J. Szabo is with the Leece Neville Company, Cleveland, Ohio.

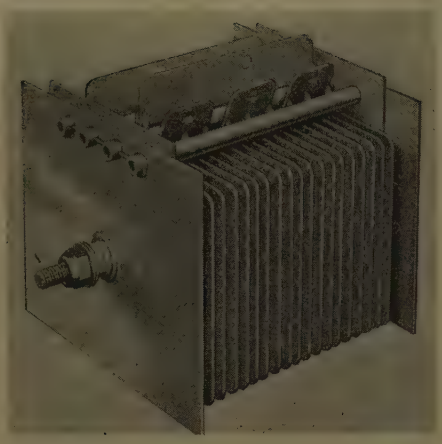

Fig. 1. Fourteen-volt 100-ampere selenium rectifier, 1946

Fig. 2. Heavy-duty railroad type of selenium rectifier, 14 volts, 125 amperes

belt-driven variable speed alternator which operates over a speed range established by the pulley diameters and the speed range of the engine. The second unit is the rectifier which converts the a-c output of the alternator into d-c power for battery charging and electrical loads on the vehicle. The third unit is the generator control unit which is very similar to the d-c generator control unit. The major difference between the d-c generator control unit and the alternator rectifier control unit is in the cutout element. The control unit for the alternator rectifier system does not have a reverse current winding on the relay, since there is no appreciable amount of reverse current discharged from the battery through the rectifier. In most applications the relay is energized or de-energized from the ignition switch on the vehicle so that the relay remains closed at all times during operation of the vehicle.

Basically the two systems serve the same function of providing electric energy to charge the battery and carry the electric loads on the vehicle. A comparison of the output characteristics of the two systems, however, shows considerable difference in the power which may be obtained from the alternator rectifier system compared to the output of the d-c generating system. There are two distinct advantages for the alternator rectifier system. One of these is more power available at lower speeds for minimum size and weight of the generating unit and other is the ability of the system to operate over a wide speed range. The alternator itself is about half the weight of a d-c generator required to generate the same amount of power at the same minimum full load speed of the unit. The other major advantage of the alternator rectifier system is the ability to produce relatively large output at low speed by taking advantage of higher belt drive ratios, and at the same time its ability to generate this high output at maximum engine operating speed with good reliability even at maximum load and speed. This permits design and application of alternator rectifier systems to produce up to 50% of maximum rated output at engine-idling speed and still be able to operate at maximum speed and output without problems of commutation and short brush life. The problems of commutation at high speed require special design considerations on d-c generators which are usually prohibitive from the cost standpoint in automotive vehicles.

The selenium rectifier is the device that permits the design of the alternator to be independent of the wide speed range and high drive ratios which are required in today's vehicle generating systems.

The selenium rectifier, being a separate unit, is located independently of the alternator and is usually mounted either directly behind the engine radiator cooling fan or in front of the engine radiator. In both of these locations, the cooling air is provided at all times while the engine is running. The rectifier is used at maximum air-blast-cooled ratings in order to keep its size, weight, and cost to a minimum. There have been a few applications of convection-cooled rectifiers such as on railraod cabbose cars, but the size and cost of the convection-cooled rectifier usually prohibits its use where air-blast cooling is available. Another method of cooling the rectifier is by locating it within a duct work which is either in the engine air intake system on diesel engines or which leads to a rectifier cooling fan on the alternator. This fan draws air through the duct work and thereby provides air-blast cooling for the rectifier whenever the alternator is rotating. The engine air-intake cooling

Fig. 3. Alternator fan duct cooling of selenium rectifier

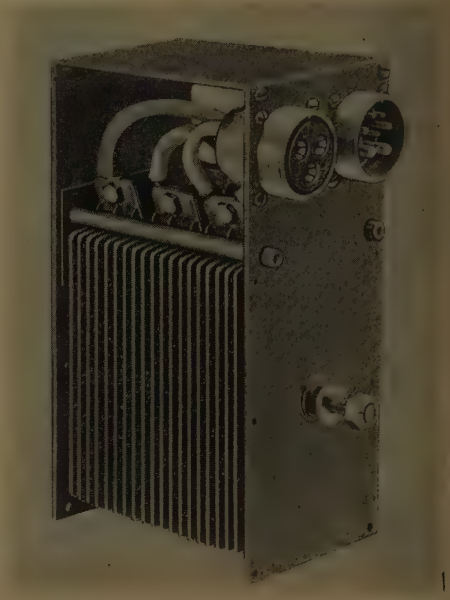

Fig. 4. Military type of selenium rectifier rated 28 volts, 100 amperes output

method mentioned previously has proved very successful on large diesel engines used in tractor-trailer combinations and also in off-highway construction equipment such as 30-ton dump trucks.

The application of selenium rectifiers in automotive vehicles presents two problems which do not usually exist in industrial applications. One of these is the problem of mechanical vibration, since the rectifiers are mounted where they are subjected to considerable vibration from the engine as well as road shock. This has required special mechanical design features in the selenium rectifiers. There has been the necessity for using a keyed construction for the plates and terminals on the center stud to keep them from rotating under vibration and causing a failure. Also there has been a special support of the terminals themselves to keep them from failing under vibration. The other major problem encountered by the selenium rectifier in automotive vehicle applications is that of exposure to extreme corrosion-causing elements. Most of the selenium rectifiers are mounted in such a location that they are exposed to dirt, road splash, and worst of all, the tons of salt spread on the highways during the winter. The road salt mixed


**Fig. 5. Selenium rectifier mounted on top of alternator**

with the slush on the pavement has required special salt spray resistant finishes on the selenium rectifiers. It is standard practice to specify the salt spray resistant finish on all selenium rectifiers used in automotive vehicle applications and even then there are still occasional failures from corrosion. The few applications which might be adequate with ordinary paint finishes do not justify the complications involved in deciding what type of finish would be good enough for various applications. These two problems have been successfully solved so that today the percentage failures are low enough to be of no concern.

The 14-volt 100-ampere selenium rectifier which was the first production application is shown in Fig. 1. This is a 3-phase bridge stack consisting of 18 cells $4^1/_8$ by 6 inches. The terminals, in addition to being keyed on the center stud, are also supported by insulator tubes to prevent failures from vibration. About 30,000 of this particular type of rectifier have been placed into service. The cells, although operating at $3^1/_2$ times normal convection rating, have given very satisfactory service.

The rectifier shown in Fig. 2 was introduced for railroad and marine use, as indicated by the rugged mechanical construction features. There are two heavy steel end plates with an insulator panel across the top supporting the large nickel-plated studs to which the leads are connected. This rectifier is rated at 14 volt, 125-ampere output, and uses 18 cells of 5- by 6-inch size. Fig. 3 shows the duct alternator fan cooling method for a rectifier of the construction shown in Fig. 2.

The next rectifier, Fig. 4, is a military unit rated at 28 volts, 100-ampere output. It consists of 18 cells, $4^1/_8$ by 6 inches, connected in a 3-phase bridge. Thousands of these are in service as part of heavy-duty alternator rectifier generating systems on military vehicles.

The combination of units, Fig. 5, shows a rectifier mounted on top of an alternator with adjustable rectifier-bracketing to permit positioning the rectifier for maximum cooling air from the radiator cooling fan.

A new type of selenium rectifier used in automotive vehicles is the one shown in Fig. 6. This uses the high current density selenium cell which permits further reduction in size and cost for the rectifier in automotive vehicle generating systems. This rectifier was introduced in 1954 with a rating of 14 volts, 50 amperes' output. It consists of six high-current-density cells of 4 by 4 inches. Comparison with previous units shown establishes the major step forward in rectifier design for smaller size and lower cost. The availability of this rectifier has been a major factor in producing a lower cost alternator rectifier system which has proved so popular for automotive applications that already about 50,000 of these rectifiers have been put into service.

The high-current-density cell having proved successful in the 14-volt 50-ampere rating is now being applied to the 14-volt 100-ampere and 150-ampere ratings in order to provide lower cost units to replace those described previously. For example, the use of the high current density cell will permit design of a 14-volt 200-ampere output rectifier no larger than the 14-volt 100-ampere heavy duty unit shown previously in Fig. 2. The high-current-density cell is quickly replacing the conventional cells for all automotive vehicle applications because of its higher output and lower cost, the two major requirements in these applications.

**Fig. 6. High-current-density 14-volt 50-ampere selenium rectifier (1954)**

The alternator rectifier system has a potential future of becoming standard equipment on all passenger cars even though its initial cost is somewhat higher than that of the conventional d-c generating system. The requirements for higher outputs, along with the more important requirement for output at engine-idling speed as well as reliability at high speed will promote the use of alternator systems within the next few years as standard equipment. The selenium rectifier plays an important part in the applications of these systems because in the past the lack of a high-output, small-size, low-cost rectifier was the main problem in applying alternator rectifier systems to vehicle usage.

## References

1. Selenium Rectifiers in Motor Vehicle Power Systems, **Glen Ramsey.** *AIEE Transactions*, vol. 68, pt. I, 1949, pp. 149–53.

2. An A-C Vehicle Generating System, **Albert D. Gilchrist.** *Electrical Engineering*, vol. 66, Aug. 1947, pp. 779–80.

# Size Reduction of Air-Borne Transformers

RAY E. LEE
NONMEMBER AIEE

SIZE and weight are very important design factors for air-borne electronic equipment. The cost of adding a pound of weight to the electronic equipment is $400 per airplane or more.[1] One very effective way to reduce electronic equipment weight is to reduce the weight of the power transformers. Much progress has been made in this direction since World War II. In 1950 17 pounds were saved in one radar set by redesigning the transformers to use improved oriented steel cores. This represented a saving of 40% of the transformer weight of this equipment. Greater savings of space and weight than this are still possible through improved transformer design.

In this paper the methods for transformer size reduction are enumerated and analyzed. Sample designs which illustrate some of the most promising techniques are described.

## Factors Affecting Size

Several of the methods for reducing transformer size and weight seem obvious, but are mentioned here because they are often neglected. For instance, 2.7 pounds were recently cut from one transformer simply by carefully re-evaluating the load and then redesigning to a more realistic value. Simplification of mounting, simplification of terminals, better physical tolerances, more exact knowledge of design limitations are all means that can result in very valuable weight and size savings. The care with which a design is made can often reduce its size as much as 25%. Large tolerances are often excused on the basis of cost, but if total cost of the increased weight were considered the cost of the closer tolerance would be justified.

Often possibilities for weight reduction are overlooked because the equipment engineer does not realize how his design affects transformer size. For instance, a plate transformer for d-c power supply will be 17 to 25% smaller if a bridge-type rectifier is used in place of one requiring a center-tapped transformer. Power supplies using capacity input filters or half-wave rectifiers will in general require larger transformers than are needed with power supplies employing choke input filters and full-wave rectification. Solid-state rectifiers and 3-phase systems result in reduced magnetic component size, because the filament transformers are eliminated, the filter chokes can be made much smaller, and the 3-phase transformer is smaller than its single-phase counterpart. Thus, considerable weight and size reduction is often possible without considering any basically new techniques.

Paper 57-1013, recommended by the AIEE Air Transportation Committee and approved by the AIEE Technical Operations Department for presentation at the AIEE Fall General Meeting, Chicago, Ill., October 7–11, 1957. Manuscript submitted July 15, 1957; made available for printing August 23, 1957.

RAY E. LEE is with the Westinghouse Electric Corporation, Baltimore, Md.

### The General Transformer Equation

The general transformer equation, discussed by Garbarino, will be used to show how various parameters affect transformer size.[2]

$$W_T = 1/45 f F_c F_i B \Delta A_c A_t \quad (1)$$

where

$A_c$ = area of core window in square inches
$A_t$ = core cross-sectional area in square inches
$W_T$ = load volt-amperes of transformer
$f$ = frequency in cycles per second
$F_c$ = winding space factor, the fraction of total window area occupied by conductor cross section
$F_i$ = core space factor
$B$ = maximum flux density in kilolines per square inch
$\Delta$ = current density in kiloamperes per square inch of conductor

By using the best ratio of copper to iron and by using the best configuration for the core and coil some size and weight reduction can usually be accomplished. Garbarino discusses this in detail in his report.[2]

If the configuration of the transformer is held constant while other parameters are varied, then the affect of these parameters on transformer volume can be investigated. When all other size-reduction methods have been considered, an optimum configuration can then be computed to give either minimum volume or minimum weight.

To obtain an expression for volume, equation 1 is rewritten:

$$A_c A_t = \frac{45 W_T}{f F_c F_i B \Delta} \quad (2)$$

$$V \propto l^3 \quad (3)$$

$$A_c \propto l^2 \quad (4)$$

$$A_t \propto l^2 \quad (5)$$

where

$V$ = volume
$l$ = any linear dimension of the transformer

Then

$$V \propto (A_c A_t)^{3/4} \quad (6)$$

$$V \propto \left(\frac{45 W_T}{f F_c F_i B \Delta}\right)^{3/4} \quad (7)$$

A configuration coefficient is defined such that:

$$V = C\left(\frac{W_T}{f F_c F_i B \Delta}\right)^{3/4} \quad (8)$$

Equation 8 shows which transformer parameters can be manipulated to reduce transformer size, but it does not show the penalties in loss, regulation, or heating that are incurred. These are discussed later. The change of size with configuration will not be discussed here since it is discussed adequately elsewhere.[2]

By examining each of the factors at the right side of this equation, it is easy to see what is necessary to reduce the size of a transformer.

Of course, if $W_T$, transformer output, is reduced the size is reduced. Some of the factors in the denominator of equation 8 must be increased to reduce the size of the transformer further.

If frequency is increased the size of the transformer can be greatly decreased, but the transformer design engineer rarely can control this factor.

Winding space factor usually varies from 0.10 to 0.40. There are great possibilities of decreasing the transformer size by increasing the winding space factor. This can be accomplished with improved manufacturing methods and improved insulation. Foil-wound coils show considerable promise as a technique for improving coil space factor.

Size can be reduced only slightly by increasing core space factor since it usually is already 0.9 to 0.95, and the maximum factor is 1.0.

Transformers are usually designed so that the flux density is a little less than that required to saturate the core; therefore, $B$ cannot be increased until a better core material is made available. Cobalt iron alloys show promise of increasing the permissible operating flux density by 25%.

Current density can be increased until loss, regulation, or heating becomes a limiting factor.

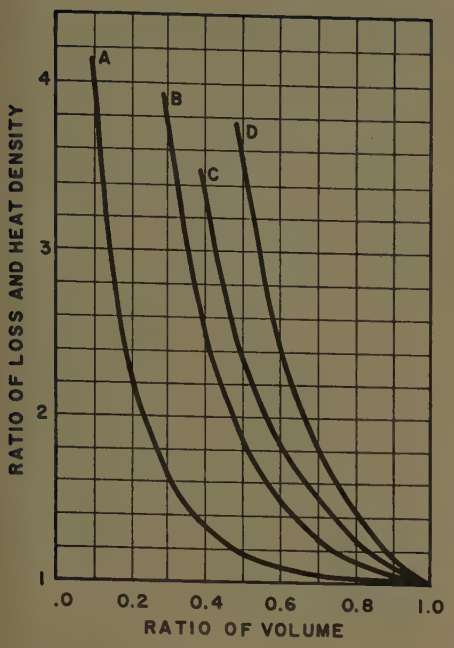


**Fig. 1. Ratio of loss and heat density increase as transformer size is reduced**

A—Loss ratio as frequency is increased
B—Heat density ratio as frequency is increased
C—Loss ratio as current density is increased
D—Heat density ratio as current density is increased

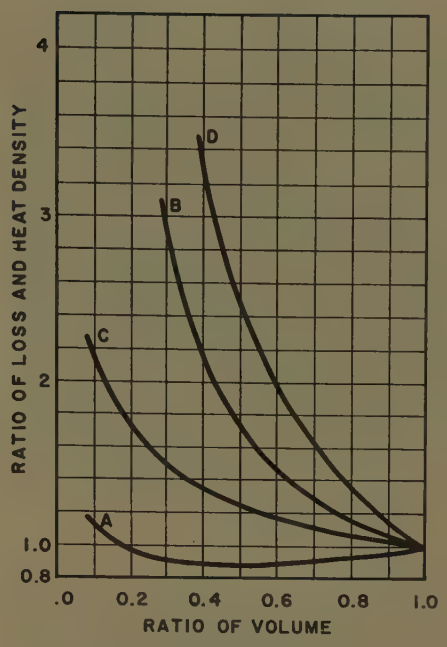


**Fig. 2. Ratio of loss and heat density as transformer size is reduced**

A—Loss ratio as coil space factor is increased
B—Heat density ratio as coil space factor is increased
C—Loss ratio as current density and flux density are increased at the same rate
D—Heat density ratio as current density and flux density are increased

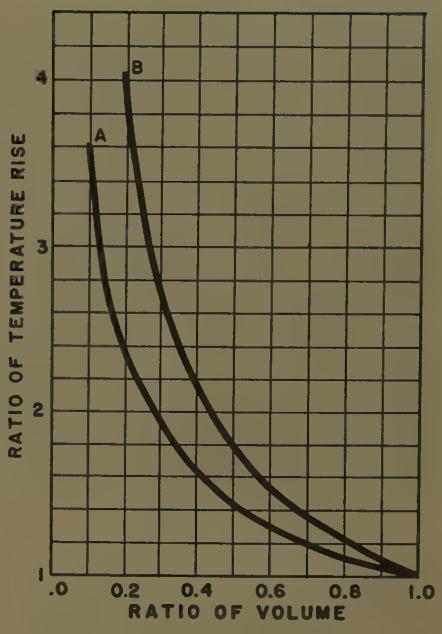


**Fig. 3. Ratio of temperature rise as transformer size is reduced**

A—Temperature rise when total heat flow is constant
B—Temperature rise when transformer is reduced by increasing current density and flux density at the same rate

### Loss and Heating

It has been shown that smaller transformers can be built if the frequency, winding space factor, flux density, current density, or any combination of these are increased. To reduce the size will usually increase the loss, but it will increase the heating even more since the increased heat is dissipated from a smaller volume. Figs. 1 and 2 show how the loss and heat density are affected as size is reduced by increasing various parameters. These curves give the ratio of loss and heat density in the transformer of reduced size to the loss or heat density of a standard design of the same configuration. It is assumed that in the standard design the loss in the coil is equal to the loss in the core; no other limitations are necessary on the standard design. Equations for curves are derived in the appendix.

The watts per cubic inch dissipated as heat are designated as heat density. The temperature rise for any configuration will increase as the heat density increases, but it will not be directly proportional to the heat density. The heat distribution between core and coil will usually change as various parameters are changed. If the heat distribution remains the same within the transformer, then the temperature rise for a given heat density will be less with a small transformer than with a large one. Fig. 3 shows how temperature rise increases as the transformer size is reduced. Curve *A* assumes the total loss remains constant and curve *B* is for the case where size reduction is accomplished by increasing *B* and Δ in the same ratio.

A few examples may show more clearly how loss and heating are affected by size reduction. If a transformer design is reduced to 70% of its former volume by increasing the current density, then it will have 50% more loss. The heat density will increase 79%, but most of the loss will be in the coil. If the first design was 96% efficient, then the new design will be 94% efficient. If this same reduction is accomplished by increasing both *B* and Δ in the same ratio, then the loss is increased only 13%; the heat density is increased 61% and the temperature rise is increased 36%. If 30% reduction is accomplished by increasing current density and winding space factor together in equal amounts, then the loss would increase 2%, heat density 46%, and temperature rise 12%.

### Heat Removal

To decrease the size of a transformer will in general increase the heat density within the transformer and this will raise the temperature unless better cooling is provided. The heat density is increased primarily because the loss is dissipated from a smaller volume. The small decrease in transformer efficiency will not usually be a limiting factor in the design.

All the heat due to loss must be removed from the transformer. There are in general two ways to dispose of the same or more heat from a smaller volume. One method is to use high-temperature insulation and let the transformer run hot. If the channels for heat flow are not improved, the temperature rises until heat flow due to the temperature gradient equals the heat originating in the transformer. It should be remembered that the higher temperature is not primarily the result of more heat, but the same heat in a smaller space; therefore, the ultimate heat sink is not increased significantly. The problem is getting the heat to that heat sink. The other method of heat removal is to provide for a better heat-conducting path between the heat source in the transformer and the ultimate heat sink. Perhaps the best design for many applications is a combination of these two heat-removal methods. Thermal conductors built into the transformer can greatly improve the heat flow and, thus, reduce the temperature rise in the transformer. Circulating or evaporating fluids are other very effective ways to obtain increased heat flow from the transformer.


Fig. 4. High-temperature transformer compared to conventional design

Fig. 5. Three-phase transformer using thermal conductors compared to one phase of conventional 3-phase design

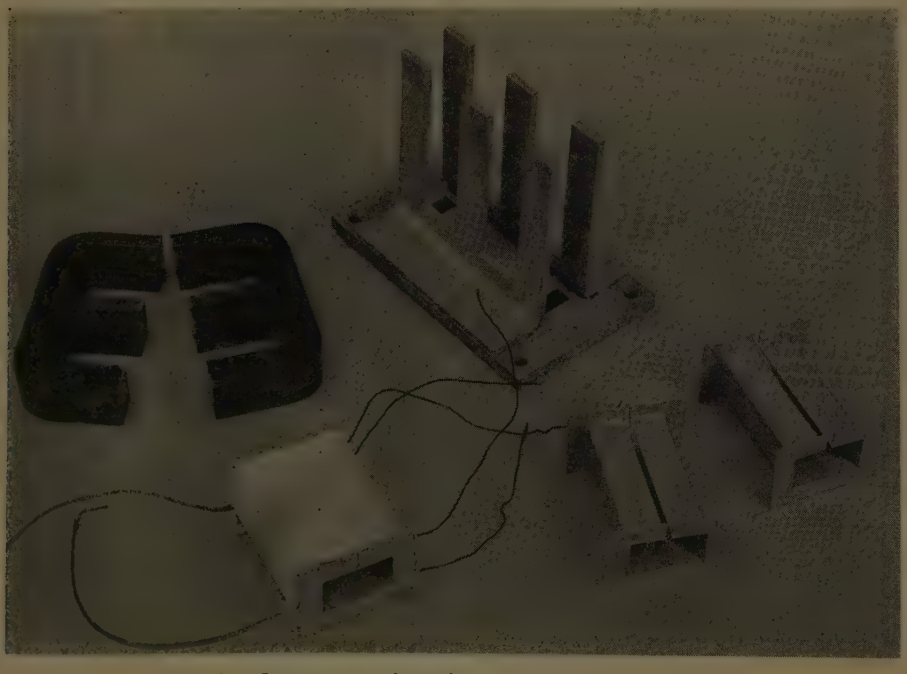

Fig. 6. Construction of transformer with thermal conductors

## Samples Illustrating Size Reduction

Fig. 4 shows on the left a transformer of reduced size which uses high-temperature insulation. At the right of Fig. 4 is a Fosterited transformer which is functionally equivalent. Except for the high-temperature silicone insulation system of the smaller transformer, the construction of the two units is similar. The smaller transformer is but one half the size and weight of the larger. High-temperature transformers similar to the one shown here have been tested under simulated operating conditions including loading, dielectric stress, vibration, humidity, thermal shock, and temperature aging for over 1,000 hours at a hot-spot temperature of 250 C (degrees centigrade) with no indications of failure.

These transformers use asbestos layer and interwinding insulation. They are encapsulated with Silastic rubber and vacuum-impregnated with a solventless silicone resin. The solventless silicone insures a thorough impregnation of the coil, while the Silastic provides for a high moisture resistance on the outside of the transformer and excellent insulation between terminals.

Fig. 5 shows on the left a 3-phase transformer of reduced size which uses metal thermal conductors to improve heat transfer in the transformer. The transformer on the right of Fig. 5 is one of three single-phase conventional transformers needed to do the same job. The 3-phase unit is built so that thermal conductors in the transformer carry the heat to the base and from there the heat passes into a "cold plate."

Fig. 6 shows the construction of the transformer. The frame is made of aluminum with the vertical members designed to conduct heat from the coil and core to the base. The coil is wound on an aluminum form with a slot to prevent a short-circuited turn. The flanges at the ends of the form keep the form from collapsing and also help to retain the wire. These flanges are insulated with split insulating washers that fit over the coil form. The core is fitted between the vertical members of the frame and the coils are fitted onto it. Close thermal contact is kept between the core, the coil, and these vertical members. Electrical insulation is insured by a tough anodized surface. The heat originating in the core flows readily through the iron of the core into the frame conductors and from there to the base. Likewise, heat from the coil flows through the thin coil section to the coil form and from there to the vertical conductors and then to the base. The base of the transformer must

**Table I. Three-Phase Transformer Performance**

Total transformer output = 590 volt-amperes
Total transformer loss = 49 watts
Transformer efficiency = 92.5%
D.C. output with silicon rectifiers = 320 volts at 1.65 amperes = 528 watts

be mounted on a cold plate. About 4 watts per square inch must be removed from the transformer base. The cold plate need not be very cold. In this instance 125 C was used and served its purpose well. The temperature rise above the base in such a transformer can be computed by adding all the incremental temperature rises along any path from the hot spot to the base of the transformer. That is,

$$T_h = T_c + T_1 + T_2 + T_3 \text{ etc.} \quad (9)$$

where

$T_h$ = hot-spot temperature
$T_c$ = base temperature

$T_1$, $T_2$, etc., are temperature rises in segments of the heat path. For any segment of the heat path

$$T = Kwd \quad (10)$$

where

$w$ = density of heat flux in watts/square inches
$d$ = length of segment in inches
$K$ = a constant of thermal resistivity which has a value of 0.1 for copper, 0.2 to 0.4 for aluminum alloys, and about 200 for the best grades of solid insulation

Tables I, II, and III give the performance of the transformer shown in Fig. 5. This,

**Table II. Three-Phase Transformer Weight Comparison**

| Old Design Item | Old Design Weight, Pounds | New Design Item | New Design Weight, Pounds |
|---|---|---|---|
| Three single-phase transformers | 7.50 | 3-phase transformer | 2.60 |
| Choke | 1.80 | Choke | 0.5 |
| Filament transformer | 0.33 | | |
| Total | 9.63 | | 3.1 |

**Table III. Hot-Spot Temperature Rise of New 3-Phase Transformer**

| Condition | Degrees, C |
|---|---|
| With cold plate and natural convection | 27 |
| With cold plate and insulating cover to eliminate convection and radiation from transformer surface | 33 |
| With natural convection and radiation only | 103 |
| Calculated temperature rise assuming conventional design and natural convection and radiation only | 127 |

although not an optimum design, demonstrates what can be accomplished.

A 3-phase core, solid-state rectifiers, and a bridge rectifier circuit also contributed to the size reduction of the magnetic components of this supply. The 3-phase core contributed about 15%, the bridge rectifier reduces the plate transformer size 25% and also reduces the filter choke size. The solid-state rectifiers make filament transformers unnecessary. Notice that over all, more than three-to-one weight reduction was accomplished.

## Conclusions

It has been demonstrated that transformer size and weight can be greatly reduced. The best results will be obtained when all the factors affecting size and weight of the design are considered. Experience has shown that usually the transformer size can be reduced to less than one half the size now being used if a higher heat density can be allowed in the smaller transformer. This paper has shown how higher heat density can be used when better cooling or high-temperature insulation are employed. The techniques described here will make possible lighter air-borne electronic equipment without sacrificing performance or reliability.

# Appendix

## Loss Equations

If transformer size reduction is accomplished by increasing frequency while holding all other variables constant, then from equation 8

$$V_f = V_1/V = (f/f_1)^{3/4} = (f_r)^{-3/4} \quad (11)$$

where

$V_f$ = the ratio of volume reduction
$V$ = volume before reduction
$V_1$ = volume after reduction
$f$ = frequency before size reduction
$f_1$ = frequency after size reduction
$f_r = f_1/f$ = ratio of frequency increase

Rearranging equation 11 becomes

$$f_r = (V_f)^{-4/3} \quad (12)$$

Similarly, when size reduction is accomplished by varying the other parameters one at a time.

$$(F_c)_r = (V_{Fc})^{-4/3} \quad (13)$$

$$B_r = (V_B)^{-4/3} \quad (14)$$

$$\Delta_r = (V_\Delta)^{-4/3} \quad (15)$$

When $B$ and $\Delta$ are changed together and at the same rate $\Delta = kB$ where $k$ is a constant. Substituting in equation 8

$$V_{\Delta B} = (B_S^2)^{-3/4} \quad (16)$$

Rearranging

$$B_S = (V_{\Delta B})^{-2/3} \quad (17)$$

where $B_S = B/B_1$ = ratio of flux increase = $\Delta/\Delta_1 = \Delta_S$ = ratio of current density increase, and $V_{\Delta B}$ = ratio of volume decrease when $\Delta$ and $B$ are increased together at the same rate.

If an existing transformer design is considered in which core loss = coil loss, then as size is being reduced:

$$\text{Loss ratio} = \frac{\text{core loss ratio} + \text{coil loss ratio}}{2} \quad (18)$$

As the frequency is increased the loss per cubic inch of iron increases as the 1.43 power of frequency. Loss per cubic inch of conductor remains constant since the current density remains constant. Then

$$L_f = \frac{V_f(f_r)^{1.43} + V_f}{2} \quad (19)$$

Substituting from equation 12

$$L_f = \frac{(V_f)^{-0.91} + V_f}{2} \quad (20)$$

where

$L_f$ = the ratio of loss increase as the transformer size is being reduced by increasing frequency while holding all other parameters constant

When the size reduction is accomplished by increasing $F_c$ the loss per cubic inch of conductor and the loss per cubic inch of core stay constant, but the ratio of conductor volume is $(F_c)_r(V_{Fc})$.

$$L_{Fc} = \frac{(F_c)_r(V_{Fc}) + V_{Fc}}{2} \quad (21)$$

Substituting from equation 13 and simplifying

$$L_{Fc} = \frac{(V_{Fc})^{-1/3} + V_{Fc}}{2} \quad (22)$$

where $L_{Fc}$ is loss ratio as the transformer size is being reduced by increasing coil space factor.

When the size reduction is accomplished by increasing current density $\Delta$, the loss per cubic inch of conductor increases as the square of current density while the core loss per cubic inch stays constant.

$$L_\Delta = \frac{V_\Delta + V_\Delta(\Delta_r)^2}{2} \quad (23)$$

Substituting from equation 15 and simplifying

$$L_\Delta = \frac{V_\Delta + (V_\Delta)^{-5/3}}{2} \quad (24)$$

where

$L_\Delta$ = loss ratio as size is decreased by increasing $\Delta$

The situation is the same when $B$ is increased except that coil loss and core loss are interchanged:

$$L_B = \frac{V_B^{-5/3} + V_B}{2} \quad (25)$$

When size reduction is achieved by increasing $B$ and $\Delta$ at the same rate, the loss per cubic inch of core increases as $B^2$ and the loss per cubic inch of coil varies as $\Delta^2$.

$$L_{\Delta B}=\frac{(V_{\Delta B})(B_s)^2+(V_{\Delta B})(\Delta_s)^2}{2} \quad (26)$$

Substituting for equation 17 and simplifying

$$L_{\Delta B}=(V_{\Delta B})^{-1/3} \quad (27)$$

where

$L_{\Delta B}$ = the loss ratio when transformer size is reduced by increasing both flux density and current density at the same rate

### Heat Density Equations

The heat density ratio is the loss ratio divided by the volume. When size reduction is accomplished by increasing frequency.

$$H_f=\frac{L_f}{V_f} \quad (28)$$

where

$H_f$ = ratio of heat dissipated per cubic inch after size reduction to heat dissipated, per cubic inch, before size reduction

The same is true for other parameters. For instance:

$$H_B=\frac{L_B}{V_B} \quad (29)$$

### Temperature Rise Equations

Assume that a transformer is to be reduced in size while total heat dissipated is to remain constant. Assume that in this transformer one half the temperature rise above ambient is at the surface of the transformer and that the other half of the temperature rise is due to temperature gradient within the transformer. Assume also that as the transformer size is reduced the relative heat distribution, thermal conductivity, and thermal emissivity remain constant. Then:

$$T_r=\frac{T_s+T_g}{2} \quad (30)$$

where

$T_r$ = ratio of the total temperature rise in the transformer of reduced size to the total in the transformer before size reduction

$T_s$ = ratio of temperature rise at the surface after size reduction to the rise at the surface before size reduction

$T_g$ = ratio of temperature rise inside the transformer after size reduction to the temperature rise before size reduction

$$T_s=\frac{1}{\text{ratio of surface area}}=\frac{1}{(V_r)^{2/3}}=V_r^{-2/3} \quad (31)$$

where

$V_r$ = the ratio of volume after size reduction to the volume before size reduction

$T_g$ = ratio of heat flow density × ratio of heat flow path length (32)

$$T_g=(V_r)^{-2/3}\times(V_r)^{1/3}=V_r^{-1/3} \quad (33)$$

Substituting equations 31 and 33 in equation 30

$$T_r=\frac{(V_r)^{-2/3}+(V_r)^{-1/3}}{2} \quad (34)$$

When size reduction is accomplished by increasing $B$ and $\Delta$ at the same rate, the relative heat distribution within the transformer remains constant. Then

$$T_{\Delta B}=L_{\Delta B}T_r \quad (35)$$

where

$T_{\Delta B}$ = temperature rise ratio in a transformer reduced by increasing $B$ and $\Delta$ at the same rate

Combining equations 27 and 35

$$T_{\Delta B}=\frac{(V_{\Delta B})^{-1}+(V_{\Delta B})^{-2/3}}{2} \quad (36)$$

## References


1. Keeping Aircraft Weight and Cost Down, **E. E. Heinemann.** *Journal*, Society of Automotive Engineers, Lancaster, Pa., vol. 63, no. 4, Apr. 1955, pp. 25–28.

2. Research and Development of New Design Methods for Power Transformers, **G. A. Forster, L. J. Stratton, H. L. Garbarino.** *Final report*, Electronics Parts and Materials Branch, Signal Corps Engineering Laboratories, Armour Research Foundation, Illinois Institute of Technology, Chicago, Ill., Mar. 1956, pp. 1–17.


# A Digital Flying Extensometer for Temper Rolling Mills


**N. S. WELLS**
MEMBER AIEE


STEEL STRIP is extremely hard after it has been cold rolled and it must then be softened by annealing. The next production process in the manufacture of tinplate is temper rolling. Temper mills are used to produce the desired surface finish in the strip with acceptable flatness plus the desired mechanical properties. The latter refers mainly to the elimination of a surface defect known as "stretcher-strain" markings which can occur in pressed-steel products. The tendency to this type of defect is directly related to the amount of yield-point elongation. If the steel can be subjected to a small amount of cold working this defect can be eliminated. The effect of various amounts of cold reduction upon the yield-point stress and the stress-strain relationship is shown in Fig. 1. It will be noted that with an extension of as little as 1.0% the yield point can be entirely suppressed.

This extension is achieved in a temper mill by a combination of strip tension and roll pressure in the two mills. Fig. 2 shows the pass line arrangement for such a mill. Certain of these mills can roll at strip speeds of 6,000 fpm (feet per minute). In all sections of the mill the strip is under substantial tension.

It is standard mill production practice to check the amount of work hardening produced in the mill by means of Rockwell hardness tests. Steel samples are taken from each coil, on the strip at the entry and exit sides of the mill. This is a spot check and can only be carried out by stopping the mill. One other method of checking strip elongation is by scribing the strip on the pay-off reel and rechecking the same scribe marks on the wind-up reel. Here a scribe gauge length of $12^1/_2$ inches is used resulting in a 1% extension figure for each 1/8-inch addition measured on the outgoing side of the mill. This scribing technique can only be carried out at a mill speed of around 200 fpm on a normal production run basis. For special tests however, the coil is run slowly through a processing line and scribed throughout its length. After temper rolling the coil is unwound and the elongation checked. This is a very costly and time consuming technique. There is therefore a definite need for an extens-


Paper 57-703, recommended by the AIEE Industrial Control Committee and approved by the AIEE Technical Operations Department for presentation at the AIEE Summer General Meeting, Montreal, Que., Canada, June 24–28, 1957. Manuscript submitted April 18, 1957; made available for printing June 14, 1957.



N. S. Wells is with The Steel Company of Canada, Ltd., Hamilton, Ont., Canada.

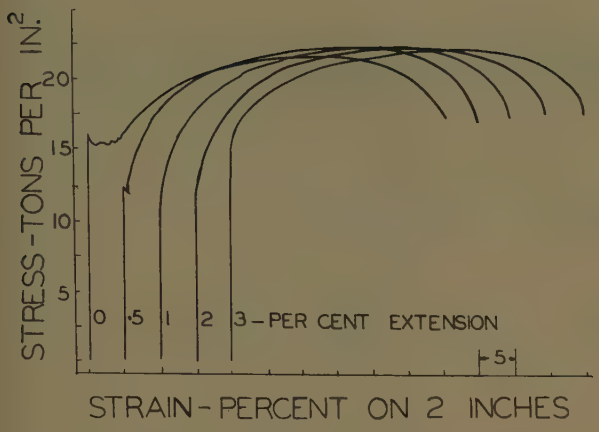


**Fig. 1 (left). The influence of cold rolling on the shape of the stress-strain curve of annealed low carbon steel**

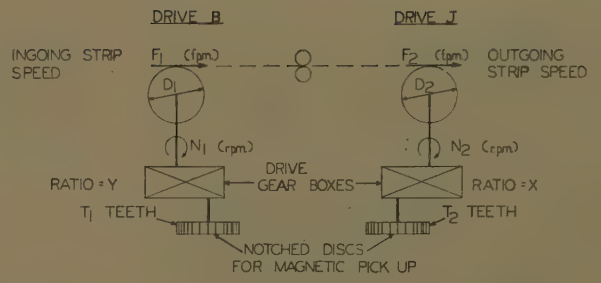


**Fig. 3 (right). Details of drives B and J**

ometer of suitable design which will permit a continuous observation and recording of strip elongation under all mill running conditions.

## Design Basis of Digital Extensometer

The strip speed at entry and exit ends of the mill is assumed to be identical to the peripheral speed of the bottom entry tension and bottom exit tension rolls respectively. This is a reasonable assumption since in both of these drives the strip is in close contact with a considerable proportion of the roll circumference and is subjected to both front and back tension.

The percentage strip elongation $E$ can be expressed as (Fig. 3):

$$E=\frac{F_2-F_1}{F_1}100\%$$

or $$\frac{N_2D_2-N_1D_1}{N_1D_1}100\%$$

If $P_1$ = pulses per minute detected by entry magnetic pick-up unit

Then

$$P_1=N_1T_1Y$$

Similarly

$$P_2=N_2T_2X$$

$$E=\frac{KP_2-P_1}{P_1}100\%$$

where $K=\text{constant}=\frac{D_2T_1Y}{D_1T_2X}$

Let $C_2$ be the total counts received at $J$ when $C_1$ counts are received at $B$, i.e., considering a per unit time basis.

If $C_1=1{,}000K$

Then

$$E=\frac{C_2-1{,}000}{1{,}000}100\%$$

This equation can be solved directly using a pair of multidecade counters.

One of these counters receives pulses from drive $B$ and is designated the "master" unit; the other is pulsed from drive $J$ and is the "slave" unit. The master unit is preset for a total pulse count of $1{,}000K$. Immediately coincidence is reached between preset and actual counts a blocking pulse switches off the pulse train to the slave counter. Then for a gated count of 1,000 on the slave unit there will be zero elongation in the strip, with the master counter preset for the correct value of $1{,}000K$.

1. For a count of 1,010, the elongation will be 1%.

2. For a count of 1,025, the elongation will be 2.5%.

The precise value of strip elongation from zero to 9.9% can therefore be directly obtained by reading the last two decades of the slave counter.

The accuracy of the results obtained is determined entirely by the accuracy of the calculated constant $K$. If a value $K^1=aK$ is used where $K$ is the correct constant value and $a$ is a factor which is not necessarily unity, the preset master count will be $1{,}000K^1$, and

$$E=\frac{KC_2-1{,}000K^1}{1{,}000K^1}100\%$$

$$=\frac{C_2-1{,}000a}{1{,}000a}100\%$$

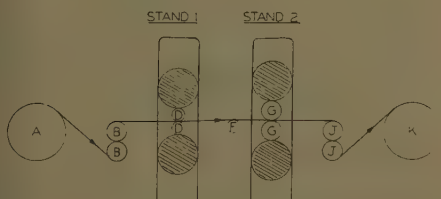


**Fig. 2. Two-stand temper mill pass line arrangement**

A—Payoff rolls
B—Tension rolls
D—Twelve-inch-diameter work rolls
F—Tensiometer roll
G—Twenty-inch-diameter work rolls
J—Exit tension rolls
K—Wind-up roll

Fig. 4 shows the resulting effects on calibration for various values of $a$. This suggests an alternative method of calibrating the extensometer using a prescribed coil and plotting actual and indicated elongations. The line $a=1.005$ is an example of some results obtained from an actual test. In this particular case the original constant was calculated to be 968 using gear ratios instead of gear tooth numbers. The value of $K$ indicated by the curve is $968/1.005=963$, which agreed with the recalculated constant using gear tooth numbers.

## Equipment Details

The general arrangement of the units comprising this extensometer is shown in Fig. 5. Noncontact magnetic pick-ups provide a simple method of counting pulses corresponding to roll revolutions, although there is the slight complication involved in mounting suitable toothed wheels. It is possible to use the actual mill rolls as the pulse producing units. In this case the outer edge of the roll has equally spaced slots milled around it. These slots need only extend a very small distance axially. This does not interfere in any way with the strip in the mill since the full face width of any roll is never fully utilized during rolling. The magnetic pick-up unit is then mounted below the roll to avoid damage to it during steel wrecks in the mill. In the 2-stand temper

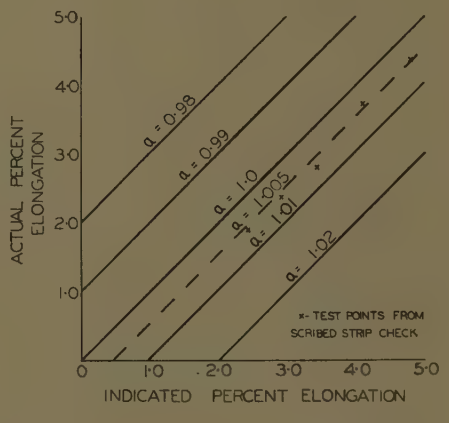


**Fig. 4. Calibration curves for various values of a**

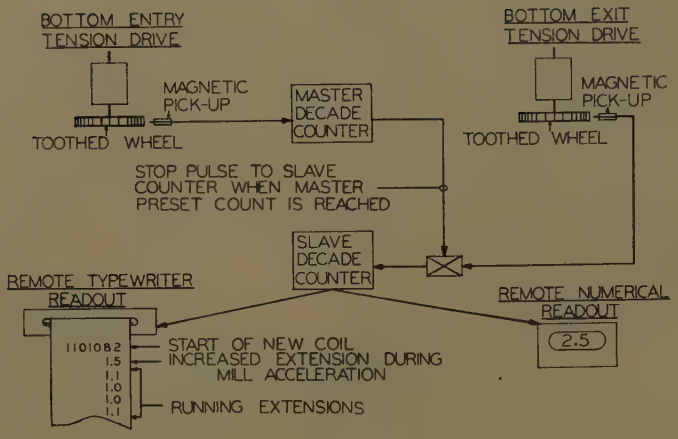


**Fig. 5. General arrangement of extensometer**

mill to which this digital extensometer has been applied, the tensiometer roll $F$ was modified in this fashion and operated satisfactorily. Using this technique it is possible to measure strip elongation on single-stand temper mills.

The particular type of magnetic units used will not follow a pulse count rate less than that corresponding to approximately 200 fpm strip speed. This is not particularly significant as this corresponds to thread speed on the mill, i.e., not a true rolling condition. The tooth numbers on the counting wheels are arranged to give a maximum count rate of 1,500 per second with the mill running at a speed of 3,000 fpm. This corresponds to a measurement of elongation on a 30-foot section of strip approximately.

Two identical 5-decade decimal counters utilizing cold-cathode glow-transfer counting tubes are used with maximum count rates of 4,000 per second. The master counter incorporates an electronic switching unit which blocks the pulse signals into the slave counter when the master preset count is reached. This preset count, i.e., $C_1 = 1{,}000K$ is set up on standard 10-position switches available on each decade. The slave counter is so arranged that remote indication is provided for the last two digits utilizing two numerical readout tubes. This information is held and displayed for a variable period of 2 to 15 seconds as desired, after which time the printed readout is typed out. Both counters are then automatically reset to zero and the complete cycle is repeated.

The print-out unit used employs a standard electric adding machine apart from the addition of an 11-key solenoid box mounted above the keys. The 60-cycle supply to the printer is removed by means of a limit switch on the main mill speed setting rheostat for strip speeds of less than 300 fpm. The solenoid keys can still be operated by the counter, but since a mechanical column transfer is used a seven figure print-out is obtained for the first reading after the supply has been restored. Identification of each new coil is readily obtained in this way. Fig. 5 indicates the type of record produced.

In this particular application the counter rack is mounted in the motor room adjacent to the mill. The numerical decimal read-out unit displaying strip extension is located at the rollers control position and the print-out unit is mounted in a suitable enclosure adjacent to the mill recorder. A test switch on the roller's visual read-out unit enables a check to be made of the two counters plus the slave pulse blocking circuit. This is achieved by switching the slave counter to a second magnetic pick-up unit on drive $B$. If everything is functioning correctly the two counters will always show the same count, which will be the master preset count. The roller's unit similarly will always show the same two digits.

## Conclusion

This digital extensometer is basically simple, the quantity of equipment involved is small and relatively cheap. There are few if any installation problems and calibration can be readily checked. This general type of equipment involving the numerical presentation of information will become general in steel plant operations in particular, and industrial concerns in general. Other types are available but would appear to be inherently more complicated.[1,2]

By using a setting on the master counter of $10{,}000K$ the extension can be read to 0.01% or more if higher powers of ten are used as settings on the master counter. The strip length over which this 0.01% reading is obtained will be 300 feet. However, if higher speed counters are used then three figure percentage elongation could still be obtained over a 30-foot strip length at a count rate of 10,000 counts per second, i.e., using more counts per foot of strip. If more counts are made per foot of strip but the $1{,}000K$ setting is used on the master counter, elongation will then be measured over 3 feet of strip and a reading will be obtained in 1/10 second approximately.

It then becomes feasible to consider a closed-loop-type of control system utilizing this digital extensometer information as the feedback in a sampling type of servo system and controlling the strip elongation in the mill to any desired set value. Results obtained on this particular temper mill indicate that running conditions obtained are very stable and the strip elongation remains essentially constant. Extension does increase during acceleration and deceleration—indicating some inaccuracy in the setting of mill inertia compensation circuits. Automatic extension control would not appear to be justified in this particular case.

However the use of this extensometer for closed loop control in other manufacturing processes can be considered. One application would be on paper machine drives where extremely accurate control of the speed difference between two adjacent stands is necessary. Here the digital extensometer could perhaps be used as a vernier-type sampling servo control in conjunction with a main section voltage control. Another measurement application would be on a multistand hot strip mill where the elongation between mills could be measured, and for known steel input thicknesses, the gauge between mills could be calculated.

## References

1. Extensometer. *U. S. patent nos. 2,447,208; 2,447,209* and *2,474,116*, United States Steel Company, Pittsburgh, Pa.

2. Baldwin Magnetic Extensometer. *Report no. MW/A/34/54*, British Iron and Steel Research Association, London, England, 1954.

# Criteria for Industrial Application of Single-Phase Transmission Lines, 400 to 20,000 Cycles

W. A. MUNSON
ASSOCIATE MEMBER AIEE

A. J. GERMAIN
NONMEMBER AIEE

SINCE the early days of alternating current, electrical engineers have designed many forms of generating devices to enable them to study the effects of different frequencies on an electric circuit or machine. This study has been a continuing one due to the foreseeable advantages of high-frequency power in certain areas.

During the past decade, the use of audio frequencies has been increasing. This increase has not been limited to merely a higher kilowatt consumption, but has also taken the form of an increased number of industrial and commercial applications. Also, the increased use of audio frequencies has resulted in different methods of generation of these frequencies.

The use of audio-frequency (a-f) power is a recognized power source, today, for such various functions as internal grinding, portable tools for high-production assembly lines, woodworking machines, industrial and commercial high-efficiency fluorescent lighting, induction heating, electroluminescence panels, and ultrasonic applications.

Table I lists the known applications and the range of frequencies presently used for the particular application.

## Methods of Generation

The methods of generating audio frequencies have kept pace somewhat with the use of audio frequencies, thus resulting in several generating devices that are now fully developed and a few newer types that are still in the developmental stage. This parallel development of generation with application has provided the impetus for some of the newer higher frequency applications.

Some of the fully developed methods are the motor-generator combinations, the electronic tube oscillator, and the spark-gap-type generator. These devices are used over a wide range of frequencies, and when coupled with frequency multipliers, are capable of producing the ultrasound frequency, 20,000 cps (cycles per second).

The motor-generator combinations, when fully developed, use a conventional motor, usually 60-cycle a-c, driving an inductor or salient-pole generator. The newer trend today is to the use of a permanent-magnet-type generator rather than those previously mentioned. However, this newer form of generator has not yet been fully developed and as such its application is still rather limited.

The new transistor oscillator is now in a full-scale development program as it is anticipated that this new form of generation will overcome many of the shortcomings of audio-frequency present generation schemes.

The normal frequencies which have been standardized on and are commercially available are 400–500 cps, 1,000 cps, 3,000 cps, 10,000 cps, and 20,000 cps. On some of the higher frequencies, 10,000 and 20,000 cps, the required frequency may be obtained through the use of a generator producing a lower frequency coupled with a frequency doubler or tripler.

## Audio-Frequency Transmission

As is the case with direct current and the conventional power frequencies, 60 cps and below, audio frequencies also require the use of metallic conductors to transmit their power to remote locations. However, unlike direct current or the conventional power frequencies, great consideration must be given to the transmission system to obtain efficient transmission of the a-f power.

The factors that must be considered with regard to the transmission circuit are the same as those for conventional power frequencies: current rating of the conductors, inductance of the conductor, and voltage and/or power loss in the transmission system. However, as all of these elements bear a relationship to frequency, minute consideration must be given to the system to obtain efficient transmission at the relatively high frequencies in question, the audio frequencies.

Fig. 1 shows the maximum allowable reactance, in ohms, which can be tolerated for various loads without leaving a rise in voltage at the point of load utilization greater than 5% after correcting the generator load to unity power factor through the use of capacitors at the load utilization point. The voltage rise of 5% is based on a nonfunctioning load and a fully loaded generator. As most a-f generators are designed to supply only a real power load, kilowatts only, the necessity for transmission system and load power factor correction is obvious. Where load fluctuations will be present, the over-all complete system must be analyzed for all possible load conditions to prevent unduly high overvoltages at the load when the generator is not fully loaded.

Thus, any transmission system selected should not exceed the maximum allowable line reactance values given in Fig. 1 if satisfactory and efficient a-f power transmission is to be obtained.

It is desirable to use standard cable if at all possible, both from the standpoint of cost and availability. Table II gives the properties for various cable combinations as shown in Fig. 2.[1] This table gives cable ratings for the commercially available standard audio frequencies. Below 400 cycles, standard 60-cycle cable data are used as a basis for choosing a transmission system.

Fig. 2 shows the arrangement of the cables as used in Table II, and also the current distribution that can be anticipated in the particular cable arrangement selected. The table gives not only the anticipated ohms but also the allowable current capacity of the particular cable arrangement as well as its expected wattage loss. All values given are on a per-foot basis and include both conductors for a single-phase 2-conductor system.

Tables III and IV[2] give characteristics of electric cables of the type usually used in the arrangement given in Fig. 2. The use of these two tables in conjunction with Fig. 2 will enable the determination of the over-all size of the transmission system.

The selection of a transmission system conductor size becomes simple by merely

Paper 57-1021, recommended by the AIEE Industrial Power Systems Committee and approved by the AIEE Technical Operations Department for presentation at the AIEE Fall General Meeting, Chicago, Ill., October 7–11, 1957. Manuscript submitted June 10, 1957; made available for printing August 13, 1957.

W. A. MUNSON and A. J. GERMAIN are both with the Westinghouse Electric Corporation, East Pittsburgh, Pa.

The authors wish to acknowledge the assistance of members of the engineering department of the Westinghouse Industrial Electronics Division in the preparation of many of the tables included in this paper, and to express their appreciation to the Ladish Company for permission to discuss the installed high-frequency system.

**Table I. Applications and Associated Frequencies**

| Frequency, Cycles | Application |
|---|---|
| 180 | Resistance welding, continuous tube mills |
| 180–360 | High-cycle tools |
| 180–420 | High-speed grinders |
| 180–720 | High-speed woodworking machines |
| 360–500 | Ozonators |
| 360–10,000 | High-efficiency fluorescent lighting* |
| 400–500 | SONAR |
| 400, 600, 800 | Aviation industry |
| 500 | Alternating current to high-voltage direct current, 20 kv to 1,500 kv (for cable testing) |
| 600, 800 | Navy |
| 960, 3,000, 4,320, 6,600, 10,000 | Induction heating |
| 3,000 | Electroluminescence panels |
| 20,000 | Ultrasound applications |

* 840 cycles is the most popular frequency at the present time for high-efficiency fluorescent lighting.

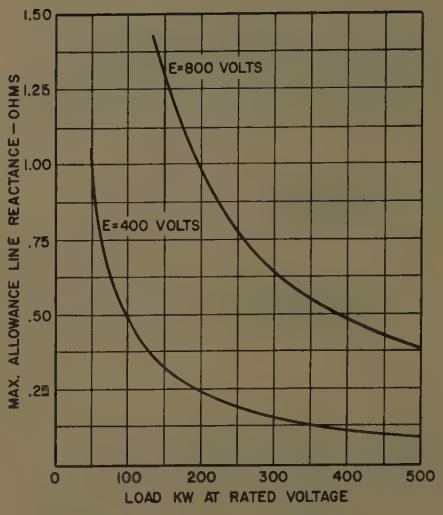


**Fig. 1. Maximum allowable line reactance based on ability to tune generator load to unity power factor with 5% rise in voltage at load utilization**

determining what current must be handled, and then making certain that the conductor reactance is not greater than the allowable maximum value as determined from Fig. 1. The third feature which must be checked is the power loss in the transmission system. For practicability, this is usually limited to 5% of the load rating. Here the 5% value is a rule-of-thumb feature and must be balanced against the increased cost of the transmission system to reduce the power loss to 5% assuming the other features, current and maximum allowable transmission reactance ohms, have been met. However, experience has indicated that a maximum loss of more than 5% is normally very uneconomical.

The presently preferred system of the various arrangements shown in Fig. 2 is the one where four conductors are used with similar poloraties opposite. This arrangement has had most success due to its relatively low value of reactance. Several large installations consisting of several generators paralleled at a central location and transmitting the power then for several hundred feet use this 4-conductor method.

Fig. 3 shows a comparison between the three systems outlined in Fig. 2. This comparison is between copper area, reactance, and resistance for various cable combinations, all of which are capable of handling the same amount of a-f current and/or power.

## Future Trends

As the use of a-f power increases, the requirement of using larger, centrally located generators becomes an economical requirement. The problem of transmitting these larger blocks of power to a point of utilization has been the subject of tremendous activity.

The coaxial system, used for many years for frequencies well above the audio range, has been vigorously investigated. The adaptability of the type of system has been enhanced through the recent development of a portable water-cooled coaxial conductor. However, such a system lends itself to relatively short runs which is not a desired feature.

Another type of transmission system, known as the concentric conductor system, has been in service for several years at the Ladish Company Forge Plant in Cudahy, Wis. This system which has been patented by Ladish has enjoyed a degree of success equal to its original expectations.

The concentric conductor system is similar to a coaxial system in that the two conductors are co-axially formed. However, whereas the inner conductor is located at the center of the cable for the coaxial system, the inner conductor of the concentric conductor system is located as tight against the outer conductor as insulation will permit. Fig. 4 shows the major difference between a coaxial system and a concentric conductor system.

The system presently in use at the afore-mentioned plant transmits 3,600 cps power at 4,800 volts which is then stepped down to either 200 or 400 volts at the various utilization points. At the present time, two 1,750-kw 3,600-cps generators are in service with a third 1,750-kw generator presently being designed to parallel with the two existing units. This third unit, when installed, will result in a total installed capacity of 5,250 kw of 3,600 cps power.

The 3,600-cycle power is distributed throughout the plant through the use of 4- and 2-inch concentric conductor transmission lines with 2-inch concentric conductors used for power take-offs and

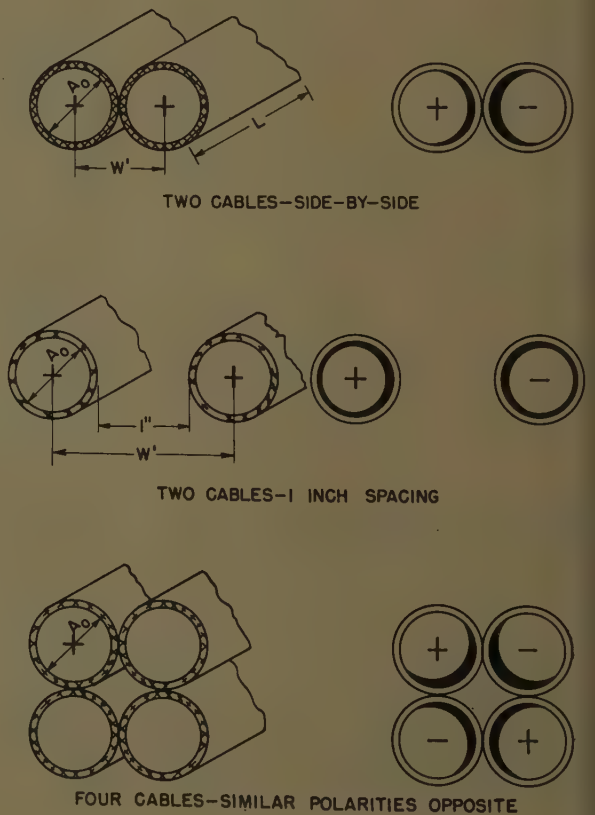


**Fig. 2. Typical conductor arrangements and current distribution in the conductors**

**Table II. Resistance and Impedance Values for Cables in Free Air: Extra Flexible Stranded Cable at 30 C Ambient Temperature,* 85 C Maximum Copper Temperature**

| Cable Size, B&S or MCM† | Two Cables, Side by Side‡ | | | | Two Cables, 1-Inch Spacing‡ | | | | Four Cables, Similar Polarities Opposite‡ | | | |
|---|---|---|---|---|---|---|---|---|---|---|---|---|
| | Watts Per Foot Run | Current Rating, Amperes | Resistance Milliohms Per Foot | Impedance, Milliohms Per Foot | Watts Per Foot Run | Current Rating, Amperes | Resistance, Milliohms Per Foot | Impedance, Milliohms Per Foot | Watts Per Foot Run | Current Rating, Amperes | Resistance, Milliohms Per Foot | Impedance, Milliohms Per Foot |
| **400–500 Cycles** | | | | | | | | | | | | |
| 14 | 8.0 | 34 | 6.7 | 6.7 | 8.0 | 34 | 6.8 | 7.0 | 11.9 | 62 | 3.4 | 3.4 |
| 10 | 8.7 | 62 | 2.45 | 2.6 | 8.7 | 63 | 2.43 | 2.25 | 12.5 | 105 | 1.2 | 1.28 |
| 6 | 11.6 | 98 | 1.2 | 1.18 | 12.0 | 110 | 1.03 | 1.35 | 14.8 | 180 | 0.47 | 0.47 |
| 4 | 11.8 | 125 | 0.7 | 0.72 | 12.2 | 140 | 0.61 | 0.95 | 14.9 | 230 | 0.29 | 0.30 |
| 2 | 12.0 | 173 | 0.45 | 0.62 | 12.7 | 190 | 0.33 | 0.82 | 15.0 | 295 | 0.19 | 0.255 |
| 1/0 | 13.6 | 240 | 0.35 | 0.53 | 14.0 | 270 | 0.187 | 0.75 | 17.8 | 410 | 0.11 | 0.22 |
| 4/0 | 15.2 | 290 | 0.3 | 0.51 | 16.3 | 345 | 0.13 | 0.67 | 20.0 | 520 | 0.075 | 0.19 |
| 250 | 17.1 | 330 | 0.22 | 0.48 | 18.8 | 395 | 0.12 | 0.63 | 22.1 | 590 | 0.065 | 0.19 |
| 350 | 18.9 | 370 | 0.18 | 0.45 | 20.4 | 450 | 0.10 | 0.59 | 24.6 | 670 | 0.054 | 0.17 |
| 500 | 20.8 | 440 | 0.15 | 0.40 | 23.0 | 600 | 0.0775 | 0.54 | 26.8 | 780 | 0.045 | 0.16 |
| **1,000 Cycles** | | | | | | | | | | | | |
| 14 | 8.0 | 34 | 6.90 | 7.0 | 8.0 | 34 | 6.82 | 7.57 | 11.6 | 58 | 3.45 | 3.5 |
| 10 | 8.7 | 59 | 2.50 | 2.82 | 8.7 | 60 | 2.40 | 3.50 | 12.5 | 100 | 1.25 | 1.41 |
| 6 | 11.6 | 98 | 1.21 | 1.76 | 12.2 | 107 | 1.06 | 2.52 | 14.8 | 176 | 0.484 | 0.704 |
| 4 | 11.3 | 123 | 0.75 | 1.37 | 12.4 | 140 | 0.630 | 2.18 | 14.9 | 224 | 0.30 | 0.548 |
| 2 | 11.5 | 151 | 0.507 | 1.17 | 12.6 | 175 | 0.410 | 1.88 | 15.0 | 272 | 0.203 | 0.468 |
| 1/0 | 13.6 | 197 | 0.350 | 1.025 | 13.1 | 234 | 0.270 | 1.71 | 17.8 | 355 | 0.140 | 0.410 |
| 4/0 | 15.2 | 240 | 0.265 | 0.915 | 16.7 | 296 | 0.190 | 1.52 | 20.0 | 433 | 0.106 | 0.366 |
| 250 | 16.9 | 270 | 0.234 | 0.890 | 19.0 | 328 | 0.176 | 1.47 | 22.1 | 487 | 0.093 | 0.356 |
| 350 | 18 9 | 305 | 0.203 | 0.816 | 20.3 | 372 | 0.147 | 1.35 | 24.6 | 550 | 0.081 | 0.326 |
| 500 | 20.6 | 358 | 0.160 | 0.752 | 24.6 | 463 | 0.115 | 1.25 | 26.6 | 645 | 0.064 | 0.301 |
| **3,000 Cycles** | | | | | | | | | | | | |
| 14 | 7.9 | 33 | 7.25 | 8.06 | 7.9 | 34 | 6.86 | 11.3 | 11.3 | 56 | 3.62 | 4.03 |
| 10 | 8.5 | 56 | 2.70 | 4.82 | 8.6 | 59 | 2.46 | 8.06 | 12.2 | 95 | 1.35 | 2.41 |
| 6 | 11.6 | 96 | 1.26 | 3.94 | 12.0 | 105 | 1.10 | 6.85 | 14.8 | 172 | 0.504 | 1.58 |
| 4 | 11.9 | 117 | 0.87 | 3.54 | 12.2 | 129 | 0.735 | 6.30 | 15.6 | 212 | 0.348 | 1.41 |
| 2 | 12.0 | 130 | 0.71 | 3.10 | 12.7 | 148 | 0.580 | 5.40 | 15.7 | 235 | 0.284 | 1.24 |
| 1/0 | 13.8 | 158 | 0.552 | 2.72 | 14.6 | 185 | 0.426 | 4.94 | 18.0 | 285 | 0.221 | 1.09 |
| 4/0 | 15.2 | 187 | 0.434 | 2.40 | 16.1 | 224 | 0.320 | 4.40 | 19.8 | 338 | 0.173 | 0.96 |
| 250 | 17.2 | 211 | 0.384 | 2.38 | 18.9 | 255 | 0.291 | 4.30 | 22.5 | 382 | 0.154 | 0.95 |
| 350 | 18.2 | 236 | 0.325 | 2.17 | 20.4 | 296 | 0.233 | 3.90 | 23.5 | 425 | 0.130 | 0.87 |
| 500 | 20.8 | 278 | 0.270 | 2.04 | 22.5 | 340 | 0.195 | 3.60 | 27.0 | 500 | 0.108 | 0.82 |
| **10,000 Cycles** | | | | | | | | | | | | |
| 14 | 8.1 | 33 | 7.44 | 16.50 | 8.1 | 34 | 6.99 | 29.80 | 13.4 | 60 | 3.72 | 8.25 |
| 10 | 8.75 | 53 | 3.10 | 13.30 | 9.0 | 56 | 2.85 | 25.30 | 14.0 | 95 | 1.55 | 6.65 |
| 6 | 11.0 | 76 | 1.93 | 11.95 | 11.6 | 82 | 1.71 | 22.13 | 14.5 | 137 | 0.772 | 4.78 |
| 4 | 11.8 | 91 | 1.42 | 10.50 | 12.0 | 100 | 1.205 | 20.00 | 15.2 | 164 | 0.568 | 4.20 |
| 2 | 12.3 | 100 | 1.23 | 10.05 | 12.8 | 113 | 1.000 | 17.40 | 15.9 | 180 | 0.490 | 4.02 |
| 1/0 | 13.5 | 117 | 0.99 | 8.29 | 15.0 | 139 | 0.775 | 15.91 | 17.3 | 210 | 0.395 | 3.31 |
| 4/0 | 15.3 | 145 | 0.725 | 7.64 | 16.6 | 176 | 0.533 | 14.10 | 20.0 | 262 | 0.290 | 3.06 |
| 250 | 17.2 | 162 | 0.655 | 7.57 | 18.6 | 194 | 0.495 | 13.70 | 22.2 | 292 | 0.262 | 3.03 |
| 350 | 19.5 | 184 | 0.575 | 6.71 | 20.4 | 222 | 0.415 | 12.67 | 25.3 | 332 | 0.230 | 2.69 |
| 500 | 21.2 | 208 | 0.480 | 6.41 | 22.7 | 258 | 0.340 | 11.83 | 27.1 | 375 | 0.192 | 2.56 |
| **20,000 Cycles** | | | | | | | | | | | | |
| 14 | 8 | 32 | 7.8 | 30.0 | 8.1 | 34 | 7.0 | 57.5 | 13.0 | 57.6 | 3.9 | 12.8 |
| 10 | 8.7 | 49.5 | 3.58 | 25.45 | 9.1 | 51.9 | 3.4 | 49.5 | 14.0 | 84 | 2.0 | 11.3 |
| 6 | 11.6 | 66.2 | 2.65 | 23.2 | 11.0 | 66.5 | 2.5 | 43.7 | 14.8 | 117 | 1.08 | 8.3 |
| 4 | 11.9 | 74.2 | 2.17 | 20.3 | 11.7 | 76.6 | 2.0 | 39.5 | 15.6 | 135 | 0.865 | 7.4 |
| 2 | 12.4 | 79.8 | 1.96 | 19.8 | 13.0 | 96.5 | 1.6 | 34.6 | 16.0 | 144 | 0.765 | 7.05 |
| 1/0 | 13.6 | 99.4 | 1.38 | 16.2 | 15.0 | 109 | 1.26 | 31.5 | 17.8 | 168 | 0.63 | 5.7 |
| 4/0 | 15.4 | 120.0 | 1.065 | 15.1 | 16.6 | 142 | 0.82 | 28.5 | 20.0 | 208 | 0.46 | 5.3 |
| 250 | 17.2 | 132.0 | 0.989 | 14.9 | 19.0 | 161 | 0.78 | 27.0 | 22.5 | 238 | 0.4 | 5.25 |
| 350 | 20.1 | 151.0 | 0.885 | 13.47 | 24.0 | 190 | 0.67 | 25.5 | 25.5 | 266 | 0.36 | 4.6 |
| 500 | 21.7 | 176.0 | 0.702 | 12.7 | 22.7 | 205 | 0.54 | 23.3 | 27.1 | 296 | 0.31 | 4.35 |

* Multiply ampere rating by following value b for rating at other than 30 C (degrees centigrade) ambient: at 20 C, by 1.08; at 40 C, by 0.90; at 50 C, by 0.79.
† Brown and Sharpe gage or thousand circular mils.
‡ For cables in nonmagnetic conduit, multiply current values by 0.73.

**Table III. Characteristics of Electric Cable: Extra Flexible, Varnished Cambric Insulation, Glyptal Treated Braid Cover, 85 C Maximum Copper Temperature**

| Size, B&S or Closest MCM* | Conductor: Number of Strands | Conductor: Size of Strands | Conductor: Insulated Thickness in 64ths | Diameter in Inches: Conductor | Diameter in Inches: Over-All | Weight Per 1,000 Feet, Pounds |
|---|---|---|---|---|---|---|
| 14 | 19 | 27 | 2 | 0.071 | 0.185 | 24 |
| 10 | 27 | 24 | 3 | 0.121 | 0.265 | 65 |
| 6 | 61 | 24 | 4 | 0.181 | 0.370 | 156 |
| 4 | 125 | 24 | 4 | 0.261 | 0.455 | 268 |
| 2 | 175 | 24 | 5 | 0.360 | 0.585 | 361 |
| 0 | 275 | 24 | 5 | 0.460 | 0.685 | 532 |
| 0000 | 550 | 24 | 5 | 0.613 | 0.855 | 976 |
| 250 | 650 | 24 | 6 | 0.673 | 0.945 | 1190 |
| 350 | 925 | 24 | 6 | 0.799 | 1.070 | 1642 |
| 500 | 1325 | 24 | 7 | 0.970 | 1.275 | 2345 |

* Brown and Sharpe gage or thousand circular mils.

**Sable IV. Characteristics of Electric Cable: Standard Strand, Varnished Cambric Insulated, Single Braided, 85 C Maximum Copper Temperature**

| Size, B&S or Closest MCM* | Conductor: Number of Strands | Conductor: Diameter of Each Strand, Inches | Insulated Thickness in 64ths | Diameter in Inches: Conductor | Diameter in Inches: Over-all | Weight Per 1,000 Feet, Pounds |
|---|---|---|---|---|---|---|
| 6 | 7 | 0.0612 | 4 | 0.184 | 0.373 | 130 |
| 4 | 7 | 0.0772 | 4 | 0.232 | 0.422 | 180 |
| 2 | 7 | 0.0974 | 4 | 0.292 | 0.482 | 265 |
| 0 | 19 | 0.0745 | 5 | 0.373 | 0.594 | 415 |
| 0000 | 19 | 0.1055 | 5 | 0.528 | 0.749 | 765 |
| 250 | 37 | 0.0822 | 6 | 0.575 | 0.828 | 908 |
| 350 | 37 | 0.0973 | 6 | 0.681 | 0.955 | 1260 |
| 500 | 37 | 0.1162 | 6 | 0.814 | 1.172 | 1866 |

* Brown and Sharpe gage or thousand circular mils.

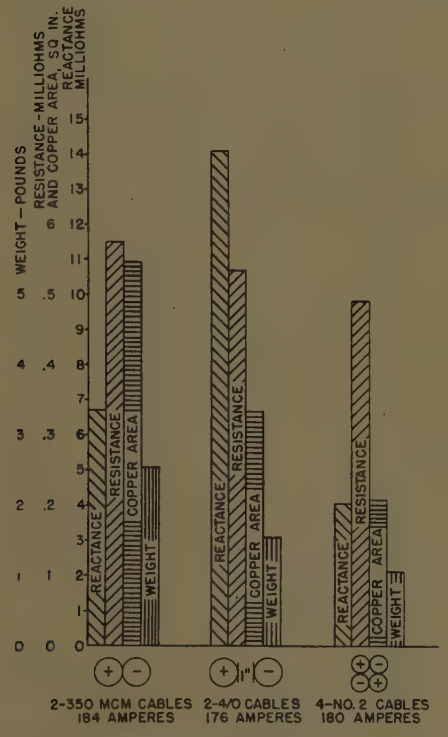


**Fig. 3. Comparison of various conductor arrangements, each capable of handling 175 amperes at 10,000 cps**

secondary distribution when required. The total length of the high-voltage (4,800-volt) distribution system is now equal to approximately 1,000 feet of 4-inch concentric conductors and 2,000 feet of the 2-inch concentric conductor. In addition, there is approximately 1,000 feet of 4-inch and 2-inch concentric conductors used for the low-voltage distribution.

The concentric conductor system has many advantages of which the following are the major ones:

1. Rigid all-metallic conductor system.
2. Grounded outer shell.
3. Very desirable electrical characteristics; i.e., low reactance, low resistance, reduced copper cross section.
4. Complete selection of power take-off fittings and expansion points.
5. Increased current capacity, if necessary, by gas or liquid cooling.
6. Relative simplicity coupled with low installation costs.

Fig. 5 shows the comparison between a concentric-conductor and a 4-conductor

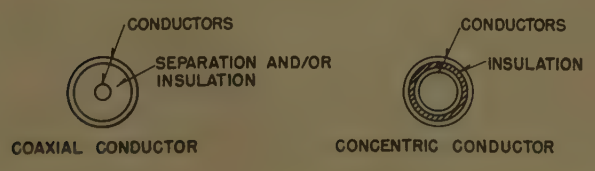


**Fig. 4. Comparison between a conventional coaxial conductor and a concentric conductor**

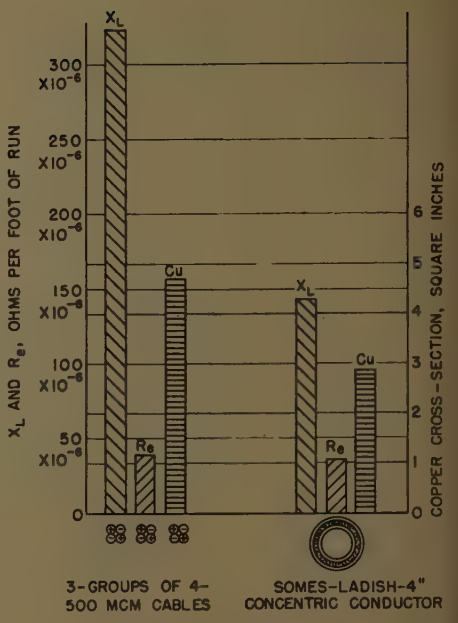


**Fig. 5. Comparison of physical characteristics for a 4-cable conductor arrangement and the Somes-Ladish 4-inch concentric conductor**

line, similar polarities opposite, for resistance, reactance, and copper cross section

## Conclusions

The information given in Tables II–IV used in conjunction with Fig. 1 will enable the engineer, who is faced with the necessity of designing an a-f transmission system, to determine what size and/or type of conductor arrangement to use. Also, the information given will enable him to allow for the required amount of space for installation of an a-f transmission system. At all times, however, it must be remembered that the system, when once selected, is not to be placed in magnetic conduit as the frequencies in question, 400 cps up to and including 20,000 cps, would induce excessive eddy current losses in conventional magnetic material conduit. Thus, for all a-f transmission systems, the conductors, when necessary to be enclosed in conduit, must be enclosed by nonmagnetic material.

## References


1. Characteristics of Single-Conductor Electric Cable at High Frequency, J. T. Sabol. *AIEE Transactions*, vol. 74, pt. III, 1955, pp. 1280–85.
2. Industrial Electronics Reference Book (book), Westinghouse Electronics Engineers. John Wiley & Sons, Inc., New York, N. Y., 1948, pp. 386–87.
3. Induction Heating (book), N. R. Stansel. McGraw-Hill Book Company, Inc., New York, N. Y., 1949, chap. 8.
4. Inductance Calculations (book), F. W. Grover. D. Van Nostrand Company, Inc., Princeton, N. J., 1946, chap. 24.

5. Standard Handbook for Electrical Engineers (book), A. E. Knowlton. McGraw-Hill Book Company, Inc., New York, N. Y., eighth edition, 1949, sects. 12–476, 12–477, 15–112.

6. Impedance Data for 400-Cycle Aircraft Distribution Systems, D. W. Exner, G. H. Singer, Jr. *AIEE Transactions*, vol. 71, pt. II, 1952, pp. 410–19.

7. Utilization of 300 to 2,000 Cycle Power in Industry, V. C. Geckler. *Proceedings*, American Power Conference, Chicago, Ill., vol. 18, 1956, pp. 482–91.

# The Selection and Use of Servo Performance Criteria

W. C. SCHULTZ
ASSOCIATE MEMBER AIEE

V. C. RIDEOUT
MEMBER AIEE

THE APPLICATION of performance criteria in the analysis, and more particularly in the synthesis, of servo systems is a matter of importance, but it is one of considerable difficulty as compared with the application of stability criteria. Although it is generally agreed that concise criteria of performance are desirable, there has been no general agreement as to what criteria should be used. This is not too surprising, for surely there should be many criteria to fit the various requirements of different servos.

Perhaps the simplest mathematical statement that can be made regarding servo performance is the error, $e(t)$, defined as the difference between the input and output,

$$e(t)=r(t)-c(t) \tag{1}$$

For comparison purposes, however, such a function of time is not a convenient expression, since, in general, it is hard to define just exactly what is meant by "comparison" of two functions. Concepts that might be borrowed from the mathematician here include "approximation in the mean," "uniform convergence," the value of the maximum absolute difference, and the like. The underlying difficulty encountered in the establishment of a general performance criterion is the choice of the best concept to use in any particular case. One very reasonable procedure is to choose, as a basis for a general criterion, a functional,[1] that is to say, a number, which is determined by the whole range of any one of a class of functions.* Although, to the authors' knowledge, no general theory has been set forth which proposes functionals as a means of stating performance criteria, there have been various proposals and suggestions of specific cases in the literature.

If $r(t)$ and $c(t)$ are stationary random processes, the ordinary mean-square measure of error,

$$E=\lim_{T\to\infty}\frac{1}{2T}\int_{-T}^{T}e^2(t)\,dt \tag{2}$$

is often used. In this paper, only transient input functions will be considered. In such cases, as discussed by Hall,[2] a measure proportional to the mean-square error may be written as

$$E=\int_0^\infty e^2(t)\,dt \tag{3}$$

An extension of equation 2 to the case in which delay (or advance) of the output is considered has been given by Spooner and Rideout.[3] Their form, called the generalized error function (GEF), may also be adapted to transient inputs and will be discussed in more detail in a subsequent section of this paper.

A simpler measure of error, proposed by Oldenbourg and Sartorious,[4] is

$$E=\int_0^\infty e(t)\,dt \tag{4}$$

A number of other measures of error have been proposed[5–10] and used, including the integral of the absolute error,

$$E=\int_0^\infty |e(t)|\,dt \tag{5}$$

One very useful measure, the integral of time multiplied by absolute error (ITAE), has been proposed by Graham and Lathrop[10–12]

$$E=\int_0^\infty t|e(t)|\,dt \tag{6}$$

Inspection of equations 2 through 6 shows that they are functionals, since once the function of $e(t)$, such as $e^2$, $e$, $|e|$, etc., is specified, together with its range, a number $E$ is obtained.

If an integral such as one of these is regarded as a satisfactory measure of error, a criterion or rule for choice of the best servo, as parameters are varied, is that this integral shall be a minimum. However, nothing has yet been said to indicate *how* the measure or measures are to be selected. A suitable measure should: (a) be responsive to the characteristics which a designer must optimize in a given servo, and (b) be susceptible to convenient computer mechanization.

In this paper some general measures of servo error will be examined and an attempt will be made to show how specific forms may be selected and used to suit the special needs of a servo designer in typical situations. As mentioned in the foregoing, only transient or step input functions will be considered. A point which should be emphasized is that the criteria to be discussed may be applied to nonlinear as well as linear servos.

## A General Mathematical Expression for Error Measure

One general form of a metric, or measure of error, is the functional

$$E=\int_0^\infty F[e(t),\,t]\,dt \tag{7}$$

where $F$ is some function of $e(t)$, and of $t$, the time measured from the initiation of the transient input $r(t)$. Equation 7 clearly includes, as special cases, equations 3–6. For example, $F$ may be the function

$$F[e(t),\,t]=t|e(t)| \tag{8}$$

so that the general form reduces to the ITAE of equation 6. Similarly, expressions can be found for $F$ corresponding to the forms of equations 3, 4, and 5. In this paper the expression in equation 7 will be considered as the general form of the

Paper 57-1033, recommended by the AIEE Feedback Control Systems Committee and approved by the AIEE Technical Operations Department for presentation at the AIEE Fall General Meeting, Chicago, Ill., October 7–11, 1957. Manuscript submitted June 7, 1957; made available for printing August 15, 1957.

W. C. Schultz and V. C. Rideout are both with the University of Wisconsin, Madison, Wis.

The research reported in this paper was supported in part by a National Science Foundation Grant.

The authors acknowledge the assistance of Prof. Preston C. Hammer of the University of Wisconsin Numerical Analysis Laboratory during the writing of this paper, and also the efforts of several graduate students of the Electrical Engineering Department in proofreading the manuscript.

* A typical functional, relative to a function $f(x)$ over the range $a<x<b$, is given by the integral $\int_a^b f(x)dx$.

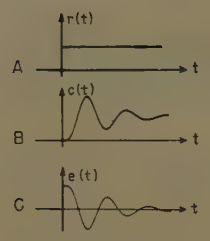


Fig. 1. Typical input, output, and error curves

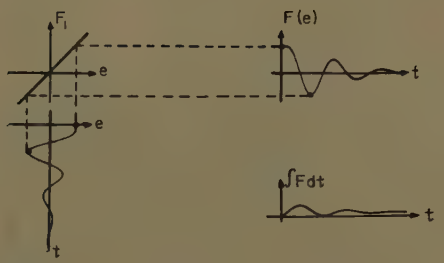


Fig. 2. Error measure for a criterion based on $F[e(t)] = e(t)$. $E = \int_0^\infty e(t)dt$

metric, and design criteria will be based on the minimization of particular forms of equation 7. Although the specific examples which have been cited to illustrate the general form have all resulted in $F$-functions which were easily expressed in a closed form, functions not so readily expressed will also be presented. Since a closed mathematical form will not then be convenient, a geometric form will be introduced. The idea of choosing a function, $F$, that will result in a measure which emphasizes certain features of the error $e(t)$ is suggested by Truxal[13] in his "importance-versus-error" curves, and by James, Nichols, and Phillips,[14] in their weight-of-error-versus-error curves.

## Geometric Interpretation

The following form of the proposed criterion, which is somewhat less general than that given in equation 7, will be used to introduce the basic approach of the method. Let the metric be given by

$$E = \int_0^\infty F[e(t)]\, dt \qquad (9)$$

This form includes the first three integrals of the Introduction, the integrated error, the integral of squared error, and the integral of the absolute error, as special cases. Equation 9 defines a class of metrics within the general form and might be called the integral of a function of error (IFE).

The $F$-function can be interpreted geometrically, and, once this is done, the way will be opened for the endless possibilities of the method. To begin, consider the integrated error metric,

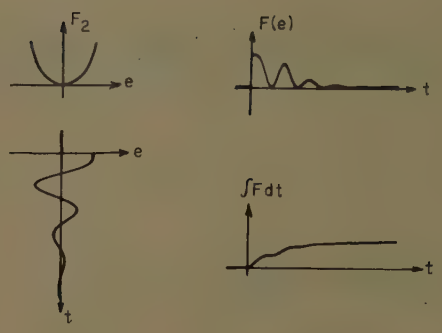


Fig. 3. Error measure for a criterion based on $F[e(t)] = e^2(t)$. $E = \int_0^\infty e^2(t)dt$

$$E = \int_0^\infty e(t)\, dt \qquad (10)$$

Fig. 1 shows a step input function, $r(t)$, and a typical output, $c(t)$. If the error is defined as in equation 1, it would appear as shown in Fig. 1(C). This error is next plotted on a composite figure, as illustrated in Fig. 2. The relationship between $F$ and $e$ is shown in the figure. This particular $F$-function, called $F_1$, simply translates $e(t)$ into itself, the integration process giving the area, $E$, under the $e(t)$ curve. Note that there is the possibility of a negative area for this metric. Now consider the metric given by equation 3,

$$E = \int_0^\infty e^2(t)\, dt \qquad (11)$$

the case illustrated in Fig. 3. The $F$-function here, called $F_2$, squares all ordinates of the error, $e(t)$; the integration gives the area under the squared-error curve. This is a form which is related to the well-known root-mean-square criterion. The third example, equation 5, is illustrated in Fig. 4. The function $F_3$ rectifies the error, and integration gives

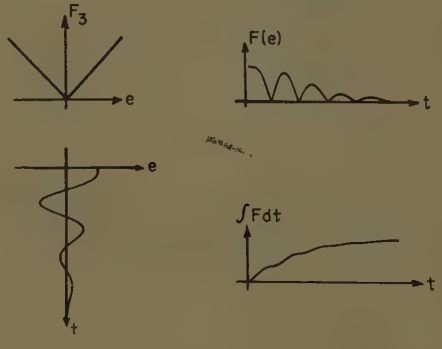


Fig. 4. Error measure for a criterion based on $F[e(t)] = |e(t)|$. $E = \int_0^\infty |e(t)|\, dt$

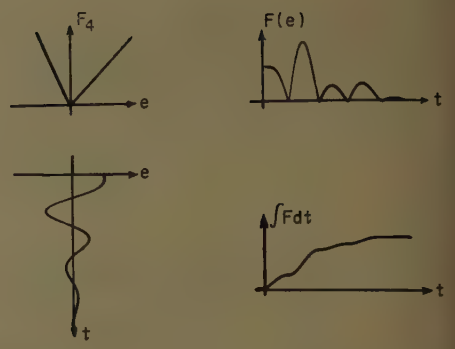


Fig. 5. Error measure for a criterion based on a modified absolute value of error

the area under the curve of absolute error. Although each geometric presentation shown has a simple corresponding analytical form, there is no reason to require only those geometric forms which do have simply expressible analytical forms. This fact gives much power to the proposed general method.

Suppose that the parameters of a servo are to be adjusted so that, for a step input, the absolute error will reduce to within some specified percentage as quickly as possible. The output of this system may show a steady oscillation, within the specified percentage limit, once this limit is first reached. The parameters of a given servo which are optimal for this case will be quite different from those for an "antiovershoot" or an "antiundershoot" case, to give two other possible examples. Another system that might be considered, the type-zero or regulator system, presents another difficulty. Since the type-zero system has a steady-state error for a step input, the integrals given by equations 3 through 6 would all fail to converge. These and other possible step-response requirements indicate the flexibility required in the general form of the metric or metrics upon which the criteria are to be based. The minimization of the integral of equation 9 is a criterion form which has the required flexibility, as will now be shown.

To illustrate the versatility of this criterion form, consider the antiovershoot case. Here the $F$-function of Fig. 4 might be modified as shown in Fig. 5 to penalize any overshoot. If overshoot is completely undesirable the $F$-function of Fig. 6 might be used, to put "full penalty" on overshoot error.

The first case mentioned, that of minimum time for the absolute error to decrease to within a specified percentage, would require the function shown in Fig. 7. In this function, typical of those with no time weighting, but in which time is to

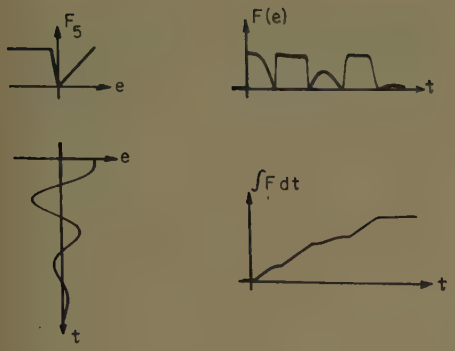


Fig. 6. Error measure for an antiovershoot criterion

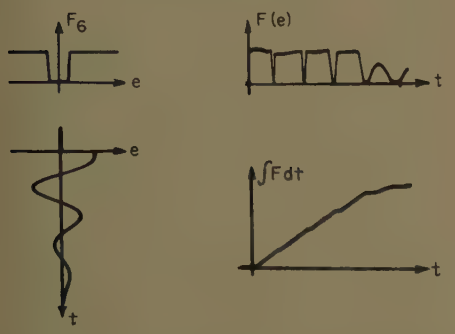


Fig. 7. Error measure for a criterion which permits a final error or error oscillation

be minimized, all error lying beyond the specified limits is equally penalized. This criterion is also one that can be used in the study of type-zero system. (Some additional $F$-functions are discussed in the appendix.)

## Computer Mechanization

The electronic differential analyzer is an invaluable tool for carrying out the computation required in the application of

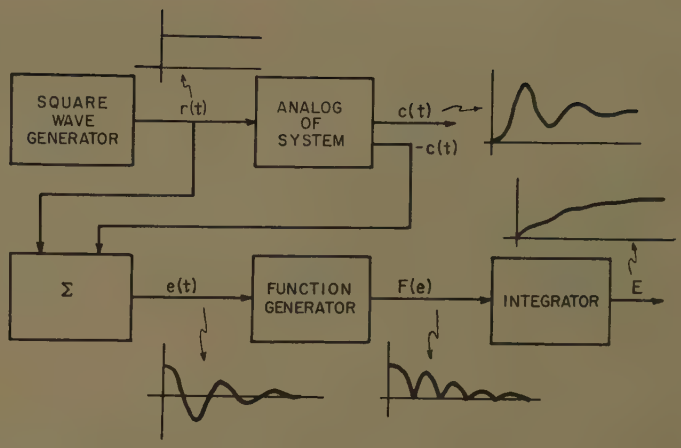


Fig. 8. Analog computer setup for determination of error measure, E. This setup can be used for optimization of the system

criteria based on equation 9. The type of computer used by the authors in this investigation is a computer of the high-speed or repetitive type, called the Wisconsin-Philbrick Computer. The computer was designed and constructed at the University of Wisconsin using Philbrick plug-in operational amplifiers and chopper-stabilizers. Because of the repetitive nature and the short (0.001-second) unit of time of the computer, the input device required is a square-wave pulse generator and the output device is a cathode-ray oscillograph. (All response curves shown in this paper are photographs of cathode-ray presentations.)

Refer to Fig. 8 for a diagram of the computer setup. The step-function is fed to the analog computer representation of the system being studied and also to a summing amplifier. The negative of the system output is added to the system input to produce the error, $e(t)$, which is then fed into a diode function generator to produce the desired $F[e(t)]$. The function generator output is then integrated and the integrator output is displayed on the oscillograph. The sequence of waveforms is illustrated in Fig. 8 for the metric of equation 5.

The method may now be summarized as follows:

1. Set the $F[e(t)]$ versus $e(t)$ characteristic on the function generator.
2. Apply $r(t)$ to the system and obtain $c(t)$.
3. Obtain $e(t) = r(t) - c(t)$.
4. Form $F[e(t)]$.
5. Integrate $F[e(t)]$ to obtain $E$.
6. Adjust the system parameters (within any given set of constraints) so that the value of $E$ is minimized.
7. Read the set of values of parameters from computer.

From this summary it can be seen that the use of the method is relatively simple if an analog computer is available. It is particularly true if the computer can work repetitively at high speed.

Two things should be emphasized at

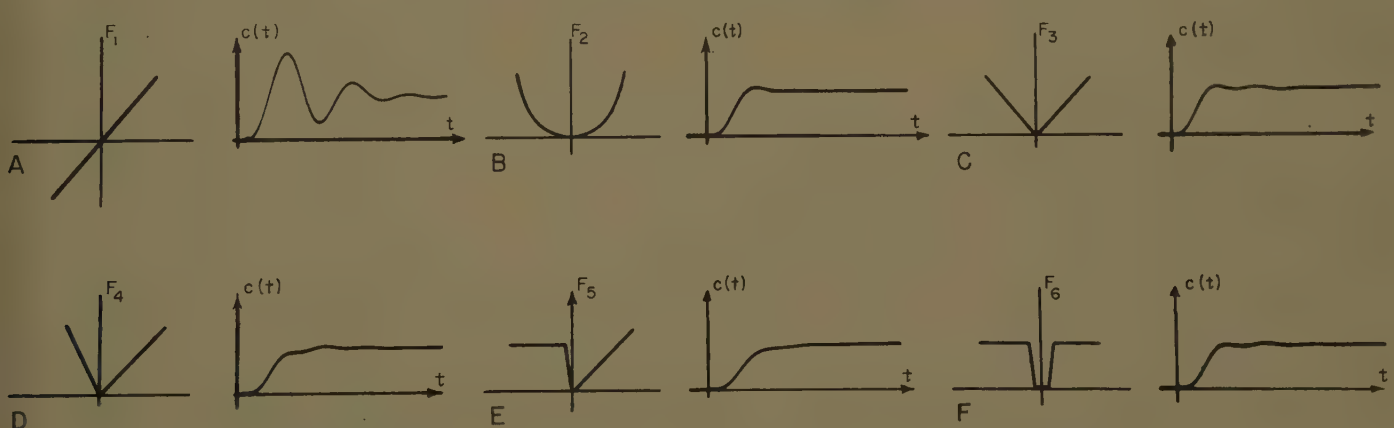


Fig. 9. Results of computer optimization of a fourth-order system for various criteria (equations 12 and 13)

| | | |
|---|---|---|
| A—$\alpha = 0.94$ | C—$\alpha = 0.94$ | E—$\alpha = 1.325$ |
| $\delta = 0.1322$ | $\delta = 0.191$ | $\delta = 0.325$ |
| $\omega_0 = 1.435$ | $\omega_0 = 1.575$ | $\omega_0 = 1.553$ |
| B—$\alpha = 1.15$ | D—$\alpha = 1$ | F—$\alpha = 1.008$ |
| $\delta = 0.324$ | $\delta = 0.16$ | $\delta = 0.205$ |
| $\omega_0 = 1.480$ | $\omega_0 = 1.687$ | $\omega_0 = 1.595$ |

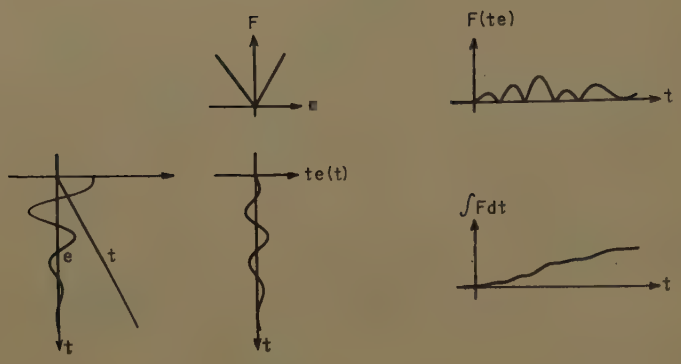


**Fig. 10. A geometric interpretation of the ITAE**

this point. First, the system being studied need not be linear, and second, the *F*-functions need not be linear. Since the electronic differential analyzer can deal with many kinds of nonlinearities, the servo designer has a powerful tool and a powerful method at his disposal. Nonlinear as well as linear systems can be studied and nonlinear or linear methods can be employed. Transients other than the step inputs considered here may, of course, be examined.

## Results

The results of computer studies of the cases shown in Figs. 2 through 7 are tabulated in Fig. 9. Fig. 9 shows several geometric forms of the *F*-function along with the transient response resulting when the corresponding integral is minimized. For purpose of illustration, all cases presented are for a system with a transfer function given by

$$\frac{C(s)}{R(s)}=\frac{1}{s^4+a_1s^3+a_2s^2+a_3s+1} \qquad (12)$$

The open-loop transfer function $G(s)$ corresponding to equation 12 is given by

$$G(s)=\frac{1}{s(s^3+a_1s^2+a_2s+a_3)}=\frac{1}{s(s+\alpha)\,(s^2+2\delta\omega_0 s+\omega_0^2)} \qquad (13)$$

The corresponding values of the coefficients are also included in Fig. 9.

## More General Cases

In equation 7 a general metric was given as

$$E=\int_0^\infty F[e(t),\,t]\,dt \qquad (14)$$

This form will now be discussed in more detail. The first example to be considered is the ITAE, which is formulated as

$$E=\int_0^\infty t\,|e(t)|\,dt \qquad (15)$$

This integral may be rewritten as

$$E=\int_0^\infty |te(t)|\,dt \qquad (16)$$

or, more generally,

$$E=\int_0^\infty F\{t\,[e(t)]\}\,dt \qquad (17)$$

This *F*-function can be interpreted as the same one used in Fig. 4 except that it is a function of $te(t)$ rather than of just $e(t)$ alone. In other words, the error input to the function generator is multiplied by the weighting function, $t$. The ITAE may therefore be represented geometrically as shown in Fig. 10. This representation now suggests a large class of metrics of the form $F\{t[e(t)]\}$, where the *F*-functions may take on the forms in Figs. 3 through 7, 9, or 12. The difference between this class and that described by equation 7 is then one of multiplying the error by $t$ before applying to the input of the *F*-function generator. An even larger class of metrics of the form $F[w(t)e(t)]$ exists, where $w(t)$ is an arbitrary weighting function. Functions that might be used as weighting functions are: $t^2$, $t^3$, $te^{-kt}$, etc.

All cases discussed so far have been metrics based on a single *F*-function. There may arise cases in some systems where more than one output exists, or where more than one system variable must be examined. For example, a system may be a position controller in which it is necessary to minimize position error, velocity error, and acceleration error in some prescribed manner. The criterion may then be to minimize a single integral of a function or functions of the respective errors, or, possibly, to minimize a sum or product of integrals of functions of the respective errors. Another extension might be one of minimizing the product of a measure of error and a measure of cost. The concept of minimizing combinations of integrals opens up another very broad area of future investigation, which cannot be further touched on here.

These investigations have included a further generalization of the proposed criterion, which is more completely described elsewhere by the authors.[15] This work resulted from an extension of work carried out by Spooner and Rideout with the generalized error function.[3] Their GEF, for random, stationary inputs, is defined as

$$E(\tau)=\lim_{T\to\infty}\frac{1}{2T}\int_{-T}^{T}[r(t-\tau)-c(t)]^2dt \qquad (18)$$

where $r(t)$ is the system input, $r(t-\tau)$ is the system input delayed by $\tau$ seconds and $c(t)$ is the system output. $\tau$ may be positive, negative, or zero. The extension to the transient input case may then be formulated as

$$E(\tau)=\int_{-\infty}^{\infty}F[e(t,\tau),\,t,\,\tau]\,dt \qquad (19)$$

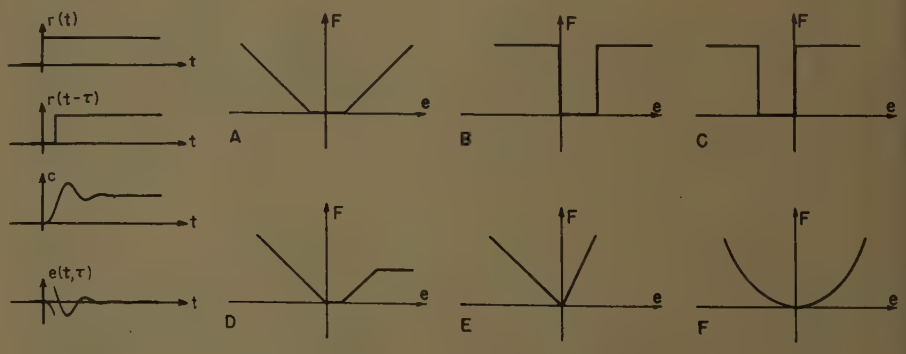


**Fig. 11 (left). Typical input, delayed input, output, and delay-error curves**

**Fig. 12 (right). Some additional F-functions**

A—Allows small final error, emphasizes all error greater than maximum allowable. The emphasis increases linearly as the magnitude of error increases
B—Antiovershoot. Allows small steady-state error, but not an overshoot
C—Antiundershoot. Allows small steady-state error, but not an undershoot
D—Ignores large initial error
E—Relative antiundershoot
F—Example of raising error e(t) to some power: $[e(t)]^{1.5}$

where $e(t,\tau)=r(t-\tau)-c(t)$. This definition of error, $e(t,\tau)$, called the delay-error, allows for a delay, $\tau$, as shown in Fig. 11. The metric, $E(\tau)$, is therefore a function of the delay, $\tau$, and the criterion may then require that $\tau$ as well as the system parameter values be varied to minimize the integral.

Special cases of equation 19 include Spooner's GEF for transient inputs,

$$E(\tau)=\int_{-\infty}^{\infty}[e(t,\tau)]^2dt \qquad (20)$$

and the ITAE of Graham and Lathrop,

$$E(0)=\int_{-\infty}^{\infty}t|e(t)|dt \qquad (21)$$

formed by setting $\tau$ equal to zero.

## Appendix. Other Metrics

Fig. 12 is included to show how the geometric interpretation of measurement of error can be extended to include many other cases. A variation of the metric given in Fig. 7 is shown in Fig. 12(A). This metric places an emphasis on any error greater than some maximum allowable error. The functions of Fig. 12(B) and Fig. 12(C) are further modifications of Fig. 7. In Fig. 12(B) the same "amount" of error is allowed, but there is a strong discrimination against overshoot. In Fig. 12(C) there is a similarity to Fig. 12(B) except that "undershoot" is discriminated against. Fig. 12(D) is an attempt to set up a metric that pays little attention to the large initial error, since $F[e(t)]$ places a limit on maximum of $e(t)$. Many possibilities exist for the extension of this concept. Fig. 12(E) is related to Fig. 5 but places emphasis on the "undershoot" error. Figure 12(F) is included to show that there might be another broad class of metrics given by

$$E_n=\int_0^{\infty}F_n[e(t)]dt \qquad (22)$$

or

$$E_n=\int_0^{\infty}|e(t)|^n dt \qquad (23)$$

where $n$ need not necessarily be an integer. For example, it might be of interest to obtain plots of $E_n$ versus $n$, over a certain range of $n$, for a given system.

Many other $F$-functions might be added to those in Fig. 12 to include metrics based on other special system requirements.

## References


1. Methods of Mathematical Physics (book), **R. Courant, D. Hilbert.** Interscience Publishers, Inc., New York, N. Y., vol. I, 1953, pp. 167–69.

2. The Analysis and Synthesis of Linear Servomechanisms (book), **A. C. Hall.** Technology Press, Massachusetts Institute of Technology, Cambridge, Mass., 1943, pp. 19–27.

3. Correlation Studies of Linear and Nonlinear Systems, **M. G. Spooner, V. C. Rideout.** *Proceedings*, National Electronics Conference, Chicago, Ill., vol. 12, 1956, pp. 321–35.

4. The Dynamics of Automatic Controls (book), **R. C. Oldenbourg, H. Sartorious.** American Society of Mechanical Engineers, 1948, pp 66–67.

5. Some Design Criteria for Automatic Controls, **Paul T. Nims.** *AIEE Transactions*, vol. 70, pt. I., 1951, pp. 606–11.

6. A Note on Control Area, **T. M. Stout.** *Journal of Applied Physics*, New York, N. Y., vol. 21, Nov. 1950, pp. 1129–31.

7. How to Specify the Performance of Closed-Loop Systems, **J. E. Gibson.** *Control Engineering*, New York, N. Y., Sept. 1956, pp. 122–29.

8. The Theory of Servomechanisms, With Particular Reference to Stabilization, **A. L. Whiteley.** *Journal*, Institution of Electrical Engineers, London, England, vol. 93, 1946, pp. 353–72.

9. A Differential-Analyzer Study of Certain Nonlinearly Damped Servomechanisms, **R. R. Caldwell, V. C. Rideout.** *AIEE Transactions*, vol. 72, pt. II, July 1953, pp. 165–69.

10. The Synthesis of "Optimum" Transient Response: Criteria and Standard Forms, **Dunstan Graham, R. C. Lathrop.** *Ibid.*, Nov., pp. 273–88.

11. The Transient Performance of Servomechanisms with Derivative and Integral Control, **Richard C. Lathrop, Dunstan Graham.** *Ibid.*, vol. 73, Mar. 1954, pp. 10–17.

12. The Influence of Time Scale and Gain on Criteria for Servomechanism Performance, **Dunstan Graham, Richard C. Lathrop.** *Ibid.*, July, pp. 153–58.

13. Control System Synthesis (book), **J. G. Truxal.** McGraw-Hill Book Company, Inc., New York, N. Y., 1955, pp. 413–14.

14. Theory of Servomechanisms (book), **H. James, N. B. Nichols, R. S. Phillips.** McGraw-Hill Book Company, Inc., 1947, pp. 308–11.

15. A General Criterion For Servo Performance, **W. C. Schultz, V. C. Rideout.** *Proceedings*, National Electronics Conference, vol. 13, 1957.

16. An Integral Criterion for Optimizing Duplicator Systems on the Basis of Transient Response, **Jack H. Crow.** *Doctor of Science Thesis*, Electrical Engineering Department, Washington University, St. Louis, Mo., June 1957.


## Discussion

**S. P. Higgins** (Minneapolis-Honeywell Regulator Company, Brown Instruments Division, Philadelphia, Pa.): The authors have made an interesting addition to the literature on criteria. In particular, they have considered nonsymmetrical weighting of error and have indicated the use of this weighting to penalize selectively overshoot and undershoot. They have also indicated a more definite break with past practice, which accepted criteria based on analytical advantages and have, thereby, taken more advantage of the power of modern computers.

Industrial process control requires that in different instances different criteria be applied. For instance, in one case, the emphasis may be on minimizing overshoot and, in another case, emphasis may be on reducing cycling to prevent effects due to coupled control systems. Also, we may wish to determine how well a system will satisfy two criteria separately by adjustment of instrument parameters. For these purposes, the approach described by the authors is of practical value.

It is, perhaps, well to keep in mind that, while simple criteria and results derived from them are needed in practical design work, the criteria on which performance is ultimately judged are generally more complex. Sometimes they can be expressed in quantitative terms. This subject has, unfortunately, not been well developed in the literature.

A minor point is brought up by Fig. 6, where the limiting on the $F_5$ values for negative errors is somewhat misleading for the case shown.

**Morton G. Spooner** (Cornell Aeronautical Laboratory, Inc., Cornell University, Buffalo, N. Y.): The authors are to be congratulated for their clearly written paper on the selection and use of servo performance criteria. The paper presents an extremely useful procedure for evaluating servo transient response performance using some chosen criteria.

The results shown in Fig. 9 are most enlightening. However, I would like to know more about the convergence of the metrics when the system parameters are adjusted. Did the analog computer clearly indicate the most desirable system parameters in all the cases considered?

The authors state that the system under test need not be linear, and also that the $F$-functions need not be linear. An interesting study in the nonlinear case would be one in which the input signal was contaminated by a random noise with a zero mean and a Gaussian distribution. The error in this case would be the uncontaminated input minus the output. Do the authors believe that the addition of noise to the input would change the optimum system parameters when some specified metric was used?

**W. C. Schultz** and **V. C. Rideout:** We wish to express our appreciation for the interest shown in the paper by Mr. Higgins and Mr. Spooner.

Mr. Higgins' remarks contribute supporting arguments to those presented in the paper, that the servo designer should not necessarily be restricted to the use of criteria which are simply analytical. The mathematical convenience of mean-square-error measures has perhaps been overemphasized to the point where mean-square measures have been used even though other metrics would have given more useful criteria. The use of computer techniques makes many other measures equally easy to use, and thus, the designer may choose the most appropriate one if such devices are employed.

In regard to Fig. 6, it is agreed that it is perhaps misleading. For the particular error curve shown, the $F_5$ curve is satisfactory, since the error does not exceed the "range" of $F_5$. If, however, the error for some other system was such that the error exceeded the maximum value shown in Fig. 6, a limit would also have to be placed on the

portion of the *F*-function in the right-hand quadrant. This limit would most likely be at the same level as that shown in the left-hand quadrant.

In regard to the remark concerning Fig. 9, we wish to thank Mr. Spooner for raising this important point. For the particular system presented, the fourth-order linear system, the computer did clearly indicate that the responses shown in Fig. 9 are the "best" system responses, relative to the several metrics. However, we wish to point out that for higher-order systems and the measure of Fig. 9(C), a series of "relative minima" were found to exist. Specifically, for an eighth-order system, the computer very quickly showed *a* minimum, but other minima were also found, and all of these minima had to be examined to establish the absolute minimum. Future work in this area will include a more rigorous mathematical approach to the problem of uniqueness.

Certain difficulties are encountered if the case where the possibility of contamination of the input signal by noise is considered. The immediate difficulty is that a continuous noise signal present at the output will result in infinite integrals. One possible modification is the use of a finite limit of integration time. Another approach would be the use of an *F*-function of the type shown in Fig 9(F) or Fig. 12(A). Although in a theoretical sense the integral would still become infinite, due to large peak noise signals, in a practical case the peak amplitudes would be limited at the output, so that an *F*-function of the type mentioned would satisfactorily handle the cases where noise was present. In general it would be expected that the "optimum" system parameters would be different for noise cases, for any given error measure.

---

# Extended Switching Criterion for Second-Order Saturated Servomechanisms

J. W. DIESEL
STUDENT MEMBER AIEE

A PRIMARY requirement in many positioning systems is that errors resulting from large input disturbances be reduced to tolerable values as quickly as possible. For a linear system, this requirement could be satisfied by making the ratio of torque to inertia sufficiently large. However, even with the best servomotor design this ratio is limited; therefore, to sufficiently reduce the response time, the designer must frequently contend with saturation in the system components and resulting saturated values of available torque. This paper deals with this saturated type of operation.

If saturation effects are present in a given control system, it is reasonable to expect that optimum response in the sense of minimum recovery time would be obtained if the corrective torque is allowed to saturate at its maximum permissible value during recovery from the disturbance, so that full available power is utilized at all times. To obtain optimum response it is also necessary that this torque be switched to its full reverse value at the proper instant during recovery. The proper instant of torque reversal is determined by a computer, which utilizes information obtained from the input and output, and manipulates the corrective torque accordingly.

Computer characteristics have been devised[1–7] for systems employing a constant maximum torque and subjected to step-displacement inputs only. Most actual systems, however, are incapable of maintaining a constant torque since the servomotor torque is usually a function of the output speed; also, most systems are excited by more complex inputs than simple displacement steps.

Accordingly, this paper extends present knowledge in two directions:

1. Controller characteristics are established for inputs composed of a combination of velocity and displacement steps.

2. Controller characteristics are established for servomotors with actual speed-torque characteristics.

This study is restricted to plants describable by a second-order equation of motion. For most positioning systems this assumption is not unreasonable. Another limitation is that the equations contain no terms dependent on the output displacement. This is necessary in order that the controller characteristics will not depend on the magnitude of the input, but only on the error between the input and the output. This requirement is equivalent to assuming no spring forces, which is usually the case for systems subjected to velocity inputs. The conclusions of the investigation are therefore quite generally applicable.

Paper 57-1036, recommended by the AIEE Feedback Control Systems Committee and approved by the AIEE Technical Operations Department for presentation at the AIEE Fall General Meeting, Chicago, Ill., October 7–11, 1957. Manuscript submitted June 10, 1957; made available for printing August 22, 1957.

J. W. DIESEL is at Washington University, St. Louis, Mo.

The material presented in this paper is based on the thesis submitted by the author in partial fulfillment of the requirements for the degree of Master of Science in Electrical Engineering at Washington University. Acknowledgment is due Professor John Zaborszky for supervising the thesis and reviewing the paper.

## Nomenclature

$c$ = normalized output or controlled variable
$r$ = normalized input or reference variable
$e$ = normalized error, $r-c$
$m$ = normalized control voltage or manipulated variable
$\tau$ = normalized time
$\Phi(m,c')$ = normalized torque as function of $m$ and $c'$
$_0$ = (subscript) indicates initial value of a variable
max = (subscript) indicates maximum value of a variable
$'$ = (superscript) indicates first derivative with respect to normalized time
$''$ = (superscript) indicates second derivative with respect to normalized time
$f(e,e',r')$ = function of $e,e',r'$ defined in text
$g(u)$, $h(u)$ = functions of $u$ defined in text
$\delta$ = function of $e'$ defined in text
$v$ = normalized speed and dummy variable of integration
$\theta_0$ = output displacement, radians
$\theta_i$ = input displacement, radians
$V$ = control voltage, volts
$t$ = time, seconds
$T$ = developed torque, foot-pounds
$\cdot$ = (superscript) indicates first derivative with respect to time, seconds
$\cdot\cdot$ = (superscript) indicates second derivative with respect to time, seconds
$K_m$ = motor gain constant, foot-pounds per volt
$\zeta_m$ = motor damping constant, foot-pound-seconds
$J$ = inertia, foot-pound-seconds squared
$\zeta_r$ = viscous damping coefficient, foot-pound-seconds
$\zeta_c$ = coulomb friction coefficient, foot-pound
$\rho_c$ = normalized coulomb friction ratio
$n$ = rotor speed, revolutions per minute
$n_s$ = synchronous speed, revolutions per minute
$R_1$ = stator resistance per phase, ohms
$X_1$ = stator reactance per phase at line frequency, ohms
$R_{2e}$ = equivalent rotor resistance per phase referred to stator, ohms
$X_{2e}$ = equivalent rotor reactance per phase at line frequency, ohms
$V_1$ = main winding voltage, volts

## System Studied

As stated previously, the investigation is directed to systems excited by a special class of inputs. Explicitly, it is assumed that the input displacement and velocity

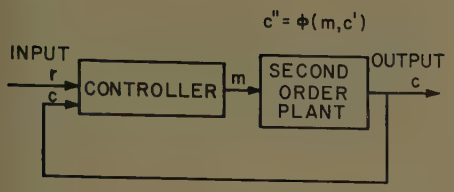


Fig. 1. Schematic diagram of general second-order positioning system

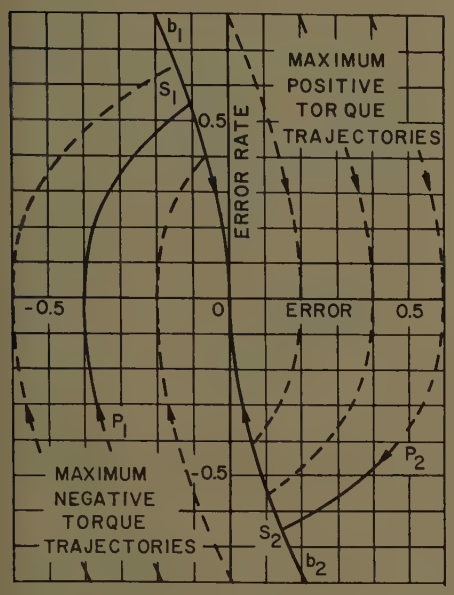


Fig. 2. Maximum torque trajectories in the phase plane

are continuous except at step-type disturbances, and that the system is allowed sufficient time to recover between such disturbances. Further, it is assumed that the input velocity does not change appreciably during the recovery period, so that only inputs with constant velocity need be considered. It then suffices to consider a single input of the form

$$r = r_0 + r_0' \tau, \quad 0 < \tau \tag{1}$$

with the initial conditions

$$c = 0, \; c' = c_0' \text{ at } \tau = 0 \tag{2}$$

The optimum control to be considered applies to any second-order plant for which the output acceleration $c''$ is a single-valued function of both the manipulated variable $m$ (see Fig. 1) and the output speed $c'$, but not the output displacement

$$c'' = \phi(m, c') \tag{3}$$

This definition includes the broad class of nonlinear characteristics of such servomotors as are used in control systems of the standard type. To simplify the analysis, it is convenient to impose the additional restrictions

$$\phi(-m, -c') = -\phi(m, c') \tag{4}$$

$$\phi(m, c') < \phi(m_{\max}, c'), \; m < m_{\max} \tag{5}$$

$$\phi(m_{\max}, c') > 0, \; c' < c_{\max}' \tag{6}$$

$$\phi(m_{\max}, c') < 0, \; c_{\max}' < c' \tag{7}$$

The symmetry condition 4 ensures that the motor can accelerate equally well in either direction. Condition 5 states that the maximum acceleration at any speed occurs at a specified maximum value of the manipulated variable $m$, which is frequently a control voltage. The maximum speed attainable by the system is defined by conditions 6 and 7. Also, the variables are assumed normalized, so that

$$m_{\max} = 1, \; c_{\max}' = 1, \; \phi(m_{\max}, 0) = 1$$

## Optimization Problem

If the input disturbance defined by equations 1 and 2 is applied to the plant, equations 3 through 7, an error in position results at $\tau = 0$. Since a second-order system does not overshoot when the error and error rate are zero at the same instant, optimum control may then be defined as that method of control which simultaneously reduces the foregoing error and error rate to zero in the least possible time.

The optimum method of control is best understood by referring to the phase plane of Fig. 2, in which the co-ordinates are the error and error rate existing in the system following the disturbance.

In general, the corrective torque is controlled by manipulating the variable $m$, the resultant response of the system then being represented by a corresponding trajectory in the phase plane. A family of such curves is obtained by setting $m$ at its maximum positive value $m_{\max}$ and prescribing various initial conditions. These curves are referred to as maximum positive torque trajectories. Similarly, a family of negative torque trajectories is obtained by setting $m = -m_{\max}$. One of the maximum positive torque trajectories passes through the origin. The portion of this curve in the upper-half plane represents motion toward the origin and is labeled $b_1$ in Fig. 2. Similarly, the portion of the negative maximum torque trajectory terminating at the origin and in the lower-half plane is labeled $b_2$. Together these curves constitute a boundary dividing the plane into two regions. This boundary is called the switching boundary for reasons which will immediately be apparent.

The optimum method of control may now be described as follows:

Whenever the error and error rate of the system are such that the representative point of the system lies to the left of the switching boundary in the phase plane, $-m_{\max}$ should be applied. Whenever the representative point lies to the right of this boundary, $+m_{\max}$ should be applied.

In Appendix I it is shown that such manipulation of $m$ indeed results in the desired optimum control. It follows that whenever the point representing the initial error and error rate lies to the left of the switching boundary, the representative point subsequently moves along a maximum negative torque trajectory with $m = -m_{\max}$ until $b_1$ is crossed. The variable $m$ is then switched to $+m_{\max}$ and the final stage of the trajectory is along $b_1$ into the origin, where the error and error rate are simultaneously zero, and the system is recovered from the disturbance. The complete trajectory during recovery would then be represented by a curve such as $P_1 S_1 O$ in Fig. 2. The correspond-

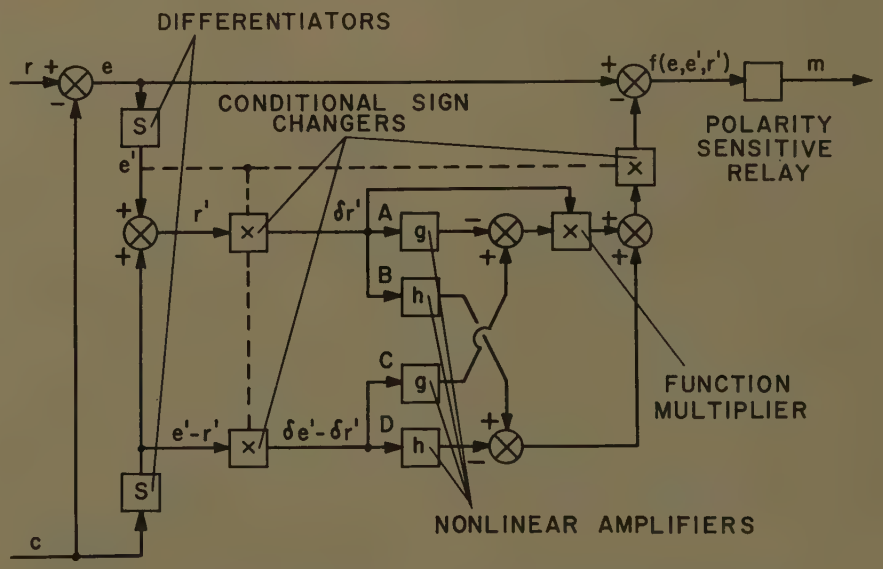


Fig. 3. Schematic diagram of computer required for optimum control

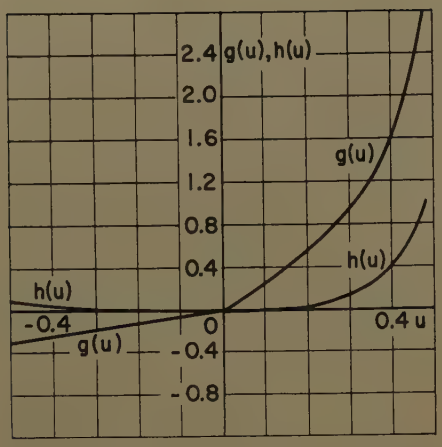


**Fig. 4. Nonlinear amplifier characteristics for plant with coulomb and viscous friction**

ing trajectory when the initial point lies to the right of the switching boundary is obvious, with the final portion of the trajectory along $b_2$. Such a trajectory is exemplified by curve $P_2S_2O$ of Fig. 2.

The equation of the switching boundary is derived in Appendix II and is given by

$$e=\delta\int_{\delta r'}^{\delta r'-\delta e'}\frac{\delta r'-v}{\phi(+m_{\max},v)}dv,\ \delta=\begin{cases}+1, & e'>0\\ -1, & e'<0\end{cases} \tag{8}$$

Note that the switching boundary depends on $r'$ the velocity of the input, and in this respect the switching criterion differs from that for systems disturbed by step displacements only, the switching boundary being independent of the input in the latter case.

The point with co-ordinates $e$, $e'$ lies to the right or left of the switching boundary depending on whether the quantity

$$f(e,e',r')=e-\delta\int_{\delta r'}^{\delta r'-\delta e'}\frac{\delta r'-v}{\phi(+m_{\max},v)}dv \tag{9}$$

is positive or negative, respectively. Accordingly, the desired manipulation of the corrective torque may be obtained if the computed quantity $f(e, e', r')$ is fed to a polarity-sensitive relay with output $\pm m_{\max}$ determined by the algebraic sign of $f(e, e', r')$. The resulting system would then provide optimum response to step displacement and velocity inputs.

Although the expression for $f(e, e', r')$ contained in equation 9 is exceedingly compact, it offers no suggestion as to how this quantity would be computed in an actual system. Equation 9 is therefore rearranged by dividing the range of integration to yield

$$f(e,e',r')=e-\delta\left\{\delta r'\left[\int_0^{\delta r'-\delta e'}\frac{dv}{\phi(m_{\max},v)}-\int_0^{\delta r'}\frac{dv}{\phi(m_{\max},v)}\right]-\left[\int_0^{\delta r'-\delta e'}\frac{vdv}{\phi(m_{\max},v)}-\int_0^{\delta r'}\frac{vdv}{\phi(m_{\max},v)}\right]\right\} \tag{10}$$

By defining

$$g(u)=\int_0^u\frac{dv}{\phi(m_{\max},v)} \tag{11}$$

and

$$h(u)=\int_0^u\frac{vdv}{\phi(m_{\max},v)} \tag{11A}$$

$f(e, e', r')$ may finally be written

$$f(e,e',r')=e-\delta\{\delta r'[g(\delta r'-\delta e')-g(\delta r')]-[h(\delta r'-\delta e')-h(\delta r')]\} \tag{12}$$

From this expression it is seen that one way to compute $f(e, e', r')$ could be that indicated in Fig. 3. This computer would require six summing junctions, a function multiplier, two differentiators, three conditional sign changers, and four nonlinear amplifiers. The nonlinear amplifiers should be synthesized to approximate the characteristics 11 and 11(A), which in turn are determined from the speed-torque characteristic 3 of the particular plant to be optimized.

In many applications, simplifying approximations might be used to determine a less elaborate computer than that indicated. Equation 12 is nevertheless significant in that it exhibits the possibility of determining $f(e, e', r')$ using only existing computer techniques.

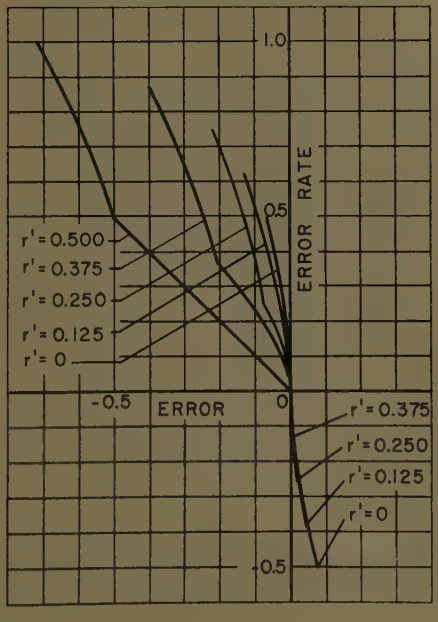


**Fig. 5. Switching boundaries for a linear plant with viscous and coulomb friction**

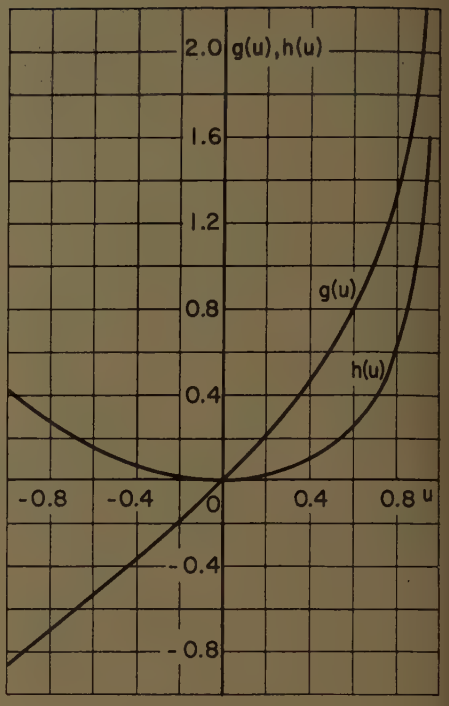


**Fig. 6. Nonlinear amplifier characteristics for the linear plant with viscous friction only**

In connection with equations 11 and 11(A), a difficulty is encountered whenever the argument $u$ approaches unity, since both $g(u)$ and $h(u)$ become unbounded in this case. Physically, this means that two of the amplifiers indicated in Fig. 3 would saturate if the input velocity were to approach or exceed the maximum output speed of the system. In this event the proper sense of corrective torque is assured if the saturated output of amplifier $A$ in Fig. 3 is made sufficiently larger than that of amplifier $B$.

## Linear Plant with Viscous and Coulomb Friction

Consider a motor described by the linear speed-torque characteristics

$$T=K_mV-\zeta_m\dot\theta_0,\ |V|\leqq V_{\max} \tag{13}$$

where the load consists of viscous and coulomb friction as well as inertia

$$T=J\ddot\theta_0+\zeta_r\dot\theta_0+\zeta_c\frac{\dot\theta_0}{|\dot\theta_0|} \tag{14}$$

The variables may be normalized by setting

$$c=\frac{(\zeta_m+\zeta_r)^2}{K_mV_{\max}J}\theta_0$$

$$m=V/V_{\max}$$

$$r=\frac{(\zeta_m+\zeta_r)^2}{K_mV_{\max}J}\theta_i$$

$$\tau=\frac{(\zeta_m+\zeta_r)}{J}t$$

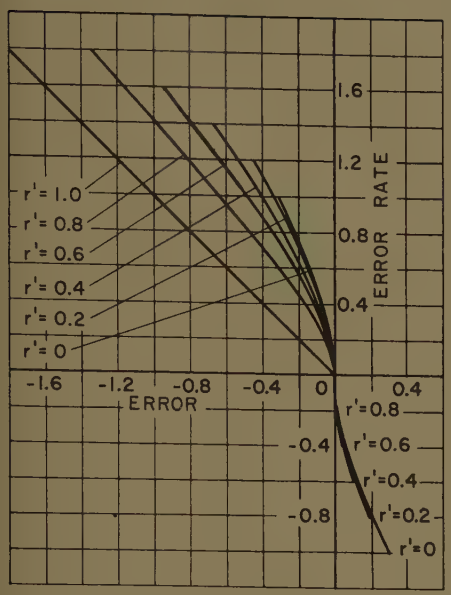


**Fig. 7. Switching boundaries for linear plant with viscous friction only**

so that equations 13 and 14 become

$$c'' = m - c' - \rho_c \frac{c'}{|c'|}, \quad \rho_c = \frac{\zeta_c}{K_m V_{\max}} \tag{15}$$

By comparing equation 15 with equation 3

$$\phi(m, c') = m - c' - \rho_c \frac{c'}{|c'|}$$

the nonlinear amplifier characteristics are then given by

$$g(u) = \int_0^u \frac{1}{1 - v - \rho_c \dfrac{v}{|v|}}\, dv = -\ln\left(1 - \frac{u}{1 - \rho_c \dfrac{u}{|u|}}\right)$$

$$h(u) = \int_0^u \frac{v}{1 - v - \rho_c \dfrac{v}{|v|}}\, dv = -u - \left(1 - \rho_c \frac{u}{|u|}\right) \ln\left(1 - \frac{u}{1 - \rho_c \dfrac{u}{|u|}}\right)$$

These characteristics are shown in Fig. 4 for $\rho_c = 0.5$. The equation of the switching boundary is obtained by substituting the foregoing expressions into equation 12, and setting the result equal to zero.

$$e = \left\{\delta\left[1 - \rho_c \frac{\delta(r' - e')}{|\delta(r' - e')|}\right] - r'\right\} \times \ln\left[\frac{1 - \rho_c \dfrac{\delta(r' - e')}{|\delta(r' - e')|} - \delta(r' - e')}{1 - \rho_c \dfrac{\delta(r' - e')}{|\delta(r' - e')|}}\right] - \left\{\delta\left[1 - \rho_c \frac{\delta r'}{|\delta r'|}\right] - r'\right\} \times \ln\left[\frac{1 - \rho_c \dfrac{\delta r'}{|\delta r'|} - \delta r'}{1 - \rho_c \dfrac{\delta r'}{|\delta r'|}}\right] - e'$$

These boundaries are shown in Fig. 5 for positive input velocities. The switching boundaries for negative input velocities are similar.

An important special case occurs when $\rho_c = 0$, corresponding to a linear plant with viscous friction only. The functions $g(u)$ and $h(u)$ are then given by

$$g(u) = -\ln(1 - u)$$
$$h(u) = -\ln(1 - u) - u$$

and the switching boundaries become

$$e = -e' + (\delta - r') \ln\left(1 + \frac{e'}{\delta - r'}\right)$$

The amplifier characteristics and switching boundaries are shown in Figs. 6 and 7, which may be compared with Figs. 4 and 5 to observe the effect of coulomb friction.

## Two-Phase Induction Motor

Because of the pronounced nonlinearity of its speed-torque characteristics and its frequent service in positioning systems, the 2-phase induction motor provides an especially practical illustration of the foregoing principles.

Before equations 11 and 12 can be applied, it is necessary to determine the speed-torque characteristics of the 2-phase induction motor, corresponding to equation 3. If the full control-winding voltage equals the main winding voltage, the torque may be expressed as

$$T = K \frac{1 - v}{X^2 v^2 - 2(X^2 + Y^2)v + 1} \tag{16}$$

where

$$K = \frac{33{,}000}{2\pi n_s \times 746} \frac{2 V_1^2 R_{2e}}{[(X_1 + X_{2e})^2 + R_1^2]}$$

$$v = n/n_s$$

$$X^2 = \frac{(X_1 + X_{2e})^2 + R_1^2}{(X_1 + X_{2e})^2 + (R_1 + R_{2e})^2}$$

$$Y^2 = \frac{R_1 R_{2e}}{(X_1 + X_{2e})^2 + (R_1 + R_{2e})^2}$$

If the quantities $X^2$ and $Y^2$ are so adjusted that the maximum torque occurs at a slip of two, so that equation 16 becomes

$$T = K \frac{1 - v}{X^2 v^2 + (3X^2 - 1)v + 1}$$

It is assumed that the load is inertial only, so that

$$T = J\ddot{\theta}_0 \tag{17}$$

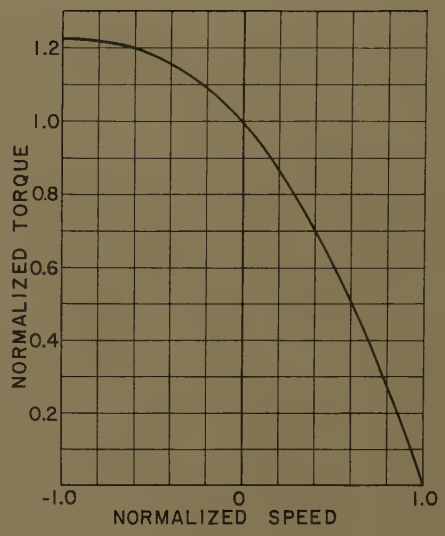


**Fig. 8. Speed-torque characteristic of 2-phase servomotor with full control-winding voltage**

The variables are next normalized by defining

$$\text{normalized time } \tau = \frac{K n_s}{J 2\pi \times 60} t$$

$$\text{normalized output } c = \frac{K n_s^2}{J(2\pi \times 60)^2} \theta_0$$

Equations 16 and 17 then combine to give

$$c'' = \phi(m_{\max}, c') = \frac{1 - c'}{X^2 c'^2 + (3X^2 - 1)c' + 1}$$

The nonlinear amplifier characteristics

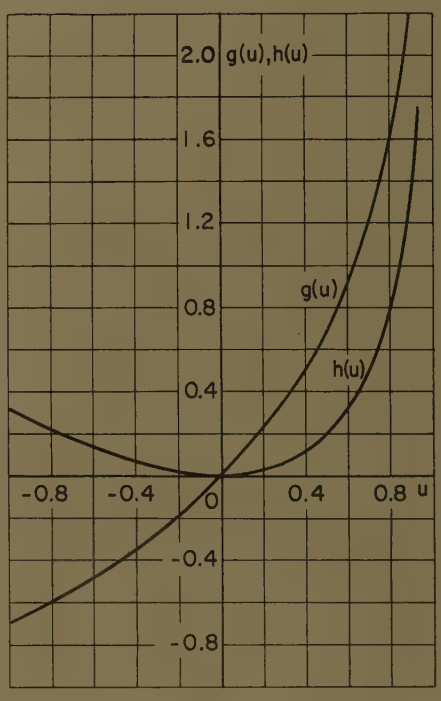


**Fig. 9. Nonlinear amplifier characteristics of computer for 2-phase servomotor**

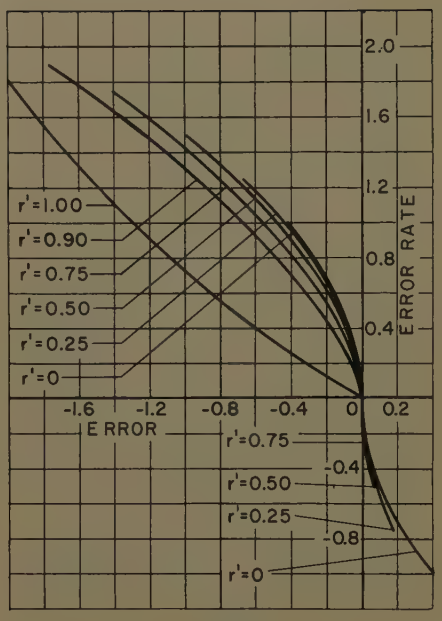


**Fig. 10. Switching boundaries for the 2-phase servomotor**

are obtained from equations 11 and 11(A)

$$g(u) = \frac{-X^2u^2}{2} - (4X^2-1)u - 4X^2 \ln (1-u)$$

$$h(u) = \frac{-X^2u^3}{3} - \frac{(4X^2-1)}{2}u^2 - 4X^2u - 4X^2 \ln (1-u)$$

If $R_1=2$ ohms, $R_{2e}=4.02$ ohms, $X_1=1$ ohm, $X_{2e}=1$ ohm, then $X^2=0.18525$. For these values of the parameters the speed-torque characteristic with full control voltage is shown in Fig. 8, and the corresponding nonlinear amplifier characteristics are shown in Fig. 9. The switching boundaries of the system are shown in Fig. 10.

## Conclusions

The extended optimum switching criterion as contained in equations 11, 11(A) and 12 is applicable to second-order systems with arbitrary nonlinear speed-torque characteristics subjected to combination step inputs of displacement and velocity. In addition to providing a more generally applicable switching criterion, the form of these equations is exceedingly useful as a guide for synthesis of the required computer. The only information needed concerning the plant is the full control-voltage speed-torque characteristic. Even though this curve may be obtainable in graphical form only, the functions $g(u)$ and $h(u)$ may be plotted therefrom, and the required nonlinear amplifiers synthesized using only these plots as a guide.

Although the complexity of the resulting computer would therefore appear to be relatively independent of the particular plant to be optimized the instrumentation involved would not be justified in many applications. The foregoing theory nevertheless might serve as a guide in designing less than optimum systems.

It should finally be observed that the saturated type of operation described in this paper is only a means of reducing the error to relatively small values following large input disturbances. Once the error is small, the system should revert to some type of continuous control. This second mode of control is necessary to provide satisfactory response to small disturbances, and to reduce errors incurred during the saturated mode of operation due to errors in instrumentation and small changes in input velocity between major disturbances.

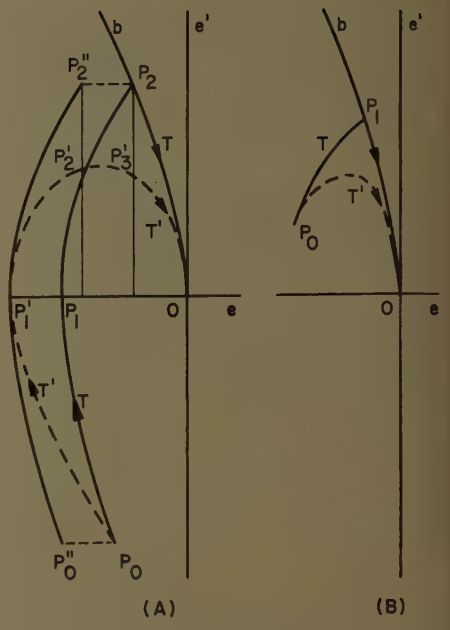


**Fig. 11. Phase-plane trajectories corresponding to optimum and less than optimum control**

## Appendix I. Determination of Optimum Method of Control

Consider the response of the system shown in Fig 1 following an input disturbance with constant velocity $r'$. It will be shown that if $m$ is manipulated according to the criterion described in the text, the resulting response is optimum in the sense of minimum recovery time. The initial conditions corresponding to the disturbance determine the initial co-ordinates $e$ and $e'$ of the representative point in the phase plane. This point is denoted by $P_0$. The trajectory in the phase plane must extent from this point to the origin, if the system is to finally recover from the disturbance, and the exact shape of the trajectory between these points is to be determined by the manner in which $m$ is varied during recovery.

If $P_i$ and $P_{i+1}$ represent points along such a trajectory, the time required to move along the curve from $P_i$ to $P_{i+1}$ is denoted by $\tau(P_i, P_i+_1)$. If the complete trajectory from $P_0$ to the origin is divided into sections by the points $P_1, P_2, \ldots, P_n$, the total time required to traverse the trajectory is $\tau=\tau(P_0, P_1)+\tau(P_1, P_2)+ \ldots +\tau(P_n,0)$. The problem is then to determine the trajectory for which $\tau$ is a minimum.

Several properties of the phase-plane trajectories are now noted:

1. The time required to move along a trajectory from a given point with abscissa $e_1$ to another point with abisscsa $e_2$ is a minimum if, along the trajectory, $|e'|$ is a maximum. This may be seen by writing

$$\tau_2-\tau_1=\int_{\tau_1}^{\tau_2} d\tau=\int_{e_1}^{e_2}\frac{1}{e'}\,de$$

where $\tau_1$ is the time at which the error is $e_1$, and $\tau_2$ is the time at which the error is $e_2$. If $e'$ is positive, $e$ increases with time and $de$ is positive. Conversely, if $e'$ is negative, $de$ is also negative. The conclusion follows immediately.

2. There is a unique positive torque trajectory and a unique negative torque trajectory passing through each point of the phase plane for which $-1+r'<e'<1+r'$.

For a given fixed value of $r'$ such that $|r'|<1$, the equation of motion of the system can be written as a second-order differential equation in $e$. The foregoing statement then follows from the theory of second-order differential equations, the limits on $e'$ being a result of equations 6 and 7 which define the maximum output speed of the system.

3. The maximum torque trajectories for a given sense of torque all have the same shape except for a translation along the error axis. The maximum torque trajectories represent solutions of a differential equation in which there are no terms dependent on the displacement of the system. For a given fixed value of $m$, all such trajectories must then have the same shape except for their position along the error axis, as determined by initial conditions.

4. If the slope of a maximum torque trajectory through a point in the phase plane is positive, it exceeds the slope of any other trajectory through the point. Similarly, if the slope of the maximum torque trajectory is negative, any other trajectory through the point has a larger slope. Since $r'$ is assumed constant, $r''=0$. Then

$$\phi(m, c') = c'' = r'' - e'' = -e''$$

$$= -\frac{de'}{de}\frac{de}{d\tau} = -\frac{de'}{de}\,e'$$

so that

$$\frac{de'}{de} = \frac{-\phi(m, c')}{e'}$$

Here $de'/de$ is the slope of the trajectory through the point. If the ordinate of the point is $e'$, then $c'=r'-e'$ is fixed, so that by equation 5, $\phi(m,c')$ is a positive maximum if $m=+1$, and a negative maximum if $m=-1$, from which the conclusion is readily deduced.

5. The slope $de'/de$ of a maximum positive torque trajectory is negative above the error axis and positive below the axis, while the slope of a maximum negative torque trajectory is positive above the axis and negative below the axis.

On a maximum positive torque trajectory, $m=+1$ so that $c''=\phi(+1, c')$ is positive, and $(de'/de)e'=e''=-c''$ is negative. The slope $de'/de$ is then negative if $e'$ is positive, and positive if $e'$ is negative. The conclusion when $m=-1$ follows in a similar manner.

Reference is now made to Fig. 11(A) in which it is assumed that $P_0$ lies to the left of the switching boundary. If $m=-1$ is initiated, the representative point moves along a maximum negative torque trajectory from $P_0$, crossing the error axis at a point $P_1$ and intersecting the switching boundary $b$ at a point $P_2$. From $P_2$ the representative point moves along the switching boundary, a positive maximum torque trajectory, into the origin. The complete trajectory described is denoted by $T$. That the general shape of this curve is as shown follows from property 5. The time $\tau$ required for recovery of the system in this case is

$$\tau=\tau(P_0, P_1)+\tau(P_1, P_2)+\tau(P_2, 0)$$

Since $T$ represents the method of control outlined in the text, it must be shown that the time required to traverse any other trajectory $T'$ from $P_0$ to 0 will exceed $\tau$.

If $m>-1$ along some other trajectory $T'$ from $P_0$, properties 4 and 5 ensure that the trajectory crosses the $e$ axis at a point $P_1'$ to the left of $P_1$. The trajectory $T'$ must then continue from $P_1'$ to 0 as indicated. Using property 2, the maximum negative torque trajectory through $P_1'$ may be obtained by shifting $P_0P_1P_2$ to the left. This curve is shown as $P_0''P_1'P_2''$. From properties 4 and 5 it is clear that $T'$ lies above $P_0''P_1'$ and below both $P_1'P_2''$ and $P_2O$, as indicated. Perpendiculars from $P_2''$ and $P_2$ to the error axis therefore cross $T'$ at points $P_2'$ and $P_3'$ as shown.

Using properties 1 and 3 gives

$$\tau(P_0, P_1')>\tau(P_0'', P_1')=\tau(P_0, P_1)$$

$$\tau(P_1', P_2')>\tau(P_1', P_2'')=(P_1, P_2)$$

$$\tau(P_2', P_3')>0$$

$$\tau(P_3', 0)>\tau(P_2, 0)$$

Since the time $\tau'$ required to traverse $T'$ is

$$\tau'=\tau(P_0, P_1')+\tau(P_1', P_2')+\tau(P_2', P_3')+\tau(P_3', 0)$$

it is seen by adding the foregoing inequalities that $\tau'>\tau$, which is the desired result.

If $P_0$ lies above the $e$ axis, as in Fig. 11(B), properties 1 through 5 ensure that the maximum torque trajectory $T$ lies above any other trajectory from $P_0$ to 0, and that the recovery time along $T$ is therefore a minimum.

The case where the initial point $P_0$ lies to the right of the switching boundary is similar to the foregoing cases.

## Appendix II. Derivation of Equation of the Switching Boundary

It is desired to determine the relation which exists between $e$ and $e'$ along a maximum torque trajectory terminating at the origin of the phase plane. To this end, it may be assumed that the error and error rate are reduced to zero at time $\tau=0$, and that prior to this time the output quantity $c$ satisfies the equation of motion 3 with $m=\pm 1$. Corresponding values of $e=r-c$ and $e'=r'-c'$ must then be found for $\tau<0$.

Since there are no spring forces in the system, the boundary condition at the origin may be expressed as

$$c=r;\ c'=r', \text{ at } \tau=0$$

with no loss of generality. The change of variables

$$v=c'$$

reduces equation 3 to the first-order equation

$$v\frac{dv}{dc}=\phi(m, v),\ m=\pm 1$$

Separating variables and integrating gives

$$c=\int_{r'}^{c'}\frac{v\,dv}{\phi(m, v)}$$

wherein the boundary conditions were used to obtain the limits of integration.

Again using the boundary conditions to establish limits of integration, $\tau$ may be obtained as

$$\tau=\int_0^{\tau}d\tau=\int_{r'}^{c'}\frac{1}{\frac{dc}{d\tau}\frac{dv}{dc}}\,dv$$

But

$$\frac{dc}{d\tau}\frac{dv}{dc}=v\frac{dv}{dc}=c''=\phi(m, v)$$

so that

$$\tau=\int_{r'}^{c'}\frac{1}{\phi(m, v)}\,dv$$

Since the integrand has the same algebraic sign as $m$ according to equations 4 and 6, the foregoing expression represents negative values of time if

$$m=+1, \text{ when } r'-c'>0$$

$$m=-1, \text{ when } r'-c'<0$$

i.e.,

$$m=\delta=\begin{cases}+1, & e'>0\\ -1, & e'<0\end{cases}$$

Since $r'$ is assumed constant and $r=0$ at $\tau=0$, the input must be given by

$$r=r'\tau,\ \tau<0$$

or, using the expression for $\tau$ found in the foregoing, it is given by

$$r=r'\int_{r'}^{c'}\frac{1}{\phi(\delta, v)}\,dv,$$

where the limits of integration and definition of $\delta$ ensure that the resulting values of $r$ correspond to negative values of $\tau$.

The foregoing expressions for $r$ and $c$ may be used to obtain $e$.

$$e=r-c=r'\int_{r'}^{c'}\frac{1}{\phi(\delta, v)}\,dv-\int_{r'}^{c'}\frac{v\,dv}{\phi(\delta, v)}=\int_{r'}^{r'-e'}\frac{r'-v}{\phi(\delta, v)}\,dv$$

To eliminate $\delta$ from the integrand, the variable of integration is changed to $u=(1/\delta)v$. Since $\delta=\pm 1$ is constant along the trajectory, $dv=\delta du$, so that

$$e=\int_{\delta r'}^{\delta r'-\delta e'}\frac{r'-\delta u}{\phi(\delta, \delta u)}\delta\,du$$

But $\phi(\delta, \delta u)=\delta\phi(1, u)$ from the symmetry condition 4. Also $\delta$ may be factored from the numerator of the integrand, using $\delta^2=+1$. The final result is

$$e=\delta\int_{r'}^{\delta r'-\delta e'}\frac{\delta r'-u}{\phi(1, u)}\,du$$

which is the desired relation between $e$ and $e'$.

## References


1. Nonlinear Techniques for Improving Servo Performance, D. C. McDonald. *Proceedings*, National Electronics Conference, Chicago, Ill., vol. 6, 1950, pp. 400–21.

2. A Phase-Plane Approach to the Design of Saturating Servomechanisms, A. M. Hopkin. *AIEE Transactions*, vol. 70, pt. I, 1951, pp. 631–39.

3. Optimization of Nonlinear Control Systems by Means of Nonlinear Feedbacks, R. S. Neiswander, R. H. MacNeal. *Ibid.*, vol 72, pt. II, Sept. 1953, pp. 262–72.

4. Errors in Relay Servo Systems, Louis F. Kazda. *Ibid.*, vol. 72, pt. II, Nov. 1953, pp. 323–28.

5. Effects of Friction in an Optimum Relay Servomechanism, T. M. Stout. *Ibid.*, vol. 72, pt. II, Nov. 1953, pp. 329–36.

6. An Investigation of the Switching Criteria for Higher Order Contactor Servomechanisms, Irving Bogner, Louis F. Kazda. *Ibid.*, vol. 73, pt. II, July 1954, pp. 118–27.

7. Analysis and Design Principles of Second and Higher Order Saturating Servomechanisms, R. E. Kalman. *Ibid.*, vol. 74, pt. II, Nov. 1955, pp. 294–310.

# A Describing Function for the Multiple Nonlinearities Present in 2-Stage Electrohydraulic Control Valves

J. ZABORSZKY
MEMBER AIEE

H. J. HARRINGTON
ASSOCIATE MEMBER AIEE

AN EARLIER PAPER[1] introduced a method for handling multiple nonlinearities through describing functions, and developed such describing functions for single-stage electrohydraulic control valves. This work is extended in this paper to 2-stage valves of the type shown in Fig. 1. Most of the essential nonlinearities are included in the describing function which is brought to a form similar to that for the single-stage valve.[1] Precalculated charts are utilized which help to make reasonable the amount of labor of computing the describing function for a specific valve. An example in the paper illustrates the use of the describing function, and very good agreement with analog computer studies is demonstrated.

## The System Studied

The type of valve shown in Fig. 1 has a second stage which is essentially identical to a single-stage valve except that the control force on the spindle is exerted through a pressure difference, $P_1-P_2$, at the spindle ends rather than directly through the torque motor. The pressure difference in turn is produced by the first stage, or hydraulic preamplifier, in which the torque motor regulates the relative flow of two leakage orifices, $O_1$ and $O_2$ respectively, and thereby creates the pressure difference, $P_1-P_2$, between the two leakage channels which are fed from the oil accumulator through two fixed orifices, $O_3$ and $O_4$ respectively. Special dashpot dampers are usually not incorporated in such valves but the leakage channels and orifices of the first stage exert a dashpot-type damping on the valve spindle.

## Nonlinearities Considered

Nonlinearities which were considered in the present study include the square-root flow-pressure relations on all six orifices; the nonlinear reaction forces[2,3] on the valve spindle, $S$, and on the torque motor flapper, $F$; coulomb friction on the valve spindle and flapper; and hysteresis in the torque-motor core. The nonlinearity of the damping is represented by the nonlinearity of the orifice flows. The oil is considered incompressible while metered by the valve, but the oil volumes stored in the actuator and tubing are to be considered compressible although for the small actuator motion involved it is fully justified to treat the compressible oil as a linear spring.

## Nomenclature

Any consistent system of units can be used for the following quantities.

$A$ = cross-sectional area of actuator piston
$A_c$ = cross-sectional area of control orifices
$A_o$ = cross-sectional area of fixed orifices
$A_v$ = cross-sectional area of valve spindle
$a, b, \ldots h$ = describing function coefficients; see equations 2 and 3 and Figs. 2–9 of reference 1
$B = 2C_qK_a \cos 69 \text{ deg}$ = reaction (Bernoulli) force coefficient[2,3]
$C_q$, $C_{qc}$, and $C_{qF}$ = discharge coefficients for metering orifices, control orifices, and fixed orifices, respectively
$D$ = distance between flapper and either control orifice when flapper is centered
$F_c$ = coulomb friction of spindle
$F_{cf}$ = coulomb friction of flapper
$f_m$ = viscous damping coefficient of second-stage spindle
$G(ju)$ = transfer function of load (see equation 36)
$I$ = torque-motor current
$I_h$ = half-width of torque-motor current hysteresis loop
$i = \dfrac{K_TI}{k_tD}$ = normalized form of $I$
$i_l$ = linearized torque-motor current
$i_1 = \dfrac{i}{1-4p_ov_t}$, $i_{1l} = \dfrac{i_l}{1-4p_ov_t}$ = modified forms of $i$ and $i_l$, respectively
$K = K_1K_LK_t$ = open-loop gain of the linearized system
$K_a$ = peripheral width of metering orifices
$K_1G_1(ju)$ = transfer function of linearized valve (equation 33)
$K_LG_L(ju)$ = transfer function of load (equation 35)
$K_tG_t(ju)$ = transfer function of torque-motor electric circuit (equation 41)
$K_v = \sqrt{1/\rho}$ constant of hydraulic fluid
$K_T$ = torque-motor force constant
$k_m$ = spring constant of spindle restoring springs
$k_t$ = spring constant of flapper restoring spring
$L_c$ = circumference of control orifices
$l$ = length of fixed orifices
$M_m$ = effective mass of spindle and restoring springs
$m$ = normalized force coefficient coupling first and second stages
$N(\psi, u)$ = describing function
$P = P_h - P_s$ = accumulator-sump pressure differential
$P_a$ = pressure differential (pressure in right chamber minus pressure in left chamber, see Fig. 1) across actuator piston
$P_h$ = high, or accumulator, pressure to valve
$P_s$ = sump pressure
$P_1$, $P_2$ = pressures in left and right chambers, respectively, of first stage
$p = P_a/P$ = normalized form of $P_a$
$p_h = P_h/P$ = normalized form of $P_h$
$p_s = P_s/P$ = normalized form of $P_s$
$p_1$, $p_2 = P_1/P$, $P_2/P$ = normalized forms of $P_1$ and $P_2$, respectively
$\bar{p}_1$ = time average value of $p_1$ or $p_2$
$p_o$ = normalized, time-average pressure drop across control orifices (equation 23)
$p_{o1}$ = normalized, time-average pressure drop across fixed orifice (equations 73 and 74)
$p_{oo}$ = modified form of $p_{o1}$ (equation 24)
$p_{p1}$ and $p_{p2}$ = periodic components of $p_1$ and $p_2$, respectively
$q$ = normalized flow coefficient of metering orifices (equation 13)
$q_c$ = normalized flow coefficient of control orifices (equation 17)
$r_o$ = radius of fixed orifices
$r_1$, $r_2$ = normalized pressure-flow coefficients of the fixed orifices (equations 15 and 16)
$T = C_qK_aK_v$ = flow coefficient of metering orifices
$t$ = time
$u = \dfrac{\omega}{\omega_n}$ = normalized frequency
$v$ = spring nonlinearity ratio (equation 9)
$v_1 = \dfrac{v_t}{1-4p_ov_t}$ = modified form of $v_t$
$v_t$ = normalized reaction (Bernoulli) force on flapper (equation 18)
$X_a$ = quantity in load monitored for feedback purposes
$X_e$ = valve spindle position from center; positive to right (Fig. 1)
$X_{eo}$ = maximum valve spindle position from center
$X_0$ = idealized actuator-piston displacement for incompressible oil and no oil-ring backlash; positive displacement from center to right (Fig. 1)
$X_{oo}$ = maximum actuator-piston displacement
$X_f$ = flapper position; positive from center to left (Fig. 1)

Paper 57-779, recommended by the AIEE Feedback Control Systems Committee and approved by the AIEE Technical Operations Department for presentation at the AIEE Summer General Meeting, Montreal, Que., Canada, June 24–28, 1957. Manuscript submitted March 25, 1957; made available for printing July 9, 1957.

J. ZABORSZKY is with Washington University, and consultant to McDonnell Aircraft Corporation, St. Louis, Mo.; and H. J. HARRINGTON is with the McDonnell Aircraft Corporation, St. Louis, Mo.

The authors wish to thank R. C. Cowles for carrying out much of the computations and algebraic operations for the material included in the paper.

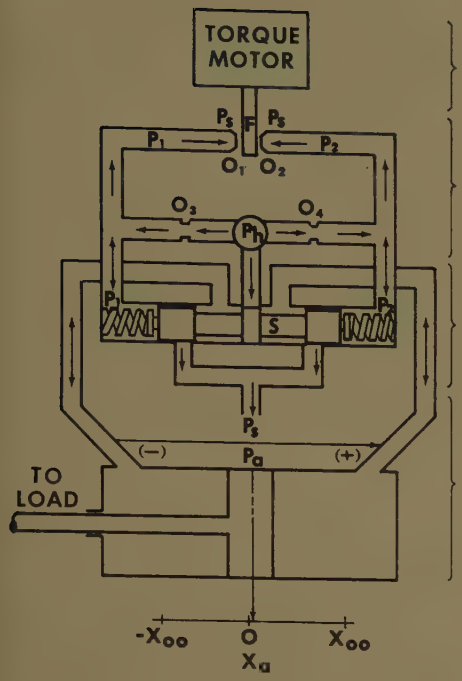


Fig. 1 (left). Sketch of a 2-stage electro-hydraulic control valve

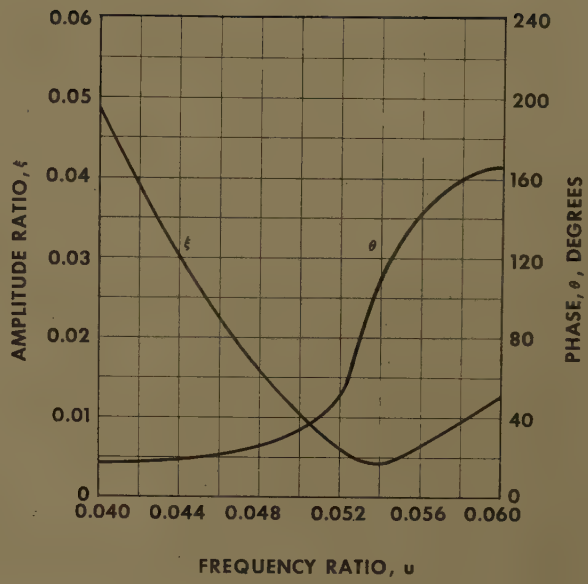


Fig. 3 (right). Frequency response of $G(ju) = \xi/\theta$ for the illustrative example

$x_a = \frac{X_a}{X_{oo}}$ = normalized form of $X_a$

$x_\epsilon = \frac{X_\epsilon}{X_{\epsilon\epsilon}}$ = normalized form of $X_\epsilon$

$x_0 = \frac{X_0}{X_{00}}$ = normalized form of $X_0$

$x_t = \frac{X_t}{D}$ = normalized form of $X_t$

$x_1'$, $x_2'$ = normalized flow rate of left and right control orifices, respectively

$x_3'$, $x_4'$ = normalized flow rate of left and right fixed orifices, respectively

$z$ = normalized pressure-force coefficient at flapper (equation 19)

$z_1 = \frac{z + v_t}{1 - 4p_0v_t}$ = modified form of $z$ (equation 68)

$\zeta$ = normalized viscous friction coefficient of spindle (equation 10)

$\zeta_c$ = normalized coulomb friction coefficient of spindle (equation 11)

$\zeta_{ct}$ = normalized coulomb friction-hysteresis coefficient of flapper and torque motor (equation 12)

$\zeta_{ct1} = \frac{\zeta_{ct}}{1 - 4p_0v_t}$ = modified form of $\zeta_{ct}$ (equation 68)

$\theta$ = phase angle of $G(ju)$

$\mu$ = viscosity of hydraulic fluid

$\xi$ = amplitude of $G(ju)$

$\rho$ = density of hydraulic fluid

$\tau = \omega_n t$ = normalized time

$\psi$ = peak amplitude of sinusoidal oscillation in pressure ratio, $p$

$\omega$ = circular frequency of a sinusoidal oscillation

$\omega_n$ = undamped natural frequency of the linearized valve spindle

## Summary of the Working Formulas for the Describing Function

The describing function is derived in Appendix I and in dimensionless form is given by:

$$N(\psi, u) = \sqrt{\frac{(1-u^2)^2 + 4u^2(\zeta+\Delta\zeta)^2}{(C+\Delta C)^2 + (S+\Delta S)^2}} \times \sqrt{\theta + \tan^{-1}\frac{S+\Delta S}{C+\Delta C} + \tan^{-1}\frac{2(\zeta+\Delta\zeta)u}{1-u^2} + 90 \text{ deg}} \tag{1}$$

where

$$C = a(u^2-1) - b2\zeta u + cv\psi - e\frac{2\zeta_c}{q\xi\psi u} \tag{2}$$

$$S = b(u^2-1) + a2\zeta u + fv\psi + h\frac{2\zeta_c}{q\xi\psi u} \tag{3}$$

and

$$\Delta\zeta = \frac{n_1}{2} \tag{4}$$

$$\Delta S = n_1 au + n_2\xi^2\psi^2 S(C^2+S^2)u^2 - \frac{2\zeta_{ct}}{q_c\xi\psi u} \times \frac{n_3C - n_4bu}{\sqrt{C^2+S^2+n_5(bC-aS)u + \frac{1}{4}n_5^2(a^2+b^2)u^2}} \tag{5}$$

$$\Delta C = -n_1bu + n_2\xi^2\psi^2 C(C^2+S^2)u^2 + \frac{2\zeta_{ct}}{q_c\xi\psi u} \times \frac{n_3S + n_4au}{\sqrt{C^2+S^2+n_5(bC-aS)u + \frac{1}{4}n_5^2(a^2+b^2)u^2}} \tag{6}$$

Equations 5 and 6 assume that terms in $\Delta S$ and $\Delta C$ which are of order $u^3$ or higher are negligible which would be true for most practical systems.

The coefficients $a$, $b$, $c$, $e$, $f$, and $h$ are the same derived for the one stage valve[1] and can be obtained from the charts of Figs. 2–9 of reference 1. The parameter $\psi$ is the peak value of the actuator pressure differential, $p$, when it is varying sinusoidally and so $\psi$ establishes the amplitude of possible oscillations. The angle $\theta$ is the phase and $\xi$ is the amplitude of the conventional linear transfer function, $G(ju)$, which links the idealized (incompressible oil and no oil-ring backlash) actuator piston motion, $x_0$, as output to the pressure differential, $p$, across the actuator as input (see equation 35). The rest of the coefficients in equations 1–6

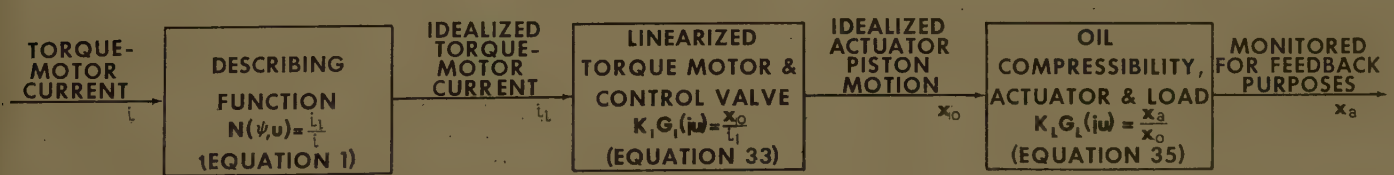


Fig. 2. Block diagram interpretation of the describing function

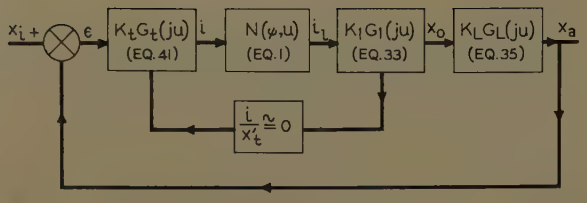


**Fig. 4. Block diagram of the system in the illustrative example**

represent the data of the valve as defined in equation 7–32 in the next section.

In the way of general comment it should be mentioned that a comparison of the describing function of the two-stage valve as given in equations 1–6 with corresponding equations for the single-stage valve[1] shows that the effect of the first stage is represented by the correction factors of $\Delta\zeta$, $\Delta S$, and $\Delta C$. With $\Delta\zeta=\Delta S=\Delta C=0$, equations 1–6 reduce to those of a single-stage valve with no dashpot damping. The latter is absent because damping is provided by the orifices of the first stage in a double-stage valve.

## Nondimensional Parameters

Nondimensional parameters which are directly involved in the computation of the describing function are defined below and can be computed from the actual valve dimensions and system parameters by the following equations:

Primary parameters:

$$\omega_n=\sqrt{\frac{k_m+BP}{M_m}} \tag{7}$$

$$u=\frac{\omega}{\omega_n} \tag{8}$$

$$v=\frac{BP}{k_m+BP} \tag{9}$$

$$\zeta=\frac{f_m}{2\sqrt{M_m(k_m+BP)}} \tag{10}$$

$$\zeta_c=\frac{F_c}{2(k_m+BP)X_{eo}} \tag{11}$$

$$\zeta_{ct}=\frac{F_{ct}+K_TI_h}{2k_tD} \tag{12}$$

$$g=\frac{\omega_nA}{T}\sqrt{\frac{1}{P}\frac{X_{oo}}{X_{eo}}} \tag{13}$$

$$m=\frac{A_vP}{X_{eo}(k_m+BP)} \tag{14}$$

$$r_1=\frac{8\mu A_vlX_{eo}\omega_n}{\pi Pr_o^4} \tag{15}$$

$$r_2=\frac{A_vX_{eo}\omega_n}{\sqrt{2P}C_{qF}K_vA_o} \tag{16}$$

$$q_c=\frac{A_vX_{eo}\omega_n}{\sqrt{2P}C_{qc}K_vL_cD} \tag{17}$$

$$v_t=\frac{8\pi C_{qc}^2PD}{k_t} \tag{18}$$

$$z=\frac{A_cP}{k_tD} \tag{19}$$

Secondary parameters:

$$\bar{p}_1=G-\sqrt{G^2-F} \tag{20}$$

$$G=\frac{\left[1+\frac{r_2^2}{q_c^2}\right]\left[P_h+\frac{r_2^2}{q_c^2}P_s\right]+\frac{r_1^2}{2q_c^2}P}{P\left[1+\frac{r_2^2}{q_c^2}\right]^2} \tag{21}$$

$$F=\frac{\left[P_h+\frac{r_2^2}{q_c^2}P_s\right]^2+\frac{r_1^2}{q_c^2}P_sP}{P^2\left[1+\frac{r_2^2}{q_c^2}\right]^2} \tag{22}$$

$$\bar{p}_o=\bar{p}_1-\frac{P_s}{P} \tag{23}$$

$$\bar{p}_{oo}=\frac{P_h}{P}+\frac{r_1^2}{4r_2^2}-\bar{p}_1 \tag{24}$$

$$\nu_1=\frac{3r_1}{2r_2}-\frac{(3\bar{p}_{oo}-\bar{p}_o)(\bar{p}_o+\bar{p}_{oo})}{\bar{p}_{oo}\sqrt{\bar{p}_{oo}}} \tag{25}$$

$$\nu_2=\frac{r_1}{2r_2}-\frac{\bar{p}_o+\bar{p}_{oo}}{\sqrt{\bar{p}_{oo}}} \tag{26}$$

$$\nu_3=-\nu_2+\frac{4r_2\bar{p}_o\sqrt{\bar{p}_o}}{q_c}\frac{z+v_t}{1-4\bar{p}_ov_t} \tag{27}$$

$$n_1=\frac{4mq_cr_2\sqrt{\bar{p}_o\bar{p}_{oo}}\,(1-4\bar{p}_ov_t)}{(1-4\bar{p}_ov_t)(q_c\sqrt{\bar{p}_o}+r_2\sqrt{\bar{p}_{oo}})+4r_2\bar{p}_o\sqrt{\bar{p}_{oo}}\,(z+v_t)} \tag{28}$$

$$n_2=\frac{q^2\nu_1^2}{2(8m\bar{p}_o)^2\nu_2\nu_3}\times\left[1+\frac{8\bar{p}_ov_t}{1-4\bar{p}_ov_t}\left(\frac{\nu_2}{\nu_1}+\frac{3q_c}{r_2\sqrt{\bar{p}_o}}\frac{\nu_2^2}{\nu_1^2}\right)\right] \tag{29}$$

$$n_3=-\frac{16mr_2\bar{p}_o\sqrt{\bar{p}_o}}{\pi q\nu_3(1-4\bar{p}_ov_t)} \tag{30}$$

$$n_4=\frac{(8mr_2\bar{p}_o)^2\sqrt{\bar{p}_o}}{\pi q\nu_2\nu_3(1-4\bar{p}_ov_t)} \tag{31}$$

$$n_b=\frac{8mr_2\bar{p}_o}{\nu_2} \tag{32}$$

## Interpretation of the Describing Function

The describing function represents the effect of the nonlinearities of the valve and accordingly it is to be inserted in the block diagram ahead of an equivalent valve which is linearized by depriving it from all nonlinearities (Fig. 2). The linearized valve has the same physical dimensions and same parameters as the actual valve but the pressure drops are frozen at their maximums in calculating the flow rates (Fig. 1) at the valve lands, and also in calculating reaction forces on the flapper and on the spindle. The flow pressure relationships of orifices $O_1$, $O_2$, $O_3$, and $O_4$ are represented by straight lines. Such a valve has a transfer function:

$$K_1G_1(ju)=\frac{x_o}{i_l}=\frac{K_1}{(ju)[(ju)^2+2(\zeta+\Delta\zeta)(ju)+1]} \tag{33}$$

$$K_1=\frac{n_1\sqrt{\bar{p}_o}}{gq_c(1-4\bar{p}_ov_t)} \tag{34}$$

which is derived in Appendix II.

The output of the valve (Fig. 2) is $x_0$ which is the idealized actuator piston motion with incompressible oil. The load then is represented in the block diagram (Fig. 2) by a transfer function:

$$K_LG_L(ju)=\frac{x_a}{x_0} \tag{35}$$

which has for its output whatever quantity $x_a$ is convenient for this purpose in the block diagram. Usually $x_a$ would be a quantity monitored for feedback purposes such as the actual actuator piston motion.

Another transfer function of the load is needed for computing the describing function (equations 1 through 6),

$$G(ju)=\xi/\theta=\frac{x_o}{\bar{p}} \tag{36}$$

which has the idealized actuator piston motion $x_o$ for its output and the pressure drop across the actuator as its input.

Both of these transfer functions include the compressibility of the oil which, however, is considered a linear spring since the actuator amplitudes are small in the phenomenon considered here. The load for both $G_L(ju)$ and $G(ju)$ is simply defined as the entire dynamic system driven by the actuator including any internal feedbacks but excluding any feedbacks which close through the describing function.

Attention should be paid to the reference directions used for $x_o$ and $\bar{p}$ in computing $G(ju)=\xi/\theta$ to avoid an uncertainly of $\pi$ in $\theta$. Those reference directions, consistent with equations 1 through 6, are stated (for $\bar{p}$ and $x_0$) in the Nomenclature.

There is no limit set on the complexity of the load except the restriction of linearity or linearizability. Transfer functions $G_L(ju)$ and $G(ju)$ are fully con-

ventional linear transfer functions. The use of the describing function is also fully conventional.

## Illustrative Example

Data of the system:

A hydraulic valve has the following nondimensional parameters:

$q=428.7$
$\zeta=0.0189$
$\zeta_c=0.00574$
$\zeta_{ct}=0$
$v=0.432$
$q_c=10.69$
$v_t=0.2696$
$m=4.168$
$z=4.226$
$r_1=2.598$
$r_2=23.50$
$p_1=0.1789$ (37)

The load is assumed to be a simple inertia with viscous friction and with a restraining spring and an elastic coupling between actuator piston and load inertia. The two transfer functions for this load will be assumed as:

$$K_LG_L(ju)=\frac{x_a}{x_0}=\frac{295.4(ju)^2+1.140(ju)+1}{104.6(ju)^4+91.58(ju)^3+347.7(ju)^2+1.648(ju)+1} \quad (38)$$

$$K_L=1.0 \quad (39)$$

$$G(ju)=\frac{x_a}{p}=\xi/\underline{\theta}=-0.01814\times\frac{104.6(ju)^4+91.58(ju)^3+347.7(ju)^2+1.648(ju)+1}{ju[206.2(ju)^3+181.2(ju)^2+102.3(ju)+1]} \quad (40)$$

The frequency response computed from equation 40 is shown in Fig. 3.

The torque motor is essentially an inductance-resistance circuit with a transfer function of:

$$K_tG_t=\frac{i}{\epsilon}=\frac{4.625}{0.5ju+1} \quad (41)$$

$K_t=4.625$

The transfer function of the linearized valve can be computed from equations 4, 25, 33, and 34 as

$\Delta\zeta=7.718$ (42)

and

$$K_1G_1(ju)=\frac{0.001591}{(ju)[(ju)^2+15.47(ju)+1]} \quad (43)$$

$K_1=0.001591$

## Block Diagram

The block diagram of the system is shown in Fig. 4. The inner loop represents the feedback caused by the back electromotive force induced in the torque motor by movement of the flapper. This inherently small effect, however, will be neglected here for brevity's sake.

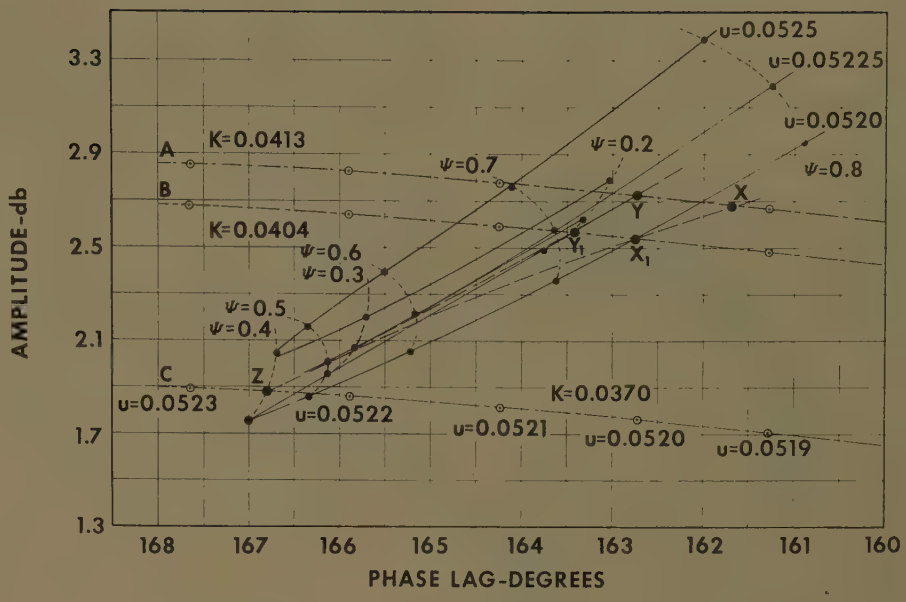


Fig. 5. A sample application of the describing function in the Nichols chart of the illustrative example

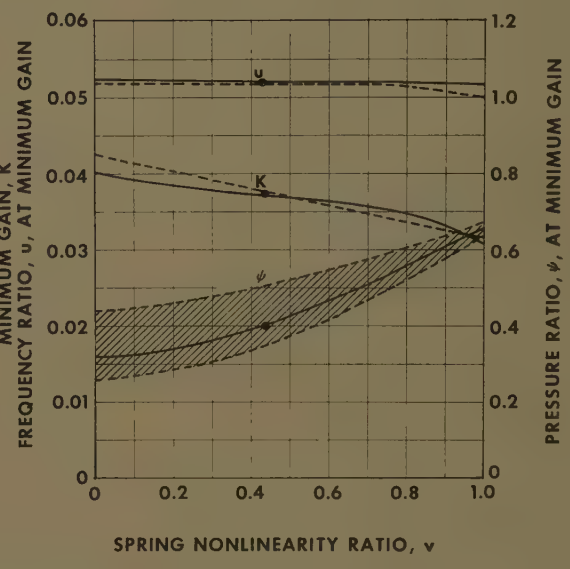


Fig. 6. Effect of the spring nonlinearity ratio, v, on the minimum gain K which is required to sustain oscillations; on the frequency, u, and the pressure amplitude, $\psi$, of these oscillations. All linear and nonlinear parameters except v have values as given in equation 37. Solid curves represent values obtained by the describing function, dashed curves were obtained by analog computer.[5] There is an uncertainty equal to the shaded area in the analog computer value of $\psi$

## Calculation of the Describing Function

The calculation of one point along the describing function will be illustrated. This will be the point at:

$u=0.05225$ (44)

$\psi=0.4$ (45)

From Fig. 3 for the selected $u=0.05225$

$\xi=0.0058$ (46)

$\theta=59.83$ deg (47)

So from Figs. 2–9 of reference 1 for $\psi=0.4$ and $\theta=59.83$

$a=1.067$
$b=0.551$
$c=0.923$
$e=0.578$
$f=0.2055$
$h=1.132$ (48)

Substituting equation 37 into equations 25 through 32

$n_1=15.44$
$n_2=6855$ (49)
$n_3=-0.0181$

Then substituting equations 37, 44, 45, 48, and 49 into equations 2, 3, 5, and 6, respectively

$S=-0.262$
$C=-1.034$ (50)

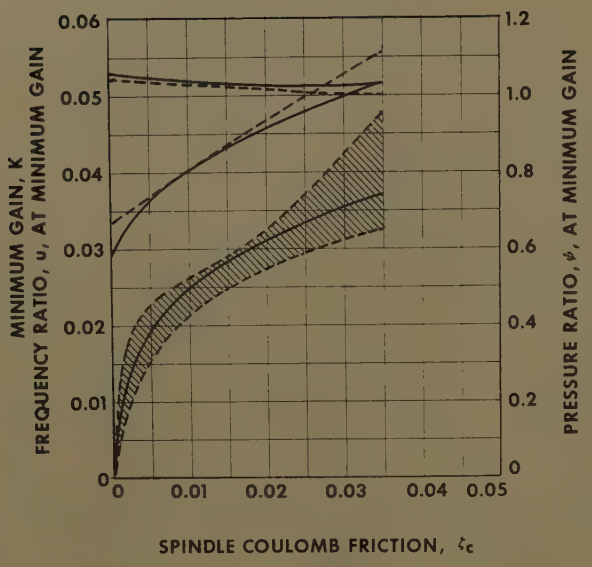


Fig. 7. Effect of the coulomb friction coefficient of the valve spindle, $\zeta_c$, on K, u, and $\psi$ of these oscillations. All linear and nonlinear parameters except $\zeta_c$ have values as given in equation 37. See Fig. 6 caption for other data

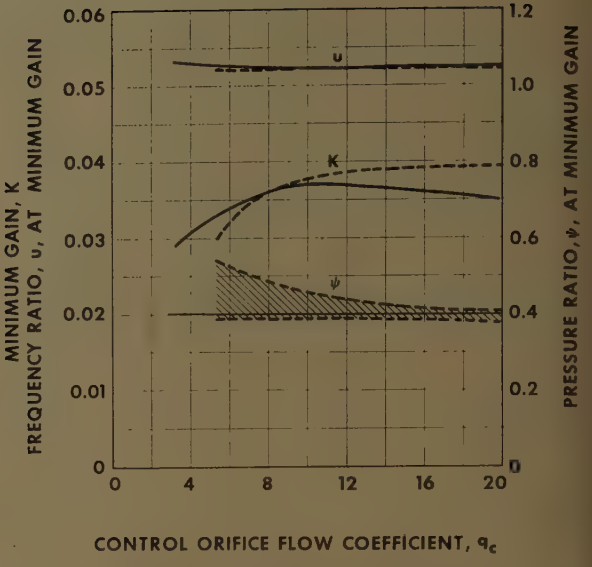


Fig. 8. Effect of the control orifice flow coefficient $q_c$, on K, u, and $\psi$ of these oscillations. All linear and nonlinear parameters except $q_c$ and $z=1.14/v_t=0.396q_c$ have values as given in equation 37. See Fig. 6 caption for other data

$$\Delta S=0.861$$
$$\Delta C=-0.444 \qquad (51)$$

Finally, substituting these along with equation 42 into equation 1

$$N(\psi, u)=0.8056\ \underline{/-13.20 \text{ deg}} \qquad (52)$$

or

$$-\frac{1}{N(\psi, u)}=1.241\ \underline{/-166.80 \text{ deg}} \qquad (53)$$

or

$$20 \log \frac{1}{|N(\psi, u)|}=20 \log 1.241$$
$$=1.88 \text{ decibels} \qquad (54)$$

$$\underline{/-\frac{1}{N(\psi, u)}}=-166.80 \text{ deg} \qquad (55)$$

The corresponding point is plotted as point $Z$ in Fig. 5. Other points of the $-1/N(\psi,u)$ curves (the grid of solid and dashed curves in Fig. 5) were obtained in similar fashion. Use has been made of a minor, desk size, digital computer in these calculations. The equations are rather ideally suited for work on such computers.

In accordance with usual describing function[4] and Nichols chart techniques, the $KG_t(ju)\ G_1(ju)\ G_L(ju)$ locus representing the linear part of the open loop is best plotted on a diaphanous sheet on the same scale as the describing function is plotted (Fig. 5). By superimposing this diaphanous sheet on the describing function with ordinate axes lined up, the effect of variations in the gain can be considered by vertically shifting the sheets so that every relative position of the $-1/N(\psi,u)$ loci and the $KG_t(ju)\ G_1(ju)\ G_L(ju)$ locus corresponds to one gain value. In Fig. 5, the $KG_t(ju)\ G_1(ju)\ G_L(ju)$ locus is shown for three gain values; curves $A$, $B$, and $C$ for gains of respectively K=0.0413, K=0.0404, and K=0.0370. Curves $A$ and $B$ each show two like-frequency intersections with the $-1/N(\psi,\ u)$ loci. These are points $X$ at $u=0.05192$ and $Y$ at $u=0.0520$ with gain $K=0.0413$, and points $X_1$ at $u=0.0520$ and $Y_1$ at $u=0.05205$ with gain $K=0.0404$. Such intersections indicate the possibility of sustained oscillations.[4] Furthermore, intersections $X$ and $X_1$ provide feasible sustained oscillations while those at points $Y$ and $Y_1$ unfeasible ones. The sustained oscillation at points $X$ or $X_1$ is feasible since a reduction of amplitude, $\psi$, carries the oscillation below the curves $A$ or $B$ indicating system instability, and so the resulting increasing amplitude returns the system into its oscillation at points $X$ or $X_1$ respectively. Conversely, an increase of amplitude, $\psi$, from its value at $X$ shifts the system into the stable region so that the increase is damped out immediately. Consequently points $X$ or $X_1$ indicate a condition where the system oscillation can be indefinitely sustained. On the other hand, sustained oscillation at points $Y$ or $Y_1$ is not practically feasible since the crossing of the two curves is reversed at $Y$ relative to the crossing at $X$. Thus, a repetition of the above discussion shows that, at the points $Y$ or $Y_1$, either an incipient decrease or an incipient increase of the amplitude becomes cumulative.

Now the behavior of the system for instance with gain $K=0.0404$ can be de-

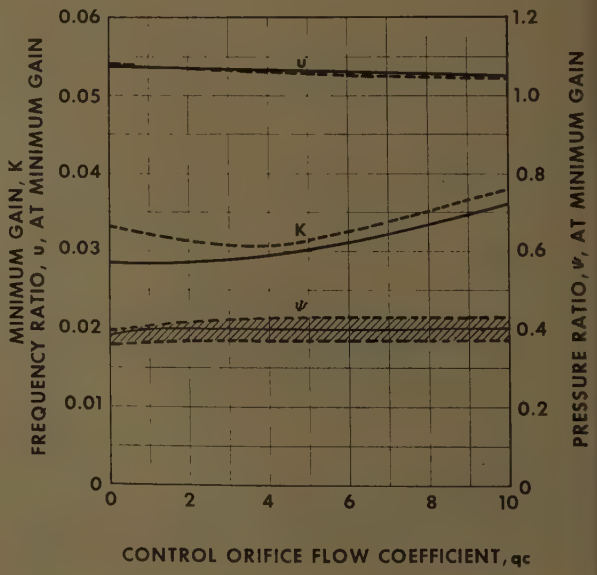


Fig. 9. Effect of the control orifice flow coefficient, $q_c$, on K, u, and $\psi$ of these oscillations. All linear and nonlinear parameters except $q_c$ and $r_1=0.1105r_3=0.2435q_c$ have values as given in equation 37. See Fig. 6 caption for other data

scribed on the basis of these results of Fig. 5. At this gain the system will not spontaneously start to oscillate; in fact oscillations started by outside disturbances shall die out unless their amplitude exceeds $\psi=0.2$ (point $Y_1$). If, however, the system is excited to an oscillation of amplitude larger than $\psi=0.2$ this oscillation will either expand or attenuate until its amplitude becomes $\psi=0.73$ (point $X_1$) where it will be sustained. With changing gain, points $X$ and $Y$ shift along the dashed curves of Fig. 5 (as may be ascertained by plotting intermediate loci of both sets). When the gain is reduced, points $X$ and $Y$ approach each other and finally, at gain $K=0.0370$ (curve $C$), they merge at point $Z$. Further reduction of gain results in no more meaningful intersections between the two sets of loci. So $K=0.0370$ is the minimum gain for the given system where sustained oscillation is marginally feasible; below this gain the system is stable in the normal linear sense. This value of gain is shown by a dark dot in Fig. 6 on the curve which shows the minimum gain for sustained oscillation as a function of the nonlinear parameter $v$. The accompanying amplitude $\psi=0.4$ and the frequency $u=0.05225$ from point $Z$ in Fig. 5 are also shown by dark dots in Fig. 6 on curves of the amplitude and frequency of the minimum-gain oscillation. Other points of the calculated curves in Figs. 7, 8, and 9 were similarly obtained.

The dashed curves in Figs. 6–9 are taken from the analog-computer studies of a companion paper[5] that fully instrumented the nonlinearities of the valve. Comparison of the calculated and measured curves shows very good agreement.

The conditions were such that it was impossible to establish accurate values of the amplitude $\psi$ at the minimum or drop out gain on the analog computer. It was possible, however, to establish the band within which $\psi$ would fall and these bands are shown in Figs. 6–9. The excellent agreement between describing function and analog computer results is evidence of the former's accuracy.

## Conclusions

In this paper a describing function has been presented which gives a complete account of the principal nonlinearities of 2-stage electrohydraulic valves, extending previous work for one-stage valves. Precalculated curves reduce the labor for computing the describing function of a specific valve to a very reasonable amount. The necessary computations are well suited for programming on smaller digital computers. It has been shown that this describing function agrees very well with analog computer results and is a powerful tool for the study of the effect of linear and nonlinear valve parameters on the dynamic operation of the valve with given loads. Such studies are helpful in selecting the best valve characteristics.

This paper also makes further use of the generalizations of the describing function method which were introduced earlier[1] for treating multiple nonlinearities and including the effect of the gain and phase of the load which is an element apart from the valve for which the describing function is being developed.

## Appendix I

The differential equations of a 2-stage hydraulic valve have been derived in a companion paper;[5] in normalized form they are for the first stage:

$$i=x_t+z(p_1-p_2)+v_t[(1-x_t)^2(p_1-p_s)-(1+x_t)^2(p_2-p_s)]+2\zeta_{ct}\frac{x_t'}{|x_t'|} \quad (56)$$

$$x_1'=x_3'-x_e' \quad (57)$$

$$x_2'=x_4'+x_e' \quad (58)$$

$$q_c x_1'=(1-x_t)\sqrt{p_1-p_s} \quad (59)$$

$$q_c x_2'=(1+x_t)\sqrt{p_2-p_s} \quad (60)$$

$$p_h-p_1=r_1x_3'+r_2^2x_3'^2 \quad (61)$$

$$p_h-p_2=r_1x_4'+r_2^2x_4'^2 \quad (62)$$

and for the second stage:

$$qx_o'=x_e\sqrt{1+\frac{x_e}{|x_e|}p} \quad (63)$$

$$m(p_1-p_2)=x_e''+2\zeta x_e'+2\zeta_c\frac{x_e'}{|x_e'|}+x_e+vpx_e \quad (64)$$

The condition studied here is that of sustained, self-excited or limit-cycle oscillations. If it is assumed that no external signal is introduced into the system then the oscillation is carried out around zero in $i$, $x_e$, $x_o$, and $x_t$ and around a constant average in case of the pressures, $p_1$ and $p_2$, in the first stage. It is then profitable to divide the pressure differences into their average and periodic components.

$$p_1=\bar{p}_1+p_{p1}(t) \quad (65)$$

$$p_2=\bar{p}_2+p_{p2}(t) \quad (66)$$

And since the valve is symmetrically built:

$$\bar{p}_1=\bar{p}_2 \quad (67)$$

Then the first-stage equations 56 through 62 can be written as:

$$i_1=x_t+z_1(p_{p1}-p_{p2})+v_1x_t^2(p_{p1}-p_{p2})-2v_1x_t(p_{p1}+p_{p2})+2\zeta_{ct_1}\frac{x_t'}{|x_t'|} \quad (68)$$

$$x_3'=x_1'+x_e' \quad (69)$$

$$x_4'=x_2'-x_e' \quad (70)$$

$$q_c x_1'=(1-x_t)\sqrt{\bar{p}_o+p_{p1}} \quad (71)$$

$$q_c x_2'=(1+x_t)\sqrt{\bar{p}_o+p_{p2}} \quad (72)$$

$$p_{o1}-p_{p1}=r_1x_3'+r_2^2x_3'^2 \quad (73)$$

$$p_{o1}-p_{p2}=r_1x_4'+r_2^2x_4'^2 \quad (74)$$

where

$$\bar{p}_o=\bar{p}_1-\bar{p}_s=\bar{p}_2-\bar{p}_s \quad (75)$$

$$p_{o1}=\bar{p}_h-\bar{p}_1=\bar{p}_h-\bar{p}_2 \quad (76)$$

To obtain the describing function, Fourier series representations will be used for $i_1$, $p_{p1}$, $p_{p2}$, $x_1'$, $x_2'$, $x_3'$, $x_4'$, $x_e$, $x_o$, and $p$. Since these functions are unknown beyond the fact that they are periodic, the coefficients of these series will be as yet unknown. It is known however that the two sides of a symmetrically built valve must oscillate exactly 180 deg out of phase with each other. So if

$$p_{p1}=\sum_{n=1}^{\infty}(p_{cn}\cos nu\tau+p_{sn}\sin nu\tau) \quad (77)$$

then there must be

$$p_{p2}=\sum_{n=1}^{\infty}[p_{cn}\cos n(u\tau+\pi)+p_{sn}\sin n(u\tau+\pi)]=\sum_{n=1}^{\infty}(-1)^n\times(p_{cn}\cos nu\tau+p_{sn}\sin nu\tau) \quad (78)$$

consequently

$$p_{p1}+p_{p2}=\sum_{n=1}^{\infty}[1+(-1)^n](p_{cn}\cos nu\tau+p_{sn}\sin nu\tau) \quad (79)$$

$$p_{p1}-p_{p2}=\sum_{n=1}^{\infty}[1-(-1)^n]\times(p_{cn}\cos nu\tau+p_{sn}\sin nu\tau) \quad (80)$$

and similarly

$$x_1'=\sum_{n=0}^{\infty}(g_n\cos nu\tau+h_n\sin nu\tau) \quad (81)$$

$$x_2'=\sum_{n=0}^{\infty}(-1)^n(g_n\cos nu\tau+h_n\sin nu\tau) \quad (82)$$

$$x_3'=\sum_{n=0}^{\infty}(e_n\cos nu\tau+f_n\sin nu\tau) \quad (83)$$

$$x_4'=\sum_{n=0}^{\infty}(-1)^n(e_n\cos nu\tau+f_n\sin nu\tau) \quad (84)$$

The definitions of equations 77 through 84 leave only a time shift of $\pi/u$ to distinguish the counterpair equations in the pairs of respectively 69 and 70, 71 and 72, 73 and 74. So these pairs now represent only one independent equation each and the set of equations 68 through 74 reduces for the first stage to:

$$i_1=x_t+z_1(p_{p1}-p_{p2})+v_1x_t^2(p_{p1}-p_{p2})-$$

$$2v_1x_t(p_{p1}+p_{p2})+2\zeta_{ct_1}\frac{x_t'}{|x_t'|} \quad (85)$$

$$x_\epsilon'=x_1'+x_\epsilon' \quad (86)$$

$$q_cx_1'=(1-x_t)\sqrt{p_o+p_{p1}} \quad (87)$$

$$p_{o1}-p_{p1}=r_1x_3'+r_2^2x_3'^2 \quad (88)$$

Eliminating $x_3'$ and $x_1'$ from 86 through 88 with equations 24 and 76

$$x_t=1+\left[\frac{r_1q_c}{2r_2^2}+q_cx_\epsilon'\right]\frac{1}{\sqrt{p_o+p_{p1}}}-\frac{q_c}{r_2}\frac{\sqrt{p_{oo}-p_{p1}}}{\sqrt{p_o+p_{p1}}} \quad (89)$$

Since $p_{p1}<<p_o$ or $p_{p1}<<p_{oo}$, binomial expansion will be used

$$\frac{1}{\sqrt{p_o+p_{p1}}}=\frac{1}{\sqrt{p_o}}\times\left(1-\frac{1}{2p_o}p_{p1}+\frac{3}{8p_o^2}p_{p1}^2-\dots\right) \quad (90)$$

$$\sqrt{p_{oo}-p_{p1}}=\sqrt{p_{oo}}\times\left(1-\frac{1}{2p_{oo}}p_{p1}-\frac{1}{8p_{oo}^2}p_{p1}^2-\dots\right) \quad (91)$$

Substituting these into equation 89 and carrying out the multiplications

$$x_t=1+\left(\frac{r_1q_c}{2r_2^2\sqrt{p_o}}+\frac{q_c}{\sqrt{p_o}}x_\epsilon'\right)\times\left(1-\frac{1}{2p_o}p_{p1}+\frac{3}{8p_o^2}p_{p1}^2-\dots\right)\times-\frac{q_c}{r_2}\sqrt{\frac{p_{oo}}{p_o}}\left(1-\frac{1}{2}\frac{p_o+p_{oo}}{p_op_{oo}}p_{p1}+\frac{3p_{oo}^2+2p_op_{oo}-p_o^2}{8p_o^2p_{oo}^2}p_{p1}^2+\dots\right) \quad (92)$$

Repeating equation 85

$$\dot{i}_1=x_t+z_1(p_{p1}-p_{p2})+v_1x_t^2(p_{p1}-p_{p2})-2v_1x_t(p_{p1}+p_{p2})+2\zeta_{ct_1}\frac{x_t'}{|x_t'|} \quad (93)$$

these two, equations 92 and 93, then represent the first stage of the valve while the second stage is described by equations 63 and 64. The two latter equations have been studied in a previous paper[1] where the assumption of a sinusoidal variation of $p$ was adopted:

$$p=\psi\cos u\tau \quad (94)$$

On this basis the first, third, and fifth harmonics of

$$x_\epsilon=\sum_{n=1,3,5}^{5}(a_n\cos nu\tau+b_n\sin nu\tau) \quad (95)$$

and the first harmonic of

$$m(p_1-p_2)=m(p_{p1}-p_{p2})=q\xi\psi u[C\cos nu\tau+S\sin nu\tau+\dots] \quad (96)$$

were determined.[1] The coefficients $a_n$ and $b_n$, as well as $S$ and $C$, were found to be functions of the amplitude, $\psi$, and frequency, $u$, of the sustained oscillation as well as the phase, $\theta$, and gain, $\xi$, of the load driven by the actuator. The latter two in turn are again functions of $u$ and $\psi$.

Consequently in extending this previous study to the first stage of the control valve the $a_n$, $b_n$, $S$ and $C$ coefficients can now be assumed known. So comparing equation 96 to equation 80

$$2mp_{c1}=q\xi\psi uC \quad (97)$$

$$2mp_{s1}=q\xi uS \quad (98)$$

$$p_{c1}=\frac{q\xi\psi uC}{2m} \quad (99)$$

$$p_{s1}=\frac{q\xi\psi uS}{2m} \quad (100)$$

and, retaining only the first two harmonics of $p_{p1}$ and $p_{p2}$, by equations 77 through 80

$$p_{p1}=\frac{q\xi\psi u}{2m}(C\cos u\tau+C_2\cos 2u\tau+S\sin u\tau+S_2\sin 2u\tau) \quad (101)$$

$$p_{p1}-p_{p2}=\frac{q\xi\psi u}{wl}(C\cos u\tau+S\sin u\tau) \quad (102)$$

$$p_{p1}+p_{p2}=\frac{q\xi\psi u}{m}(C_2\cos 2u\tau+S_2\sin 2u\tau) \quad (103)$$

where the second harmonic $C_2=2m\ p_{c2}/q\xi\psi u$ and $S_2=2m\ p_{s2}/q\xi\psi u$ is unknown since it is not directly dependent on the second stage, being absent in $p_{p1}-p_{p2}$, which represents the coupling between the two stages.

Substitution of equations 95 and 101 into equation 92 and application of some well known trigonometric identities results in a form

$$x_t=\sum_{n=0,1,2}[k_n(a_n,b_n,S,C,S_2,C_2)\cos nu\tau+l_n(a_n,b_n,S,C,S_2,C_2)\sin nu\tau] \quad (104)$$

Now for a symmetrically built valve $x_t$ must not contain second or zero order harmonics since its oscillations will have to be performed symmetrically around zero. So

$$k_0(a_n,b_n,S,C,S_2,C_2)=0 \quad (105)$$

$$k_2(a_n,b_n,S,C,S_2,C_2)=0 \quad (106)$$

$$l_2(a_n,b_n,S,C,S_2,C_2)=0 \quad (107)$$

Equations 106 and 107 can be used to eliminate $S_2$ and $C_2$ from $k_1$ and $l_1$. Equation 105 could be used for a more accurate establishment of $\bar{p}_1$. Then there remains:

$$x_t\cong k_1(a_n,b_n,S,C)\cos u\tau+l_1(a_n,b_n,S,C)\sin u\tau \quad (108)$$

This now is substituted along with equations 102 and 103 into equation 93, and after further use is made of common trigonometric identities and transformations paralleling those in reference one.

$$\dot{i}_1=\frac{qg_c}{2\sqrt{p_o}\Delta\zeta}\xi\psi u[(C+\Delta C)\cos u\tau+(S+\Delta S)\sin u\tau+\dots] \quad (109)$$

is established. The resulting equations for $S$, $C$, $\Delta S$, and $\Delta C$ are presented in equations 2, 3, 5, and 6 respectively.

A further word is required in connection with handling of the $x_t'/|x_t'|$ term in equation 93. This is a unit amplitude square wave which for a moderately distorted waveform of $x_t$, as is encountered here, will be essentially in phase with the base harmonic of $x_t'$. So the base harmonic of the square wave in turn is

$$\frac{x_t'}{|x_t'|}=+\frac{4}{\pi}\times\left[\frac{l_1}{\sqrt{k_1^2+l_1^2}}\cos u\tau-\frac{k_1}{\sqrt{k_1^2+l_1^2}}\sin u\tau\right] \quad (110)$$

Equation 109 can be written in complex form as

$$\dot{i}=\frac{\xi\psi u}{K_1}\sqrt{(C+\Delta C)^2+(S+\Delta S)^2}\times\underline{/-\tan^{-1}\frac{S+\Delta S}{C+\Delta C}} \quad (111)$$

Dividing this into the corresponding equation 121 for the linear valve, equation 1 for the describing function results.

In the preceding derivation the effects of all included nonlinearities on the first harmonic are considered. The effects which are exerted by the higher harmonics on the first through the nonlinearities are included, however the number of these higher harmonics are restricted to the second or the third in most cases.

In conflict with normal describing function practice the output rather than the input is taken as sinusoidal. This approach has been adopted earlier[1] for mathematical expediency and the results here are found to be equally as good as in that previous work.[1]

## Appendix II

The linearized form of equations 85 and 88 is defined as respectively

$$i_{1l}=x_t+z_12p_{p1} \quad (112)$$

$$x_3'=x_1'+x_\epsilon' \quad (113)$$

$$q_cx_1'=(1-x_t)\sqrt{p_0}+\frac{p_{p1}}{2\sqrt{p_o}} \quad (114)$$

$$x_3'=\frac{1}{2r_2^2}[-r_1+\sqrt{r_1^2+4r_2^2p_{o1}}]-\frac{1}{\sqrt{r_1^2+4r_2^2p_{o1}}}p_{p1} \quad (115)$$

and for the second stage linearized from equations 63 and 64

$$qx_o'=x_\epsilon \quad (116)$$

$$m2p_{p1}=x_\epsilon''+2\zeta x_\epsilon'+x_\epsilon \quad (117)$$

Solving equations 113 through 115 and making use of equations 75,76 and 24 and the condition that for the linearized valve $p_{p1}$ is a pure sinusoidal quantity, there result equation 20 and

$$x_t=\frac{q_c}{\sqrt{p_0}}x_\epsilon'+\frac{q_c}{\sqrt{p_o}}\times\left[\frac{1}{\sqrt{r_1^2+4r_2^2p_{o1}}}+\frac{1}{2g_c\sqrt{p_0}}\right]p_{p1} \quad (118)$$

Substituting equation 118 into equation 117 and making use of equations 4 and 116 gives the following:

$$2\Delta\zeta \frac{\sqrt{p_o}}{q\, q_c} i_{1l} = x_o''' + 2(\zeta+\Delta\zeta)x_o'' + x_o' \quad (119)$$

Defining

$$K_1 = 2\Delta\zeta \frac{\sqrt{p_o}}{q\, q_c(1-4p_o v_l)} \quad (120)$$

Equation 119 can be written with $x_0 = \xi\psi/\theta$ as

$$i_l = \frac{1}{K_1} \xi\psi u \sqrt{(1-u^2)^2+4(\zeta+\Delta\zeta)^2u^2} \Big/ \theta + 90 \text{ deg} - \tan^{-1}\frac{2(\zeta+\Delta\zeta)u}{1-u^2} \quad (121)$$

and the transfer function of the linearized valve

$$\frac{K_1 G_1(ju)}{} = \frac{x_o}{i_l} = K_1 \frac{1}{ju[(ju)^2+2(\zeta+\Delta\zeta)(ju)+1]} \quad (122)$$

## References


1. A Describing Function for Multiple Nonlinearities Present in Electrohydraulic Control Valves, J. Zaborszky, H. J. Harrington. *AIEE Transactions*, vol. 76, pt. I, May 1957, pp. 183–90.

2. Steady-State Axial Forces on Control Valve Pistons, Shih-Ying Lee, J. F. Blackburn. *Transactions*, American Society of Mechanical Engineers, New York, N. Y., vol. 74, 1952, pp. 1005–11.

3. Berechnung von Ausfluss und Ueberfallzahlen, R. Von Mises. *Zeitschrift des Vereines Deutscher Ingenieure*, Dusseldorf, Germany, vol. 61, May-June 1917, pp. 447–52.

4. Sinusoidal Analysis of Feedback-Control Systems Containing Nonlinear Elements, E. Calvin Johnson. *AIEE Transactions*, pt. II, July 1952, pp. 169–81.

5. Generalized Charts of the Effects of Nonlinearities in 2-Stage Electrohydraulic Control Valves, J. Zaborszky, H. J. Harrington. *Ibid.*, vol. 76, pt. II, 1957 (Jan. 1958 section), pp. 401–08.

6. Generalized Charts of the Effects of Nonlinearities in Electrohydraulic Control Valves, J. Zaborszky, H. J. Harrington. *Ibid.*, vol. 76, pt. I, May 1957, pp. 191–98.

7. A Method for the Selection of Valves and Power Pistons in Hydraulic Servos, F. C. Paddison, W. A. Good. *Report CM-717*, Applied Physics Laboratory, Johns Hopkins University, Baltimore, Md., Jan. 26, 1952.


(*Joint discussion with following paper, page 408*)

# Generalized Charts of the Effects of Nonlinearities in 2-Stage Electrohydraulic Control Valves


J. ZABORSZKY
MEMBER AIEE

H. J. HARRINGTON
ASSOCIATE MEMBER AIEE


THIS paper, which is an extension of previous work,[1,2] presents a collection of charts derived from full instrumentation on an analog computer of the equations of a closed-loop control system controlled by a 2-stage electrohydraulic control valve of the type shown in Fig. 1. The curves included in this paper show variations in the performance of the control system under the effect of variations of the individual linear and nonlinear parameters of the valve itself and of the other parts of the control system. Usually just one parameter was varied at a time while the other linear and nonlinear components had a constant, nominal value. In some cases, however, as many as three parameters were varied simultaneously. The resulting curves are presented in a general normalized way which permits the use of these results in drawing conclusions on valves of different physical dimensions. As a whole, these results are believed to promote a better understanding of the performance of valves of this type. The results listed have also been used to test the accuracy of theoretical investigations.[3]


Paper 57-780, recommended by the AIEE Feedback Control Systems Committee and approved by the AIEE Technical Operations Department for presentation at the AIEE Summer General Meeting, Montreal, Que., Canada, June 24–28, 1957. Manuscript submitted March 25, 1957; made available for printing July 9, 1957.



J. Zaborszky is with Washington University, and consultant to McDonnell Aircraft Corporation, St. Louis, Mo.; and H. J. Harrington is with McDonnell Aircraft Corporation, St. Louis, Mo.



The authors wish to thank R. C. Cowles for carrying out much of the computations for the material included in this paper.


## The System Studied

The study refers to a 2-stage 4-port electrohydraulic valve of the type shown in Fig. 1. The first-stage hydraulic amplifier of this valve regulates by the flapper, $F$, of the torque motor the relative flow of two orifices $O_1$ and $O_2$, and through this device regulates the pressures $P_1$ and $P_2$ of two leakage paths, which in turn are being fed by two fixed orifices $O_3$ and $O_4$. The $P_1-P_2$ pressure difference is then used to move the spindle of the second stage of the valve against restoring springs and dynamic forces.

This type of system contains a large number of nonlinearities. The flow relations on all six orifices are quadratic or a combination of linear and quadratic. There are reaction or Bernoulli forces on both the main valve spindle and the flapper of the torque motor. There is coulomb-type friction on the valve spindle and, in some cases, on the flapper; also there is hysteresis in the torque motor. The combination of orifices $O_1$, $O_2$, $O_3$, and $O_4$ exerts a dashpot-type nonlinear damping on the valve spindle. All these effects, as shown by the equations of Appendixes I and II, were instrumented on the analog computer.

The valve was incorporated in a closed-loop control system as shown in Fig. 2 in block diagram. This system, which also was instrumented on the analog computer, consists of a pure inertia-type load driven by an actuator with elastic coupling between the load and the actuator and a linear restoring spring on the inertia. Viscous and coulomb friction on the actuator and load are assumed, as are additional nonlinear damping terms on the load which are dependent on its acceleration and displacement respectively. The feedback is from the actuator through an electric network. There also is an inner loop resulting from a counter electromotive force induced in the torque motor by the motion of the flapper. The equations for these parts of the system are given in Appendix III. The nominal normalized parameters of the studied system are given in the section of Nominal Parameter Values.

## Scope of the Study

The study summarized was concerned with the sustained or limit-cycle oscillations of the system. There are several possible types of oscillations of this kind in the system. Some can be attributed predominantly to a single nonlinearity, for instance coulomb friction on the valve spindle. Others accompany some linear

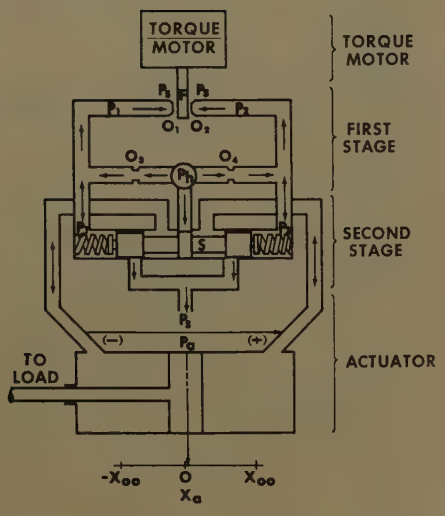


Fig. 1 (left). Sketch of a 2-stage electrohydraulic control valve

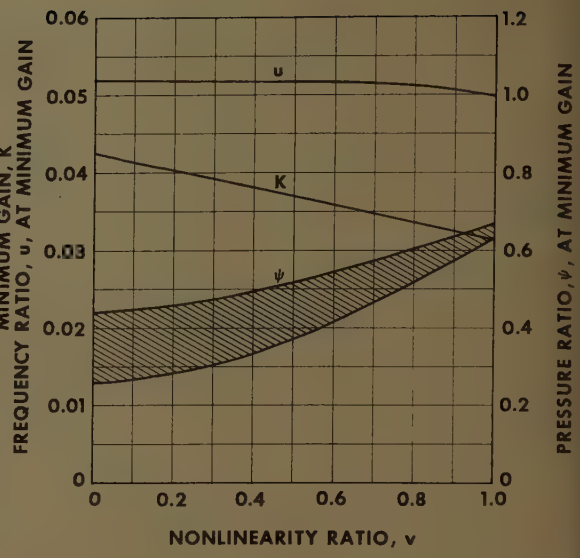


Fig. 3 (right). Effect of the spring nonlinearity ratio, v, on the minimum gain K which is required to sustain oscillations, on the frequency, u, and the pressure amplitude, $\psi$, of these oscillations. All linear and nonlinear parameters except v have values as given in Nominal Parameter Values section. There is an uncertainty equal to the shaded area in the values of $\psi$ in this curve and in Figs. 4, 15, and 16

resonance peak of the system, such as those around the natural frequency of the load inertia or of the valve spindle inertia. The latter usually show the influence of a large number of nonlinearities simultaneously.

The present study is mainly concerned with the oscillations around the resonant frequency of the load. This appears to be the most significant of the oscillations; not so much because it is highly sensitive to most nonlinear effects simultaneously, but because this tends to be the condition setting the stability margin for a system of this kind. Accordingly the study was directed mainly at finding the minimum or drop out gain, that is the smallest gain which makes it possible to maintain an oscillation, near the resonant frequency of the load. Variations of this gain with various linear and nonlinear parameters were determined. The frequency and amplitude of these sustained oscillations at the drop out gain was also established, these being functions of the gain in nonlinear systems.

The following sections discuss the effects of the various linear and nonlinear parameters in connection with the charts. The information is believed to be conveyed most effectively by the charts which will be commented on briefly.

## Effects of the Various Linear and Nonlinear Parameters

### Effect of Reaction (Bernoulli) Forces on the Valve Spindle

The parameter $v$ expresses what portion of the total spring constant on the valve spindle is derived from the reaction or Bernoulli forces[4,5] caused by the flow through the valve with zero load on the actuator piston. This reaction force is proportional to the valve opening; in this it acts as a linear spring. However, it is also proportional to the pressure drop across the valve, and this latter in effect represents a nonlinear feedback to the valve spindle. Fig. 3 shows the effects of $v$ on the valve performance. Increasing $v$ may be seen to exert a strong destabilizing effect, a strong reduction of frequency, $u$, and also a strong increase of amplitude $\psi$. Nevertheless the effect of $v$ appears to be much less on the 2-stage valve than on the single-stage one.[1,2] This may be a result of the damping action of the first-stage orifices.

### Effect of Coulomb Friction at Various Parts of the System

Coulomb friction at any part of the system exerts a marked effect on the performance. Figs. 4–9 show the effect of coulomb friction at the valve spindle, the actuator, and the load. It should be noted that in all of these coulomb friction exhibits a strong stabilizing effect (an increasing minimum gain for sustained oscillations) with very little effect on the frequency, $u$, and amplitude, $\psi$, of these oscillations, except when the coulomb friction is on the valve spindle. In the latter case the amplitude increases substantially with increasing amounts of coulomb friction and drops to zero at no coulomb friction. This does not mean that nonlinear oscillations are not possible without coulomb friction; however the nature of such oscillations changes. With coulomb friction, at the nominal parameters the oscillation is of the hard type, meaning that there is a drop-out gain which maintains an oscillation with a finite amplitude, but upon a slight reduction of this drop-out gain the oscillations disappear altogether. Without coulomb friction, at the nominal parameters the oscillation is of the soft type: the oscillation would start at a certain drop-out gain value with negligible amplitude and the amplitude would gradually increase with increasing gain. Theoretical studies based on describing functions[1,3] indicate that a drop-out gain of the discontinuous or hard type will be present without

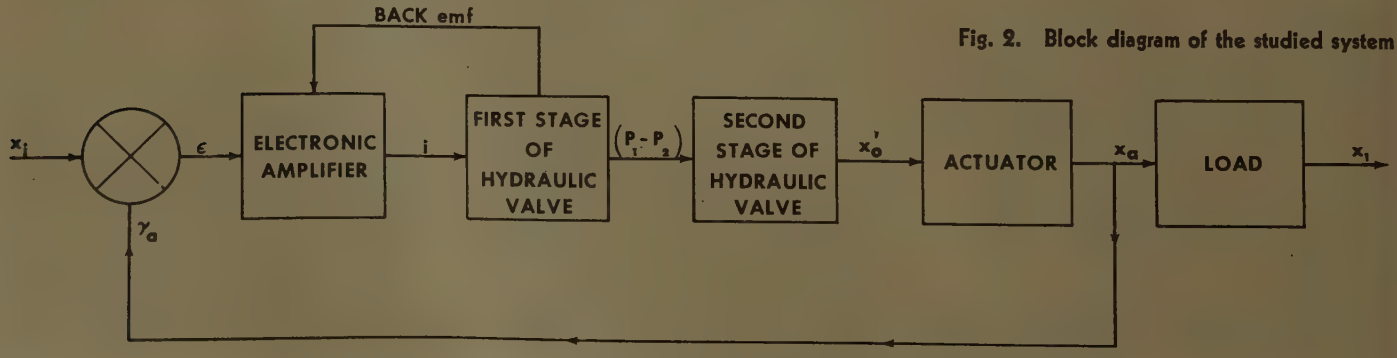


Fig. 2. Block diagram of the studied system

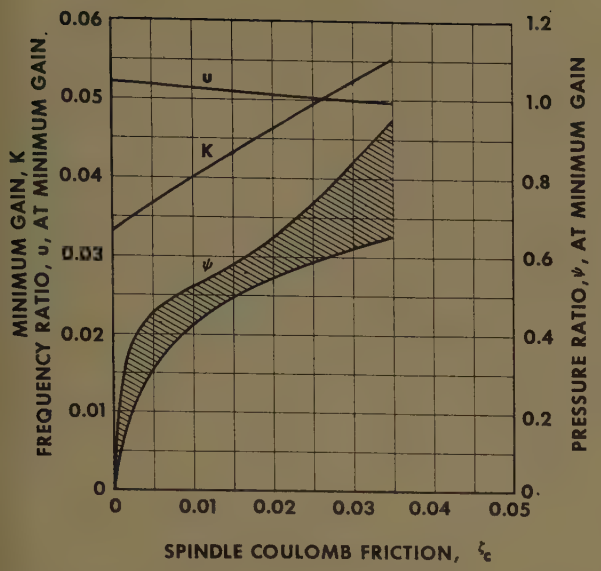


Fig. 4. Effect of the coulomb-friction coefficient of the valve spindle, $\zeta_c$, on K, u, and $\psi$ as in Fig. 3. All parameters except $\zeta_c$ are given in values section

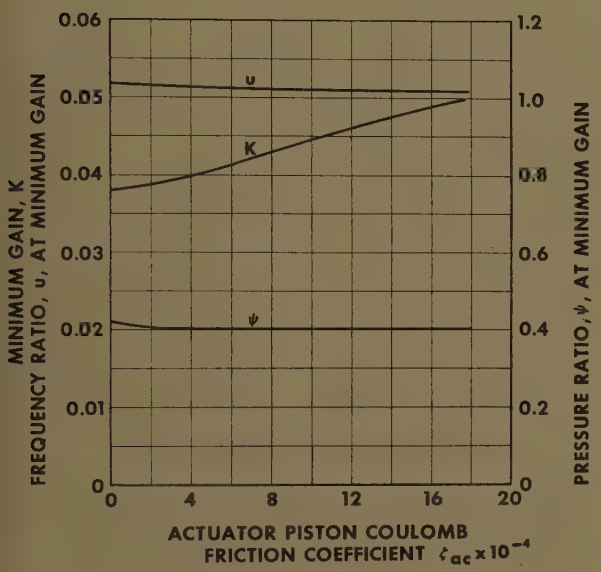


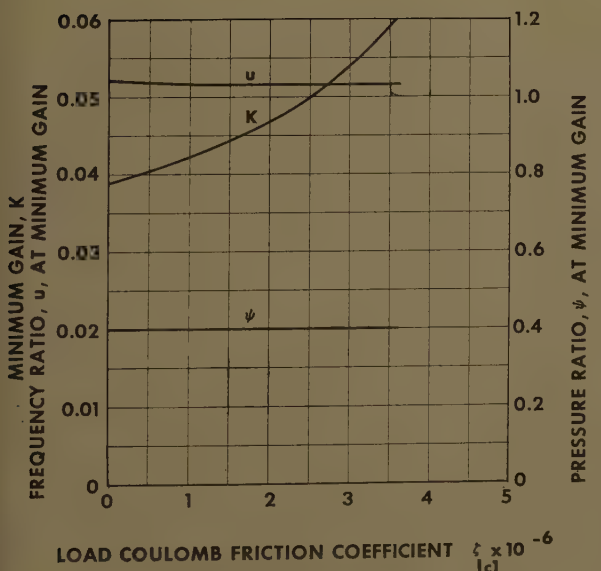


Fig. 7 (right). Effect of the displacement dependent coulomb friction coefficient, $\zeta_{lc2}$, on K, u, and $\psi$ as in Fig. 3. All parameters except $\zeta_{lc2}$ and $\zeta_{lc1}=\zeta_{lc3}=0$ are given in values section

Fig. 5 (left). Effect of the coulomb friction on the actuator piston, $\zeta_{ac}$, on K, u, and $\psi$ as in Fig. 3. All parameters except $\zeta_{ac}$ are given in values section

Fig. 8 (right). Effect of the acceleration dependent coulomb friction coefficient of the load, $\zeta_{lc3}$, on K, u, and $\psi$ as in Fig. 3. All parameters except $\zeta_{lc3}$ and $\zeta_{lc1}=\zeta_{lc2}=0$ are given in values section

Fig. 6 (left). Effect of the coulomb friction coefficient of the load, $\zeta_{lc1}$, on K, u, and $\psi$ as in Fig. 3. All parameters except $\zeta_{lc1}$ and $\zeta_{lc2}=\zeta_{lc3}=0$ are given in values section

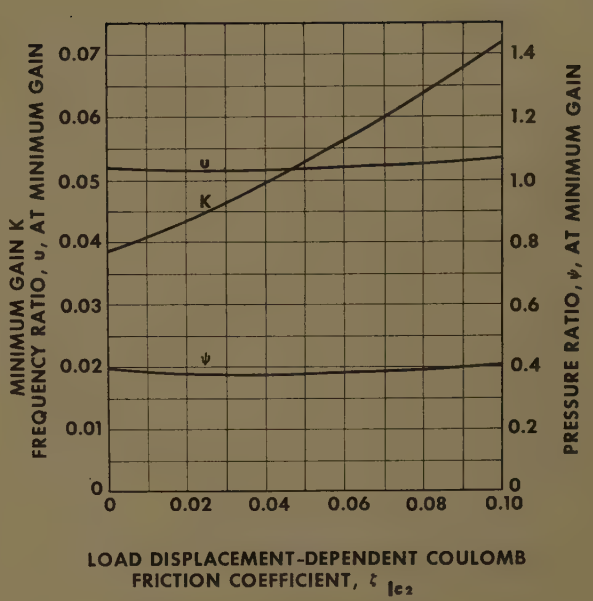


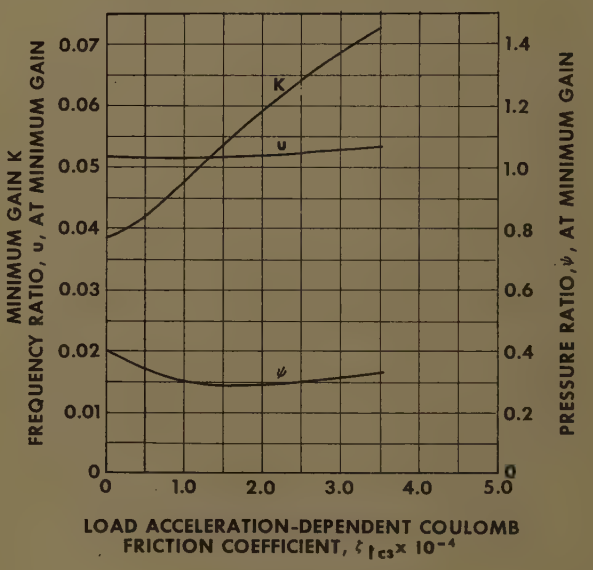


Fig. 9 (below). Effect of the simultaneous variations of the three types of load coulomb friction coefficient $\zeta_{lc1}$, $\zeta_{lc2}$ and $\zeta_{lc3}$ on K, u, and $\psi$ as in Fig. 3. All parameters except $\zeta_{lc1}$ and $\zeta_{lc2} = 403\ \zeta_{lc3} = 1.74 \times 10^5\ \zeta_{lc1}$ are given in values section

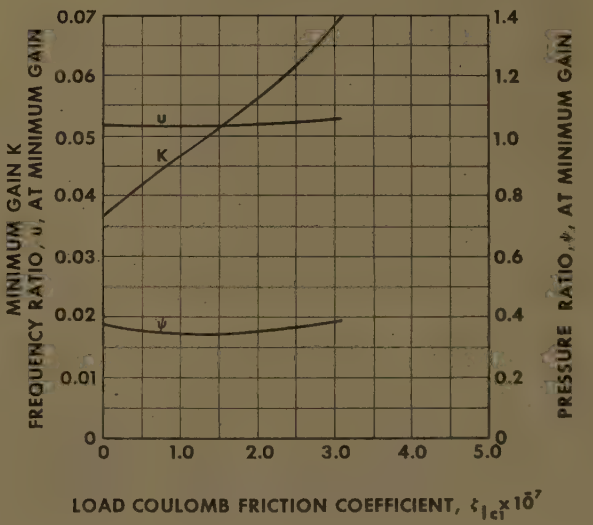

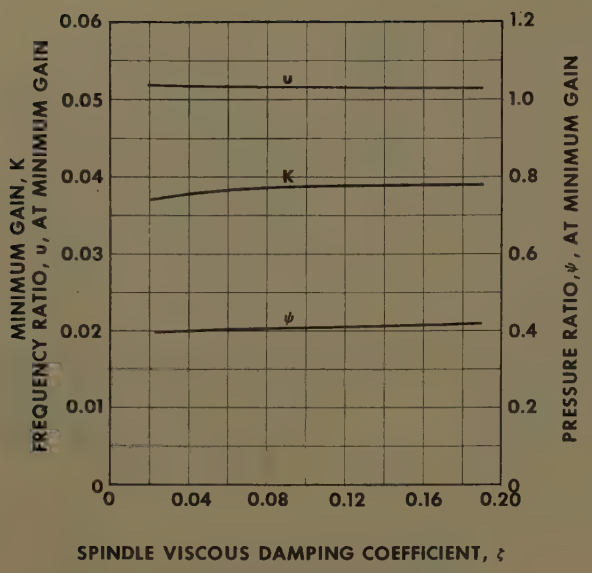


Fig. 10 (left). Effect of the viscous friction on the valve spindle, $\zeta$, on K, u, and $\psi$ as in Fig. 3. All parameters except $\zeta$ are given in values section

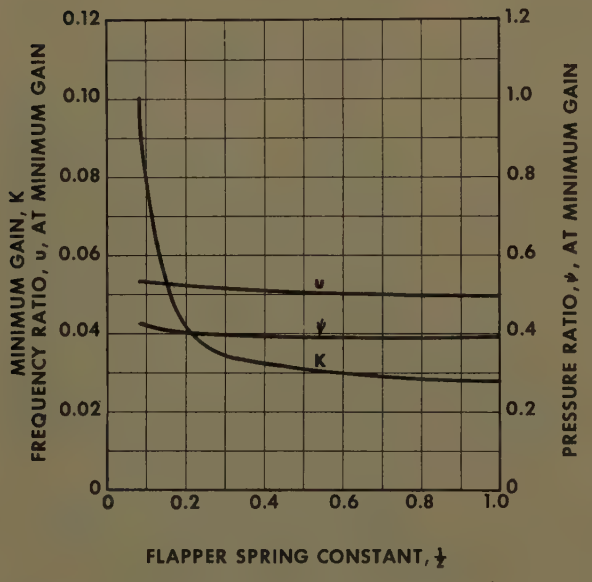


Fig. 11 (left). Effect of the flapper spring constant, 1/z, on K, u, and $\psi$ as in Fig. 3. All parameters except 1/z and $v_t = 0.0638z$ are given in values section

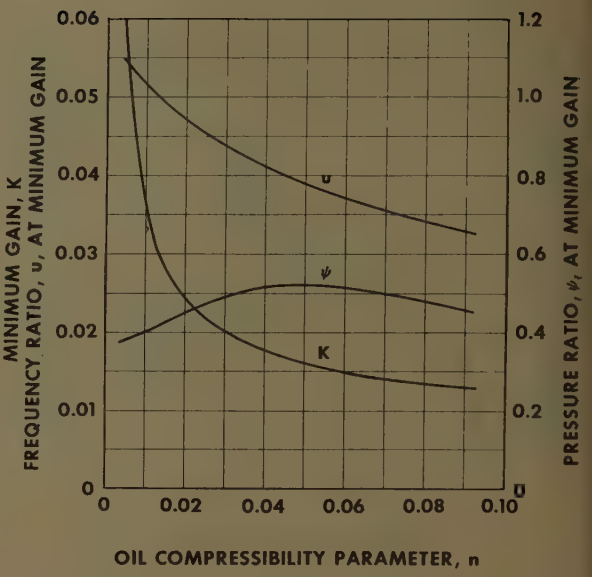


Fig. 12 (right). Effect of the oil compressibility, n, on K, u, and $\psi$ as in Fig. 3. All parameters except n are given in values section

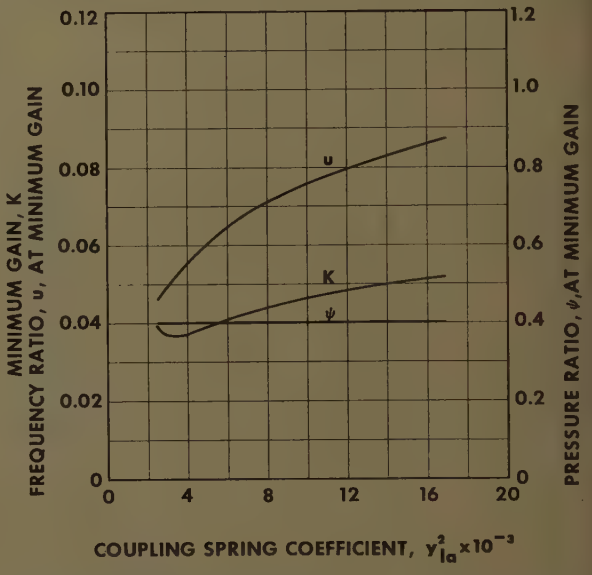


Fig. 13. Effect of the coefficient, $y_{1a}^2$, of elasticity of coupling between actuator and load on K, u, and $\psi$ as in Fig. 3. All parameters except $y_{1a}^2$ are given in values section

coulomb friction also if the parameter $v$ exceeds substantially the value of the $v$ in the Nominal Parameter Values section.

If it appears to be a paradox that coulomb friction should have a stabilizing effect, it should be remembered that the oscillation considered here is the one around the linear resonance condition of the load; at this point coulomb friction is only one of the parameters influencing the oscillations. At a much higher gain and much lower frequency in the studied system another sustained oscillation could be observed which was produced predominantly by the coulomb friction in the valve.

Some discussion of the three types of coulomb friction considered on the load is necessary. All are coulomb type in the sense that they act in a direction opposite to the direction of the velocity, $x_l'$, and that their magnitude is independent of the velocity. But while $\zeta_l c_l$ represents

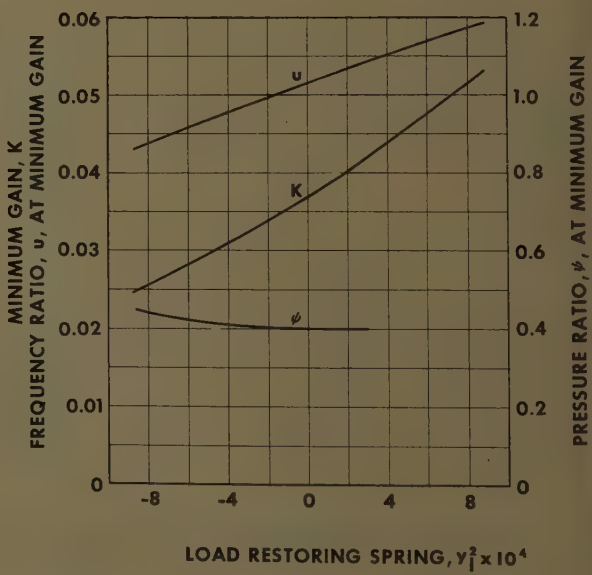


Fig. 14. Effect of the coefficient, $y_1^2$, of restoring spring of the load on K, u, and $\psi$ as in Fig. 3. All parameters except $y_1^2$, are given in values section

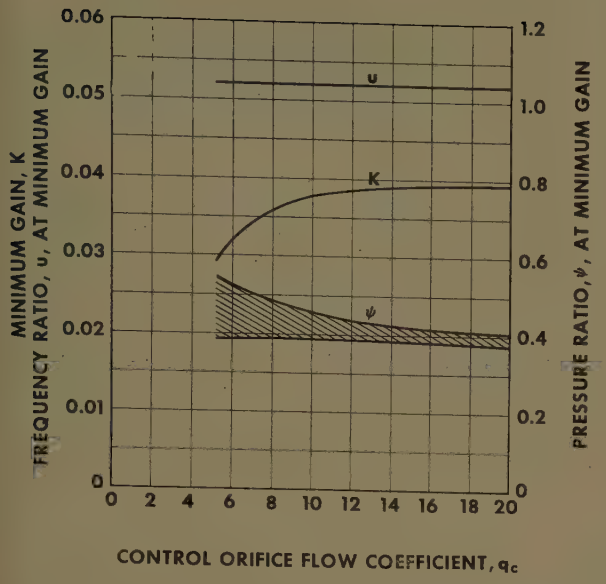


Fig. 15 (left). Effect of the control orifice flow coefficient, $q_c$, on K, u, and $\psi$ as in Fig. 3. All parameters except $q_c$ and $z = 1.14/v_t = 0.396 \times q_c$ are given in values section

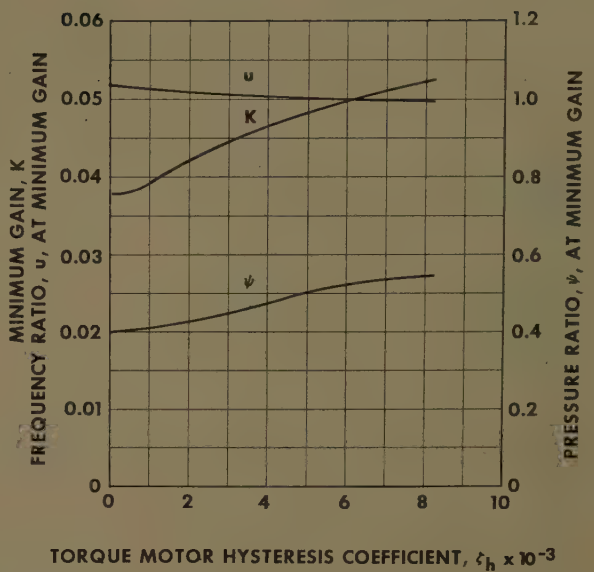


Fig. 16 (below). Effect of the control orifice flow coefficient $q_c$, on K, u, and $\psi$ as in Fig. 3. All parameters except $q_c$ and $r_1 = 0.1105$ $r_2 = 0.2435 q_c$ are given in values section

Fig. 17. Effect of the torque motor hysteresis coefficient, $\zeta_h$ on K, u, and $\psi$ as in Fig. 3. All parameters except $\zeta_h$ are given in values section

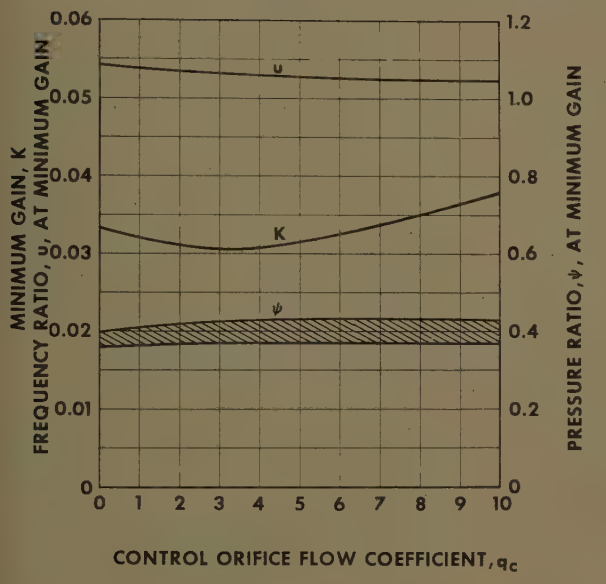


Fig. 18 (right). Effect of the normalized sump pressure, $p_s$ on K, u, $\psi$ as in Fig. 3. All parameters except $p_s$ are given in values section

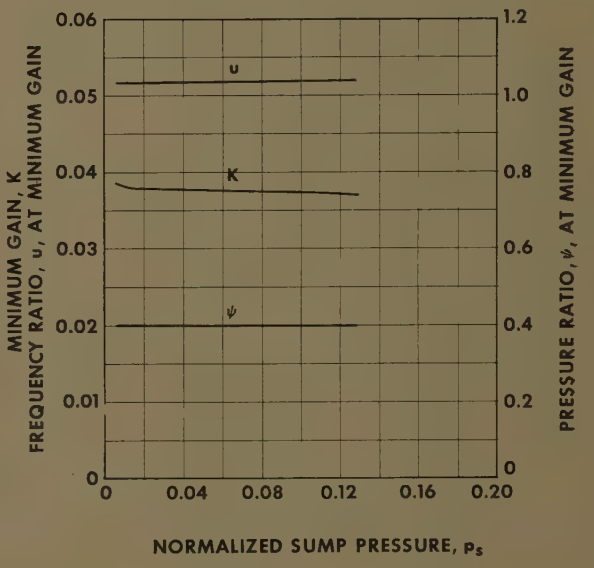


a conventionally interpreted coulomb friction, the forces associated with $\zeta_1 c_2$ and $\zeta_1 c_3$ are respectively proportional to the absolute value of the displacement, $|x_l|$, and the absolute value of the acceleration, $|x_l''|$. Such friction components may arise on some loads when respectively the center of the restoring torque and the center of gravity of the load inertia do not coincide with the axis of the load. In such cases displacement or acceleration shall result in pressure and friction at the hub of the load.

All three afore-mentioned types of coulomb friction, according to Figs. 6, 7, and 8 have the same general effect but the acceleration induced appears to be the most effective. Fig. 9 shows the simultaneous effects of the three types of coulomb friction terms mixed in a definite arbitrary ratio.

### Effect of Viscous Friction at the Valve Spindle

According to Fig. 10 the effect of viscous friction of the valve spindle is a stabilizing one; a predictable result. Fig. 10 also shows, however, the slight effect from this source.

### Effect of the Various Elastic Elements of the System

The effects of the various elastic elements within the system are illustrated by Figs.11–14. From these figures it may be observed that harder springs (smaller $n$, larger $y^2_{1a}$ or $y^2_1$) always lead to a marked increase in the frequency of oscillations and, except for small values of $y^2_{1a}$, tend to have a stabilizing effect on the system. The amplitude of the oscillations is affected but slightly. Finally, the flapper spring constant $l/z$, is effective mainly if it is quite soft; then softer spring means more stability. The effec, of the flapper spring constant on fret quency or on amplitude is always small-however. The physical significance of decreasing the flapper spring constant is to emphasize the importance of the pressure and Bernoulli forces acting on the flapper; apparently these forces act as a stabilizing dynamic feedback for the system.

### Effect of the Flow Coefficient of the Control Orifice

The effect of the flow coefficient of the control orifice was studied under two conditions as recorded in Figs. 15 and 16. The former chart signifies variations in the dimensional parameter, $D$, while the latter allows an over-all change in first-stage flow rates.

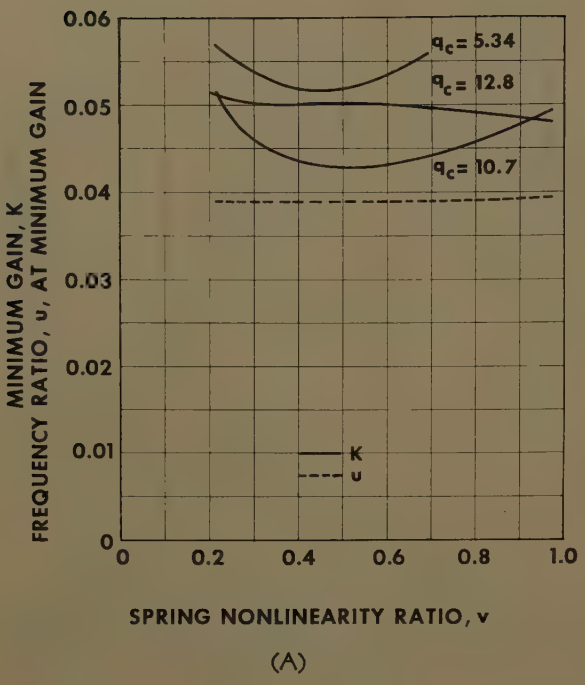


(A)

Fig. 19(A). Effect of the spring nonlinearity ratio, v, and of the flow coefficient, $q_c$, on K, u, and $\psi$ as in Fig. 3. All parameters except v, $q_c$, $r_1 = 0.1105$ $r_2 = 0.2435 q_c$, and $y_{1a}^2 = 0.00169$ are given in the values section

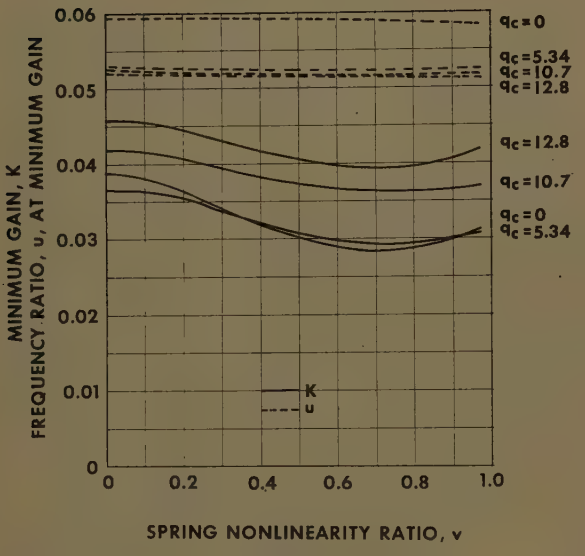


(B)

Fig. 19 (B). Effect of the spring nonlinearity ratio, v, and flow coefficient, $q_c$, on K, u, and $\psi$ as in Fig. 3. All parameters except v, $q_c$, $r_1 = 0.1105 \times r_2 = 0.2435$ $q_c$, and $y_{1a}^2 = 0.00338$ are given in the values section

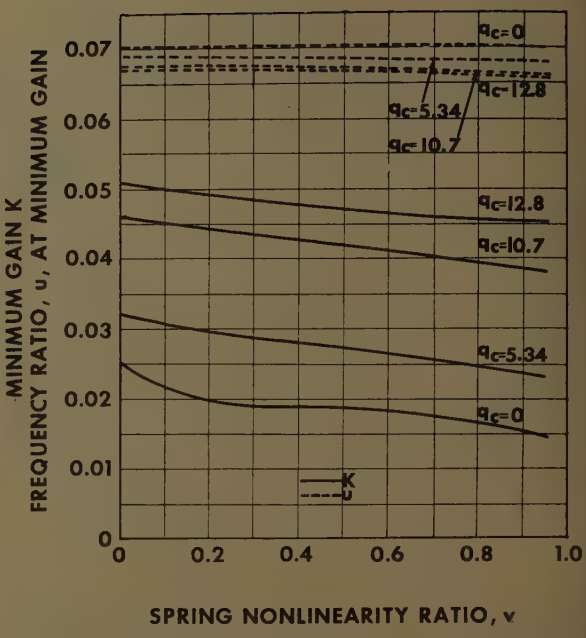


(C)

Fig. 19(C). Effect of the spring nonlinearity ratio, v, and flow coefficient, $q_c$, on K, u, and $\psi$ as in Fig. 3. All parameters except v, $q_c$, $r_1 = 0.1105$ $r_2 = 0.2435 q_c$, and $y_{1a}^2 = 0.00677$ are given in the values section

### Effect of the Hysteresis in the Torque Motor

This effect is shown in Fig. 17 and is found to be somewhat stabilizing at the mode of oscillation near the resonant frequency of the load. In this it is similar to the effects of coulomb friction in various parts of the system as should be expected.

### Effect of Normalized Sump Pressure

The effect of sump pressure is quite negligible according to Fig. 18, at least within the studied range over which this pressure has been varied.

### Simultaneous Variation of Three Parameters

The three parameters selected for variation in obtaining Figs. 19(A), 19(B), and 19(C) are

1. The spring nonlinearity ratio, $v$, of the valve which has a rather dominating effect on the performance.

2. The stiffness, $y_{1a}^2$, of the linkages between actuator piston and load inertia which determines primarily the frequency of the oscillations.

3. The flow parameter, $q_c$, of the control orifice.

It is interesting that with the two stage valve the effect of $v$, the spring nonlinearity ratio, is highly dependent on the parameters $y_{1a}^2$ and $q_c$. In fact even the tendency of variation with $v$ can be reversed; with some $q_c$ and $y_{1a}^2$ combinations it is stabilizing, with others it is destabilizing. Increasing $y_{1a}^2$ is generally destabilizing and results in increasing the frequency, $u$. However the destabilizing effect of $y_{1a}^2$ is also strongly dependent on the other two parameters, the effect being much less pronounced for large values of $q_c$ for example. The same strong interdependence is apparent in the generally stabilizing effect of increasing $q_c$. These results indicate that caution should be exercised in applying the results presented in the charts when the parameter values differ strongly from those chosen as nominal in this study.

### Effects of Gain Variations

An interesting peculiarity of the sustained oscillations which were studied here is illustrated by Fig. 20. This shows the variations of frequency, $u$ and amplitude-$\psi$, with the gain above the drop-out gain which for the set of parameters used in Fig. 20 is $K = 0.04$. Above this gain value the oscillations diverge rather rapidly in amplitude. However stable oscillations are again resumed at about $K = 0.18$ and these latter oscillations converge with increasing gain. The frequency is near the natural frequency of the load for both oscillations. A loop in the Nichols chart of the system together with describing function considerations[3] indicates the presence of these two stable oscillating regions.

## Conclusions

The results of the analog computer study of 2-stage electrohydraulic control valves is presented. It would be a rather impossible task to vary all the numerous linear and nonlinear parameters simultaneously over their practical ranges. Consequently only a maximum of three parameters has been varied in this fashion,

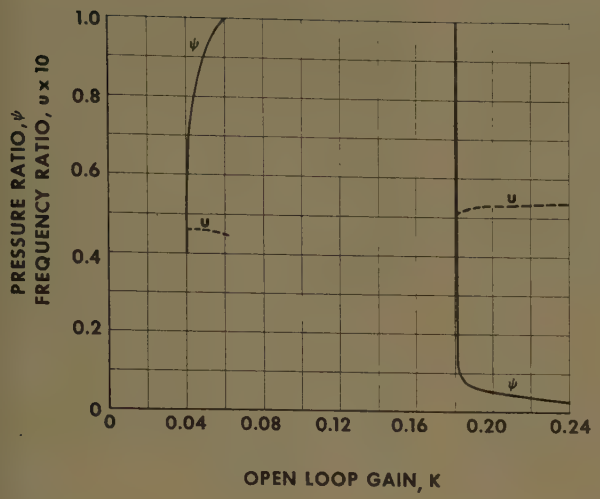


Fig. 20 (left). Loci of frequency, u, and pressure amplitude, $\psi$, of sustained oscillations versus gain, K. All parameters except $y_{la}^2 = 0.00254$ are given in values section

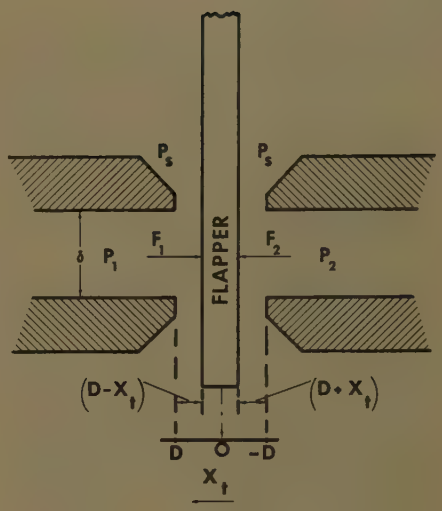


Fig. 21 (right). Sketch of the control orifice

and in most of the study all parameters but one were kept at the constant values given in the section of Nominal Parameter Values. Even so it is believed that the results of the study as summarized in the curves are useful in gaining insight into the influences of various linear and nonlinear parameters on the operation of systems with two stage hydraulic valves. Even the drawing of semi-quantitative conclusions on the basis of the curves seems fairly safe if the normalized system parameters do not deviate very far from the nominal values given. The normalized form of presentation enhances the usefulness of the results.

## Nomenclature*

Any consistent system of units can be used for the quantities defined in the following.

$D$ = distance between flapper and either control orifice when flapper is centered; see Fig. 21

$E = X_t - K_f X_0$ = servo error

$F_{ac}$ = coulomb-friction force of actuator piston

$f_a$ = viscous damping coefficient of actuator piston

$F_{lc1}$ = coulomb-friction force of load

$F_{lc2}$ = coefficient of amplitude-dependent coulomb friction of load

$F_{lc3}$ = coefficient of acceleration-dependent coulomb friction of load

$f_l$ = viscous damping coefficient of load

$h_a = \dfrac{AP}{M_a X_{oo} \omega_n^2}$ = normalized form of $A$

$[I]_h$ = torque motor current distorted by hysteresis

$[i]_h = \dfrac{K_T}{Dk_t}[I]_h$ = normalized form of $[I]_h$

$k = \dfrac{X_{oo}}{X_{lo}}$ = proportionality factor

$K_{at}$ = coefficient of back electromotive force (emf) induced by motion of flapper in magnetic field

$k_{at} = \dfrac{K_{at} K_T}{k_t L}$ = normalized form of $K_{at}$

$K_f$ = electrical gain of feedback transducer; see $E$

$K_{la}$ = spring constant of linkage between actuator piston and load

$K_T$ = force constant of torque motor

$k_t$ = equivalent spring constant of flapper restoring spring (including magnetic forces)

$L$ = inductance of torque motor coil

$l_a = \dfrac{\mu_a K_f K_T X_{oo}}{D k_t L \omega_n}$ = normalized form of $\mu_a$

$K_l$ = restoring spring constant of load

$M_a$ = mass of actuator piston

$M_l$ = mass of load

$n = \dfrac{V_o P}{4\beta A X_{oo}}$ = normalized oil compressibility parameter

$R$ = resistance of torque motor coil

$r = \dfrac{R + r_p}{L\omega_n}$ = normalized form of $R + r_p$

$r_p$ = plate resistance of output stage of electronic amplifier

$V_o$ = total volume of oil on both sides of the actuator piston between the piston and the valve

$w = \sqrt{\dfrac{K_{la}}{M_a \omega_n^2}}$ = normalized form of the undamped natural frequency of the actuator piston

$X_f$ = input emf to the servo

$x_t = \dfrac{X_t}{K_f X_{oo}}$ = normalized form of $X_t$

$X_l$ = displacement of the load

$X_{lo}$ = maximum displacement of load from center

$x_l = \dfrac{X_l}{X_{lo}}$ = normalized form of $X_l$

$y_l = \sqrt{\dfrac{K_l}{M_l \omega_n^2}}$ = normalized form of the undamped natural frequency of the load referred to $K_l$ when $K_{la}$ is assumed zero

$y_{la} = \sqrt{\dfrac{K_{la}}{M_l \omega_n^2}}$ = normalized form of the undamped natural frequency of the load referred to $K_{la}$ when $K_l$ is assumed zero

$\beta$ = bulk modulus of the oil

$\delta$ = diameter of control orifice; see Fig. 21

$\epsilon = \dfrac{E}{K_f X_{oo}}$ = normalized form of $E$

$\zeta_a = \dfrac{f_a}{2\sqrt{M_a K_{la}}}$ = normalized form of $f_a$

$\zeta_{ac} = \dfrac{F_{ac}}{2M_a X_{oo} \omega_n^2}$ = normalized form of $F_{ac}$

$\zeta_h = \dfrac{K_T I_h}{2k_t D}$ = normalized hysteresis coefficient

$\zeta_{lc1} = \dfrac{F_{lc1}}{2M_l X_{lo} \omega_n^2}$ = normalized form of $F_{lc1}$

$\zeta_{lc2} = \dfrac{F_{lc2}}{2M_l \omega_n^2}$ = normalized form of $F_{lc2}$

$\zeta_{lc3} = \dfrac{F_{lc3}}{2M_l}$ = normalized form of $F_{lc3}$

$\mu_a$ = gain of electronic amplifier

$\omega_n = \sqrt{\dfrac{k_m + BP}{M_m}}$ = undamped natural frequency of the linearized valve spindle

* Additional notation may be found in a companion paper.[1]

## Nominal Parameter Values

| | |
|---|---|
| $h_a = 0.0260$ | $v_t = 0.2696$ |
| $k = 1.00$ | $w^2 = 0.489$ |
| $k_{at} = 0.322$ | $y_l^2 = 0$ |
| $l_a = 9.26$ | $y_{la}^2 = 0.00338$ |
| $m = 4.168$ | $z = 4.226$ |
| $n = 0.00920$ | $\zeta = 0.0190$ |
| $p_h = 1.023$ | $\zeta_a = 0.626$ |
| $p_s = 0.0234$ | $\zeta_{ac} = 0$ |
| $q = 428.7$ | $\zeta_c = 0.00574$ |
| $q_c = 10.69$ | $\zeta_h = 0$ |
| $r = 2.0$ | $\zeta_l = 0.0333$ |
| $r_1 = 2.598$ | $\zeta_{lc1} = 0$ |
| $r_2 = 23.50$ | $\zeta_{lc2} = 0$ |
| $v = 0.432$ | $\zeta_{lc3} = 0$ |

## Appendix I. Derivation of the Equations of the First Stage of the Valve

The various equations shall be written first in dimensional form and then normalized.

1. Flow relations on the two control orifices $O_1$ and $O_2$

$$Q_1 = \sqrt{2}\, C_{qc} K_v L_c (D - X_t) \sqrt{P_1 - P_s} \qquad (1)$$

$$Q_2 = \sqrt{2}\, C_{qc} K_v L_c (D + X_t) \sqrt{P_2 - P_s} \qquad (2)$$

These are simply the general flow relations for sharp-edged orifices (assuming $D \ll \delta$) with $P_1 - P_s$ and $P_2 - P_s$ being the respective pressure drops across the orifices and $L_c(D - x_t)$ and $L_c(D + x_t)$ the respective orifice cross sections (Fig. 21). Normalized, equations 1 and 2 become

$$q_c x_1' = (1 - x_t) \sqrt{p_1 - p_s} \qquad (3)$$

$$q_c x_2' = (1+x_t)\sqrt{p_2 - p_s} \quad (4)$$

It should be noted that the flows $Q_1$ and $Q_2$ are normalized in terms of equivalent valve spindle speed; the speed at which the valve spindle would push the amount of flow in question before it. This principle will be applied in what follows to all flows in the first stage.

2. Flow relations on the fixed orifices $O_3$ and $O_4$.

$$P_h - P_1 = \frac{8\mu l}{\pi r_o^4} Q_3 + \frac{1}{(\sqrt{2}\, C_{qF} K_v A_o)^2} Q_3^2 \quad (5)$$

$$P_h - P_2 = \frac{8\mu l}{\pi r_o^4} Q_4 + \frac{1}{(\sqrt{2}\, C_{qF} K_v A_o)^2} Q_4^2 \quad (6)$$

These equations take into consideration the fact that orifices $O_3$ and $O_4$ tend to consist of narrow tubes of considerable length. Accordingly the first terms on the right give the pressure drop for the laminar flow in these narrow tubes, while the second terms are the pressure drops caused by the discharge at the tube ends. Normalized, equations 7 and 8 become

$$p_h - p_1 = r_1 x_3' + r_2^2 x_3'^2 \quad (7)$$

$$p_h - p_2 = r_1 x_4' + r_2^2 x_4'^2 \quad (8)$$

3. Continuity relations for the two leakage channels:

$$Q_3 - Q_1 = A_v \dot{X}_\epsilon \quad (9)$$

$$Q_4 - Q_2 = -A_x \dot{X}_\epsilon \quad (10)$$

which simply expresses the fact that the difference of the oil volume flowing through either pair of fixed and control orifices in series is used to replace oil behind the spindle when the latter is moving. The oil is considered incompressible in these passages which is justified by the small volume and rather uniform pressure. In normalized form, equations 9 and 10 become

$$x_3' = x_1' + x_\epsilon' \quad (11)$$

$$x_4' = x_2' - x_\epsilon' \quad (12)$$

4. Dynamics of the torque motor flapper:

$$K_T[I]_h = k_t X_t + A_c(P_1 - P_2) + (F_1 - F_2) \quad (13)$$

On the left-hand side stands the electric torque delivered by the torque motor to the flapper, $[I]_h$ being the torque motor current as modified by the hysteresis. On the right the first term is the mechanical spring action on the flapper, which may be its own elasticity, the second term is the force on the flapper which results from the static pressure difference in the two leakage channels. The last term finally represents the reaction forces from the fluid flow and this term merits a few words of explanation. These reaction forces derive from the change of momentum occurring when the fluid that is coming in along the axis of the channel leading to the control orifices discharges radially along the surface of the flapper (Fig. 21). The corresponding reaction force on the two sides of the flapper will be:

$$F_1 = \rho Q_1 V_1 = \rho Q_1^2 \frac{1}{A_c} \quad (14)$$

$$F_2 = \rho Q_2 V_2 = \rho Q_2^2 \frac{1}{A_c} \quad (15)$$

Substituting equation 1 and 2 into 14 and 15, respectively, and the latter in turn into equation 13 there results after normalizing:

$$[i]_h = x_t + z(p_1 - p_2) + v_t[(1-x_t)^2(p_1 - p_s) - (1+x_t)^2(p_1 - p_2)] \quad (16)$$

## Appendix II. Equations of the Second Stage of the Valve

These equations have been derived[1,2] with a slight difference and they are in normalized form:

$$m(p_1 - p_2) = x_\epsilon'' + 2\zeta x_\epsilon' + 2\zeta_o \frac{x_\epsilon'}{|x_\epsilon'|} + x_\epsilon + vp|x_\epsilon| \quad (17)$$

and

$$g x_o' \sqrt{1 + p\frac{x_\epsilon}{|x_\epsilon|}} \quad (18)$$

One difference with reference 1 or 2 is the left hand side of equation 17 which for the one stage valve[1,2] is the force exerted by the torque motor on the valve spindle, and for the 2-stage valve of course is the force exerted by the static pressures at the two ends of the spindle. The other difference is the absence in equation 17 of an explicit dashpot-type damping term, since dashpot damping also is now implicit in $(p_1 - p_2)$.

## Appendix III. Differential Equations Exclusive of Control Valve

With the exception of the acceleration- and position-dependent coulomb friction terms of the load, the equations given here are identical to those derived in reference 2. Consequently, the equations will be only summarized in their non-dimensional form.

1. Compressibility of oil in actuator cylinder

$$x_a - x_o = np \quad (19)$$

2. Equations of motion of the actuator piston

$$x_a'' + 2\zeta_a w x_a' + 2\zeta_{ac}\frac{x_a'}{|x_a'|} + w^2(x_a - x_l/k) + h_a p = 0 \quad (20)$$

3. Equation of motion of the load

$$x_l'' + 2\zeta_l y_{la} x_l' + [2\zeta_{lc1} + 2\zeta_{lc2}|x_l| + 2\zeta_{lc3}|x_l''|]\frac{x_l'}{|x_l'|} + y_{la}^2(x_l - k x_a) + y_l^2 x_l = 0 \quad (21)$$

Here it is assumed that coulomb friction varies directly with bearing normal force loading and that the latter varies linearly with both the absolute value of load position and of load acceleration.

4. Equation of error signal

$$\epsilon = x_t - x_a \quad (22)$$

5. Differential equation of amplifier and torque motor

$$a\epsilon = i' + ri + k_a x_t' \quad (23)$$

This equation differs from its counterpart in reference 2 only in that the back emf term is now derived from flapper rate, $x_t'$, rather than spindle rate, $x_\epsilon'$.

## References


1. A Describing Function for Multiple Nonlinearities Present in Electrohydraulic Control Valves, **J. Zaborszky, H. J. Harrington.** *AIEE Transactions*, vol. 76, pt. I, May 1957, pp. 183–90.

2. Generalized Charts of the Effects of Nonlinearities in Electrohydraulic Control Valves, **J. Zaborszky, H. J. Harrington.** *Ibid.*, pp. 191–98.

3. A Describing Function for the Multiple Nonlinearities Present in 2-Stage Electrohydraulic Control Valves, **J. Zaborszky, H. J. Harrington.** *Ibid.*, pt. II, 1957 (Jan. 1958 section), pp. 394–401.

4. Steady-State Axial Forces on Control Valve Pistons, **Shih-Ying Lee, J. F. Blackburn.** *Transactions*, American Society of Mechanical Engineers, New York, N. Y., vol. 74, 1952, pp. 1005–11.

5. Berechnung von Ausfluss und Ueberfallzahlen, **R. Von Mises.** *Zeitschrift des Vereines Deutscher Ingenieure*, Düsseldorf, Germany, vol. 61, May-June 1917, pp. 447–52.


## Joint Discussion of Papers 57-779 and 57-780

**L. R. Axelrod** and **W. L. Kinney** (Cook Research Laboratories, Morton Grove, Ill.): The authors of this paper and its companion paper are to be complimented for their efforts in applying describing function techniques to the multiple nonlinearities present in an electrohydraulic servo valve. Our organization has also been studying this type of valve, but the analytical aspects of the study have been principally centered around use of small perturbation techniques to establish suitable transfer functions for these valves. This work has been done during the past 4 years under various Air Force contracts and has led to a successful method of predicting dynamic response from system static characteristics. Our present program consists in part of simulating an electrohydraulic servo valve as a function of its internal operating characteristics on an analogue computer. Hence, this paper appeared at a very opportune time.

The authors' use of dimensionless (normalized) quantities was, from our standpoint, an unfortunate choice since the effect on valve operation as caused by a change in one physical parameter became somewhat obscured. Also, since no numerical values for the physical parameters were given it was impossible to compare

the authors' normalized servo system to typical systems which we have used to experimentally verify our analytical approach to this problem. If the author's have attempted any experimental verification of their analytical solution, a discussion of this work would be enlightening.

We agree with the author's statement that electrohydraulic valve controlled systems contain a large number of nonlinearities. However, it is our opinion that some of the more significant of these were not included. Items such as torque-motor saturation, flow saturation in first and second stages, pressure saturation, reduction in maximum available pressure at small spool displacements (a problem at higher frequencies), and amount of under or overlap all may be significant in an actual valve and should be considered in a complete analysis.

**J. Zaborszky and H. J. Harrington:** The comments of Messrs. Axelrod and Kinney are appreciated. It would seem, however, that the use of a normalized treatment should facilitate rather than hinder the comparison of the results of this paper and its companion[1] to their physical systems. For this sort of comparison, of course, it is necessary to compute the normalized parameters from the physical parameters of their system. This can be accomplished with the set of equations 7 through 32 of the first paper[1] and the notations of both papers. If then the normalized parameters so obtained do not match those of the lilustrative example of the paper, results corresponding to the illustrative example, but for the system in question, can be obtained through comparatively little effort with the methods introduced in the papers. In other words, the use of the nondimensional or normalized treatment makes the results universally comparable to any physical system. On the other hand, if the analysis of the paper should have been carried out for a specific physical system, then comparison to physical systems of differing parameters would be impossible. The physical system for which the illustrative example was worked used a typical high-speed 5-gallon-per-minute 2,000-pound-per-square-inch valve, and experimental studies gave equally as good agreement with the theoretical work as that indicated in earlier papers[2,3] for the single-stage valve.

It appears to the authors that all of the nonlinear effects mentioned by the discussers are included in the papers with the exception of over or underlap and of torque motor saturation. However, over or underlap are not universally significant in all valves. Torque motor saturation does not enter into the phenomenon studied since the amplitude of the electric current remains small although the pressure and flow amplitudes are relatively large. Both flow and pressure saturation are definitely included in the orifice flow equations for both stages of the valve.


REFERENCES

1. See reference 3 of the paper.
2. See reference 1 of the paper.
3. See reference 2 of the paper.


# The Lightweight Train—Its Power Supply for Auxiliaries


J. L. SWARNER
ASSOCIATE MEMBER AIEE


FOR MANY YEARS the "iron horse" rode alone having no equal or competition. The railroad conquered the wilderness with a belch of smoke and tied the far places together with ribbons of steel. Legends were woven around it and ballads created. Excesses brought about legal restrictions, but still the railroad prospered.

Born along with the present century was the horseless carriage which would not last, but did. The idea of mass production and the assembly line developed along with the automobile. The two teamed up to produce millions of offspring, rapidly and economically. The iron horse lost many of his riders to the family car.

During this so-called industrial revolution the railroads and their suppliers followed diametrically opposite paths from the general industrial pattern. Automobiles provided the method, but household appliances and practically every other industry employed mass production and assembly lines to provide a cheaper, better product to sell at a lower price.

Not so with the railroad industry, and by this term is included the equipment suppliers to the roads. Passenger cars were custom-built to individual railroad specifications. In the period 1945 through 1953, Pullman-Standard built 1,235 domestic nonsleeper passenger cars from 151 different floor plants for 41 different customers; 43% of these had less than three and 73.5% had less than seven cars per plan. In this same period, Pullman-Standard built 913 domestic sleeping cars, excluding troop sleepers, from 66 different floor plans and 36 different railroads. Of these, 21% had less than three and 42.5% had less than seven cars per plan. While there are six basic types of sleeping accommodations, 25 different types were engineered and built. To point this condition further, practically all of these sleeping cars were turned over to the Pullman Company to operate and to maintain. The Pullman Company, in order to operate this varied mass of cars, conducted extensive surveys and was able to achieve a degree of standardization by changing the cars after they took them over. A typical example concerns the batteries. Cars were received by the Pullman Company with 33 different types of batteries. With a minimum of structural change on the cars, this number was or is being reduced to nine as the batteries wear out.

With the appearance of the lightweight trains, built late in 1955 or in the early part of 1956, a 20-year cycle was completed. In 1934 Pullman-Standard, in co-operation with the Union Pacific Railroad, built a unit train with matched power, central auxiliary electric power, and light weight. It was a so-called tubular type, with a smaller cross section than standard. It weighed 1,110 pounds per foot of length, including the locomotive.

Since 1934, cars have been getting progressively heavier. Table I shows this trend from the 1,110 pounds per foot of the City of Salina to the 1,900 pounds per foot of length of the 1955 train.

The concept of something new in railroad passenger equipment was developed by necessity. A method must be found to make this operation desirable to the public and profitable to the railroads. There has been much publicity and speculation about the so-called lightweight trains. With their sleek lines, underslung bodies, matched power locomotives, and 120 miles per hour (mph) speed,


Paper 56-256, recommended by the AIEE Land Transportation Committee and approved by the AIEE Technical Operations Department for presentation at the AIEE 1956 Winter General Meeting, New York, N. Y., January 30–February 3, 1956. Manuscript submitted November 21, 1955; made available for printing June 14, 1957.



J. L. SWARNER is with the Pullman-Standard Car Manufacturing Company, Chicago, Ill.



The author wishes to acknowledge information on the bus duct given by W. A. Kuhar and Gerald Panulla of the Roller-Smith Corporation, Bethlehem, Pa.

Table I. Train Weight Trend 1934 to 1955, Complete Trains Including Locomotive

| Train | Length of Train, Feet-Inches | Weight of Train, Pounds | Weight per Feet, Pounds |
|---|---|---|---|
| City of Salina, 1934 (Union Pacific) | 204- 5 | 232,540 | 1,110 |
| Green Diamond (Illinois Central) | 328- 6 | 476,800 | 1,146 |
| City of Portland, 1936 (Union Pacific) | 454-11 | 615,580 | 1,350 |
| City of Los Angeles (Union Pacific) | 713-11 | 1,005,640 | 1,410 |
| City of Denver (Union Pacific) | 864- 0 | 1,332,840 | 1,540 |
| Conventional 6-car train, 1955 | 580- 3 | 1,104,300 | 1,900 |
| Train *X* | 497-10 | 383,000 | 770 |

Table II. Weight Comparison of Car Electric Systems

| System | Per-Car Weight with Complete Electric Equipment, Pounds | Total Weight of Electric System for Train, Pounds |
|---|---|---|
| Axle-generator battery system, 110 volts d-c with amplidyne | 12,586 | 75,516 |
| Car equipment for train *X*, power source in locomotive | 1,303 | 11,727 |
| Central power equipment in locomotive | | |
| New York Central | 15,500 | |
| New York, New Haven & Hartford | 38,522 | |
| Net difference for complete train system, axle generator versus train *X* | | |
| New York Central | | 48,289 |
| New York, New Haven & Hartford | | 25,267 |
| Diesel-generator system 120 volts d-c | 10,200 | 61,200 |
| Net difference for complete train system, diesel generator versus train *X* | | |
| New York Central | | 33,973 |
| New York, New Haven & Hartford | | 10,951 |

Weights estimated: one locomotive for New York Central train, 300 kw; two locomotives for New York, New Haven & Hartford train, 250 kw in each locomotive.

they have been proclaimed as the salvation of railroad passenger business, in an era of increasingly tight competition; see New York Central train *X* in Fig. 1. But these trains will not live up to expectations, unless the following factors are given serious consideration and application:

1. Weight reduction without sacrifice of traditional railroad comfort and convenience to be accomplished by: use of new materials and techniques, providing energy for train auxiliaries from a common source. Of these two, the latter offers the greatest opportunity.

2. Sufficient standardization to permit production of car units in quantities, allowing for mass-production techniques.

3. A unit cost, which will allow the railroads to provide a better service, at equal or lower cost than other forms of transportation.

4. The reduction of maintenance and servicing, by intelligent design and use of proved components.

Using the foregoing as a basis, the electric system for lightweight trains can be selected.

## Growth of Car-Auxiliary-Power Requirements

More than 125 years ago, the application of lighting started the demand for car auxiliaries for passenger comfort and safety. It was in 1825 that Thomas Dixon, operating a horsedrawn coach between Stockton and Darlington, on the Liverpool and Manchester Railroad, bought candles for his passengers to hold in the car. For the next 100 years, the primary motivation, for auxiliary energy on railroad passenger cars, was the need for light.

The invention of the electric incandescent lamp, preceded a few years by the development of the storage battery by Plante, opened the way for the application of electric auxiliary power to a car. In 1881, the London, Brighton and South Coast Railroad put the incandescent lamps and the storage battery together on a passenger car.

In 1894, the New Jersey Central Railroad made the first installation of an axle-generator system in the United States. This system gradually took over until 1934, when its use was practically universal.

Then came the application of air conditioning to passenger cars in the 1930's. The auxiliary-power demand jumped from 5 kw to 25 kw. The need for consideration of a more suitable power system was created. The recent building of cars with large glass areas, such as the dome-type cars and high-level cars, further increased car auxiliary loads due to air-conditioning requirements. Modern passenger cars demand anywhere from 20 to 40 kw of connected load.

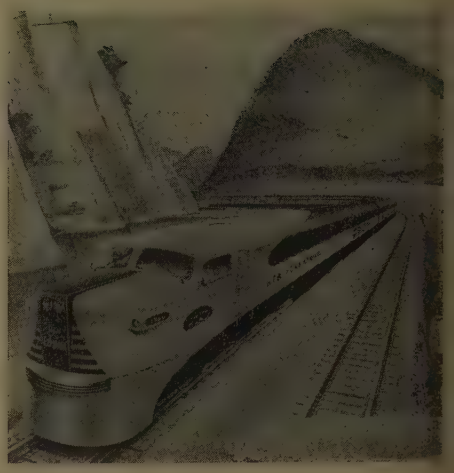

Fig. 1. Artist's conception of New York Central's train X

## Selection of Electric Power Source for a Train

There are three possible methods of providing power for auxiliaries on passenger cars. The axle-driven generator and associated battery, the diesel-driven generator for the individual cars, and a central source of power feeding the cars through a trainline. To apply any one of these to the lightweight train, the system must be compatible with the fundamental concepts of the new trains, as outlined previously.

Both the axle-generator system and the diesel-driven generator must be mounted under the car floor. The new trains, with their lowered floor heights, do not provide the necessary clearances.

In examining the characteristics of the axle-generator system further, the weights and cost must conform to the original premises. Table II is a comparison of a recent 110-volt d-c coach with an amplidyne invertor, a diesel-driven alternator system applied to the same type of car, and Pullman-Standard's train *X* which uses a central power source of 480 volts, 3 phase a-c. Fig. 2 is a similar comparision for a 32-volt car versus train *X*. Here again, the evident weight advantage of the central power source recommended its use.

Table III is an analysis of the horsepower requirements necessary for producing electric power by means of axle-driven generators. The efficiencies used and the horsepower to transport one ton of weight over level tangent track were taken from data determined in extensive Association American Railroads tests in 1937. This table indicates a 2.11-horsepower(hp) - per - kilowatt average from 30 to 90 mph. If axle-generated power was furnished for train *X*, it would require 50% of one locomotive's output,


**Fig. 2. Comparison: 32 volt d-c versus train X**

**Table III. Horsepower Required for Auxiliary Power**

Six-Car Conventional Coach Train, Axle-Generator System and Train X

| Item | 30 MPH | 50 MPH | 70 MPH | 90 MPH |
|---|---|---|---|---|
| Efficiency of generator and drive | 79 | 77 | 75 | 72 |
| Input hp at car axle for 20-kw general output | 34 | 34.7 | 35.8 | 37.3 |
| Input hp at rail at 5% loss | 35.8 | 36.5 | 37.7 | 39.2 |
| Drawbar hp required for six cars to generate 20-kw output | 214.8 | 219.0 | 226.2 | 235.2 |
| Drawbar hp required to transport each extra ton of equipment | 0.24 | 0.53 | 1.06 | 2.16 |
| Drawbar hp required to transport axle-generator equipment, one car | 1.34 | 2.96 | 5.92 | 12.05 |
| Drawbar hp required to transport six cars of axle-generator equipment | 8.04 | 17.76 | 35.52 | 72.30 |
| Total drawbar hp for six cars, sum of fourth and seventh items | 222.12 | 236.76 | 261.52 | 307.5 |
| Hp per kw output | 1.77 | 1.95 | 2.18 | 2.56 |
| Drawbar hp required to generate 270 kw for train *X* by means of axle generators | 478 | 526 | 589 | 692 |
| Engine hp required to generate 270 kw for train *X*, diesel-alternator set, 1.44 hp per kw | 389 at all train speeds | | | |
| Drawbar hp required to transport train *X* auxiliary-power equipment | | | | |
| One locomotive | 1.86 | 4.10 | 8.21 | 16.74 |
| Two locomotives | 3.72 | 8.20 | 16.42 | 33.48 |
| Total hp required for auxiliary power on train *X* | | | | |
| One locomotive | 390.86 | 393.1 | 397.21 | 405.74 |
| Two locomotives | 392.72 | 397.2 | 405.42 | 422.48 |

or 543-hp average, to turn the generators, whereas, only 397 hp would be necessary with a direct diesel-driven alternator. Since the primary source of power in both cases is a diesel engine, the advantage clearly lies with the central diesel-alternator set providing all train power.

Fig. 3 is a comparision of train resistances of the conventional 6-car coach train with axle-generator equipment and train *X*. Here is shown, graphically, the train resistance due to axle-generator drag. The primary purpose of a locomotive is to move the train. It appears that its horsepower could be more efficiently employed in increased acceleration rates and schedule speeds.

One important factor in obtaining the objective of low operating costs is the elimination of all items possible, and the arrival at a simple system made up of proven components, and available from mass-production sources. Referring to Fig. 2, there are six major items of equipment per car, which are special to the railroad industry and which require constant servicing and maintenance. If the axle generator and drive were replaced by a small diesel generator, the status is the same except for the increased function of diesel-engine repair, and fuel-oil and cooling service. All of this equipment, except for control panels, is mounted under the car where it is subjected to the worst possible operating conditions and where servicing and replacement are inconvenient and uncomfortable.

The car components of the electric power system for train *X* are as follows:

1. Locomotive Equipment
   a. Diesel generator.
   b. Engine-generator controls.
2. Car Equipment
   a. Three-phase bus-bar trainline.
   b. Automatic 3-phase trainline couplers.
   c. Power transformer.
   d. Magnetic contactors.

With one exception, these are items common to industry in general, and are produced by a number of reliable manufacturers at highly competitive prices. To illustrate the comparision between costs of equipment now used on passenger cars and what it is possible to use, Table IV is an example for d-c motors versus a-c motors in the horsepower ratings normal to railroad cars.

## Selection of Power Trainline

From a previous study made in 1939, a trainline of two no. 4/0 conductors in parallel would be required for a 300-kw trainline. The weight of this trainline, for

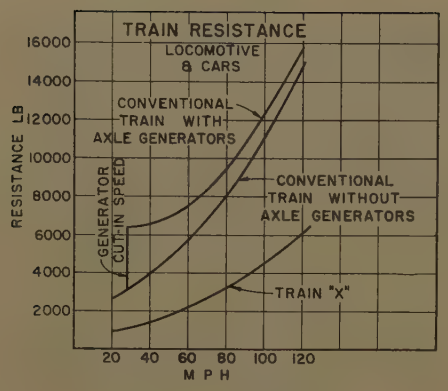


**Fig. 3. Train resistance**

train *X*, would have been 5,684 pounds, exclusive of end connectors or couplers.

An aluminum bus-bar system of standard manufacture, completely assembled with covers and hangers, rated at 600 amperes (amp), weighed 6 pounds per foot or 2,307 pounds for the train. The aluminum bus-bar system was selected. Voltage-drop calculations are shown in the Appendix.

The total maximum load on the trainline is 270 kw, or 325 amp at −20 F (degrees Fahrenheit) in the heating season. It is hoped that sufficient data can be obtained during the train's operation to arrive at a load factor for future trainline calculations.

## Power Trainline Connectors

Train *X* is made up of four cars, each consisting of two permanently connected units, and a center car; see Fig. 4. The trainline is carried between the two permanently coupled ends of the 2-section car by means of bolted jumpers, near the roof of the car.

At the coupled ends, the power trainline is coupled automatically at the same time as the mechanical coupling. The power trainline coupler is mounted above the inner diaphragm, where it is protected from the weather and road-bed dirt. It is also so located as to be inaccessible for accidental contact with live surfaces; see Fig. 5.

Auxiliary 480-volt contacts remove the load from the coupler on uncoupling, and do not apply the load until the cars are coupled. In this way, the power contacts never have to make, or break current. The contacts are designed to carry 400 amp continuously.

This unique method of power connections between cars removes all high-voltage power from the vicinity of all other electric circuits and permits keeping the 480 volts overhead, out of reach, for the entire length of the train.

The mechanical coupler carries 42 control wires, all at 64 volts, for brake, signal, locomotive, and miscellaneous control circuits. When two locomotives are used, the rear locomotive is controlled from the front end.

## Car or Unit Power System

Fig. 6 shows the basic power system on each unit of train *X*. Light weight, simplicity, and maximum utilization of standard components were governing factors. Power is taken from the 3-phase bus-bar trainline to a 3-pole magnetic contactor, with overloads on each phase.

All loads possible are fed directly from the 480 volts. Air-conditioning motors and all heating elements operate on 480 volts. This permits the use of a small transformer for lighting and miscellaneous loads only. Lighting is fluorescent, with 199/216-volt ballasts. The few incandescent lamps operate on 120 volts.

The transformer is connected delta-Y. The primary side is 480 volts delta-connected, the secondary is Y-connected for 208/120 volts.

On stand-by service, the insertion of the stand-by power plug isolates the unit from the train by locking out the power contactor to the trainline. The secondary of the transformer, i.e., the 208/120-volt side, becomes the primary and 480 volts is taken from the delta side for circuits of this voltage.

**Table IV. Comparative Cost D-C Versus A-C Motors, Cost of A-C Motor Is 100%**

| Size, Hp | Cost of 220/440-Volt 3-Phase A-C Motor, Per Cent | Cost of 32-Volt D-C Motor, Per Cent |
|---|---|---|
| 25 | 100 | 372 |
| 15 | 100 | 410 |
| 2 | 100 | 294 |
| 1 | 100 | 330 |
| 1/2 | 100 | 227 |

The overhead electric heat is locked out on stand-by, primarily due to capacity of yard stand-by power supplies. This limitation permitted using a smaller transformer than would have been possible if all 27 kw of electric heat were to be drawn from wayside power. It was considered that, at all times the train was in service, the head-end power system would be connected and in operation, and stand-by service would only be used for a detached unit in the yards.

## Heating System

The same basic requirements for a modern train of the new design must be applied to all components. The heating system, traditionally steam on present equipment, will be all electric on train *X*. The following three systems were given serious consideration and engineering study:

1. A water-loop system, in which water is passed through a heat exchanger in the locomotive where it absorbs waste engine heat. This water is then circulated through a closed loop, the length of the train. Controls at each car select the amount of hot water necessary to maintain car tempera-

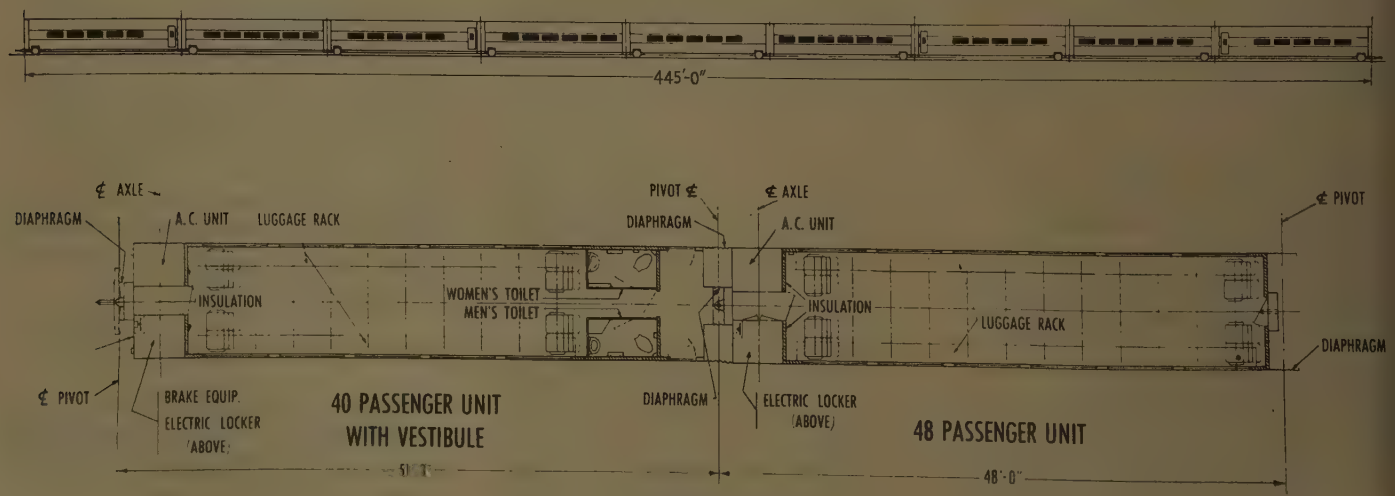


**Fig. 4. Consist of train X**

Fig. 5 (above). Power coupler

Fig. 6 (right). Basic power circuit, train X

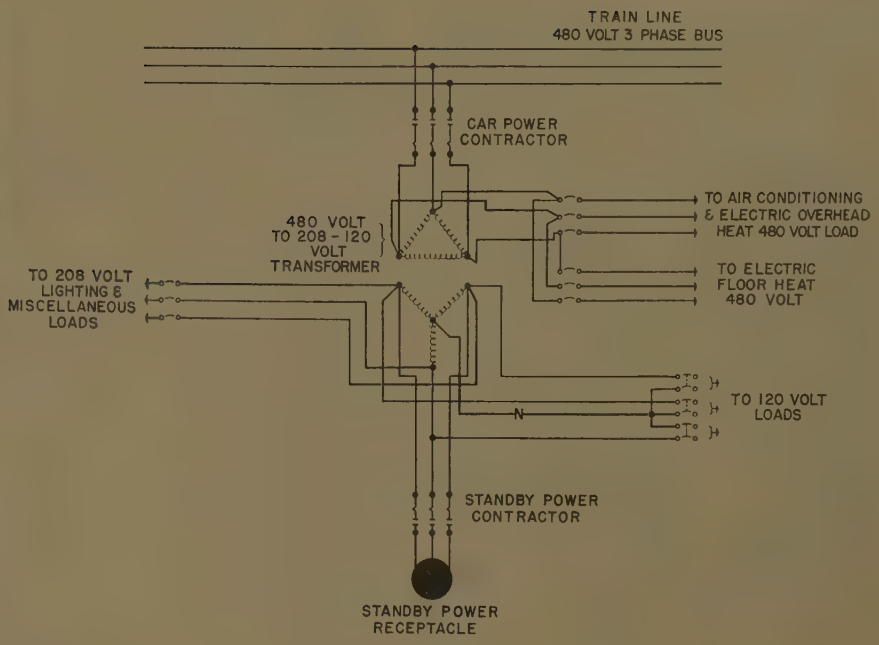


**Table V. Comparative Weights of Heating System's Trailing Units**

| System | Weight Per Unit, Pounds | Weight Per Train, Pounds |
|---|---|---|
| Water loop | 1,434 | 12,906 |
| Steam | 470 | 4,230 |
| Unit boiler and radiation | 936 | 8,424 |
| Electric | 150 | 1,350 |

ture. In warm weather, the water is chilled by a refrigeration system in the locomotive and is used to cool the cars.

2. A unit oil-fired boiler on each car, for either hot water or steam heating.
3. All-electric heating.

The water-loop-system engineering studies showed that sufficient heat would be available from the engines to maintain a desirable car temperature, except under light engine loads in severe weather. Electric heat was used to supplement when engine heat was insufficient. This system also indicated desirable operating economies by use of engine waste heat. However, other factors influenced against its use. These were: size of trainline pipe required, complexity of providing smooth flow, automatic coupling of the fluid line between units, antifreeze protection, and insulation of trainline and intercar connections for chilled water.

The unit oil-fired burner, one per car, required an electrical supply for the operating motor and controls, fuel tanks, filling devices, safety devices, and water supply. While this system of producing heat is more efficient than the generation of electric power by diesel engine, and conversion of power to heat, the maintenance of the oil-burner installation would more than offset any gain in efficiency. The filling of fuel tanks, establishment of wayside fueling facilities, and numerous units to maintain were not considered desirable.

The conventional steam-heating system, where steam is fed from a boiler in the locomotive through a steam trainline, is subject to relatively high losses in transmission, possible freeze-up, and complexity of providing automatic coupling between units. A steam boiler would have to be installed in the locomotive, in addition to the auxiliary generator for other auxiliaries.

The electric system offered the most over-all advantages; see Table V. Experience has proved the very low maintenance cost of this method of heating. Transmission losses are very low, and methods of coupling transmission lines between cars is simple, compared with other systems. Only one source of energy is required, per train, for all auxiliaries. Only one energy transmission line is necessary.

The electric heating system is composed of low-maintenance items of standard manufacture, namely strip heaters and contactors.

The electric heating system has two elements: the overhead unit, incorporated in the air-conditioning unit to temper fresh air, consists of an 18-kw finned-rod unit; the floor heat is made up of strip heaters, approximately 6 feet long, having a total capacity of 9 kw. Only two sizes of floor heat strips are used through-

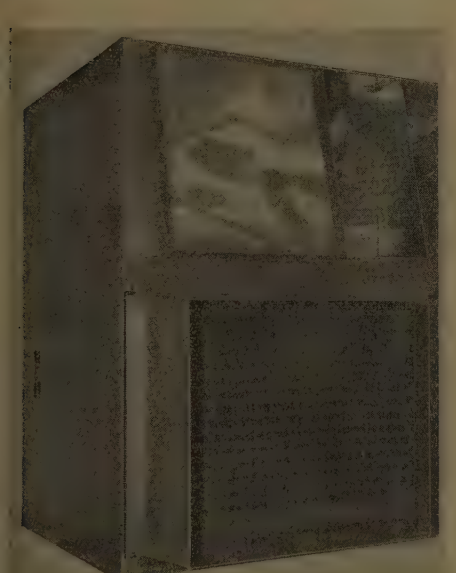

Fig. 7. Air-conditioning units, air-intake side

Fig. 8. Air-conditioning unit, cover removed

Fig. 9. Car interior

## Table VI. Load Analysis, 48-Passenger Unit

Four Cars Per Train; Length, 48 Feet

| Items | Kw | PF | Kva | Kv | $I_L$ | $\phi$, Degrees | $I_L \cos\phi$ | $-jI_L \sin\phi$ |
|---|---|---|---|---|---|---|---|---|
| **Cooling Season*** | | | | | | | | |
| Compressor motor | 5.60 | 0.85 | 6.58 | 0.48 | 7.92 | 31.8 | 6.730 | 4.17 |
| Condensor motor | 1.49 | 0.81 | 1.84 | 0.48 | 2.21 | 35.9 | 1.790 | 1.30 |
| Fan motor | 0.75 | 0.76 | 0.98 | 0.48 | 1.18 | 40.5 | 0.766 | 0.897 |
| Direct-diffused light | 0.79 | 0.90 | 0.88 | 0.48 | 1.06 | 25.8 | 0.955 | 0.411 |
| Indirect light | 0.79 | 0.90 | 0.88 | 0.48 | 1.06 | 25.8 | 0.955 | 0.411 |
| Miscellaneous light | 0.45 | 1.0 | 0.45 | 0.48 | 0.541 | 0 | 0.541 | 0 |
| Coffee warmer | 0.60 | 1.0 | 0.60 | 0.48 | 0.721 | 0 | 0.721 | 0 |
| | 10.47 | | | | | | 12.458 | 8.189 |
| **Heating Season†** | | | | | | | | |
| Fan motor | 0.75 | 0.76 | 0.98 | 0.48 | 1.18 | 40.5 | 0.766 | 0.897 |
| Direct-diffused light | 0.79 | 0.90 | 0.88 | 0.48 | 1.06 | 25.8 | 0.955 | 0.411 |
| Indirect light | 0.79 | 0.90 | 0.88 | 0.48 | 1.06 | 25.8 | 0.955 | 0.411 |
| Miscellaneous light | 0.45 | 1.0 | 0.45 | 0.48 | 0.541 | 0 | 0.541 | 0 |
| Coffee warmer | 0.60 | 1.0 | 0.60 | 0.48 | 0.721 | 0 | 0.721 | 0 |
| Overhead heat Δ | 18.0 | 1.0 | 18.0 | 0.48 | 21.6 | 0 | 21.600 | 0 |
| Floor heat Δ | 7.5 | 1.0 | 2.5 | 0.48 | 9.03 | 0 | 9.030 | 0 |
| | 28.88 | | | | | | 34.568 | 1.419 |

* Without night light $I_L = 15.3/\underline{32.4}°$, pf = 0.845.

† Pf = 0.998.

## Table VII. Load Analysis, 40-Passenger Center Car

One Car Per Train; Length, 48 Feet; Outside Temperature, 20 F; Inside Temperature, 75 F

| Items | Kw | PF | Kva | Kv | $I_L$ | $\phi$, Degrees | $I_L \cos\phi$ | $-jI_L \sin\phi$ |
|---|---|---|---|---|---|---|---|---|
| **Cooling Season*** | | | | | | | | |
| Compressor motor | 5.60 | 0.85 | 6.58 | 0.48 | 7.92 | 31.8 | 6.730 | 4.17 |
| Condensor motor | 1.49 | 0.81 | 1.84 | 0.48 | 2.21 | 35.9 | 1.790 | 1.30 |
| Fan motor | 0.75 | 0.76 | 0.98 | 0.48 | 1.18 | 40.5 | 0.766 | 0.897 |
| Direct-diffused light | 0.99 | 0.90 | 1.10 | 0.48 | 1.32 | 25.8 | 1.190 | 0.575 |
| Indirect light | 0.99 | 0.90 | 1.10 | 0.48 | 1.32 | 25.8 | 1.190 | 0.575 |
| Miscellaneous light | 0.15 | 1.0 | 0.15 | 0.48 | 0.181 | 0 | 0.181 | 0 |
| | 9.97 | | | | | | 11.847 | 7.517 |
| **Heating Season†** | | | | | | | | |
| Fan motor | 0.75 | 0.76 | 0.98 | 0.48 | 1.18 | 40.5 | 0.766 | 0.897 |
| Direct-diffused light | 0.99 | 0.90 | 1.10 | 0.48 | 1.32 | 25.8 | 1.190 | 0.575 |
| Indirect light | 0.99 | 0.90 | 1.10 | 0.48 | 1.32 | 25.8 | 1.190 | 0.575 |
| Miscellaneous light | 0.15 | 1.0 | 0.15 | 0.48 | 0.181 | 0 | 0.181 | 0 |
| Overhead heat Δ | 18.00 | 1.0 | 18.0 | 0.48 | 21.6 | 0 | 21.600 | 0 |
| Floor heat Δ | 9.00 | 1.0 | 3.0 | 0.48 | 10.83 | 0 | 10.830 | 0 |
| | 29.88 | | | | | | 35.727 | 2.047 |

* Without night lights $I_L = 14/\underline{32.4}°$, pf = 0.845.

† Pf = 0.997.

## Table VIII. Load Analysis, 40-Passenger Vestibule Unit

Four Cars Per Train; Length, 51 Feet, 3 Inches; Outside Temperature, 20 F; Inside Temperature, 75 F

| Items | Kw | PF | Kva | Kv | $I_L$ | $\phi$, Degrees | $I_L \cos\phi$ | $-jI_L \sin\phi$ |
|---|---|---|---|---|---|---|---|---|
| **Cooling Season*** | | | | | | | | |
| Compressor motor | 5.6 | 0.85 | 6.58 | 0.48 | 7.92 | 31.8 | 6.730 | 4.17 |
| Condensor motor | 1.49 | 0.81 | 1.84 | 0.48 | 2.21 | 35.9 | 1.790 | 1.30 |
| Air-circulation fan motor | 0.75 | 0.76 | 0.98 | 0.48 | 1.18 | 40.5 | 0.766 | 0.897 |
| Direct diffused lighting | 0.79 | 0.90 | 0.88 | 0.48 | 1.06 | 25.8 | 0.955 | 0.411 |
| Indirect lighting | 0.85 | 0.90 | 0.94 | 0.48 | 1.13 | 25.8 | 1.020 | 0.492 |
| Miscellaneous lighting | 0.76 | 1.0 | 0.76 | 0.48 | 0.914 | 0 | 0.914 | 0 |
| Water cooler | 0.19 | 0.60 | 0.32 | 0.48 | 0.385 | 53.2 | 0.231 | 0.308 |
| | 10.43 | | | | | | 12.406 | 7.578 |
| **Heating Season†** | | | | | | | | |
| Air-circulation fan motor | 0.75 | 0.76 | 0.98 | 0.48 | 1.18 | 40.5 | 0.766 | 0.897 |
| Direct diffused light | 0.79 | 0.90 | 0.88 | 0.48 | 1.06 | 25.8 | 0.955 | 0.411 |
| Indirect light | 0.85 | 0.90 | 0.94 | 0.48 | 1.13 | 25.8 | 1.020 | 0.492 |
| Miscellaneous light | 0.76 | 1.0 | 0.76 | 0.48 | 0.914 | 0 | 0.914 | 0 |
| Overhead heat Δ | 18.0 | 1.0 | 18.0 | 0.48 | 21.6 | 0 | 21.600 | 0 |
| Floor heat Δ | 9.0 | 1.0 | 3.0 | 0.48 | 10.83 | 0 | 10.830 | 0 |
| Water cooler | 0.19 | 0.60 | 0.32 | 0.48 | 0.385 | 53.2 | 0.231 | 0.308 |
| | 30.34 | | | | | | 36.316 | 2.108 |

* Without night light $I_L = 14.5/\underline{31.5}°$, pf = 0.853.

† Pf = 0.997.

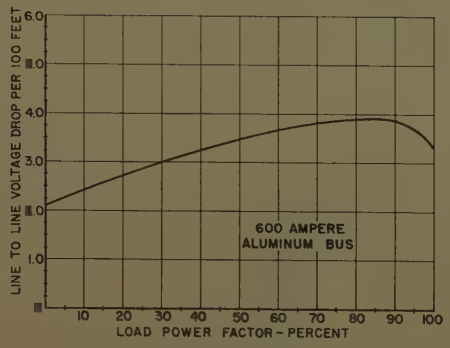


**Fig. 10. Line-to-line voltage drop for train X**

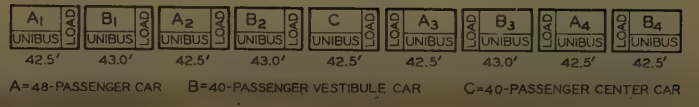


**Fig. 11. Schematic of train X**

out the train. The vestibule section, of the 2-section car, has a special-length heater in the toilets. All other units in the train are exactly alike and interchangeable.

To meet the need for two steps of heating, and to save weight and cost, the heaters are connected in delta, for full heat, and reconnected in Y for low heat. Therefore, there are 18 kw of electric heat at the high setting and 6 kw at the low connection, for the overhead air tempering. On the floor heat, the high setting is 9 kw, the low setting is 3 kw.

## Air-Conditioning System

Each unit of train *X* has a 6-ton air-conditioning unit, which is a complete package, assembled, charged with Freon 12, and tested at the factory; see Figs. 7 and 8.

The unit is designed to be installed in the car through removable panels on the side of the car. The removable panels contain the condenser air inlet, the fresh-air grille, and the exhaust outlet. Electric connections to the units are plugs and receptacles. Duct connections must be completed, for car air supply and recirculated air, after the unit is bolted in place. Condenser air discharge is through the bottom of the car.

Here again, every effort was made to design an air-conditioning system which was lightweight, exactly identical for each car unit, easily replaceable, and made up of proven components The compressor is the sealed type. All motors are 440 volt, 3 phase, 60 cycle. All contactors and controls are mounted in a box, as an integral part of the unit. With spare units available, the railroad will be able to service them in the shop under ideal conditions, and not hold a car out of service.

In the design of the package system, it has been determined that any of the refrigeration equipment suppliers can produce a unit to be applied in the same location, and to conform to outside dimensions and air openings. In this way, standardization is achieved without limiting selection of equipment.

## Lighting

The design of the lighting system is based on the same general stipulations as for the rest of the train. In addition, the illuminations will:

1. Eliminate glare sources.
2. Provide well-diffused illumination.
3. Maintain a high level of 40 foot-candles on the reading plane.
4. Permit group lamp replacement and cleaning at normal intervals.

The illumination in the passenger compartment consists of two components. One component is a large luminous element, which forms the lower surface of the main air duct. Two rows of rapid-start 48T12 fluorescent lamps are mounted on strips, at the top of the air duct, to provide even illumination of diffusing panel; see Fig. 9. The inside of the duct is a white plastic coating. The second element is indirect lighting, on each side of the air diffusers, which parallel the luminous panels. Here too, the 48T12 rapid-start lamp is used. Either the direct diffuser, the indirect, or both can be used as desired. All circuits are balanced across the 3-phase lines. Ballasts are rated 199/216 volts. Three lighting levels are available at approximately 15 foot-candles with indirect only, 30 foot-candles with direct diffused only, 40 to 50 foot-candles with both. The use of cool white deluxe lamps provides good color rendition to complement the color schemes.

An incandescent night-light circuit is included in the direct-diffused element, to provide a very low level, for service where passengers might desire to sleep.

Emergency lights are provided in each unit by means of a standard 6-volt storage-battery unit, complete with automatic charging facilities.

## Conclusions

To arrive at a low first cost for a lightweight train with low operating cost, the power for train auxiliaries must come from a central source.

The use of equipment peculiar to the railroads, such as axle generators, battery, or small individual power plants, is unnecessary and undesirable.

The use of a nominal 440-volt 3-phase system allows the use of standard, proven, industrial equipment, available from many different sources at competitive prices.

The use of 3-phase power permits an air-conditioning system employing a sealed compressor and brushless motors for fan and condensor drives.

The heating system achieves the utmost in simplicity, with low maintenance.

## Appendix

The load and trainline voltage-drop calculations for train *X* are shown in Tables VI through VIII. The end connections are not considered. Fig. 10 shows the line-to-line voltage drop for train *X*, and Fig. 11 is a schematic of train *X*. Using the calculated values of power factors (pf) from Tables VI through VIII, the current for each car is calculated as follows. For a 48-passenger unit

$$I_L = \frac{kw}{\sqrt{3} V_L \cos 0} = \frac{9.97 \times 10^3}{(\sqrt{3})(480)(0.845)} =$$

14.2 amp (cooling season)

$$I_L = \frac{29.88 \times 10^3}{(\sqrt{3})(480)(0.997)} =$$

36.2 amp (heating season)

For a 40-passenger vestibule unit

$$I_L = \frac{10.43 \times 10^3}{(\sqrt{3})(480)(0.853)} =$$

14.7 amp (cooling season)

$$I_L = \frac{30.34 \times 10^3}{(\sqrt{3})(480)(0.997)} =$$

36.5 amp (heating season)

For a 40-passenger center unit

$$I_L = \frac{10.47 \times 10^3}{(\sqrt{3})(480)(0.845)} =$$

15.0 amp (cooling season)

$$I_L = \frac{28.8 \times 10^3}{(\sqrt{3})(480)(0.998)} =$$

34.8 amp (heating season)

In the cooling season, with pf = 0.85, the following may be calculated

voltage drop = 3.91 volts per 100 feet

For the 600-amp bus

voltage drop = $6.51 \times 10^{-5}$ volts per amp per foot

The current $I_L$ is calculated for a 48-passenger car (A), a 40-passenger vestibule car (B), and a 40-passenger center car (C) as follows

$I_L = 14.2$ amp at 0.85 pf for A
$I_L = 14.7$ amp at 0.85 pf for B
$I_L = 15.0$ amp at 0.85 pf for C

## References


1. Realistic Goals for Railway Passenger Car Design, T. C. Gray. *Mechanical Engineering*, New York, N. Y., vol. 77, Mar. 1955, pp. 225–30. (condensed)

2. The Steam Locomotive (book), Ralph P. Johnson. Simmons-Boardman Publishing Corporation, New York, N. Y., 1942, revised 1944.

3. Car Lighting by Electricity (book), Charles W. T. Stuart. *Ibid.*, 1923.


## Discussion

H. F. Brown (Gibbs & Hill, Inc., New York, N. Y.): This is a timely paper. Since so many different voltages have been used both in the United States and abroad for train lighting and heating, it would be of interest to learn from the author just what systems were considered and compared, economically, before the 440-volt 3-phase 60-cycle system was finally adopted.

It may well be that such a study, if made, would have an important bearing later, if railroad electrification with commercial frequency were to be adopted in this country. The 1,000-volt single-phase a-c trainline with simple single-conductor jumpers between cars would seem to have attractive possibilities. This is widely used in Europe.

In Fig. 3 is shown a curve of train resistance for train *X* compared with a conventional train. If the values shown for the train resistance for train *X* are converted into horsepower per ton, the values obtained by so doing would be as follows:

| | | | | | | |
|---|---|---|---|---|---|---|
| Speed in mph.. | 30.. | 50.. | 70.. | 90.. | 120 |
| Hp per ton.... | 0.48.. | 1.32.. | 2.5.. | 4.5.. | 9.6 |

The values shown for horsepower per ton in Table III, the fifth item, are much lower than these values. Since these figures have an important bearing on the further calculations tabulated in Table III, it would appear to be in order to re-examine the values shown in this item.

In the eleventh item of Table III, the statement is made that the engine horsepower requirements are constant throughout the speed range when taken from a head-end supply. In one sense this is true, but since the prime mover must also move the weight of the auxiliary-power generating equipment, whether located on the cars or on the locomotive, it must devote the same increase in horsepower for each ton of added weight in either case, for a fair comparison, as the speed of the train increases.

Actually, the locomotive must supply nearly 30 hp more to move the weight of the head end and car equipment shown for train *X* at 90 mph than for 30 mph. If this power for auxiliaries comes from the main engine, there is this much less for traction. It is not much, but it should be taken into account for a fair comparison with axle-generator equipment. Train *X* is shown as weighing 770 pounds per foot including the locomotive. On this basis, it is only fair to include in the paper the horsepower of the engine for traction purposes since this will greatly influence the permissable maximum locomotive weight.

Since the lightweight train has been associated with high-speed trains in all recent publicity in the popular and technical press, attention is called to the increasing amount of horsepower per ton required for higher speeds than those now attained by conventional trains. To obtain speeds of 100 mph, or more, there must be available for traction capacities greater than 10 horsepower per ton to accelerate a train on level track up to these high speeds. Since self-propelled locomotives of any type now made in the United States at least are limited to about 13 or 14 hp per ton of locomotive weight, and since this is rapidly reduced as train weight, no matter how light, is added, it will be seen that it is almost a physical impossibility to design even a lightweight train for such speeds as 120 mph, unless the prime mover is designed to carry passengers.

In Europe, very high speed tests were recently made by the French railways, three cars weighing 101 tons were hauled by an electric locomotive weighing 80 tons. When this train of 181-ton total weight attained the maximum speed of 206 mph, it was taking more than 10,000 hp from the overhead contact system. This is just an indication of the way the power requirements increase as the speed increases, which seems to have been overlooked in some of the so-called high-speed-train designs being proposed in the United States.

The lightweight train will certainly save power at all speeds, when compared with conventional trains at the same speeds. The real problem is to obtain enough power for the speeds desired. It would appear that electrification offers the only practical solution for high speeds at the present time.

---

# Multiple-Unit-Rectifier Motive Power—Inductive Co-ordination Considerations on the New York, New Haven & Hartford Railroad

L. J. HIBBARD, MEMBER AIEE
F. T. GARRY, ASSOCIATE MEMBER AIEE
G. N. LOOMIS, NONMEMBER AIEE

WHEN the New York, New Haven & Hartford Railroad ordered ten ignitron locomotives and 100 rectifier multiple-unit (MU) cars for use in their electrified territory, the communications engineers of the New Haven Railroad and of the Southern New England Telephone Company (SNET) were concerned with the possible increased levels of noise that might be encountered on their exposed lines.

While it was known from Pennsylvania Railroad tests and Westinghouse laboratory tests that filters could be applied to reduce the $I \cdot T$* product of such equipment, a question arose as to the cumulative effect of a combination of ignitron locomotives and MU cars operating in the same vicinity.

A pioneer rectifier MU car has been in continuous service with originally applied apparatus on the Pennsylvania Railroad for almost 6 years, since July 14, 1949, without an a-c filter. However, this car only draws approximately 52 amp (amperes) from the 11-kv catenary during acceleration.[1]

Two pioneer 6,000-hp (horsepower) rectifier locomotives have been in use on the Pennsylvania Railroad since July 1951. Each 2-cab locomotive normally draws 750 to 800 amp from the 11-kv trolley under full-load conditions, but sometimes draws 800 to 850 amp for 15 to 20 minutes with occasional short-time peaks of 1,000 amp.

There was no evidence that the two 6,000-hp locomotives had a directly additive effect on each other and laboratory tests definitely indicated that the additive effect of a large number of rectifier motive-power units should never be very pronounced. However, the New Haven commitment involved the first large-scale use of rectifier motive power in the world and test results from the application have been awaited with keen interest.

The 100 rectifier MU cars represent a potential of approximately 40,000-wheel-hp continuous load and a potential of approximately 62,000-wheel-hp accelerating load. The ten rectifier locomotives represent a potential of approximately 40,000-wheel-hp continuous and approximately 80,000-wheel-hp accelerating load.

*$I \cdot T$ represents the current in amperes supplied to the motive-power unit times the telephone influence factor which has a different weighting for each frequency in the voice range, based on telephone receiver response.

Paper 55-207, recommended by the AIEE Land Transportation Committee and approved by the AIEE Technical Operations Department for presentation at the AIEE Summer General Meeting, Montreal, Que., Canada, June 24–28, 1957. This paper was previously presented as a Conference Paper at the 1955 Winter General Meeting. Manuscript submitted October 21, 1954; made available for printing May 17, 1957.

L. J. HIBBARD is with Westinghouse Electric Corporation, East Pittsburgh, Pa.; F. T. GARRY is with the Southern New England Telephone Company, New Haven, Conn.; and G. N. LOOMIS is with the New York, New Haven & Hartford Railroad Company, New Haven, Conn.

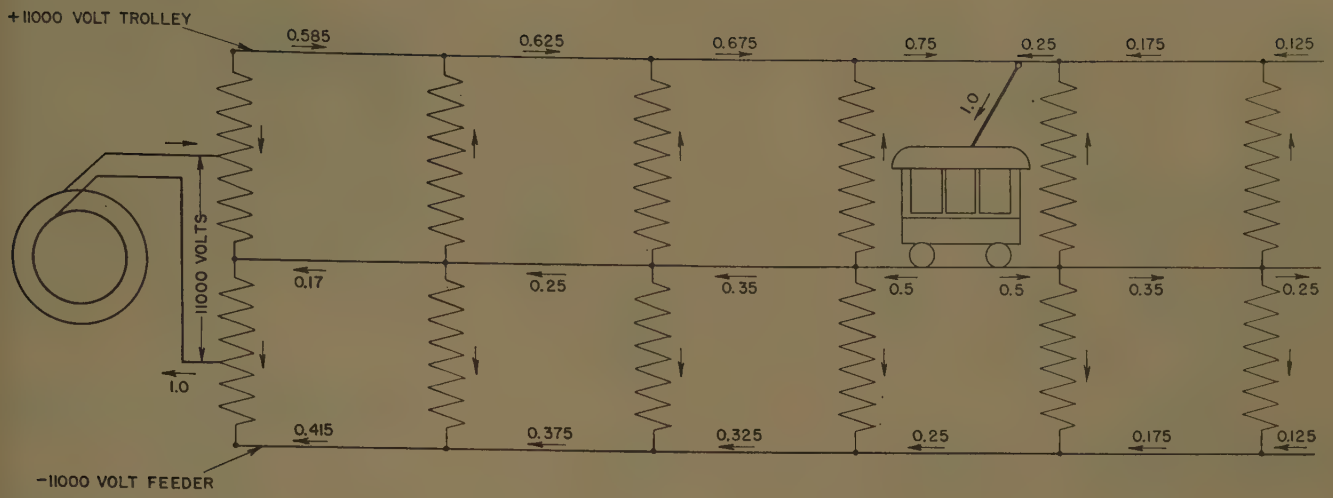


**Fig. 1. Single-phase system with autotransformers**

## Factor Involved in Co-ordination Problem

Telephone circuits that pass through alternating magnetic fields will have extraneous currents induced in all connected telephone receivers. These extraneous currents interfere with telephonic transmission if they are in the audio- or noise-frequency range, and are of appreciable magnitude compared with normal voice currents.

The over-all effect of a given inductive exposure depends on three factors: 1. inductive susceptiveness of the telephone system, 2. inductive coupling, and 3. inductive influence of the power system.

If any of these three factors could be reduced to zero, the inductive effects would disappear. Inductive susceptiveness and inductive influence can be kept to a low value but cannot at the present state of the art be reduced to zero. To reduce couplings to zero would require large separations between the power and telephone systems, which is almost always impracticable in connection with power and telephone distribution systems and often difficult in connection with power transmission systems. The practical solution to most inductive problems, therefore, lies in keeping both susceptiveness and influence at a reasonably low value and using such measures as can be readily applied to limit coupling, e.g., telephone cable sheath shielding.

Control of telephone susceptiveness is largely a matter of controlling unbalance. Control of power-system influence is almost entirely a matter of controlling harmonics.

The voltage induced in telephone circuits can be resolved into two components:

1. Metallic-circuit induction. Unequal voltages will be induced in the two con-

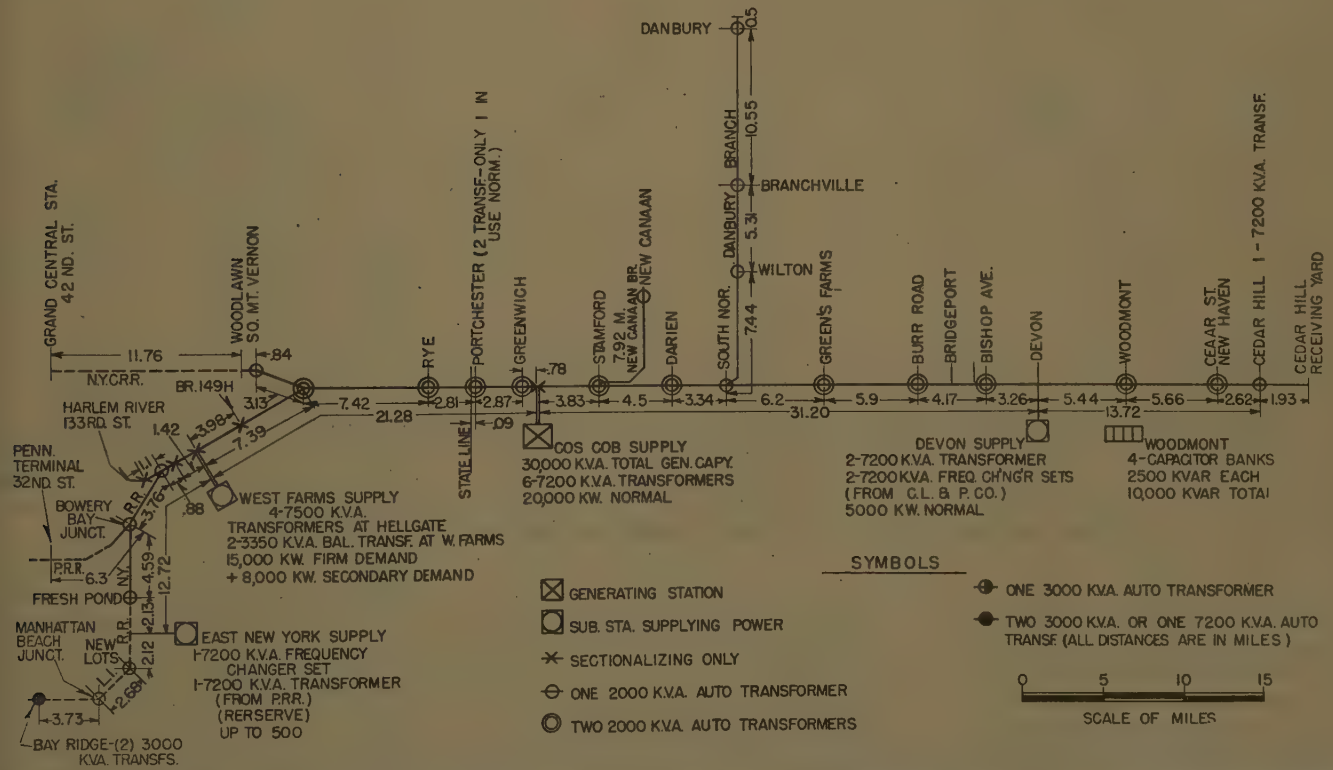


**Fig. 2. New York, New Haven & Hartford Railroad electrified zone showing sources and distribution of power, transformer locations, and spacing**

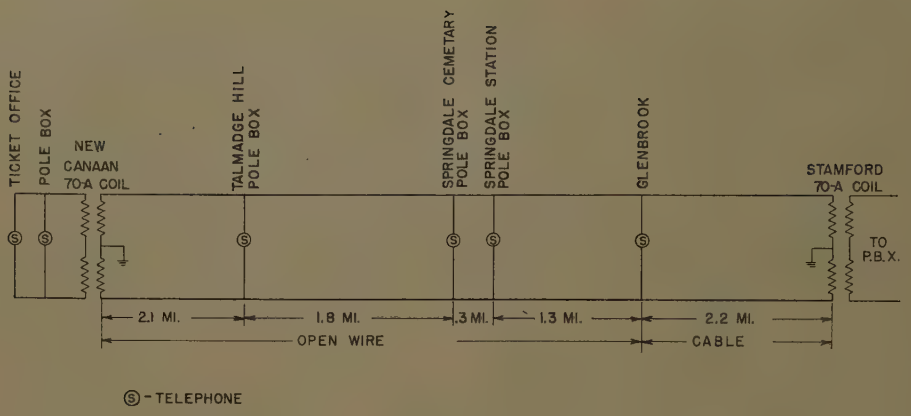


**Fig. 3. Diagram of the railroad's test circuit on the New Canaan branch**

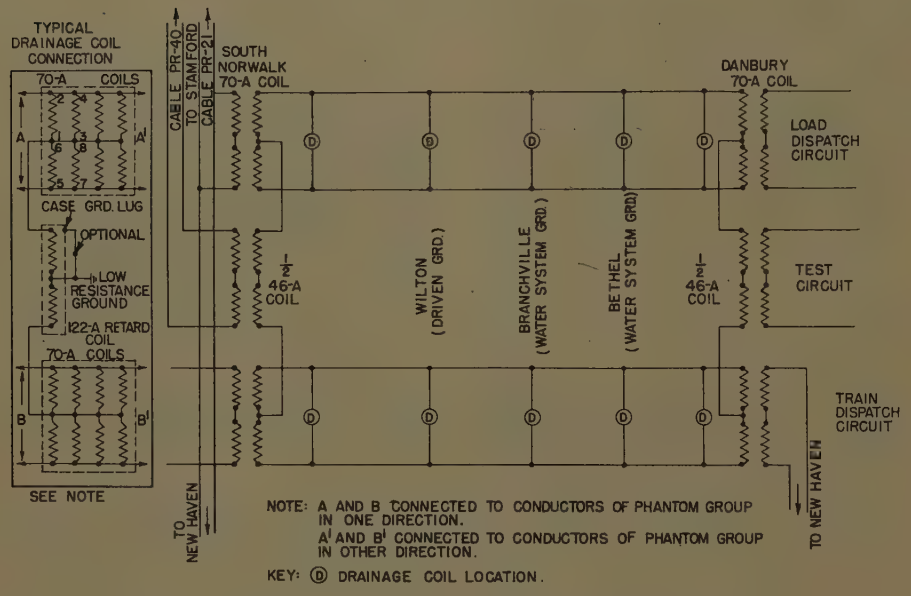


**Fig. 4. Diagram of the railroad's test circuit on the Danbury branch**

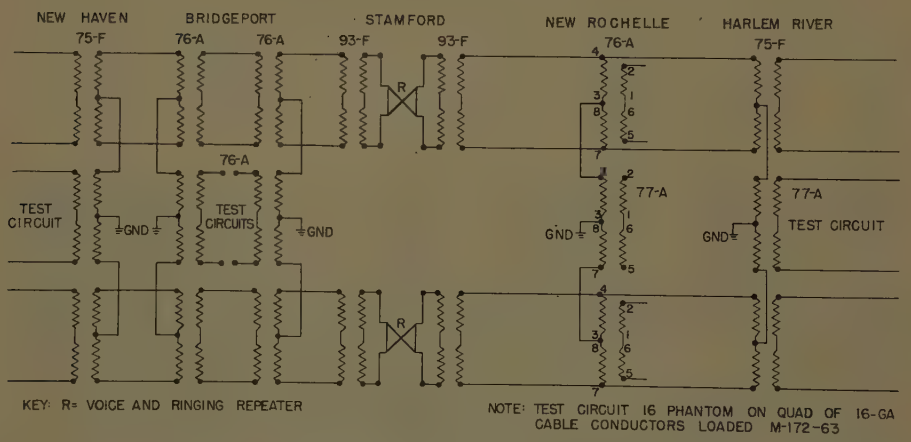


**Fig. 5. Diagram of the railroad's test circuit on the main line between Stamford and Bridgeport**

ductors of a telephone circuit if the two conductors are located in different field strengths of an a-c field.

2. Longitudinal-circuit induction.

If the two conductors of a telephone circuit are subjected to the same average field strengths by means of transpositions, the voltages induced in the two conductors of a given circuit by an a-c field will be equal.

Longitudinal voltages impressed on a perfectly balanced circuit cause no current in connected telephone receivers.

For telephone cable circuits, only the magnetic longitudinal coupling factors are of importance. The metallic-circuit voltages are negligible because of the juxtaposition of the wires and frequent twist.

Open-wire lines will have longitudinal induction and may or may not have harmful values of metallic-circuit induction and electrostatic induction depending on the type of exposure and effectiveness of the transpositions.

## Railroad Propulsion System and Communication Lines Involved

### Railroad Propulsion System

The electrification of the New York, New Haven & Hartford Railroad includes the main line from Woodlawn to New Haven, the New Canaan branch, the Danbury branch, the Harlem River branch, and the New York Connecting Railroad.

Power is supplied from overhead catenaries at 11,000 volts, 25 cycles, single phase. In the major part of the electrification, the trolley-rail circuit is fed by autotransformers, which, with the trolley rails and feeders, form a 3-wire 22,000/11,000-volt system having 22,000 volts between the trolleys and feeders, and 11,000 volts between rails and either trolleys or feeders. At the time of the completion of the Harlem River—New Haven communication cable in 1918, power was fed to the propulsion system only at Cos Cob, Conn., where the railroad's main generating station is located, and at the West Farms, N.Y., substation, where power was purchased from the United Electric & Power Company (now Consolidated Edison Company). In later years, additional power-supply stations were established at Devon and East New York by interconnection, through suitable conversion machinery, with the 60-cycle systems of the Connecticut Light & Power Company and the Consolidated Edison Company respectively.

The main-line a-c electrification is 64 miles long, with four tracks extending from New Haven to Woodlawn, N.Y., where trains for Grand Central Terminal in New York City transfer to the 650-volt d-c electrification of the New York Central Railroad.

The New Canaan branch is a single-track line extending about 8 miles from Stamford to New Canaan with frequent stretches of 1% upgrade, going toward New Canaan. This branch was stub-end fed from Stamford for both series of tests. Subsequent to the tests, a 22-kv feeder has been extended from Stamford to a transformer at New Canaan.

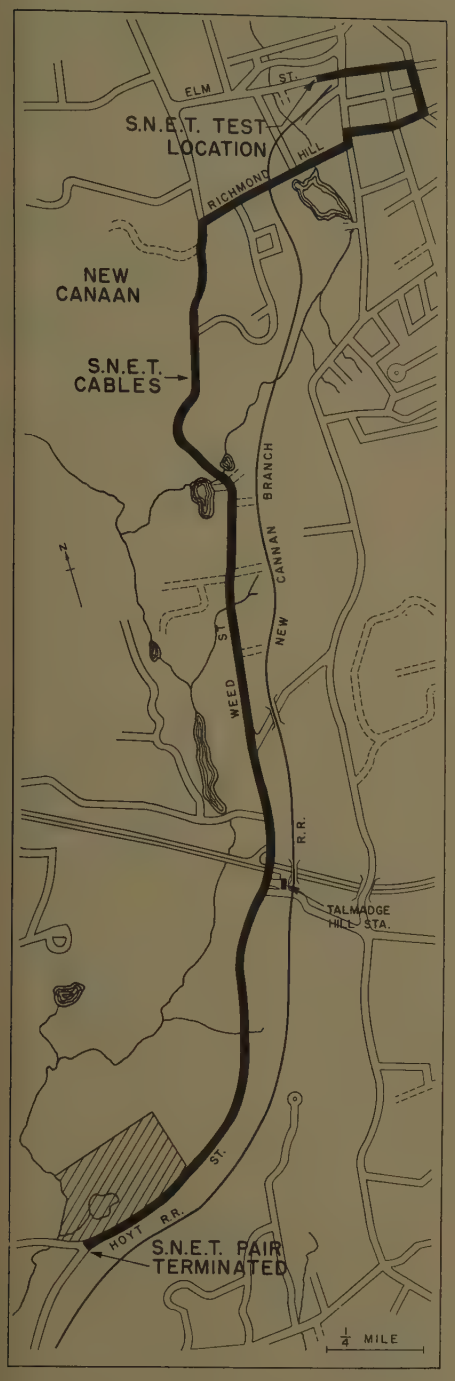


Fig. 6. Map of the New Canaan branch test area

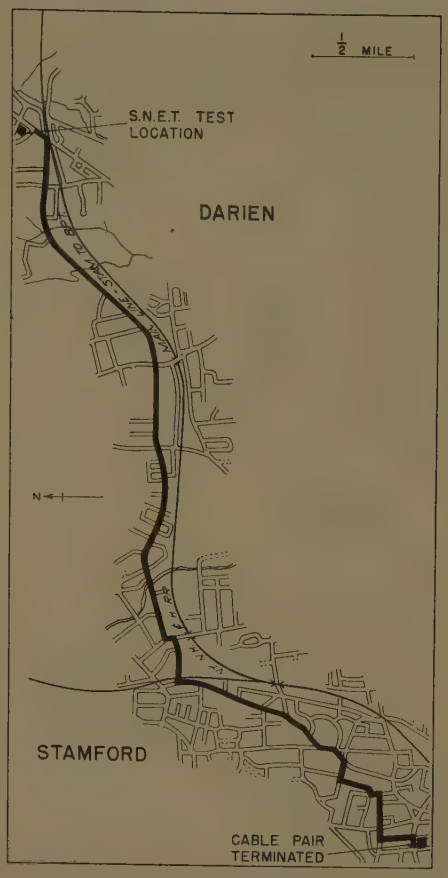


Fig. 7. Map of the test area on the main line between Stamford and Bridgeport

Table I. Maximum I·T Product, Single MU Car

| Test Series | One Car: No Cans | One Car: One Can | One Car: Two Cans |
|---|---|---|---|
| First | | | |
| Maximum db reading | 60 | 60 | 52 |
| $I \cdot T$ | 1,728 | 1,728 | 692 |
| Second | | | |
| Maximum db reading | 63 | 60 | 54 |
| $I \cdot T$ | 2,440 | 1,728 | 776 |
| Third | | | |
| Maximum db reading | 63 | 59.5 | 53 |
| $I \cdot T$ | 2,440 | 1,640 | 776 |

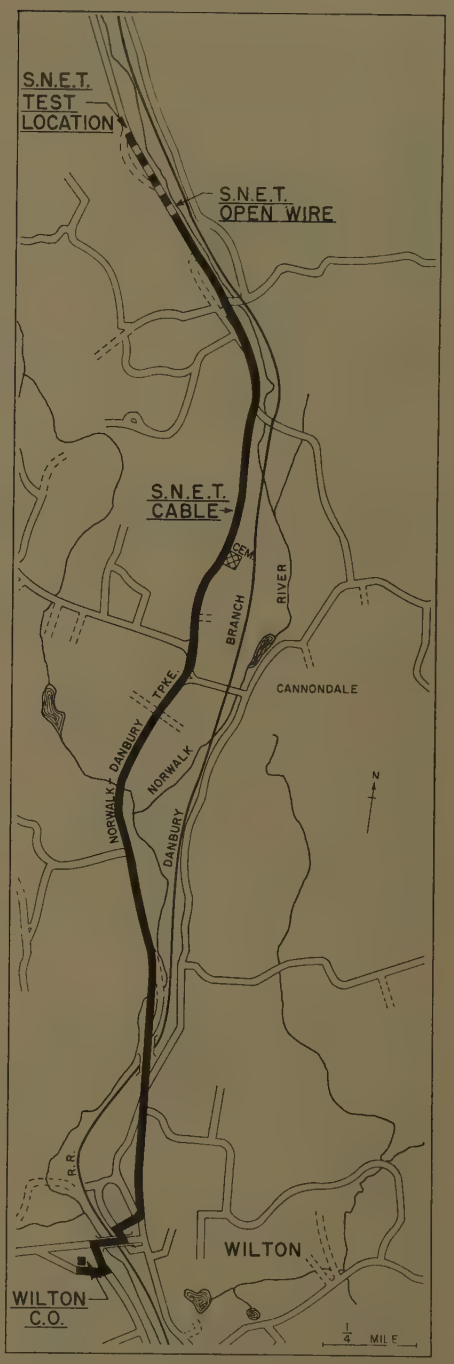


Fig. 8. Map of the Danbury branch test area

An installation of one series-track booster transformer at Springdale Cemetery and a 3-ohm air-core reactor in the trolley at Stamford was used to limit the magnitude and path of short-circuit currents during the tests. The booster transformer has since been removed.

The Danbury branch, also a single-track line, extends about 24 miles from South Norwalk to Danbury. High-speed circuit breakers are installed in the feeder and trolley wires on the Danbury side of the autotransformer at South Norwalk to limit the duration of short-circuit currents.

Autotransformers for feeding the Danbury trolley are located at South Norwalk, Wilton, Branchville, and Danbury. The autotransformer at Branchville is provided with a booster winding and a section break iu the trolley wire, so that the trolley voltage on the Danbury side of Branchville can be raised to 12 kv.

The Harlem River branch is about 12 miles long, extending from New Rochelle Junction on the main line to Harlem River yard in New York. From New Rochelle Junction to Port Morris there are four tracks, and from Port Morris to Harlem River there are two.

The New York Connecting Railroad joins the Harlem River branch at Port Morris and extends to the Bay Ridge Terminal on Long Island. Through passenger trains from New Haven to points west of New York leave the New York Connecting Railroad at Bowery Bay Junction, Long Island, and pass from there through the Pennsylvania Station, New York, over the Pennsylvania electrification. There are four tracks from Port Morris to Bowery Bay, two tracks from Bowery Bay to Bay Ridge Terminal, and two tracks from Bowery Bay to Harold Avenue.

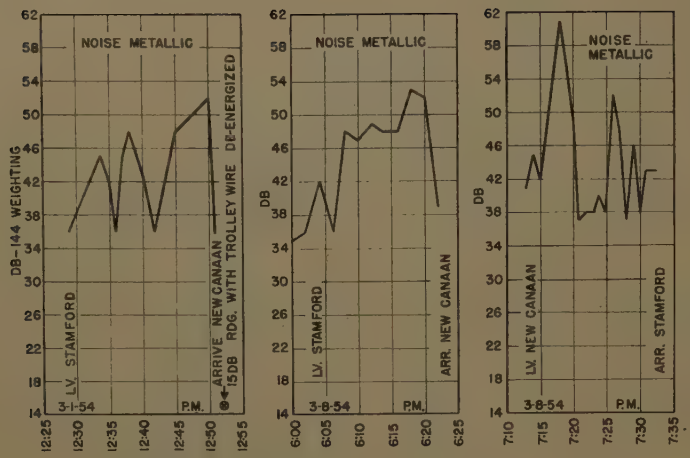


**Fig. 9. Data obtained on railroad test circuit with existing motive power on the New Canaan branch**

**Table II. New Haven Railroad Noise-Test Results**

Test Runs With Single-Phase Series-Motor Motive Power

| Test No. | Date | Equipment | Route | Train No. | Maximum Metallic Noise, Db |
|---|---|---|---|---|---|
| 1 | March 1, 1954 | MU car with two trailers | Stamford to New Canaan | N-28 | 52 |
| 2 | March 8, 1954 | locomotive 310 and eight cars | Stamford to New Canaan | 332 | 53 |
| 3 | March 8, 1954 | locomotive 310 and ten cars | Stamford to New Canaan | N-43 | 61 |
| 4 | July 8 1954 | locomotive 315 and eight cars | South Norwalk to Danbury | 140 | 50 |
| 5 | July 13, 1954 | electric locomotive and eight cars | South Norwalk to Danbury | 356 | 50 |

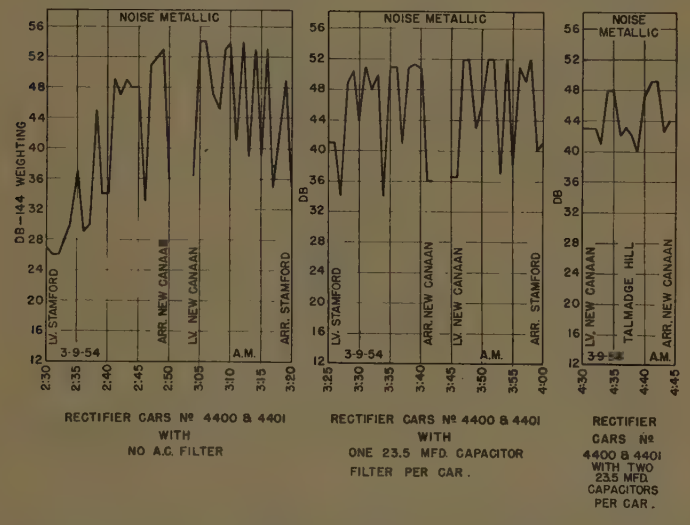


**Fig. 10. Data obtained on railroad test circuit with rectifier cars on the New Canaan branch**

**Table III. New Haven Railroad Noise-Test Results**

Test Runs on MU Cars, March 9, 1954, on New Canaan Branch

| Test No. | Time, A.M. From | Time, A.M. To | No. of MU Cars | Filters Per Car | Train From | Train To | Maximum Metallic Noise on New Canaan Freight and Ticket Line, Db |
|---|---|---|---|---|---|---|---|
| 1 | 2:18 | 2:52 | 2 | 0 | Stamford | New Canaan | 53 |
| 2 | 3:04 | 3:24 | 2 | 0 | New Canaan | Glenbrook | 54 |
| 3 | 3:25 | 3:42 | 2 | 1 | Glenbrook | New Canaan | 51.5 |
| 4 | 3:45 | 4:04 | 1 | 1 | New Canaan | Glenbrook | 52 |
| 5 | 4:30 | 4:44 | 2 | 2 | New Canaan | Talmadge Hill | 49 |
| 6 | 4:46 | 5:00 | 1 | 2 | New Canaan | Talmadge Hill and return | 51 |
| | 5:10 | | 1* | 2 | New Canaan | Stamford | 52 |

* Second car towed.

Figs. 1 and 2 show schematically the trolley and feeder circuits involved in the co-ordination tests.

### Communication Lines, New York, New Haven & Hartford Railroad

Prior to 1919, the New Haven Railroad had used an open-wire line situated along its right of way to take care of its telephone and telegraph traffic. During the years of 1916 through 1918 it installed a cable from New Haven, Conn., to Harlem River, N. Y. After the cable was installed, all communications between New Haven and Harlem River were handled by means of cable conductors. The cable includes train-and load-dispatching circuits; tie lines between the railroad's switchboard at Harlem River, New Haven, and intermediate points; way-station circuits, etc.; and also a few telegraph circuits.

The cable contains 45 pairs of conductors enclosed in a lead sheath; there are 32 pairs of 16 gage copper, 12 pairs of 13 gage copper, and 1 pair of 10 gage. One quad of the 16 gage conductors is enclosed in a second sheath at the center of the cable.

The length of the cable between Harlem River and New Haven is about 67 miles; for a total of about 15 miles it is laid underground between or near the tracks, and the rest of it is aerial cable following generally the route of the old open-wire line. The effective separation of the cable from the center line of the catenary system is about 60 feet.

There are also two open-wire circuits extending from Stamford to New Canaan, and four open-wire circuits from South Norwalk to Danbury, all of which have been equipped with drainage because of their close proximity to the trolley and feeder wires. The Danbury circuits consist of two physical and one phantom group of no. 9 Brown & Sharpe gage copper wire. Both the Danbury and New Canaan communication circuits are carried along the railroad right of way and are horizontally separated from the trolley by about 25 feet.

The New Haven Railroad operates circuits in a cable between Harlem River and Bay Ridge, carried for most of the distance along the right of way of the New York Connecting Railroad.

At points where the railroad circuits connect with those of the Bell System, repeating coils are used to separate the two metallic circuits.

Western Electric repeating coils are installed on the main-line circuits for drainage at the following locations: New

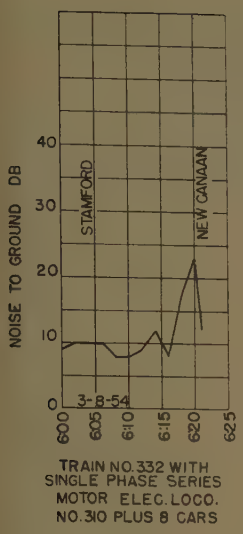


**Fig. 11. Data obtained on SNET test circuit with existing motive power on the New Canaan branch**

**Table IV. SNET Noise-Test Results**

Test Runs on New Canaan Branch with Single-Phase Series Motive Power and 2-Car MU Train, March 8 and 9, 1954

| Test No. | Time From | Time To | No. of MU Cars | Filters Per Car | Train From | Train To | Maximum Noise to Ground |
|---|---|---|---|---|---|---|---|
| 1 | 6:02 | 6:21 p.m. | 0 | 0 | Stamford | New Canaan | 23 |
| 2 | 2:43 | 3:12 a.m. | 2 | 0 | Woodway | New Canaan and return | 30 |
| 3 | 3:34 | 3:51 a.m. | 2 | 1 | Woodway | New Canaan and return, Talmadge Hill | 27 |
| 4 | 4:33 | 4:43 a.m. | 2 | 2 | New Canaan | Talmadge Hill and return | 22.5 |

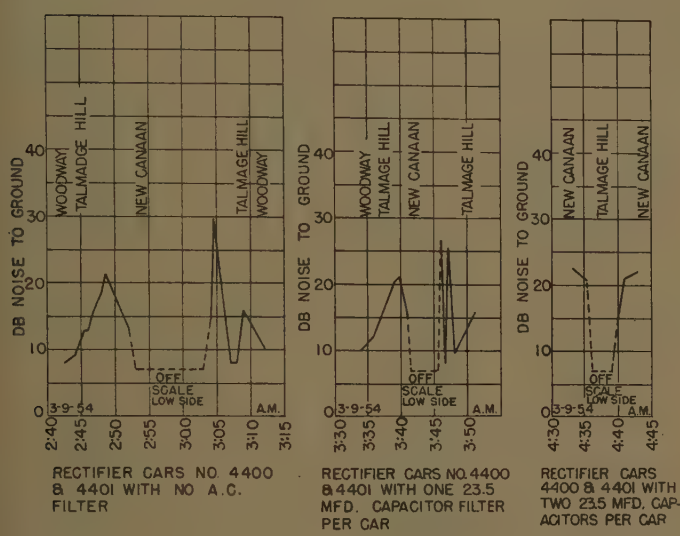


**Fig. 12. Data obtained on SNET test circuit with rectifier cars on the New Canaan branch**

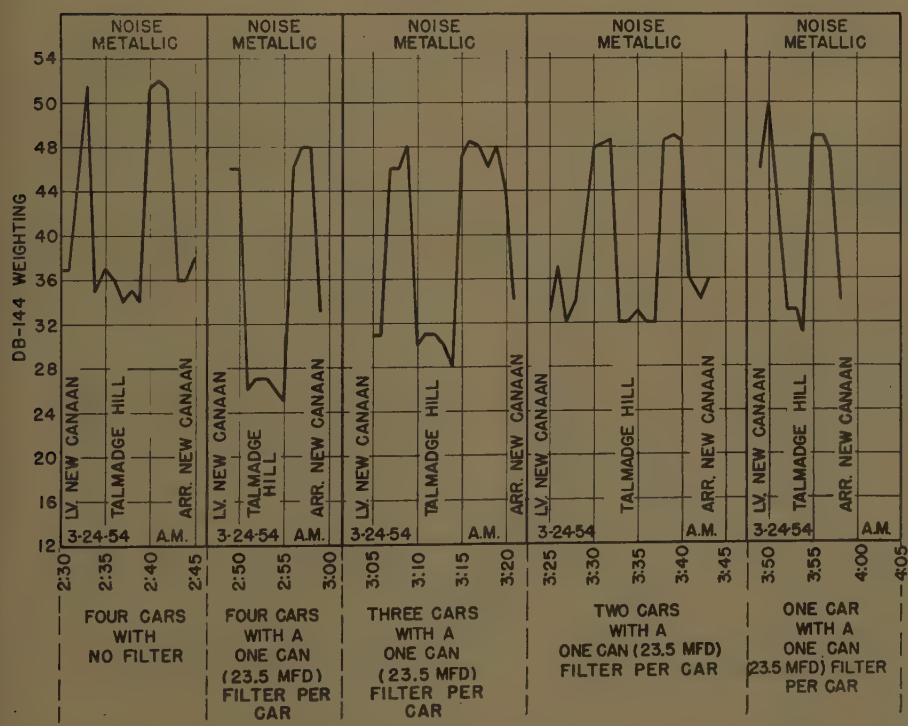


**Fig. 13. Data obtained on railroad test circuit with rectifier cars on the New Canaan branch**

Haven, Devon, Bridgeport, South Norwalk, Port Chester, New Rochelle, South Mount Vernon, and Harlem River.

Drainage was provided for the New Canaan loop from Stamford by connecting the *70-A* drainage coil at Stamford as a repeating coil, the secondary being connected to the New Canaan loop with the mid-point of the coil grounded. A *70-A* coil was connected across the loop at New Canaan and grounded at its mid-point. Drainage was provided at five points on the Danbury branch.

Figs. 3 through 5 show schematically the railroad communication circuits and drainage provisions used in the co-ordination tests.

### Communication Lines, SNET

Figs. 6 through 8 show, respectively, the exposures to the SNET plant on which measurements were made of longitudinal-induction effects arising from the railway motive-power equipment on the New Canaan branch, the main line, and the Danbury branch. In the first two instances, all cable circuits were used with the far-end terminated in a balanced impendance to ground. On the Danbury branch, the test location was at the end of an open-wire line about 1/2 mile in length. These open-wire circuits were connected to cable pairs that had been terminated in a balanced impedance to ground at the Wilton central office.

## Co-ordinated Noise and Influence Tests

### Exposure Locations

The first series of tests to determine the effect of rectifier motive power on neighboring communication circuits was made on March 9, 1954, with two rectifier cars (4400 and 4401) on the New Canaan branch, with a stub-end trolley feed to New Canaan from Stamford.

The second series of tests was made on March 24, 1954, with six rectifier cars on

(*Continued on page 424.*)

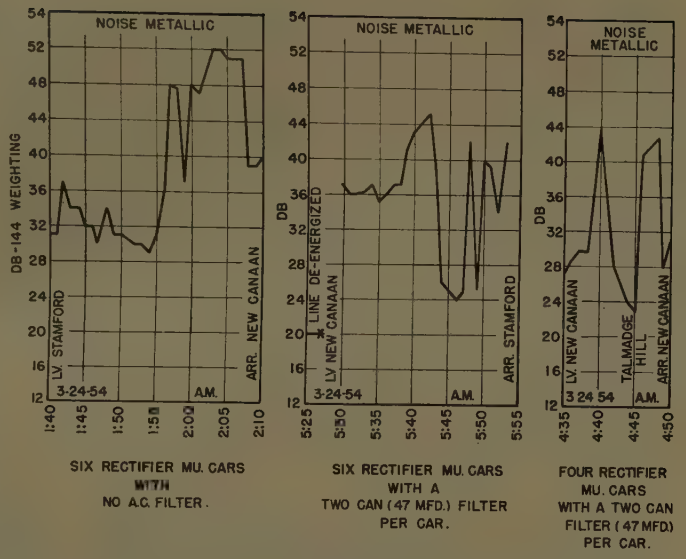


**Fig. 14. Data obtained on railroad test circuit with rectifier cars on the New Canaan branch**

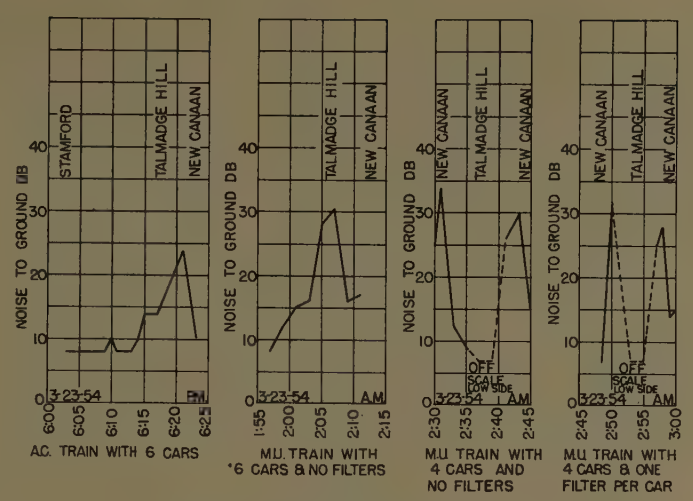


**Fig. 15. Data obtained on SNET test circuit with rectifier cars and an a-c train on the New Canaan branch**

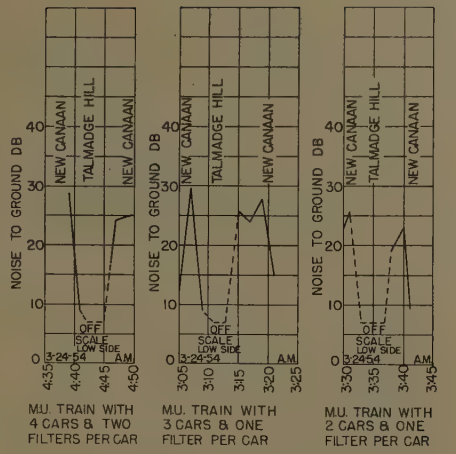


**Fig. 16. Data obtained on SNET test circuit with rectifier cars on the New Canaan branch**

## Table V. New Haven Railroad Noise-Test Results

Test Runs on MU Cars, March 24, 1954, on New Canaan Branch

| Test No. | Time, A.M. From | Time, A.M. To | No. of MU Cars | Filters Per Car | Train From | Train To | Maximum Metallic Noise on New Canaan Freight and Ticket Line, Db |
|---|---|---|---|---|---|---|---|
| 1 | 1:33 | 2:10 | 6 | 0 | Stamford | New Canaan | 52 |
| 2 | 2:30 | 2:45 | 4 | 0 | New Canaan | Talmadge Hill and return | 52 |
| 3 | 2:49 | 3:00 | 4 | 1 | New Canaan | Talmadge Hill and return | 48 |
| 4 | 3:05 | 3:21 | 3 | 1 | New Canaan | Talmadge Hill and return | 48.5 |
| 5 | 3:25 | 3:43 | 2 | 1 | New Canaan | Talmadge Hill and return | 49 |
| 6 | 3:49 | 3:58 | 1 | 1 | New Canaan | Talmadge Hill and return | 50 |
| 7 | 4:35 | 4:50 | 4 | 2 | New Canaan | Talmadge Hill and return | 44 |
| 8 | 4:59 | 5:23 (reactor cut out) | 6 | 2 | New Canaan | Talmadge Hill and return | 48 |
| 9 | 5:28 | 5:53 | 6 | 2 | New Canaan | Stamford | 45 |

## Table VI. SNET Noise-Test Results

Test Runs on New Canaan Branch With Single-Series Motive Power and MU Cars, March 23 and 24, 1954

| Test No. | Time From | Time To | No. of MU Cars | Filters Per Car | Train From | Train To | Maximum Noise to Ground |
|---|---|---|---|---|---|---|---|
| 1 | 6:03 | 6:24 p.m. | 0 | 0 | Stamford | New Canaan | 24 |
| 2 | 1:52 | 2:13 a.m. | 6 | 0 | Stamford | New Canaan | 30.5 |
| 3 | 2:29 | 2:45 a.m. | 4 | 0 | New Canaan | Talmadge Hill and return | 34 |
| 4 | 2:48 | 3:00 a.m. | 4 | 1 | New Canaan | Talmadge Hill and return | 31.5 |

## Table VII. New Haven Railroad Noise-Test Results

Test Runs on MU Cars, March 26, 1954, on Main Line Between Stamford and Devon, Six Cars

| Test No. | Time From | Time To | Filters Per Car | Train From | Train To | Maximum Metallic Noise Measured at Bridgeport, on New Haven-Harlem River Line, Db: No. 7 West | No. 7 East |
|---|---|---|---|---|---|---|---|
| 1 | 9:10 a.m. | 11:06 a.m. | 0 | Stamford | Devon | 26.5 | 10 |
| 2 | 11:07 a.m. | 12:03 p.m. | 1 | Devon | Stamford | 25 | 10 |
| 3 | 12:04 p.m. | 12:47 p.m. | 2 | Stamford | Bridgeport | 20.5 | |
| 4 | 2:27 p.m. | 2:58 p.m. | 0 | Bridgeport | Stamford | 28.5 | |

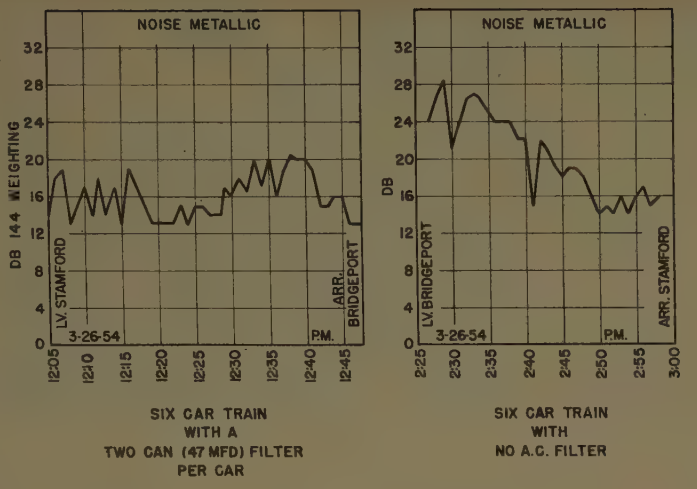


Fig. 17. Data obtained on railroad test circuit with rectifier cars on the main line between Stamford and Bridgeport

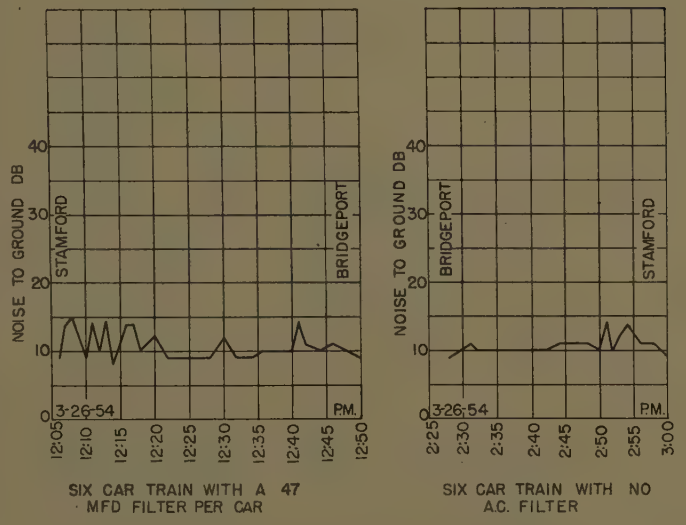


Fig. 18. Data obtained on SNET test circuit with rectifier cars on the main line between Stamford and Bridgeport

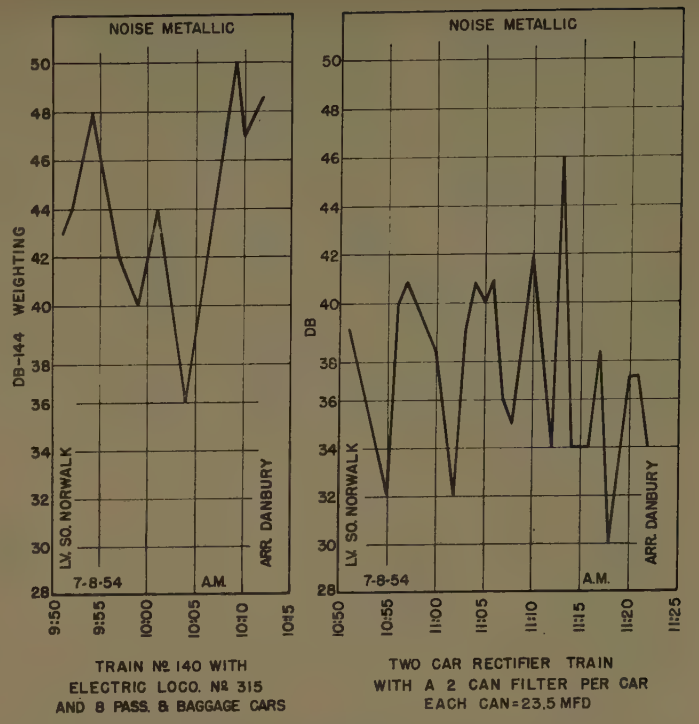


Fig. 19. Data obtained on railroad test circuits from tests on the Danbury branch

**Table VIII. SNET Noise-Test Results**

Test Runs on Main Line Between Stamford and Bridgeport With MU Cars, March 26, 1954

| Test No. | Time From | Time To | No. of MU Cars | Filters Per Car | Train From | Train To | Maximum Noise to Ground |
|---|---|---|---|---|---|---|---|
| 1 | 12:04 | 12:47 p.m. | 6 | 2 | Stamford | Bridgeport | 15 |
| 2 | 2:27 | 2:56 p.m. | 6 | 0 | Bridgeport | Stamford | 14 |

**Table IX. New Haven Railroad Noise-Test Results**

Test Runs of MU Cars, July 8, 1954, on Danbury Branch

| Test No. | Time From | Time To | No. of MU Cars | Filters Per Car | Train From | Train To | Maximum Metallic Noise, Phantom Circuit, Db |
|---|---|---|---|---|---|---|---|
| 1 | 10:51 | 11:22 a.m. | 2 | 2 | South Norwalk | Danbury | 46 |
| 2 | 12:33 | 1:21 p.m. | 2 | 2 | Danbury | South Norwalk | 46 |
| 3 | 2:38 | 3:17 p.m. | 2 | 2 | South Norwalk | Danbury | 48 |
| 4 | 9:51 | 10:12 a.m. | train no. 140, electric locomotive no. 315 | | South Norwalk | Danbury | 50 |

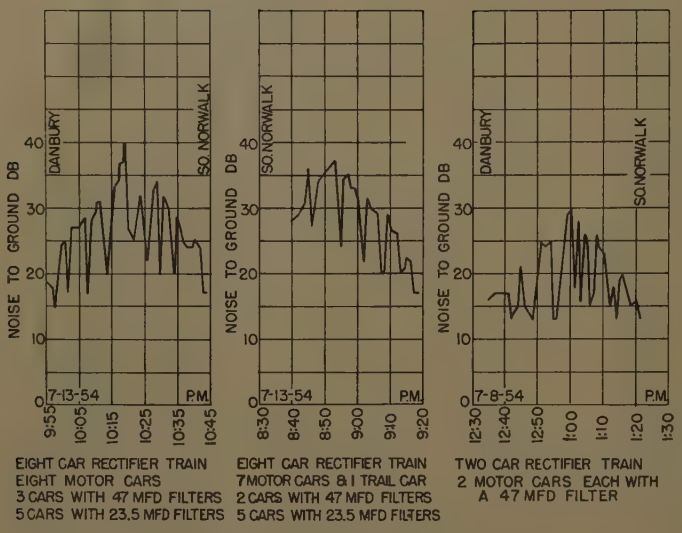


**Fig. 20. Data obtained on SNET test circuit with rectifier cars on the Danbury branch**

**Table X. SNET Noise-Test Results**

Test Runs on Danbury Branch With MU Cars, July 8 and 13, 1954

| Test No. | Time From | Time To | No. of MU Cars | Filters Per Car | Train From | Train To | Maximum Noise to Ground |
|---|---|---|---|---|---|---|---|
| 1 | 9:56 | 10:43 p.m. | 8 | 3 ..... 2<br>5 ..... 1 | Danbury | South Norwalk | 40 |
| 2 | 8:31 | 9:16 p.m. | 8 | 3 ..... 2<br>5 ..... 1 | South Norwalk | Danbury | 37.5 |
| 3 | 12:33 | 1:21 p.m. | 2 | 2 | Danbury | South Norwalk | 30 |

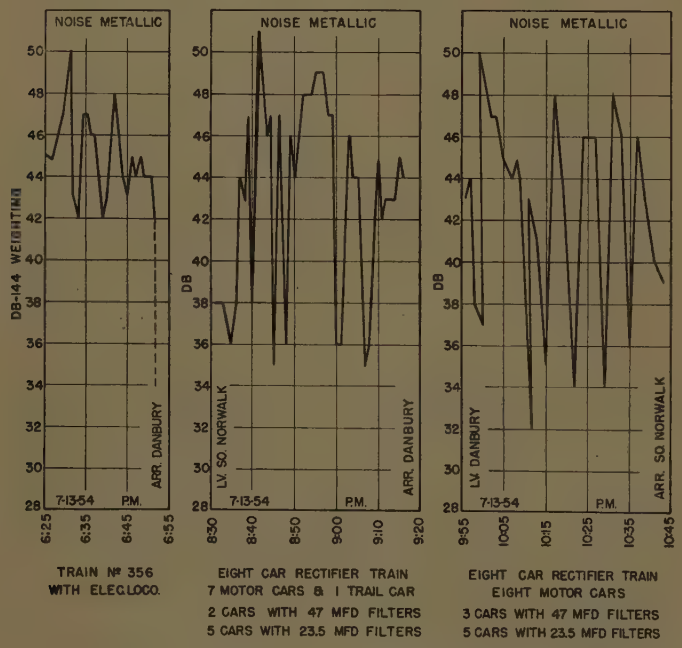


**Fig. 21. Data obtained on railroad test circuit from tests on the Danbury branch**

**Table XI. New Haven Railroad Noise-Test Results**

Test Runs of MU Car, July 13, 1954, on Danbury Branch

| Test No. | Time From | Time To | No. of MU Cars | Filters Per MU Car | No. Train Cars | Train From | Train To | Maximum Metallic Noise, Phantom Circuit, Db |
|---|---|---|---|---|---|---|---|---|
| 1 | 6:24 | 6:52 p.m. | train 356 and electric locomotive | | | South Norwalk | Danbury | 50 |
| 2 | 8:31 | 9:16 p.m. | 7 | 2 ..... 2<br>5 ..... 1 | 1 | South Norwalk | Danbury | 51 |
| 3 | 9:56 | 10:43 p.m. | 8 | 3 ..... 2<br>5 ..... 1 | | Danbury | South Norwalk | 50 |

the New Canaan branch. The third series was made on March 26, 1954, on the main line between Stamford and Bridgeport with six rectifier cars. The fourth series was made on July 7, 1954, on the Danbury branch with two rectifier cars. The fifth series was made on July 13, 1954, with eight rectifier cars on the Danbury branch.

### Measuring Instruments

Rectifier car no. 4400 was used on the first three series of tests. This test car was equipped with meters, cathode-ray oscilloscopes, speedometer, and a *2-B* noise meter. Table I shows maximum single-car-trolley ampere $I \cdot T$ values for these three tests. Tape recorders were used during all tests to record the railroad's test circuit noises; and also in the New Canaan tests to record the telephone company's test circuit noises.

*2-B* noise meters were used to measure metallic noise on all railroad test circuits. Noise to ground could not be measured due to drainage circuit connections.

*2-B* noise meters were used to obtain noise to ground readings on selected SNET telephone circuits. Metallic noise was too low to measure. All db (decibel) readings taken were with 144 receiver weighting.

### Discussion of Test Data

#### *First Series of Tests at New Canaan*

Fig. 9 and Table II show the noise readings obtained on the railroad test telephone line at New Canaan with single-phase series-motor motive power.

Fig. 10 and Table III show the corresponding reading for one and two rectifier MU cars with and without a-c filters.

Figs. 11 and 12 and Table IV show the SNET test line readings, for both a-c motor and rectifier MU car operation.

#### *Second Series of Tests at New Canaan*

Figs. 13 and 14 and Table V show the noise readings obtained on the railroad test circuit with one to six rectifier cars.

Figs. 15 and 16 and Table VI show the SNET test circuit readings for these conditions with a 6-car train with a-c series-motor locomotive.

#### *Third Series of Tests, on Main Line*

Fig. 17 and Table VII show the noise readings obtained on the railroad test circuit with six rectifier cars.

Fig. 18 and Table VIII show SNET test circuit readings for these conditions.

#### *Fourth Series of Tests, on Danbury Branch*

Fig. 19 and Table IX show the noise readings on the railroad test circuit with

two rectifier cars and with a single-phase series-motor locomotive.

Fig. 20 and Table X show SNET test circuit reading under these conditions except no tests were made during a-c series-motor operation.

*Fifth Series of Tests, on Danbury Branch*

Fig. 21 and Table XI show the noise readings on the railroad test circuit with eight rectifier cars and with an a-c series-motor locomotive.

Fig. 20 and Table X show the corresponding SNET test circuit readings except no tests were made during a-c series-motor operation.

NOISE, MU RECTIFIER MOTIVE POWER

The most predominant and most characteristic sound produced by nonfiltered single-phase rectifier motive power is a "buzz" similar to the sound of a small buzzer. The buzz in the communication circuit is induced by the high rate of change in the catenary current and flux during the angle of overlap.

The voltage induced in the exposed communication circuit appears as a pulse in voltage during the angle of overlap. The value of induced voltage for any given exposure varies directly with the load current being commutated and it varies inversely with the angle of overlap.

The pulse in voltage in the communication circuit occurs every half-cycle and will be positive and negative during alternate half-cycles.

## Conclusions

The test results indicate the following:

1. A large number of rectifier motive-power units do not have a directly additive effect on each other.

2. MU rectifier motive power without a-c filters produces approximately the same noise levels as existing motive power under similar load conditions.

3. MU rectifier motive power with a-c filters produces lower noise levels than existing motive power under similar load conditions.

## Reference

1. RECTIFIER MOTIVE POWER—INDUCTIVE COORDINATION CONSIDERATIONS, E. B. King, K. H. Gordon, L. J. Hibbard. *AIEE Transactions*, vol. 73, pt. II, July 1954, pp. 107–18.

# Discussion

**E. A. Binney** (English Electric Company, Ltd., Bradford, England): In this very interesting paper the authors have shown records which indicate the noise found in open telephone lines paralleling a track, under varying current conditions in the catenary. It is, however, difficult to compare the results obtained with the locomotive-hauled trains and the MU cars with rectifiers, since the corresponding current are not given. It is clear that the MU cars cause no direct additive effect, but would this be true of a locomotive having, say, the power of six MU cars?

Two years ago a 25-cycle 6,600-volt system of the British Railways was converted to a 50-cycle 6,600-volt system, and the original MU cars having two single-phase motors were replaced by new cars with rectifier equipment, in this case there being four motors per car of 200 hp.

Prior to the change, noise tests were carried out on a telephone circuit paralleling the tracks, using a single motor coach (with two 200-hp single-phase motors) taking about 40 amp from the overhead. The psophometer readings obtained reached values of 8 millivolts, this being nearly twice the recognized maximum permissible in the United Kingdom, although the telephone lines had been used under these conditions for many years (under protest). Subsequently, similar tests were carried out with a single rectifier-type MU car drawing a maximum current of 200 amp during starting. The corresponding readings reached a value of 30 millivolts. A further test at 60 line amp gave 11 millivolts. From these results it appears that the interference value is roughly proportional to the current drawn by the rectifier car, and that at equal currents for the 25-cycle single-phase load and rectified 50-cycle load the interference is of the same order.

As might be surmised, these telephone wires were cabled and buried before operation on the new system commenced. I think it can be assumed that this step will be necessary on all 50/60-cycle single-phase traction systems, whatever type of motive power is employed.

Of greater interest, in my opinion, is the possible effect of harmonics due to 50-cycle traction on the power system or systems supplying the substations. It would be interesting to know the magnitude of the various harmonics due to traction currents which might be measured on the secondary and primary side of the West Farm supply, which would appear to be the only station connected to the system having nontraction demand.

**H. S. Ogden** (General Electric Company Erie, Pa.): The paper provides a record of a number of miscellaneous tests with reference to the subject of telephone interference on a particular railroad. The data given do not lend themselves readily to other applications. They are valuable in that they provide a qualitative summary of what happens when rectifier motive-power units are applied in rather large numbers.

Having been invited to participate as an observer in some of the tests described, it was my good fortune to be able to obtain some readings which may have a more general application than those given in the paper. On the first tests on the New Canaan branch, it was possible to measure the total rail return current from the train undergoing tests between Springdale Cemetery and New Canaan Station at the former location. Although the scale of the ammeter in use was such that it would not indicate currents under 120 amp (approximately current for two cars), fairly complete observations were made on a 4-car train with zero, one, and two capacitor cans per car. A shunt and noise meter in series with the ammeter permitted the inherent noise, and thus the telephone influence factor, of the propulsion current to be determined. When multiplied by the ammeter reading, the $I \cdot T$ product for the circuit became available. At the same instant that these meter readings were taken, corresponding noise measurements were made on the freight and ticket office telephone line at the New Canaan Station. The information so obtained has been plotted in Fig. 22. The curves indicate a reasonably close correlation between the $I \cdot T$ product for the different numbers of capacitors per car and the noise reading on the phone line. Within a reasonable amount of error, considering the test conditions, the curves show that doubling the $I \cdot T$ product changes the db level on the phone line by 6 db, which, because of the logarithmic nature of the db unit, is the correct ratio. The following simple manipulation proves this statement. By definition

$$\text{db} = 20 \log_{10}(I \cdot T) \quad (1)$$

Doubling the $I \cdot T$ product gives

$$\text{db}' = 20 \log_{10}(2 \times I \cdot T) \quad (2)$$

$$\text{db}' = 20 (\log_{10} 2 + \log_{10} I \cdot T) \quad (3)$$

$$\text{db}' = 20 \log_{10} 2 + 20 \log_{10} I \cdot T \quad (4)$$

Substituting the numerical value of $20 \log_{10}$ 2 and db from equation 1 and rearranging gives

$$\text{db}' = \text{db} + 6$$

Thus doubling the $I \cdot T$ product increases the original db level by six units.

The $I \cdot T$ product decrease from 7,800 for no cans to approximately 2,000 with two cans per car, and the telephone-line noise level decreased from 51.5 db to 44 db. Talking over the line was entirely possible with a noise level of 51.5 db resulting from the rectifier. The buzz of the rectifier seemed to fade out when voice frequencies were present and was only noticeable when there was no talking.

A 1955 paper[1] contains a discussion on some of the theoretical aspects of telephone interference, and included therein is an oscillograph wave shape (Fig. 9) showing an induced wave on a telephone line on the test floor. A wave shape identical in all respects to this was obtained on the freight and ticket office telephone line at the New Canaan Station during these tests. A copy of this oscillogram is shown in Fig. 23. A single capacitor per car sufficed to remove the spike shown on the oscillogram.

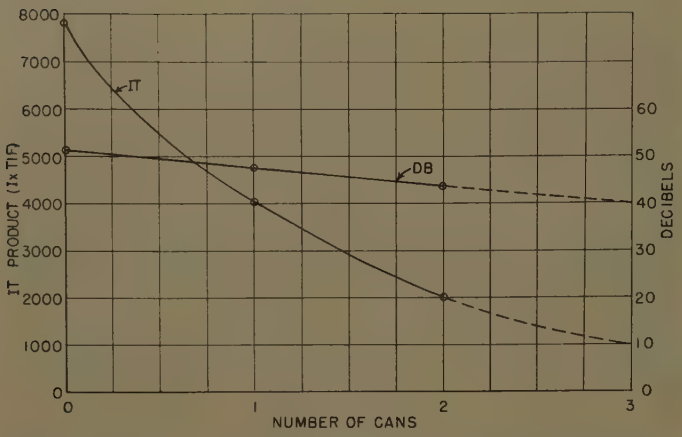


**Fig. 22 (above). Tests of 4-car train on New Canaan branch, March 24, 1957; total I·T from Springdale Cemetery readings, and db metallic on freight and ticket office line versus number of cans per car**

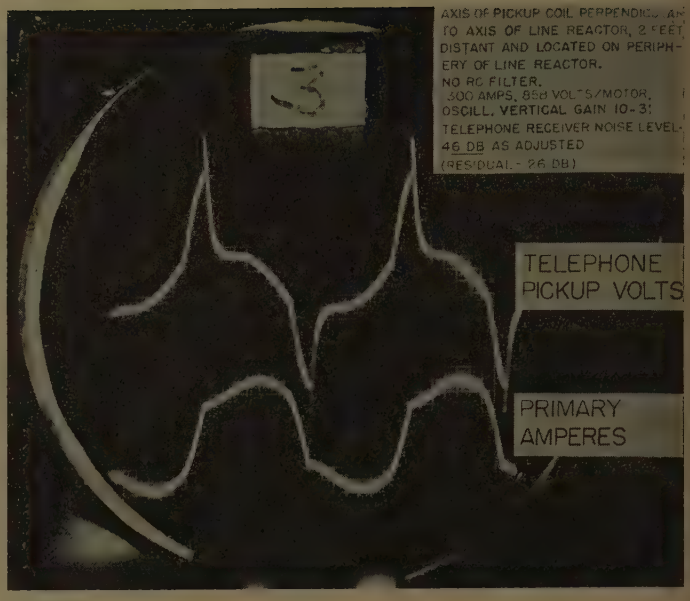


**Fig. 23 (right). Oscillogram of test on ticket office telephone line at New Canaan branch**

Where observations were made on telephone lines encased in cable, it was impossible to obtain the characteristic "pick-up" wave shape mentioned in the foregoing and, as stated in the paper, the influence was of very small proportions.

The authors omitted any reference to the use of tape recorders in studying telephone influence on the New Haven Railroad. An excellent presentation describing the use of tape recorders in connection with tests on the Pennsylvania Railroad was made by Mr. Hibbard and others (see reference 1 of the paper). I believe the use of tape recorders would bear mentioning again since, on some of the tests covered by the paper, tape recorders were placed at a number of locations on the New Haven telephone system, such as at the New Canaan ticket office, the Bridgeport wire chief's office, and at the New Haven dispatcher's office. These were in operation throughout the tests on the New Canaan branch and permitted personnel, then busily engaged with the conduct of the tests at the New Canaan ticket office, to study the record of test noise on the telephone lines at these specified points at their leisure a day or so later.

### Reference

1. Considerations in the Development of a High-Power Rectifier Locomotive, H. S. Ogden. *AIEE Transactions*, vol. 74, pt. II, July 1955, pp. 169–76.

**H. F. Brown** (Gibbs & Hill, Inc., Pennsylvania Station, New York, N. Y.): Those familiar with inductive co-ordination problems involving single-phase railway-traction circuits and the paralleling of communication lines will recognize in this paper familiar territory and utilities involved. Ever since 1909, the New Haven Railroad and the SNET, with the American Telephone and Telegraph Company and Bell Laboratory engineers, have closely co-operated in the understanding and solutions of their mutual problems due to induction. That both the railway and the communication systems have successfully extended their facilities in this territory during the intervening years indicates how satisfactory have been the relations between these companies, and how successful have been the mitigative methods developed.

The information presented will not only be of value when future equipment of this type is considered for use in the United States, but will be studied with keen interest abroad, where rectifier equipment is being used or considered for single-phase railway electrification using commercial frequency.

The harmonics from rectifier apparatus whether used in fixed substations for d-c traction, or on mobile equipment of the type described in the paper, have always presented a problem to the communication interests. It is gratifying to learn from the test data and experience already accumulated that this new type of motive power for railway electrification, which combines so well the best features of the d-c and a-c systems, requires but simple and relatively inexpensive mitigative apparatus. The railroad, the telephone, and manufacturing companies involved are all to be congratulated and complimented on another good example of engineering co-operation.

It seems fitting here to pay tribute to one of the authors of this paper, L. J. Hibbard. That the rectifier car and locomotive have been so successfully developed is due largely to his untiring efforts. The electrical industry and the railroads are greatly indebted to him for his enthusiasm in the application of this apparatus, and for his contributions to the solution of the engineering problems involved.

**L. J. Hibbard, F. T. Garry,** and **G. N. Loomis:** It is predicted that communication inductive co-ordination considerations in connection with single-phase rectifier motive-power applications to the world's railroads will become increasingly unimportant in the future.

From the communication standpoint, the extensive replacement by railway and telephone companies of open wire with cable, with its inherent shielding and close pair spacing, as well as the increasing use of carrier and short wave have made the communication plant less susceptive. Another factor has been the general policy of telephone companies for many years to avoid long and close inductive exposures to existing or potential railroad electrifications.

Our experiences in the United States to date indicate the only inductive communication problems that may be involved with applications of rectifier motive power to new or existing electrifications will be the railroads' own private communication lines. These problems can be met on existing communication lines where trouble is encountered by simple and inexpensive filtering equipment on the motive-power units.

These problems will disappear on the modern railroads of the future, equipped with modern communication systems. Hurricanes, ice storms, and other acts of nature combined with economics will force the modern railroad to use modern communication systems even if they are not electrified.

Extensive electrification is taking place in other parts of the world with rectifier motive power at commercial frequencies. To our present knowledge, no communication problems have been encountered and it has not been necessary to apply filtering equipment to the rectifier motive-power units.

In reply to Mr. Binney's question we did not measure the rectifier harmonics on the primary side of the West Farm substation. However, tests made in the laboratory at East Pittsburgh indicate that existing New Haven motive-power equipment with single-phase series commutator motors produce as high a value of harmonics in the supply system as are produced with the new rectifier motive units.

Several studies have been made in recent years relative to supplying power to single-phase railways from existing power systems at commercial frequency. The studies indicate that such a procedure is entirely practical. This conclusion is borne out by experiences in France.

# Some Applications of Magnetic Amplifiers in Aircraft Generator Protective Systems

D. L PLETTE
ASSOCIATE MEMBER AIEE

J. W. BUTLER
ASSOCIATE MEMBER AIEE

CONSIDERABLE progress has been made during the years 1951 through 1956 toward improving the performance and reliability of aircraft generator regulation[1] and excitation systems. Much of this progress has been made possible by the use of static magnetic components and metallic dry disk rectifiers combined in such a way that the result is good reliability and accurate, predictable performance.

During this same period the increasing dependance of the airplane upon its electrical system has made it necessary to consider protective systems to prevent the destruction of critical load equipment due to a failure in any part of the electrical system. The majority of the protective devices utilized in these systems depends on the calibrated operation of relays. These relays are normally operated with coil voltages which are fairly critical. At rated system voltage and frequency, the coil voltage is either slightly lower than that necessary to pick up the relay or slightly higher than that at which the relay will drop out. This condition is brought about by the desirability of detecting frequency and voltage changes in the order of 5% to 15% from rated. As a result of this practice, these protective devices are sensitive to acceleration, shock, and vibration and their exact operating points are often rather unpredictable. Since the relays are generally not designed to withstand the vibration forces present in aircraft with critical coil voltages applied, vibration isolators are required for the equipment to prevent malfunctioning of these devices.

Paper 57-481, recommended by the AIEE Air Transportation Committee and approved by the AIEE Technical Operations Department for presentation at the AIEE East Central and Middle Eastern District Meeting and Air Transportation Conference, Dayton, Ohio, May 7–9, 1957. Manuscript submitted February 7, 1957; made available for printing July 29, 1957.

D. L. PLETTE and J. W. BUTLER are with the General Electric Company, Waynesboro, Va.

The authors wish to acknowledge the assistance of H. H. Britten, P. D. Corey, and J. L. Lotts, who contributed substantially to the development work on which this paper is based.

It is felt that the reliability and accuracy of the protective system can be much improved by the use of magnetic amplifiers, which can be used in such a manner that they supply essentially full voltage or zero voltage to the coil of a relay, thereby making the relay relatively insensitive to acceleration, shock, and vibration. This paper will describe some applications of magnetic amplifiers in aircraft generator protective systems.

## Reasons for Use of Magnetic Amplifiers

Magnetic amplifiers provide an accurate and predictable means of obtaining power amplification. It is therefore possible to operate voltage comparison circuits and frequency comparison circuits at a fairly low power level. The error signal obtained from these comparison circuits can then be amplified to a power level sufficient to operate a reliable standard relay, supplying essentially full-on or full-off voltage to the relay coil.

The resulting use of standard, noncritical relays enables the protective system to withstand rigid shock, vibration, and acceleration specifications without the need for shock mounts or vibration isolators. Magnetic amplifiers also provide an accurate and reliable means of producing time delay. By utilizing the magnetic properties of the core, fixed time delay as well as inverse time delay can be obtained. By the proper selection of core materials and rectifiers, magnetic amplifiers will perform accurately and reliably over the range of −55 to +125 C (degrees centigrade).

## Circuit Description

### Magnetic-Amplifier Undervoltage Relay

Individual phase undervoltage protection is often required in protective systems to protect load equipment from sustained undervoltage because of any of the following:

1. Loss of excitation.
2. Open-generator phase windings or feeder (under conditions of system loading which produce undervoltage on one or more phases).
3. Bus faults or feeder faults which are not cleared either by protective devices or by burning clear.

Individual phase undervoltage protection may be obtained by utilizing a magnetic amplifier as shown in Fig. 1. The voltage on each phase ($E_{ac}$) is rectified and filtered to produce voltage ($KE_{dc}$) which is compared to the reference voltage. With rated voltage on each phase, the direct voltage produced by each sensing network is higher than the reference voltage and rectifiers 1REC, 2REC, and 3REC are blocking. If any one or all three direct voltages drop below the reference voltage, current flows from the reference through the control winding and rectifier. This causes the magnetic amplifier to reduce its output to a very low value, thereby de-energizing the relay. As soon as all three direct voltages are equal to or higher than the reference voltage, the magnetic amplifier will increase its output and energize the relay. Different settings of the undervoltage relay are obtained by the use of different fixed resistors for $1R$, $2R$, and $3R$.

### Magnetic-Amplifier Overvoltage Relay

Highest-phase overvoltage protection is commonly required in protective systems to give the maximum overvoltage protection to load equipment. This protection is characterized by an inverse time-voltage relationship. Extreme overvoltages are allowed to exist for only a very brief time. On the other hand, slight overvoltages are allowed to exist for a longer time before the overvoltage protection is energized.

Highest-phase overvoltage protection with inverse time delay may be obtained by utilizing a magnetic amplifier as shown in Fig. 2.

The three line-to-neutral voltages $E_{Aac}$, $E_{Bac}$, $E_{Cac}$ are rectified and filtered in such a manner that the output voltage $E_{0dc}$ is roughly proportional to the highest of the three line-to-neutral voltages. A portion of this voltage is then compared with the voltage reference. Under rated voltage conditions, this voltage $E_{2R} = [2R/(1R+2R)] \times E_{0dc}$ is less than the reference voltage and rectifier 1REC is blocking. As the voltage on any one or all phases of the system rises, the voltage $E_{2R}$ will finally exceed the reference voltage and cause voltage to be impressed across control winding $F_1$-$F_2$ on the magnetic amplifier ($1SX$). The characteristic of the voltage across this winding as a

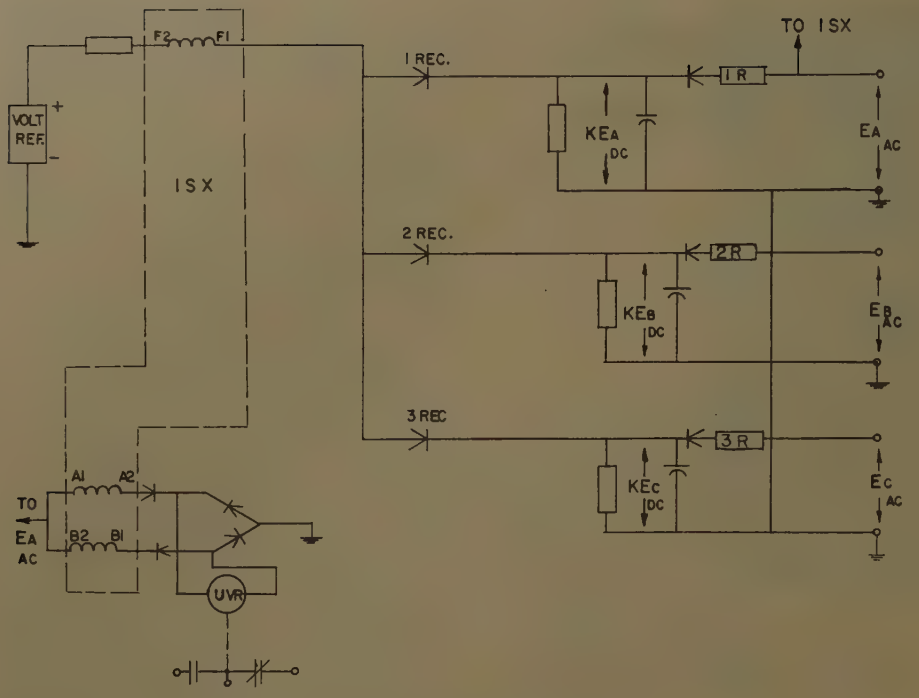


Fig. 1. Undervoltage relay circuit

function of line-to-neutral voltage is shown in Fig. 3. The exact value of this voltage for a particular value of $E_{0dc}$ will depend upon the reference voltage and the values of resistors $1R$, $2R$, and $3R$.

An understanding of how the magnetic amplifier produces a time delay characteristic may be obtained by considering Fig. 4, which shows a hysteresis loop of the square-loop core material utilized in the magnetic amplifier. By means of bias winding $F_3$-$F_4$, the core material is initially saturated in the negative direction. By winding gate windings $A_1$-$A_2$ and $B_1$-$B_2$ with a very large number of turns, the a-c flux excursion in the core can be made very small compared to the saturation flux density of the material. Its effects can therefore be neglected in calculating the flux change caused by application of the voltage $E_c$ to the control winding $F_1$-$F_2$ of the magnetic amplifier.

The time delay characteristics of this magnetic amplifier thus depend on the voltage $E_c$ as follows:

$$E = N\frac{d\phi}{dt}\times 10^{-8} \qquad (1)$$

$$E_c = N_c A_{Fe}\frac{dB}{dt}\times 10^{-8} \qquad (2)$$

$$\int_0^t E_c dt = \frac{N_c A_{Fe}}{10^8}\int_{-B_s}^{+B_s} dB \qquad (3)$$

$$K_{volt-sec} = \int_0^t E_c dt = \frac{N_c A_{Fe} 2B_s}{10^8} \qquad (4)$$

These equations indicate that for a given magnetic amplifier with saturation flux density $B_s$, control winding turns $N_c$, and total cross sectional area of both cores equal to $A_{Fe}$, a definite number of volt-seconds are required to cause the flux density to change from $-B_s$ to $+B_s$ or a total excursion of $2B_s$. At such time as the cores are saturated, the output voltage of the magnetic amplifier will suddenly increase causing the relay to be energized.

When the overvoltage is removed, thereby reducing the voltage $E_c$ to zero, the output of the magnetic amplifier is quickly reduced to a very low value, thus de-energizing the relay. The bias winding $F_3$-$F_4$ will then cause the cores to be reset to the negative saturation value. Complete resetting is normally accomplished in 1 to 2 seconds after which the time delay action can be repeated with excellent accuracy.

$$K_{volt-sec} = \int_0^t (E_{ac} - E_{ut})dt \qquad (5)$$

where $E_{ac} > E_{ut}$

Typical values of $K$ required for use with present-day excitation systems vary from 2.0 to 5.0 volt-seconds.

The ultimate trip voltage of the relay is determined primarily by the reference voltage, the ratio of $E_{ac}$ to $E_{0dc}$, and the resistance values of $1R$ and $2R$. The volt-second characteristic is then determined primarily by the core characteristics, the number of control winding turns, and the resistance of $3R$. A family of constant volt-second curves is shown in Fig. 5.

Once a particular volt-second characteristic has been established for the overvoltage relay, it is possible by analysis of oscillographic data to determine whether a particular overvoltage transient in the system would cause tripping of the overvoltage relay. If not, the amount of margin remaining before tripping occurs can be easily determined.

## Magnetic-Amplifier Fixed Time Delay Relay

In the magnetic-amplifier overvoltage relay, the inverse time delay characteristic is obtained by applying varying voltages to the control winding $F_1$-$F_2$ of the amplifier. If, instead, a fixed control winding voltage is applied, the time required

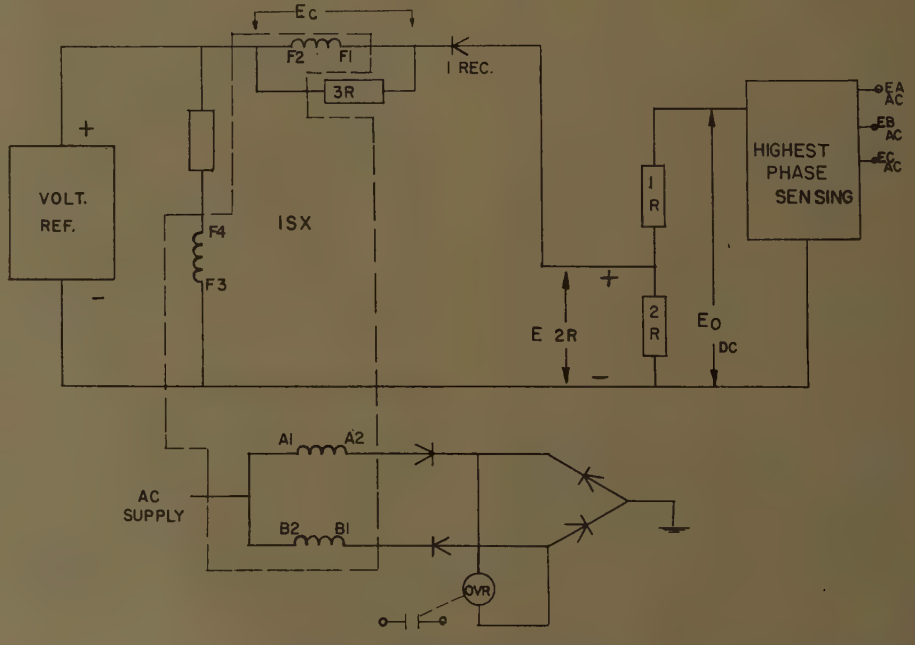


Fig. 2. Overvoltage relay circuit

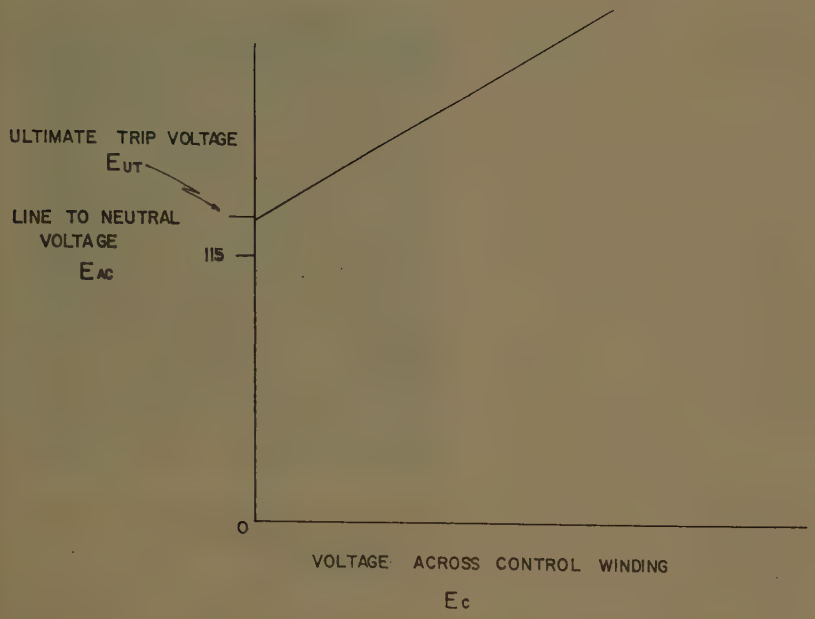


Fig. 3. Overvoltage relay comparison circuit characteristic

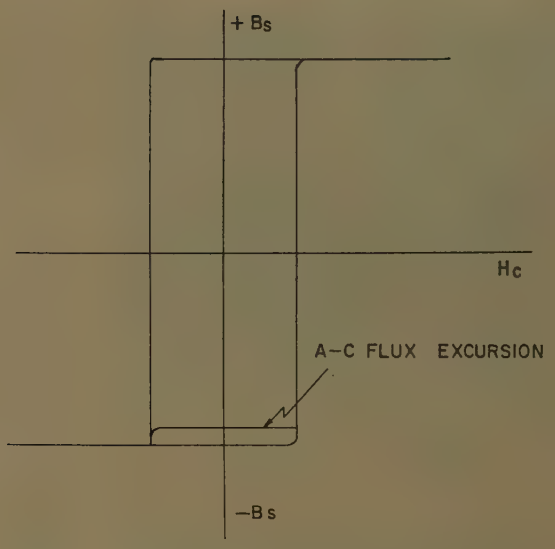


Fig. 4. Hysteresis loop of square loop core material

Fig. 5 (below). Overvoltage relay time delay curves

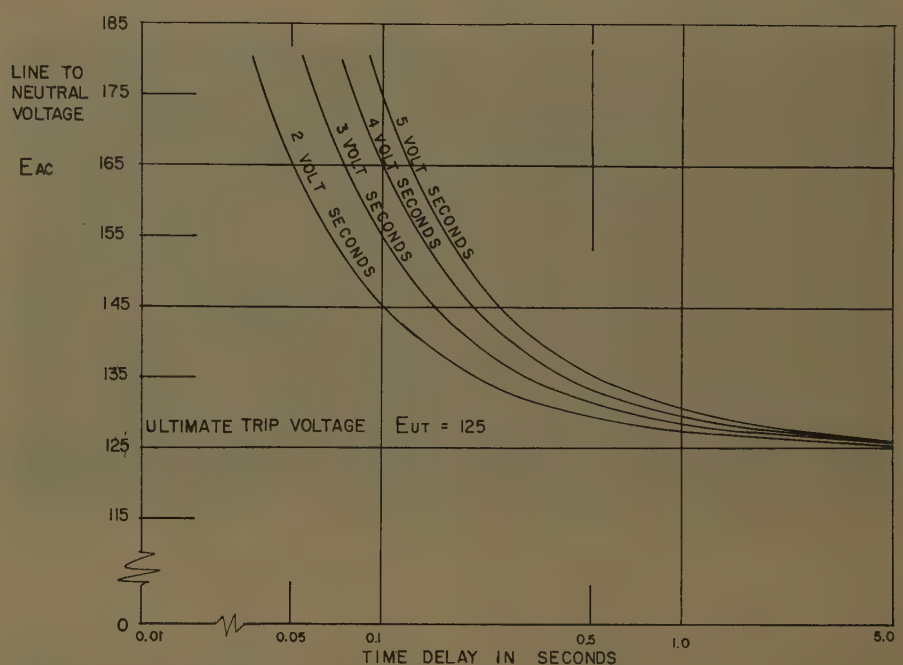


to change the flux level in the cores from negative to positive saturation will be a fixed time. Thus the same basic magnetic-amplifier time delay circuit can be utilized to obtain a fixed time delay as well as an inverse time delay.

### Magnetic-Amplifier Underfrequency Relay

Underfrequency protection is often required in aircraft electric systems to prevent overheating of various types of load equipment. Transformers, magnetic amplifiers, and induction motors are examples of loads which cannot normally tolerate application of rated voltage at frequencies under their minimum design frequency.

An underfrequency may be brought about by any number of factors, such as:

1. Engine idle at low speed on direct-driven generators.
2. Failure of constant speed drive or associated controls.
3. Excessive load torque requirement imposed on a constant speed drive during a low-input speed or low-input energy condition.
4. Jet engine failure and windmilling during flight (even with constant speed drive).
5. Short-time underfrequency during normal engine shutdown and starting.

One method of providing underfrequency protection is the use of a magnetic-amplifier type of underfrequency relay. The circuit for a magnetic-amplifier type of underfrequency relay is shown in Fig. 6. The current in control winding $F_3$-$F_4$ of the magnetic amplifier is proportional to the voltage applied to the circuit and is essentially independent of

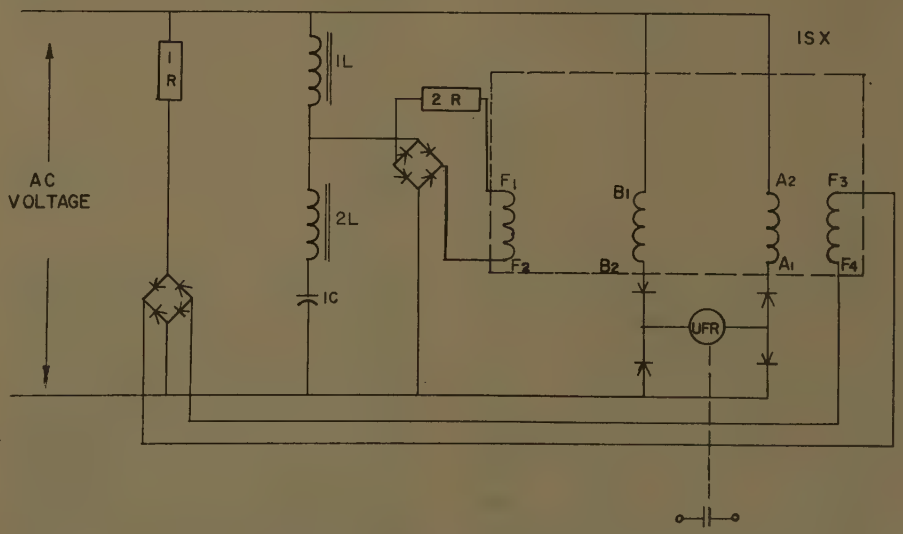


Fig. 6. Underfrequency relay circuit

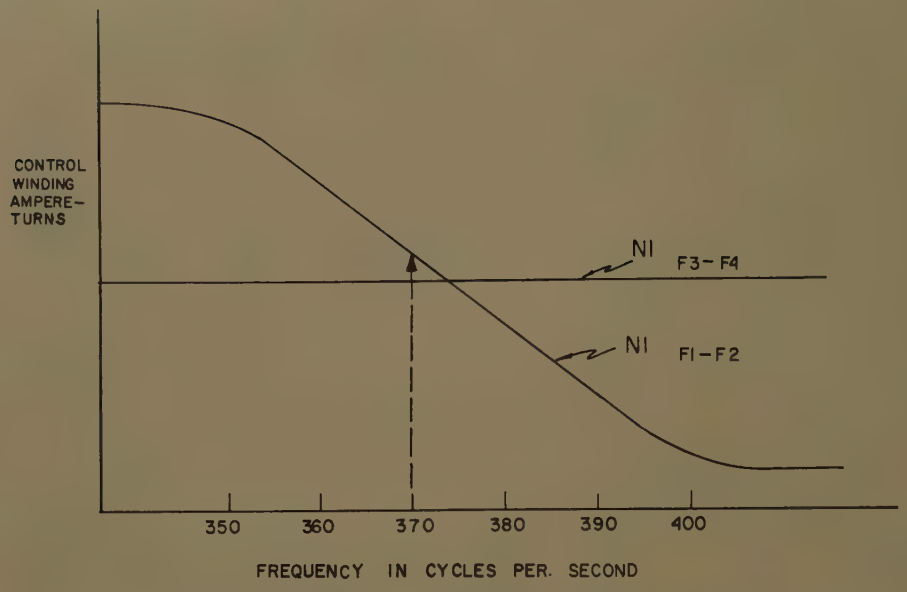


**Fig. 7. Characteristics of frequency comparison circuit with constant input voltage**

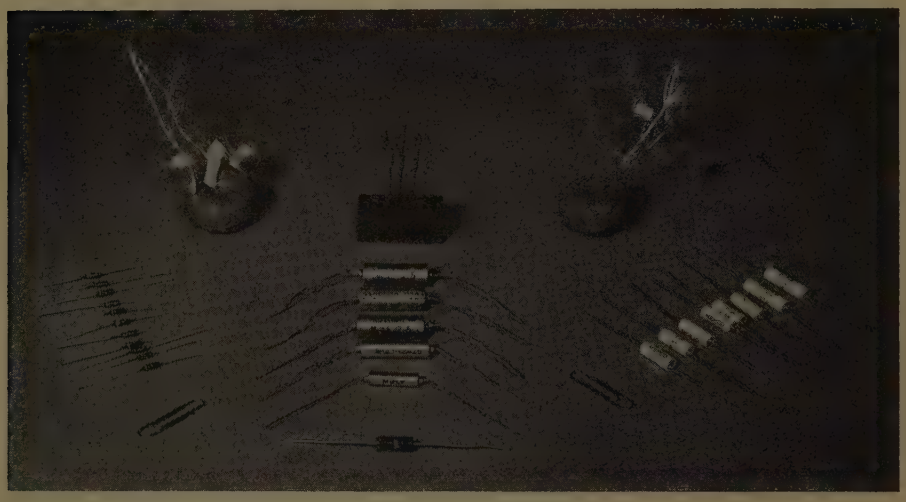

**Fig. 8. Component parts of undervoltage relay assembly**

the frequency. The current in control winding $F_1$-$F_2$ is proportional to the applied voltage, but varies appreciably also as a function of frequency. The variation of the current as a function of frequency is caused by the tuned filter composed of the linear reactors $1L$ and $2L$ and capacitor $1C$.

Fig. 7 shows the characteristic of the ampere-turns in control windings $F_1$-$F_2$ and $F_3$-$F_4$ as a function of frequency. Since the voltage effects are balanced out due to the bucking effects of the windings, the curve of Fig. 7 is shown for constant voltage input. The direction of current flow in winding $F_3$-$F_4$ is from $F_3$ to $F_4$, and therefore provides positive ampere-turns tending to increase the amplifier output. The direction of current flow in winding $F_1$-$F_2$ is from $F_2$ to $F_1$, and therefore provides negative ampere-turns tending to decrease the amplifier output. For the case shown, at frequencies above 370 cps (cycles per second), the magnetic amplifier will have essentially full output and the relay will be energized. As soon as the frequency drops slightly below 370 cps the negative ampere-turns will exceed the positive enough to reduce the amplifier output to essentially zero and the relay will be de-energized.

The exact frequency at which the relay will pick up and drop out is dependent primarily upon the values of $1R$, $2R$, $1L$, $2L$, and $1C$ as well as the number of turns in control windings $F_1$-$F_2$ and $F_3$-$F_4$. In practice, for slight changes in frequency setting, $1R$ is varied in resistance value.

In most of the systems where this underfrequency relay has been used, the generator has incorporated within its frame a small permanent-magnet auxiliary generator. This auxiliary generator is utilized for a number of purposes in the regulation, excitation, and protection systems. By sensing the frequency of this permanent-magnet generator, the underfrequency relay can provide performance which is unaffected by loss of voltage on one or more phases of the main aircraft electrical system.

An inverse time underfrequency characteristic may be obtained by use of the same basic circuit.[2] The tuned circuit range of linearity must be extended, and to accomplish this an amplifier similar to the overvoltage relay magnetic amplifier must be utilized.

## Packaging Problems and Considerations

In making the product or physical design of a protective control panel utilizing magnetic amplifier circuits, a number of considerations confront the product designer. The following is only a partial list of items for consideration:

1. General specifications which equipment must meet.
2. Adaption of the product design to the available components that individually will meet the electrical and environmental requirements.
3. Adaption of the design for ease of manufacturing, testing, and servicing.

### General Specification Requirements

The unit must operate reliably under the normal military aircraft environmental conditions, including high and low temperature, altitude, humidity, salt spray, fungus, shock, acceleration, vibration, and others. Perhaps the requirements presenting the greatest problems to the designer are the high temperatures (120 degrees centrigrade, minimum requirement), vibration (resonances resulting from an applied vibration of 10 $g$ from 60 to 500 cps minimum), and shock (equivalent to 15 $g$ as a minimum requirement). Minimum size and weight are obviously of the utmost importance.

As additional design objectives, it is considered preferable to avoid the use of any adjustable resistors or potentiometers, as well as vibration isolators. Adjustable resistors and potentiometers are potential contributors to unreliability in aircraft equipment. This is because of their basic construction requirement for a moving member, their exposed electrical contact surfaces, and their susceptibility to damage from well-meaning but inexperienced aircraft mechanics. Vibration isolators rob valuable space and result in

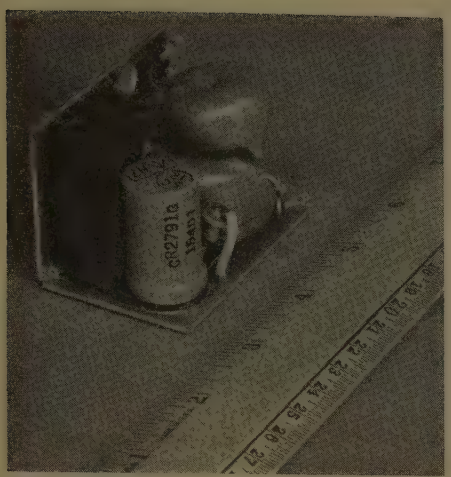

Fig. 9. Overvoltage relay assembly before casting, bottom view

larger and therefore potentially heavier products.

### Component Considerations

Not only have protective systems gradually included more protective and control functions, but the application of magnetic amplifiers to these individual functions results in the use of larger numbers of components in each function. For example, the undervoltage relay circuit described in this paper actually consists of 29 electrical components, including rectifiers, resistors, capacitors, a relay, and a saturable reactor; see Fig. 8. Admittedly, most of these components are extremely small and dissipate only negligible amounts of power. However, since failure of any component could result in unsatisfactory operation of the undervoltage relay, considerable thought must be given to the mounting and the wiring of each component. If conventional packaging techniques are used, an extreme amount of attention and time must be given to detailed design, quality of workmanship, and thorough inspection, in order to achieve the required reliability. In spite of the fact that each individual component can pass rigid vibration specifications, it may be difficult for the overall assembly to meet these requirements, without the use of vibration isolators.

### Adaptability to Manufacturing and Servicing

Products with large numbers of components tightly packaged are inherently difficult to manufacture. Only with extreme care on the part of the workman and the designer can a reliable assembly be built. In addition, if a unit fails to pass its electrical production test, it is often difficult to locate the faulty component or wiring error. The same problem exists when a malfunctioning unit is overhauled after being in service. Undoubtedly complete assemblies are often discarded due to the difficulties in locating and replacing the defective component.

### Solution to the Problem

One solution to these problems is the use of modular subassemblies. In each subassembly, components are assembled and wired by the use of printed circuits and dip soldering, and are then cast into a rigid block by the addition of an epoxy resin and filler.

Some characteristics of the material actually used and an ideal casting material are compared in Table I. Due to the excellent insulating properties of the casting material used, clearances between points of different potential can be reduced without fear of failure. Failures due to shifting of components and wiring early in life are eliminated. All components and wiring within the cast block are protected from the adverse affects of humidity, salt spray, fungus, and altitude. Vibration problems are lessened since all components and wiring are held rigidly in place and vibrate as one mass. This prevents failure due to minor resonances at extremely high frequencies. Even short-time exposure to temperatures over the maximum continuous ambient temperature will not harm components since the heat actually takes appreciable time to reach the components.

The use of printed wiring reduces the possibilities of wiring errors and wire breakage in manufacture. Dip soldering, when controlled properly, produces a uniform electric connection which is easily inspected. Most components require no additional mounting other than that provided by the printed wiring board.

A complete protective panel thus consists of a number of functional subassemblies plus a few miscellaneous components that do not lend themselves to casting due to their large power dissipation or large physical size. Each subassembly can be separately assembled, wired, tested, cast, and retested, prior to being placed in the final over-all equipment enclosure. Final-production electrical testing and inspection serve to check miscellaneous components and interconnecting wiring, as well as to recheck each function after its integration into the protective system. The use of the same functional subassemblies in different protective systems improves manufacturing efficiency and reduces product design time on new protective systems.

The use of adjustable resistors, rheostats, and potentiometers is eliminated wherever possible by designing circuits which do not require adjustment to meet prescribed limits, even considering the worst combinations of component tolerances. Where this is impractical, a fixed resistor of the correct value is selected in preliminary test and is then wired into the subassembly prior to casting. After casting, the subassembly

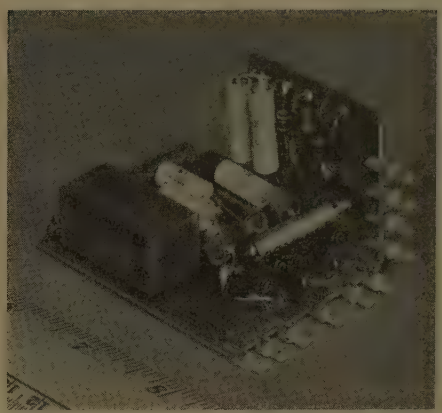

Fig. 10. Undervoltage relay assembly, less magnetic amplifier, before casting

Table I

| | Ideal Requirements | Actual Characteristics |
|---|---|---|
| Viscosity, prior to casting | low | low at elevated temperature |
| Pot life | as long as possible | 29 days when stored at room ambient |
| Cure time | as short as possible | 2 to 3 hours |
| Cure temperature | low, below 120 C | 110 C |
| Shrinkage | kept to minimum | approximately 1% |
| Coefficient of expansion | kept to minimum | $3.2\times10^{-5}$/C |
| Heat conductivity | good | less than $4.8\times10^{-4}$ cal/sec/cm²/C/cm.* |
| Exothermic temperature | as low as possible | 160 C |
| Bond strength | high | excellent to metals |
| Shear strength | high | excellent to 160 C |
| Dielectric strength | high | over 400 volts/mil |
| Resistance to environmental conditions | high | excellent |
| Insulation | above 10 megohms per mil | over 100 megohms/mil |
| Density | low | 0.036 pound per inch³ |

* Calories per second per square centimeter per C per centimeter.

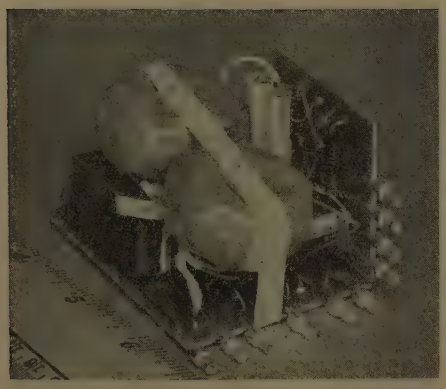

Fig. 11. Undervoltage relay assembly before casting

Fig. 12. Overvoltage relay assembly before casting, back view

will be interchangeable with all other similar cast blocks even though different resistors might have been selected for each block.

Testing and overhauling equipment in the field is greatly simplified by the cast subassembly approach. A brief check of the over-all equipment will generally indicate trouble in a particular function. By merely replacing that complete function, the equipment can be restored to normal operating condition without need for any adjustment. The cost of replacing complete subassemblies instead of individual components is at least partially offset by a simplified stocking problem and greater speed in repairing equipment.

### Packaging of Specific Modular Blocks

In the product designs of each of the modular blocks, there has been an attempt to secure mechanically all the components directly to the printed board in

Fig. 13. Cast unit showing inserts for mounting

order to facilitate the assembling and to prevent wire breakage during manufacture. For example, the overvoltage relay shown in Fig. 9 has all its components mounted directly to the printed boards. In the undervoltage relay, the large number of parts mentioned previously (Fig. 8) are mounted directly to the two printed circuit boards with the exception of the saturable reactor; see Fig. 10. The two cores of the saturable reactor are separate for better space utilization and are held in proper position for casting by a short length of high-temperature glass tape; see Fig 11.

Since the height of the components varies greatly, mounting them on a single printed circuit board results in poor space utilization and extra weight in casting material. Using two printed circuit boards in parallel presents problems in assembly and test due to the relative inaccessibility of the components. The use of two printed boards mounted at right angles to each other affords a good compromise between ease of manufacture and minimum weight and size; see Figs. 9 through 11. The right-angle connections are made with wire jumpers.

Delicate components such as magnetic amplifiers which are sensitive to minute changes in pressure must be protected with a rubberlike compound before casting to prevent any changes in electrical characteristics caused by a difference in the thermal expansion of the component and the casting compound; see Fig. 11. The terminals used are of the solder type rather than the plug-in type. Better reliability is obtained from a soldered connection since the electrical contact is not

Fig. 14. Typical single-generator protective panel, less cover

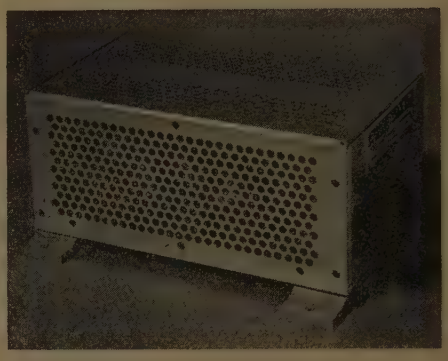

Fig. 15. Single-generator protective panel

dependent upon mechanical pressure and proper alignment. The terminals are placed on the edge of each printed board rather than on the surface of one board to make the casting operation easier; see Fig. 12. The assembly is placed in the mold with the terminals at the top, the casting compound is poured until the printed circuit board is covered, and only the terminals are left exposed. Steel inserts molded into each subassembly serve as a method of mounting the modular blocks; see Fig. 13.

### Typical Protective Panel

A typical aircraft protective panel utilizing the modular construction is shown in Fig. 14. This unit provides highest-phase overvoltage protection, individual-phase undervoltage protection, underfrequency protection, transformer-rectification, and field flashing. The four cast assemblies are placed side by side in the rear of the panel with a sheet metal framework wrapped around them and a center support section in front. This enables all the assemblies to be securely fastened on at least three surfaces. This basic construction is extremely rigid and passes the vibration requirements easily.

The uncast components are mounted on

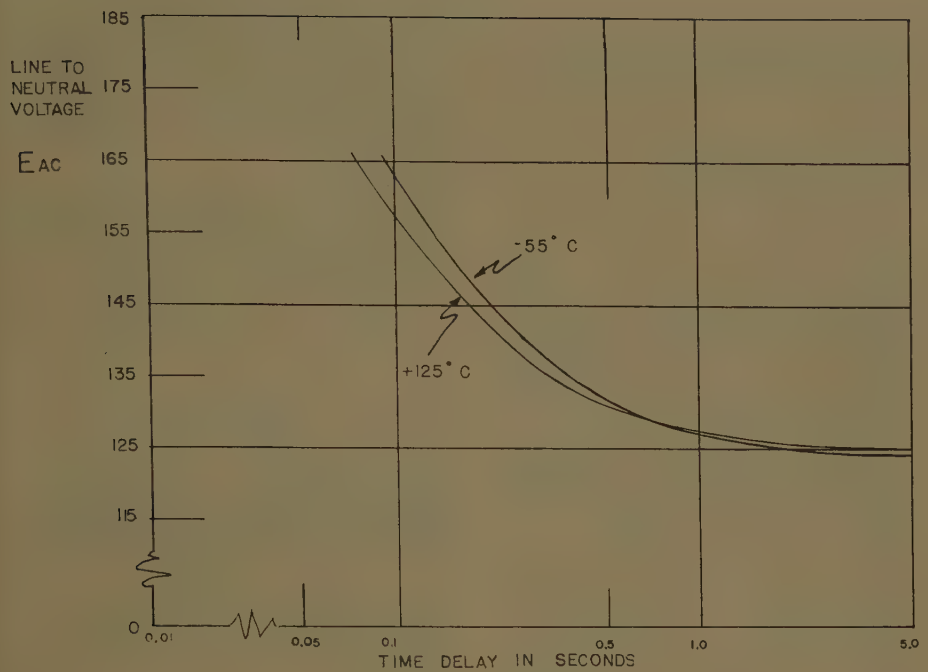


**Fig. 16. Overvoltage relay variation with temperature**

either the printed board or any of the available sheet metal surfaces. The complete protective panel weighing $6^1/_2$ pounds is shown in Fig. 15.

## Results

1. The magnetic-amplifier type of overvoltage relay in its final form weighs 0.7 pound and is 2 by 2 by 2.8 inches. The electrical performance over the temperature range of −55 C to +125 C is shown in Fig. 16.

2. The magnetic-amplifier type of undervoltage relay weighs 0.75 pound and is 1.9 by 2.4 by 2.9 inches. Over the temperature range of −55 C to +125 C, the drop-out voltage varies ±2%. The differential between pickup and dropout is one volt, based on line-to-neutral voltage.

3. The magnetic-amplifier type of underfrequency relay weighs 0.95 pound and is 2.1 by 2.4 by 2.9 inches. Over the temperature range of −55 C to +125 C, the drop-out frequency varies ±3 cps. The differential between the pickup and dropout frequencies is 2 cps.

## Conclusions

The use of magnetic amplifiers in aircraft generator protective systems results in highly accurate and predictable operation of the various protective functions. By eliminating the use of less reliable components such as adjustable resistors and poorly applied relays, the level of component reliability can be made very high. The use of cast subassemblies makes possible a high degree of reliability for the over-all assembly, without the requirement for vibration isolators. The use of modular subassemblies reduces product design time and simplifies the manufacturing and servicing of equipment. The size and weight of these protective devices are small, thereby making all the other advantages possible without increasing the weight and space requirements in the aircraft.

## References

1. The Development of a Static Voltage Regulator for Aircraft A-C Generators, H. H. Britten, D. L. Plette. *AIEE Transactions*, vol. 74, pt. II, 1955(Jan. 1956 section), pp. 438–43.

2. Invfrse-Time Underfrequency Relay, R. G. Hoft. *Ibid.*, vol. 75, pt. I, 1956 (Jan. 1957 section) pp. 625–29.

# LATE DISCUSSION

The following discussion, based on a 1956 paper, was recently received from abroad.

## Fundamental Relation of A-C Servo Systems

**Discussion of paper 56-792, "Envelope Transfer Function Analysis in A-C Servo Systems," by M. Panzer, published in AIEE Transactions, part II, November 1956, pages 274–79.**

**Amos Nathan** (Technion, Israel Institute of Technology, Haifa, Israel): What may well be called the fundamental relation of a-c servo systems was recently announced by Panzer and also by Levenstein.[1] Because of its importance, a much simplified proof is here presented.

Following Panzer's notation we state the problem as follows:

A linear transducer of transmittance $G(p)$, i.e.,

$$E_0(p)=G(p)E_i(p) \tag{1}$$

is fed with the input

$$e_i(t)=e_s(t)\cos\omega_c t=Re\{e_s(t)\epsilon^{i\omega_c t}\} \tag{2}$$

It is required to obtain the output $e_0(t)$ in the form

$$e_0(t)=Re\{[s_o(t)+iS_Q(t)]\epsilon^{i(\omega_c t+\phi)}\} \tag{3}$$

$\phi$ being an arbitrary constant.

To solve, let us transform equations 2 and 3, obtaining

$$E_i(p)=Re\{E_s(p-i\omega_c)\} \tag{2A}$$

$$E_0(p)=Re\{[S_D(p-i\omega_c)+iS_Q(p-i\omega_c)]\epsilon\}^{i\phi} \tag{3A}$$

where we have used the well-known relation

$$\mathcal{L}\{f(t)\epsilon^{\alpha t}\}=F(p-\alpha)$$

Substituting equations 2(A) and 3(A) into equation 1 and noting the reality of $G(p)$

$$Re\{[S_D(p-i\omega_c)+iS_Q(p-i\omega_c)]\epsilon^{i\phi}\}=Re\{G(p)E_s(p-i\omega_c)\} \tag{4}$$

which is satisfied by

$$S_D(p)+iS_Q(p)=G(p+i\omega_c)E_s(p)\epsilon^{-i\phi} \tag{5}$$

This solves the problem, $e_0(t)$ being given by equations 3 and 5.

Introducing

$$G_D(p)=S_D(p)/E_s(p)$$
$$G_Q(p)=S_Q(p)/E_s(p) \tag{6}$$

and noting the reality of $S_D$ and $S_Q$ we can write equivalently:

$$G_D(p)=Re\{G(p+i\omega_c)\epsilon^{-i\phi}\} \tag{5A}$$
$$G_Q(p)=Im\{G(p+i\omega_c)\epsilon^{-i\phi}\}$$

REFERENCE

1. ON THE DESIGN OF A-C NETWORKS FOR SERVO COMPENSATION, H. Levenstein. *Transactions*, Professional Group on Automatic Control, Institute of Radio Engineers, New York, N. Y., Feb. 1957, pp. 39–55.

# ERRATA

**"Design and Calculation of Induction-Heating Coils" by R. M. Baker, published in Applications and Industry, March 1957, pages 31–40.**

Equation 25, page 34, should read:

$$X_e=\frac{8\pi^2 f N_c^2 10^{-9}}{R_e} \tag{25}$$

Equation 26, page 34, should read:

$$X_e=\frac{8\pi^2 f N_c^2 10^{-9}}{l_c}\left(\frac{l_c}{R_e}\right) \tag{26}$$

# Applications and Industry Index for 1957

## 1. Technical Subject Index



### B



### C



### D

## E



## F



## G



## H



## I



## J



## L

## M



## N



## O



## P



## Q



## R



## S

## T



## U



## V



## W



## Z



# 2. Author Index



## B



## C



## D



## E

## W



## Y



## Z

## Power Apparatus and Systems—December 1957



## Conference Paper Open for Discussion

Conference paper listed below has been accepted for AIEE Transactions and is now open for written discussion until February 26. Duplicate double-spaced typewritten copies of each discussion should be sent to Edward C. Day, Assistant Secretary for Technical Papers, American Institute of Electrical Engineers, 33 West 39th Street, New York 18, N. Y., on or before February 26.

Preprints may be purchased at 40¢ each to members; 80¢ each to nonmembers if accompanied by remittance or coupons. Please order by number and send remittance to:

AIEE Order Department
33 West 39th Street
New York 18, N. Y.

57-990 Transient Protection Conditions in Pipe-Line Stations....Turner

# AIEE PUBLICATIONS

| | Member Prices | Nonmember Prices |
|---|---|---|
| **Electrical Engineering** | | |
| Official monthly publication containing articles of broad interest, technical papers, and three news sections: Institute Activities, Current Interest, and Electrical Engineering Education. Automatically sent to all members and enrolled students in consideration of payment of dues. | | annually $12* per year |
| * Subscription price and $1.00 extra for foreign postage both payable in advance in New York exchange. | | Single copies $1.50 |
| **Bimonthly Publications** | | |
| Containing all officially approved technical papers collated with discussion (if any) in three broad fields of subject matter as follows: | | |
| | annually | annually |
| Communication and Electronics | $2.50† | $5.00‡ |
| Applications and Industry | $2.50† | $5.00‡ |
| Power Apparatus and Systems | $2.50† | $5.00‡ |
| † Members may elect to receive any one of the three bimonthly publications in consideration of payment of dues without additional charge. | | |
| ‡ Subscription price and 50 cents extra for foreign postage both payable in advance in New York exchange. | | |
| Single copies may be obtained when available. | $1.00 each | $1.00 each |
| **AIEE Transactions** | | |
| An annual volume in three parts containing all officially approved technical papers with discussions corresponding to six issues of the bimonthly publication of the same name bound in cloth with a stiff cover. | | |
| | annually | annually |
| Part I Communication and Electronics | $3.00 | $ 6.00** |
| Part II Applications and Industry | $3.00 | $ 6.00** |
| Part III Power Apparatus and Systems | $3.00 | $ 6.00** |
| Annual combination subscription to all three parts (beginning with vol. 74 for 1955). | $9.00 | $12.00*** |
| Annual combination subscription to any two parts. | | $10.00*** |
| ** Subscription price and 75 cents extra for foreign postage both payable in advance in New York exchange. | | |
| *** Subscription price and $1.00 extra for foreign postage both payable in advance in New York exchange. | | |
| **Electrical Engineering and Transactions** | | |
| An annual combination subscription to both publications (effective April 1, 1955). | | $20.00§ |
| § Subscription price and $2.00 extra for foreign postage both payable in advance in New York exchange. | | |
| **AIEE Standards** | | |
| Listing of Standards, test codes, and reports with prices furnished on request. | | |
| **Special Publications** | | |
| Committee reports on special subjects, bibliographies, surveys, and papers and discussions of some specialized technical conferences, as announced in ELECTRICAL ENGINEERING. | | |

---

Discount 25% of above nonmember prices to college and public libraries. Publishers and subscription agencies 15% of above nonmember prices. For available discounts on Standards and special publications, obtain price lists from Order Department at Headquarters. Send all orders to:

Order Department
American Institute of Electrical Engineers
33 West 39th Street, New York 18, N. Y.